Copyright

by

Meredith Anne Bush

2016

The Dissertation Committee for Meredith Anne Bush certifies that this is the approved version of the following dissertation:

STRATIGRAPHIC SIGNATURES OF CONVERGENT OROGENESIS FROM THE PLATE INTERIOR: STUDIES FROM TIBET AND THE SOUTHERN ROCKY MOUNTAINS

Committee:

Brian Horton, Supervisor

Daniel Stockli

Ronald Steel

Jacob Covault

Michael Murphy

STRATIGRAPHIC SIGNATURES OF CONVERGENT OROGENESIS FROM THE PLATE INTERIOR: STUDIES FROM TIBET AND THE SOUTHERN ROCKY MOUNTAINS

by

Meredith Anne Bush, B.A.; M.S.I.S.

Dissertation

Presented to the Faculty of the Graduate School of

The University of Texas at Austin

in Partial Fulfillment

of the Requirements

for the Degree of

Doctor of Philosophy

The University of Texas at Austin

December 2016

Acknowledgements

This research is the product of discussions with friends and colleagues around the world. I am indebted to numerous collaborators, research group members, committee members, and the people who helped me make connections to field and laboratory resources in both China and the southern Rocky Mountains – too many individuals to name.

Funding for these projects was cobbled together from institutional support from the Jackson School of the Geosciences at the University of Texas, graduate student grants from professional organizations including the Geological Society of America, the American Association of Petroleum Geologists, the International Association of Sedimentologists, the Colorado Scientific Society, and the Gulf Coast Association of Geological Societies. Thanks to these organizations for continuing to support research by graduate students, allowing us to design original projects independent from industry or federal funding sources.

This research was inspired by landscape of the American west, and the teachers at Colorado College and during the University of Texas summer field camps who have fostered my continued investigation of these regions. It would not have been possible without a lifetime of support from my family.

Stratigraphic signatures of convergent orogenesis from the plate interior: studies from Tibet and the southern Rocky Mountains

Meredith Anne Bush, Ph.D.

The University of Texas at Austin, 2016

Supervisor: Brian K. Horton

Fundamental questions remain in geology regarding the growth and development of the continental landscape. The existence of major mountain belts and high plateaus in the plate interior, over a thousand kilometers from a plate boundary, requires a complex combination of tectonic and climatic pre-conditions combined with inherited structures, active tectonics, geodynamic processes, and climatic feedback. Through these studies of the basin records of orogenesis in the Qaidam basin of northern Tibet and the southern Rocky Mountain basins of North America, we provide new constraints on the timing of deformation, the development of proximal basins, and the evolution of continental-scale drainage patterns in two of the most prominent modern mountain belts.

Three studies are presented in this dissertation, each investigating a different aspect of continental plate-interior basin development. In Chapter 2, the Cenozoic sedimentary record from the Qaidam basin is investigated through a sedimentological and multi-proxy provenance study. Provenance and stratigraphic analysis reveals syn-

collisional exhumation of the Eastern Kunlun Shan and Qilian Shan, marking the early establishment of the borders of the Tibetan plateau. Chapter 3 investigates the record of easternmost Laramide deformation in the southern Rocky Mountains. Detrital zircon U-Pb geochronology of Cretaceous through Eocene sedimentary units in the Raton basin provides new constraints on the uplift and exhumation of the Sangre de Cristo range, revealing initial exhumation of Laramide basement material in the Campanian, the formation of a drainage divide within the Sangre de Cristo range by the Paleocene, and continued exhumation through the Eocene. The final study (Chapter 4) looks at regional patterns of uplift, exhumation, and drainage reorganization during the latest Cretaceous through Eocene in the southern Rocky Mountains. Initial Laramide-style deformation introduced basement material into the basins while maintaining integrated basins, while continued exhumation throughout the Paleogene resulted in partitioning of basins into more localized depocenters. Provenance analysis of strata from the San Juan, Galisteo-El Rito, and Raton basins reveals new depositional ages, as well as patterns of basin filling and drainage integration during Laramide thrusting, pluton emplacement in the San Juan mountains, and the transition to south-directed continental drainage systems that terminate in the Gulf of Mexico.

Together, these studies provide a framework for understanding the co-evolution of sedimentary basins and mountain belts in the plate interior based on the recognition of initial deformation, continued exhumation and drainage integration, and partitioning of basins due to the formation of topographic barriers.

Table of Contents

List of Tables

List of Figures

Chapter 1: Introduction

Understanding the development of the continental landscape is important for predictions involving source-to-sink sedimentary systems, boundary conditions in paleo-climate modeling, and to explore the links between surface processes and geodynamics. Accurate reconstructions of the growth of intra-plate mountain ranges as well as their associated basins are necessary for scientists involved in the ongoing exploration of the geological history of the Earth.

Two vast mountain belts crossing the major continental landmasses dominate the modern terrestrial landscape (Fig. 1.1). The Tethyan ranges of Eurasia and the Cordilleran ranges of the Americas are the dramatic manifestation of Phanerozoic convergent plate tectonics. The sedimentary record stored in basins proximal to these mountain belts serves as an archive of both local and regional landscape evolution: the stratigraphy and composition of the basins is dependent upon both climatic and tectonic conditions in the sediment source area, while the basin architecture is a product of the rheology and deformation history of the lithosphere (Dickinson, 1974; Flemings and Jordan, 1989; Jordan, 1995).

The studies that compose this dissertation add another dimension to the significant contributions from earlier researchers regarding the tectonics of continents, complementing work by structural geologists and sedimentologists alike (Dewey and Bird, 1970; Atwater, 1970; Coney, 1972; Powell et al., 1973; Jordan, 1981.) In particular, these studies look at the paired deformation and sedimentation that occurs in "far-field" zones related to convergent tectonics, where mountain belts are found greater than 1000 km from the plate boundary. This dissertation focuses on reconstructing the evolution of

the plate-interior landscape from the provenance record, investigating and ultimately comparing the development of the continental interior from the Tibetan plateau and from the Cordilleran (Laramide) deformation front in the southern Rocky Mountains.

MOTIVATION

In continental mountain ranges, detection of initial uplift is often problematic due to the removal of material from mountain ranges during exhumation (which could otherwise provide thermochronological constraints on cooling) and the reorganization of drainage systems during subsequent growth of the orogen (which obfuscates the early record of sedimentary response to deformation). The Qaidam basin of the Tibetan plateau and the basins of the southern Rocky Mountains (specifically, the San Juan, Galisteo-El Rito, and Raton basins) were selected for research based on the preserved sedimentary successions spanning a complete episode of orogenesis.

The aim of this research has been to understand the landscape evolution of mountain ranges bounding basins in the most distally deformed regions of the continental plate interior, in order to facilitate future interpretations of the tectonic evolution of plate interior systems from the depositional record. The following objectives were established to achieve these goals:

1) Characterize the sedimentary history preserved in plate interior basins throughout an episode of mountain building, identifying major shifts in depositional styles and provenance signatures. Develop an understanding for the partitioning of sediment between the proximal and distal zones of an orogen.

2) Determine the effect of topographic barrier formations on mountain-front basins, evaluating the impact on both local and regional depositional patterns.

All study areas preserve a succession of nonmarine, siliciclastic basin fill that records plate interior mountain building. In the Qaidam basin, the Cenozoic strata record deformation on the Tibetan plateau, including the uplift of the Qilian Shan-Nan Shan, Kunlun Shan, Altyn Shan and other related ranges. In the southern Rocky Mountains, the San Juan, Galisteo-El Rito, and Raton basins record the uplift of ranges east of the Sevier fold-thrust belt and Colorado Plateau, specifically the San Luis highlands, Nacimiento range, and Sangre de Cristo range. These basins are intermediate depositional repositories in the continental-scale source to sink systems, a critical link between the deformation and exhumation records from the source areas and the stratigraphic record preserved in the sink. Methods and data tables are provided in the appendices.

OVERVIEW OF CHAPTERS

This dissertation is composed of three separate manuscripts that focus on the evolution of basins in the continental plate interior. Basin records of subsidence patterns, depositional environments, and provenance evolution from the pre-deformation to post-deformation phases are used to evaluate the influence of the paleo-geographic, paleo-tectonic, and paleo-climatic changes in the basins. Chapter 2 examines the Cenozoic evolution of the northern margin of the Tibetan plateau, based on field and laboratory data from the Qaidam basin. Chapters 3 and 4 focus on Laramide-age basins of the southern Rocky Mountains in North America, examining the patterns of mountain

building and reorganization of sedimentary systems during the Cretaceous through Eocene.

Chapter 2, entitled “Growth of the Qaidam Basin during Cenozoic exhumation in the northern Tibetan Plateau: Inferences from depositional patterns and multi-proxy detrital provenance signatures”, has been published in Lithosphere in 2016 (Bush et al., 2016b). This manuscript presents a multi-proxy provenance analysis from the Qaidam basin, reconstructing the uplift of the Qilian Shan-Nan Shan and Eastern Kunlun Shan in the northern Tibetan plateau.

Chapter 3, entitled “Detrital record of initial basement exhumation along the Laramide deformation front, southern Rocky Mountains”, has been published in Tectonics in 2016 (Bush et al., 2016a). This manuscript uses detrital zircon U-Pb geochronology from the Cenozoic section in the Raton basin to pinpoint the timing of initial Laramide deformation in the Sangre de Cristo range and the rerouting of fluvial systems.

Chapter 4, entitled “Deformation and basin development in the Southern Rocky Mountains, 35° to 38° N” is in review at the Geological Society of America Bulletin. This study examines the Cretaceous-Eocene provenance record from the San Juan, Galisteo-El Rito, and Raton basins, providing a reconstruction of continent-scale drainage and sediment dispersal systems during the Laramide orogeny.

Chapter 5 briefly summarizes the major conclusions of each study, and provides a synthesis of the patterns of both deformation and drainage reorganization recognized in these plate-interior basins.

REFERENCES

Atwater, T., 1970, Implications of plate tectonics for the Cenozoic tectonic evolution of western North America: Geological Society of America Bulletin, v. 81, p. 3513.

Bush, M.A., Horton, B.K., Murphy, M.A., and Stockli, D.F., 2016a, Detrital record of initial basement exhumation along the Laramide deformation front, southern Rocky Mountains: Tectonics, doi: 10.1002/2016TC004194.

Bush, M.A., Saylor, J.E., Horton, B.K., and Nie, J., 2016b, Growth of the Qaidam Basin during Cenozoic exhumation in the northern Tibetan Plateau: Inferences from depositional patterns and multiproxy detrital provenance signatures: Lithosphere, v. 8, p. 58–82, doi: 10.1130/L449.1.

Coney, P.J., 1972, Cordillaran tectonics and North American plate motion: American Journal of Science, v. 272, p. 603–628.

Dewey, J.F., and Bird, J.M., 1970, Mountain belts and the new global tectonics: Journal of Geophysical Research, v. 75, p. 2625–2646, doi: 10.1029/JB075i014p02625.

Dickinson, W.R., 1974, Plate tectonics and sedimentation: Tectonics and sedimentation, v. 22, p. 1–27.

Flemings, P.B., and Jordan, T.E., 1989, A synthetic stratigraphic model of foreland basin development: Journal of Geophysical Research, v. 94, p. 3851–3866.

Jordan, T.E., 1995, Retroarc foreland and related basins, in p. 331–362.

Powell, C., and Conaghan, P., 1973, Plate tectonics and the Himalayas: Earth and Planetary Science Letters, v. 20, p. 1–12.

Ryan, W.B.F., S.M. Carbotte, J.O. Coplan, S. O'Hara, A. Melkonian, R. Arko, R.A. Weissel, V. Ferrini, A. Goodwillie, F. Nitsche, J. Bonczkowski, and R. Zemsky, 2009, Global Multi-Resolution Topography synthesis, Geochem. Geophys. Geosyst., 10, Q03014, doi:10.1029/2008GC002332.

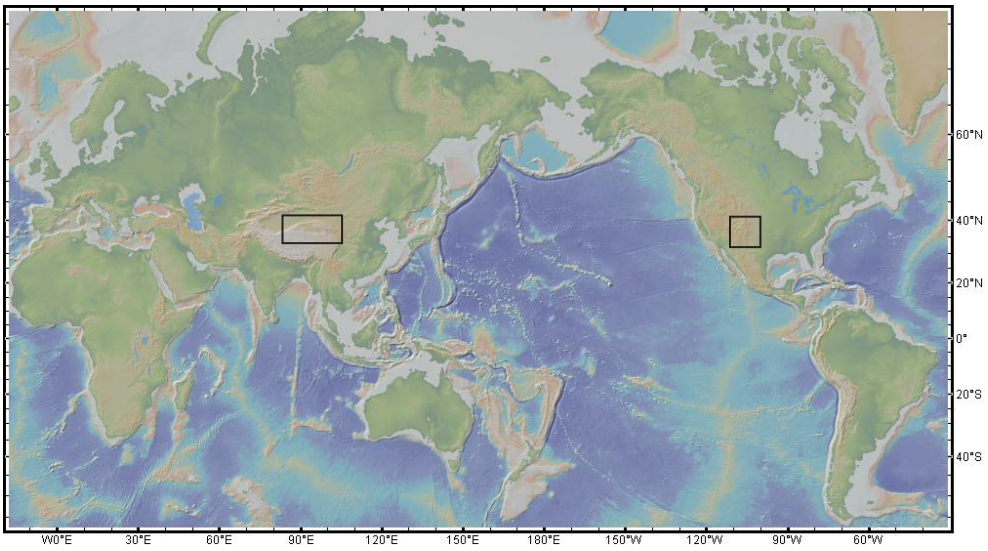

Figure 1.1: Global shaded relief map. Black rectangles define study regions, the Qaidam basin of the northern Tibetan plateau (Chapter 2) and the southern Rocky Mountains of North America (Chapters 3 and 4). Map produced with GeoMapApp (http://www.geomapapp.org), with base map from Ryan et al., 2009.

Chapter 2: Growth of the Qaidam Basin during Cenozoic exhumation in the northern Tibetan Plateau: Inferences from depositional patterns and multi-proxy detrital provenance signatures[1]

ABSTRACT

Sedimentologic and provenance analyses for the Qaidam Basin in the northern Tibetan Plateau help elucidate the stratigraphic signatures of initial deformation and exhumation in basin-bounding ranges. The basin recorded sedimentary transitions in response to uplift and unroofing of several distinctive source regions. Along the NE basin margin, a detrital record of exhumation and basin isolation is preserved in the 6200 m thick Cenozoic succession at the Dahonggou anticline. An upsection shift from axial fluvial and marginal lacustrine deposition to transverse fluvial sedimentation suggests progradation and increasingly proximal sediment sources, reflecting activation and advance of crustal deformation. Provenance results from sandstone petrology, U-Pb geochronology, and heavy mineral analyses indicate initial late Paleocene–early Eocene derivation from igneous, metamorphic, and sedimentary sources, consistent with Permian-Triassic arc rocks dominating the southern (Kunlun Shan) or southwestern (Qimen Tagh) basin margins. Upsection variations in sediment composition and detrital zircon U-Pb age distributions are attributed to Eocene–Oligocene derivation from lower Paleozoic and Mesozoic igneous and metamorphic rocks of the central to northern Qilian Shan-Nan Shan. A disappearance of igneous and persistence of metamorphic sources is

[1] This chapter was published in January 2016. Author contributions to the authorship are as follows: M. Bush: 75%, J. Saylor: 15%; B. Horton: 5%; J. Nie: 5%

Bush, M.A., Saylor, J.E., Horton, B.K., and Nie, J., 2016, Growth of the Qaidam Basin during Cenozoic exhumation in the northern Tibetan Plateau: Inferences from depositional patterns and multiproxy detrital provenance signatures: Lithosphere, v. 8, p. 58–82, doi: 10.1130/L449.1.

consistent with derivation from the southern Qilian Shan-Nan Shan during early–middle Miocene shortening along the frontal Nan Shan-North Qaidam thrust belt. These results are supported by paleocurrent analyses revealing an Eocene shift from roughly E-directed (axial) to SW-directed (transverse) dispersal of sediment. Variations in lithofacies, composition, U-Pb ages, and paleoflow are consistent with late Paleocene–early Eocene exhumation in the Kunlun Shan followed by middle Eocene–middle Miocene exhumation in the Qilian Shan-Nan Shan. The upsection disappearance and reappearance of diagnostic U-Pb age populations can be associated with progressive unroofing of multiple thrust sheets, successive input of sedimentary and magmatic sources, and southward encroachment of Qilian Shan-Nan Shan shortening into the Qaidam Basin. The sedimentary record presented here indicates that during the Paleogene the unified Qaidam-Tarim Basin was partitioned and uplifted as it was incorporated into the growing Tibetan Plateau. Comparison with basins on and surrounding the Tibetan Plateau suggests that basement strength and lateral homogeneity, and formation of syndepositional structural dams are among the primary controls on formation of giant sedimentary basins.

INTRODUCTION

The 5–14 km thick Cenozoic succession in the Qaidam Basin (Fig. 2.1) provides an important detrital record of the intraplate response to the India-Asia collision. Growth of this internally drained basin at ~2500 m elevation has been ascribed to northward advance of Neogene collisional deformation and accompanying flexural subsidence (Meyer et al., 1998; Métivier et al., 1998; Tapponnier et al., 2001). However, evidence for pre-Neogene shortening in the northern Tibetan Plateau contradicts the proposed

systematic northward propagation of deformation. Specifically, rapid late Eocene-Oligocene sedimentation and tectonic rotation (Horton et al., 2004; Dupont-Nivet et al., 2004; 2008), exhumational cooling (Clark et al., 2010), and thrust faulting (Duvall et al., 2011) indicate early deformation in northeastern Tibet (see review by Yuan et al., 2013). These findings highlight the limited understanding of early Cenozoic deformation and plate-interior basin evolution within the Tibetan plateau.

Contrasting reconstructions have been proposed for mountain ranges bounding the Qaidam Basin. To the south, the eastern Kunlun Shan recorded pre-Cenozoic deformation (Cheng et al., 2015), an early phase of Eocene shortening (Jolivet et al., 2003; Yin et al., 2007a; Duvall et al., 2013), and complex Oligocene to Quaternary transpressional deformation ranging from ~30–20 Ma in the central range (Mock et al., 1999; Wang et al., 2004; Yuan et al., 2006; Clark et al., 2010; Mao et al., 2014) to 12–8 Ma in the west and 8–5 Ma in the east (Duvall et al., 2013). Left-lateral slip on the Kunlun fault initiated by middle–late Miocene time (Kirby et al., 2003; Fu and Awata, 2007; Duvall et al., 2013). To the north, the Qilian Shan-Nan Shan may record early Cenozoic faulting and middle–late Cenozoic migration of deformation and sedimentation to the south and east (Yin et al., 2008a). In contrast, thermochronology studies in the northern Qilian Shan identify bedrock cooling at 12–6 Ma (Zheng et al., 2010; Craddock et al., 2011b).

Continuous sediment accumulation in the Qaidam Basin from the Paleogene–Holocene may record the onset of exhumation in basin-bounding ranges, and associated changes in sediment sources. However, the Qaidam Basin epitomizes the challenge posed by plate-interior basins in which multiple sediment sources are characterized by

similar lithologies, compositions, or thermal histories (e.g., Graham et al., 1993). Sediment provenance tracers are often consistent with multiple potential sources and do not point to systematic upsection changes in sediment sourcing (Rieser et al., 2005, 2006a, 2006b; Zhuang et al., 2011b, Jian et al., 2013; Cheng et al., 2015). However, application of multiple provenance techniques has identified changes in sediment sources (e.g., Hanson, 1999).

This study addresses the evolution of the Qaidam Basin by integrating multiple sedimentologic and provenance records from the northeastern margin of the basin to evaluate Cenozoic exhumation patterns in major basin-bounding ranges. Uniting stratigraphic and sedimentologic relationships with multiple provenance techniques, including petrographic, U-Pb geochronologic, heavy mineral, and paleocurrent analyses sheds light on the growth of flanking ranges and associated evolution of Qaidam depositional systems. Interpretations of detrital zircon U-Pb results are guided by multi-dimensional scaling (MDS), a visualization technique representing statistical similarity among samples. Collectively, these datasets identify the early intraplate response to the India-Asia collision through identification of non-uniform exhumation along Qaidam Basin margins.

GEOLOGIC SETTING

The Qaidam Basin is surrounded by diverse igneous and metamorphic rocks comprising Precambrian basement, Paleozoic-Mesozoic magmatic arc, and accretionary prism assemblages overlapped by Mesozoic–Cenozoic basin fill. Flanking ranges (Fig. 2.1) include the Qilian Shan-Nan Shan system to the north, Kunlun Shan to the south, Altyn Shan to the west, and Ela Shan and Dulan-Chaka highland to the east.

The basin is commonly modeled as a rigid block composed of strong lithosphere and continental basement (Clark and Royden, 2000; Braitenberg et al., 2003; Dayem et al., 2009). Crystalline basement in northern Tibet is composed of the Qilian and Qaidam terranes: Proterozoic and Paleozoic assemblages accreted to the Tarim and Sino-Korean cratons during Paleozoic-early Mesozoic closure of Tethys (Hsü et al, 1995; Sobel and Arnaud, 1999; Yin and Harrison, 2000; Yin et al., 2007b; Pullen et al., 2008; Gehrels et al, 2011).

To the north-northeast, the Qilian Shan-Nan Shan (Fig. 2.1, 2.2) forms a major NW-trending fold-thrust belt overprinting a system originally formed during early Paleozoic collision and arc accretion and later reactivated during Mesozoic-Cenozoic extension, contraction, and strike-slip deformation (Ritts and Biffi, 2001; Jolivet et al., 2001; Xiao et al., 2009; Yan et al., 2010; Zheng et al., 2010). Synorogenic deposits in the adjacent Hexi Corridor document the onset of crustal shortening in the northern Qilian Shan by the Miocene (Wang and Coward, 1993; George et al., 2001; Bovet et al., 2009).

To the south, the E-trending Eastern Kunlun Shan (Fig. 2.1, 2.2) is a transpressional fold-thrust system overprinting a Permian–Triassic magmatic arc (Dewey et al, 1988; Mock et al., 1999; Jolivet et al., 2001, 2003; Xiao et al., 2002; Mo et al., 2007; Yuan et al., 2009; Clark et al., 2010) and early Paleozoic arc in the westernmost Qimen Tagh range (Li et al., 2013). Left-lateral displacement along the Kunlun fault is thought to have initiated with late Miocene extension in southern Tibet and continues to the present (Van der Woerd et al., 1998; Lin et al., 2002; Fu and Awata, 2007; Kirby et al., 2007; Duvall et al., 2013).

To the northwest, the NE-striking Altyn Tagh fault (Fig. 2.1, 2.2) persists for 1600 km, with left-lateral displacement absorbed by NE-SW shortening in the Qilian Shan-Nan Shan. Altyn Tagh deformation initiated between 49 and 30 Ma, with strike-slip motion dominant by Miocene time and progressively decreasing strike-slip motion (Jolivet et al., 2001; Yin et al., 2002; Wang et al., 2005) related to a shift from lateral extrusion to crustal shortening (Yue et al., 2003; Ritts et al., 2008; Yin et al., 2008a; 2008b).

To the east, the Qaidam Basin is flanked by the Ela Shan range and Dulan-Chaka highland (Fig. 2.2), which form the boundary between Qaidam and externally drained Neogene basins of northeastern Tibet. These include the Miocene-Pliocene Gonghe, Xunhua, and Chaka basins, which occupy the Yellow River headwaters (Craddock et al., 2011b; Lease et al., 2011; Lu et al., 2012; H.-P. Zhang et al., 2012).

Ages of the Paleocene–Quaternary succession in the Qaidam Basin, based on nonmarine fossil assemblages and magnetostratigraphy (Fig. 2.3), have been extrapolated across the basin on the basis of seismic reflectors (QBGMR, 1991; Rieser et al, 2005, 2006a). However, ages from critical sedimentary sections are often only broadly constrained due to a lack of key marker beds. This study presents sedimentologic and multi-proxy provenance results for the northern basin margin (Fig. 2.2, 2.4), complementing magnetostratigraphic, paleoclimatologic, and paleontological data from the Dahonggou and Huaitoutala anticlines (Fang et al., 2007; Wang et al., 2007; Lu and Xiong, 2009; Zhuang et al., 2011; Song et al., 2013a; 2013b). Ages used here are consistent with the regional study conducted by Zhuang et al. (2011) and published magnetostratigraphic results from the two sections examined here (Fang et al., 2007; Lu and Xiong, 2009). A 6200 m thick stratigraphic section was measured on the southern

limb of the Dahonggou anticline west of Xitieshanzhen (37.5486°N 95.1655°E). Continuous exposures include the upper Paleocene–Eocene Lulehe (~1100 m), Eocene Xiaganchaigou (~2400 m), Oligocene Shangganchaigou (~1300 m), lower Miocene Xiayoushashan (~800 m), middle-upper Miocene Shangyoushashan (~300 m), upper Miocene-Pliocene Shizigou (300 m), and overlapping Quaternary Qigequan formations (Fig. 2.3). Although the lower 3500 m of the Cenozoic succession remains poorly dated, magnetostratigraphic and sedimentologic studies of neighboring sections have constrained the age of the upper part of the section between 34 and 8 Ma, and provided documentation of general lithologic trends of upper stratigraphic levels (Lu and Xiong, 2009; Zhuang et al., 2011).

POTENTIAL SEDIMENT SOURCES

Potential sediment sources include mountain ranges surrounding the Qaidam Basin on all flanks (Fig. 2.2). Buried sedimentary and metamorphic units form the Qaidam basement, which could also have provided sediment during early basin filling. Below we highlight the characteristic crystallization ages, lithologies, and heavy mineral constituents of each of these sources.

Southern Sources

Along the southern basin margin, the Eastern Kunlun Shan east of ~92°E (Fig. 2.1, 2.2) is principally composed of Permian–Middle Triassic (260–210 Ma) plutons with isolated lower Paleozoic granitic rocks (450–380 Ma) (Fig. 5C) (Harris et al., 1998; Roger et al., 2003; Mo et al., 2007; Pullen et al., 2008; Yuan et al., 2009; McRivette, 2011; J.Y. Zhang et al., 2012) intruding late Proterozoic to Paleozoic metamorphic basement rock. Heavy minerals associated with magmatic and metamorphic basement

(pyroxene, hornblende, epidote, garnet) are expected from the Kunlun Shan. In contrast to the East Kunlun Shan, Early Paleozoic (513-420 Ma) subduction-related intrusions occupy the Qimen Tagh (Li et al., 2013). Farther south, gneissic basement rocks north of the Kunlun fault yield Paleoproterozoic ages (Zhang and Zheng, 1994). Upper Carboniferous to Lower Permian shallow-marine sedimentary and volcanic strata are unconformably overlain by Jurassic-Cenozoic nonmarine strata (Mock et al., 1999). Southeast of the Kunlun Shan is the Songpan Ganzi Basin (Fig. 2.1), a belt of Middle–Upper Triassic deep-marine clastic deposits with a broad mixture of Permian-Triassic, middle Paleozoic, and rare Precambrian detrital zircon age populations (Fig. 2.5A) from the North China block, South China block, Kunlun, and Qiangtang terranes (Weislogel et al., 2006, 2008, 2010; Enkelmann et al, 2007; Ding et al., 2013).

Directly south of the Eastern Kunlun Shan, the Hoh Xil Basin contains Cenozoic siliciclastic rocks characterized by Neoproterozoic, Paleozoic and Permian-Triassic sources (Fig. 2.5B) derived from the Lhasa and Qiangtang terranes as well as the Eastern Kunlun Shan (Dai et al., 2012; Staisch et al., 2014).

Eastern Sources

To the east, Proterozoic metamorphic basement, Paleozoic–Mesozoic sedimentary and meta-sedimentary units and Permian–Triassic granitoids are exposed in the Ela Shan and Dulan-Chaka highland (Fig. 2.2). These ranges divide the Qaidam Basin from Cenozoic intermontane basins of northeastern Tibet. Basement is composed of early Proterozoic high-grade metamorphic rocks, Paleozoic-Mesozoic sedimentary and low-grade metamorphic rocks, and extensive Permian–Triassic igneous bodies (Fig. 2.5G; Liu et al., 2004; Wu et al., 2004; Chen et al., 2012; Duvall et al., 2013).

Western Sources

The Altyn Shan to the west of Qaidam Basin include Archean–lower Paleozoic magmatic arc, accretionary prism, and related sedimentary successions. The Altyn Tagh fault (Fig. 2.1, 2.2), which bisects the Altyn Shan, is a 1600-km long left-lateral fault. Sedimentary units exposed in the Altyn Shan include Neoproterozoic quartz arenite and marbleized stromatolitic limestone (Gehrels et al., 2003a). Paleoproterozoic (1.6-2.0 Ga), Neoproterozoic (922-928 Ma), and Ordovician-Silurian (430–480 Ma), and Permian (260-280 Ma) zircon U-Pb ages are common in igneous and metamorphic basement of the Altyn Shan (Fig. 2.5F; Gehrels et al., 2003b).

Northern Sources

Finally, north of the basin, localized ultra-high pressure metamorphic complexes, magmatic arcs, and recycled sedimentary units comprise the northern Qaidam and Qilian Shan-Nan Shan region (QBGMR, 1991). These sedimentary and magmatic units are underlain by Proterozoic and Archean crystalline basement (Yin and Harrison, 2000; Gehrels et al., 2003a, 2003b). The Qilian Shan-Nan Shan (Fig. 2.1, 2.2, 2.5D) includes the North Qaidam terrane of Proterozoic gneiss overlain by Paleozoic metasedimentary rocks (QBGMR, 1991). Early Paleozoic arcs developed along the southern margin of the North China craton (Yin and Harrison, 2000; Xiao et al., 2009), including marine sedimentary rocks, ophiolites and ultra high-pressure metamorphic complexes (Menold et al., 2009; Xiao et al., 2009). Heavy mineral provinces of the southern Qilian Shan-Nan Shan can be expected to contain high volumes of epidote, hornblende, garnet, rutile, and metamorphic accessory minerals such as kyanite, andalusite and sillimanite. The Qilian Shan-Nan Shan contains isolated Permian-Triassic plutons (Chen et al., 2012). Silurian–

Ordovician strata are dominated by 450–490 Ma U-Pb ages from a local volcanic source and a minor Proterozoic component (Gehrels et al., 2011). In addition, recycling of Mesozoic and late Paleozoic sedimentary units would provide Permian–Triassic aged zircons, such as the unimodal 270–280 Ma population observed in Jurassic sandstones associated with magmatic ages in the Kunlun arc (Yan et al., 2010; Gehrels et al., 2011).

Local Basement Sources

Neoproterozoic and lower Paleozoic metamorphic rocks, flysch, and carbonates form part of the Qaidam basement beneath Mesozoic-Cenozoic basin fill (Wang and Coward, 1990; Xia et al., 2001; Chen et al., 2012). Jurassic–Cretaceous nonmarine rocks exposed on the northern Qaidam margins and in well logs (QBGMR, 1991) were sourced from early exhumation in the Qilian and Altyn Shan (Ritts and Biffi, 2001; Sobel et al., 2001; Gehrels et al., 2003b).

SEDIMENTOLOGY AND DEPOSITIONAL ENVIRONMENTS

We recognize major depositional shifts based on facies distributions of six formations (Fig. 2.6). Initial coarsening (Lulehe) was followed by fining (Xiaganchaigou), continued fining and transition from fluvial to marginal lacustrine deposits (Shangganchaigou), and final coarsening (Xiayoushashan, Shangyoushashan and Shizigou).

Lulehe Formation

Description: Fine-grained, distinctively red deposits of the lower Lulehe (0–220 m) are characterized by trough cross-stratified and horizontally bedded sandstone (Fig. 2.7A) with laminated mudstone lenses and pebble lags above sharp bases (Fig. 2.8F). Fine- to medium-grained sandstone packages contain downstream accretion surfaces and are

typically 3–7 m thick and 10–20 m wide with lenticular geometries. These fine upward into mudstone intervals up to 3 m thick which feature mottling and variable destruction of primary sedimentary structures.

The upper Lulehe (220–1100 m) contains 1–5 m thick lenticular beds of polymict, poorly sorted, clast-supported, granule-cobble conglomerate interbedded with medium- to coarse-grained, trough-cross stratified sandstone (Fig. 2.7B; Fig. 2.8A). Conglomerate beds have sharp erosional surfaces incising up to 1 m into underlying beds and a matrix of poorly sorted, calcite-cemented sandstone. These beds pinch out laterally, fine upward to coarse-grained sandstone, and include horizontally stratified, imbricated, and structureless varieties. Overlying conglomerate beds are horizontally laminated or structureless red mudstone beds 2-5 m thick (Fig. 2.8H).

Interpretation: Lower Lulehe levels represent a moderate-energy fluvial system with stable floodplains. The sharp bases, gradational upper surfaces, and low width-to-thickness ratios of the sandstones are similar to sand bodies typical of channel-fill deposits (e.g., Friend et al., 1979; Tornqvist, 1993). Structureless red mudstones are interpreted as overbank deposits with subaerial exposure and pedogenesis. Trough cross-stratified sandstone bodies, stable overbank deposits, and lack of laterally accreting bar forms are consistent with a low-sinuosity channel belt in a sandy, low- to moderate-gradient braided or anastomosing fluvial system with multiple channels, down-stream accreting barforms and vertical aggradation (Cant and Walker, 1978; Ethridge et al., 1999; Makaske, 2001). We interpret the increase in grain size and sand to mud ratio in the upper 20 m of this interval as a transition to a higher competence fluvial system.

Upper Lulehe conglomerate beds preserve channel thicknesses 1–5 m thick (Fig. 2.7B). Clast support, imbrication, poor sorting, coarse grain size, and scoured bases indicate deposition by a higher energy system (Nemec and Steel, 1984; Smith, 1990). Structureless and horizontally stratified conglomerate beds are considered components of downstream migrating compound bars (Miall, 1977). This interval is consistent with a transition to a higher-gradient gravelly braided fluvial system, although the presence of mudstone beds indicates highly variable flows.

Xiaganchaigou Formation

Description: The intermediate succession (1100–3550 m) contains finer material with few gravel clasts (Fig. 2.7C). The deposits consist of multi-story sand bodies in 5–10 m thick packages with sharp bases, commonly fining upward in the basal 50 cm, and are composed of 5–10 cm thick beds of horizontally and ripple cross-stratified, fine- to very fine-grained silty sandstone (Fig. 2.8B). The packages contain mudstone drapes and interbeds and are capped by 1–3 m thick mudstone intervals displaying blocky soil aggregates (peds), pedogenic slickensides, carbonate nodules, red and green mottling, rhizoliths, and moderate bioturbation.

Above 1250 m, interbedded sandstone and mudrock deposits dominate, featuring upward coarsening and thickening intervals of laminated mudstone and massive to horizontally stratified, laterally continuous sandstone sheets 0.5–2 m thick (Fig. 2.8C). In sharp contact with these interbedded deposits, trough cross-stratified, medium-grained sandstone packages reach 20–40 m (up to 75 m) thick (Fig. 2.8I). These thick sandstone packages persist to ~3550 m, with mudstone intervals increasing above the ~3000 m level.

Interpretation: Upward fining mudstone, cross-bedded sandstone, and interbedded paleosols represent a fine-grained fluvial system with pedogenically modified overbank settings. Trough cross-stratified sandstones indicate dune migration, with laminated mudstones resulting from low-flow isolation of dunes and mud deposition (Smith, 1990). Stability of the surrounding floodplain is suggested by ubiquitous root traces, mottling, and soil structures. Lack of distinctive soil profiles points to aggradational alluvial soils (Besly and Fielding, 1989). Thick sandstone bodies are typical of amalgamated channels in a high-sinuosity channel belt; upward coarsening and thickening mudstone and sandstone intervals represent crevasse splays. These overbank, channel margin, and in-channel deposits are considered representative of a meandering fluvial system (e.g., Nanson, 1980; Kraus, 1996).

Shangganchaigou Formation

Description: The Shangganchaigou (3550-4805 m) shows continued fining and is dominated by laminated mudstone and ripple laminated fine-grained sandstone (Fig. 2.7D). Thin beds (0.5–2 m) of mottled, nodular mudstone coarsen upward into fine-grained structureless or cross-laminated sandstone (Fig. 2.8K). These thinly bedded heterolithic deposits are commonly incised by upward fining, lenticular cross-laminated sandstone bodies. Cross-laminae are generally asymmetric, with occasional symmetrical cross-laminae (Fig. 2.8C). Rare lateral accretion surfaces in sandstone beds are less than 1 m thick.

Interpretation: Thin-bedded sandstone and laminated to structureless mudstone of this association are attributed to floodplain deposition, based on upward coarsening packages and association with channel sandstones (Porter and Gallois, 2008). Mudstone

packages capping channel sandstones indicate phases of channel abandonment. Lack of lacustrine ichnofacies, freshwater fish fauna (Wang et al., 2007), soft sediment deformation, and lacustrine carbonate or beach facies helps rule out an open lacustrine setting, though such facies are identified in the distal basin (Zhuang et al., 2011). These deposits likely represent an alluvial plain with splays into shallow ephemeral lakes, as expressed by bidirectional ripples and thick mudstone packages.

Xiayoushashan, Shangyoushashan and Shizigou Formations

Description: Upper stratigraphic levels (4805–6200 m) comprise the second major coarse-grained interval (Fig. 2.7E). Deposits are dominated by normally graded, trough cross-stratified conglomerate and medium- to very coarse-grained sandstone (Fig. 2.8E). Beds are 1–4 m thick, with sharp bases and lenticular geometries (Fig. 2.8L). At 4800–5800 m, <1 m thick beds of mottled, structureless siltstone are interbedded with fine- to very fine-grained structureless to ripple cross-laminated sandstone. The frequency and thickness of granule-pebble conglomerate beds increase upsection (4805–5787 m), with capping deposits (above 5787 m) dominated by clast-supported, planar to trough cross-stratified, imbricated conglomerate containing sandstone lenses and clasts up to 1 m in diameter.

Interpretation: Lithofacies and stratal geometries are characteristic of a sandy to gravelly braided fluvial system (Rust, 1972; Cant and Walker, 1978). Normally graded, trough cross-stratified, clast-supported conglomerates are consistent with dune migration in fluvial channels during flood and waning flow conditions (Miall, 1977). Absence of matrix-supported debris flow conglomerates and sandy sheetflood deposits preclude a proximal alluvial fan setting. Coarse grain size, cross-stratification, erosive bases and

lenticular bed geometries are representative of proximal deposition in an aggradational, low-sinuosity channel belt. The upward thickening and coarsening pattern likely indicates a progradational system in which coarse-grained transverse fluvial systems advanced into the basin.

Regional Evolution of Depositional Systems

Shifting depositional systems are evidenced by facies variations and grain-size trends in the Dahonggou section, consistent with other studies of Cenozoic strata across the basin (e.g., Bally et al., 1986; Hanson et al., 2001; Zhuang et al., 2011). Coarse intervals represent basinward progradation, potentially linked to climate change and/or deformation shifts in source regions, or reduced accommodation in proximal basin settings. Fine intervals may represent changing basin architecture in response to differential subsidence, cutoff of basin outlets and resulting internal drainage, and/or varying sediment discharge in response to changes in climate, source lithologies, and drainage divide position.

The first major shift is represented by the Eocene transition from a low-gradient fluvial system (lower Lulehe Formation) to coarse-grained braided river system (upper Lulehe). The red color, palynologic data (Miao et al., 2008), weathering indices (Chemical Index of Alteration, Plagioclase Index of Alteration, Chemical Index of Weathering, and modified Chemical Index of Weathering from Song et al., 2013b) are consistent with strong chemical weathering and linked to a warm, wet climate. Similar deposits are observed along strike to the northwest at Lake Mahai and Lulehe (Fig. 2.2; Zhuang et al., 2011), suggesting regional drainage reorganization of a braided fluvial system.

The Xiaganchaigou Formation is characterized by thick multi-story channel stacking within a lower gradient, sandy fluvial system. These deposits can be correlated with coarser meandering fluvial deposits at the Lake Mahai and Lulehe sections (Fig. 2.2; Yin et al., 2008a, b; Zhuang et al., 2011).

The Shangganchaigou Formation is composed of interbedded paleosol, channel belt, and marginal lacustrine deposits of a distal fluvial system with small lake basins (Smith et al., 2008; Hamer et al., 2007). During this phase, the depocenter was situated in the western basin (Ganchaigou and Hongshanhan sections of Zhuang et al., 2011; Fig. 2.2), where laminated mudstones and evaporites indicate profundal and hypersaline lacustrine environments (Bally et al., 1986). Adjacent to the depocenter are marginal lacustrine clastic and calcareous mudstones, including subaerial mudcracks and subaqueous algal stromatolites, ostracods, and pisoliths (Hanson et al., 2001). During endorheic periods, a central evaporative lake was likely quite shallow, resulting in significant shoreline advance and retreat.

Miocene-Pliocene deposits are clast-supported conglomerate and coarse-grained trough cross-bedded sandstones of braided fluvial systems. The interval at Dahonggou exceeds 1000 m, but thins to ~600 m at Lake Mahai (Zhuang et al., 2011). Upward coarsening and thickening of this conglomeratic succession is attributed to progradation of a proximal fluvial system, possibly a fluvial megafan (Horton and DeCelles, 2001) derived from a large hinterland catchment area in the southern Qilian Shan fold-thrust belt. This interval is coincident with a regional tectonic reorganization proposed for northeastern Tibet.

SEDIMENT PROVENANCE

A multi-proxy provenance approach (paleocurrent, sandstone petrographic, detrital zircon U-Pb geochronologic, and heavy mineral analyses) for the 6200 m-thick Dahonggou section (Fig. 2.4, 2.6) helps constrain topographic development of several ranges around the basin. To constrain lateral variability, U-Pb results are also presented for the 1400 m-thick Huaitoutala section ~100 km to the E (Fig. 2.3, 2.4), where Miocene and younger deposits (magnetostratigraphy from Fang et al., 2007) are exposed in the hanging wall of the Eastern Luliang, Xitie Shan, and Lenghu thrust system of the southern Qilian Shan-Nan Shan.

Paleocurrent Analysis

Paleocurrents from 30 localities help constrain dispersal patterns and indicate a major switch in paleoflow. At each locality, paleoflow was determined from measurements of at least 10 imbricated clasts or 15 trough limbs. Data (Fig. 2.9) show a major switch from E-directed flow for the lower Lulehe Formation (4 sites, 220-500 m, Fig. 2.6) to principally SW-directed flow for upper sites (29 sites, 1100-6200 m, Fig. 2.6). Paleocurrents at the base of the section point to an axial fluvial system flowing from the west, eliminating the northeastern region as a primary source during the early Cenozoic. In contrast, SW-directed flow for upper levels is comparable to the modern configuration, revealing transverse dispersal away from the Qilian Shan-Nan Shan since the Eocene.

Sandstone Petrography

Sixty-seven petrographic thin sections of medium-grained sandstone samples were examined, with fourteen selected for point counting using the Gazzi-Dickinson method

(Gazzi, 1966; Dickinson, 1970; 1985). These submature, moderately sorted feldspathic litharenites–litharenites (mean composition $Q_{63}Ft_{10}RF_{27}$)(Folk, 1980; Fig. 2.10) preserve unstable metamorphic rock fragments (range 3-18%, mean 11%) and heavy minerals including kyanite, sillimanite, garnet, zircon, and chlorite. Polycrystalline quartz with extensive grain-boundary migration is common. Sedimentary rock fragments are also common throughout the section (range 2-14%, mean 7%).

Petrographic data are comparable to sandstones from the same units in the western Qaidam Basin, though our samples contain a higher ratio of metamorphic to volcanic rock fragments (Rieser et al., 2005). Mesozoic sandstones from the northeastern basin are quartz- and feldspar-rich ($Qm_{62}F_{24}Lt_{14}$), with fewer rock fragments (Ritts, 1998). Compositional data indicate recycled orogenic and collisional suture/fold-thrust belt sources (Fig. 2.10, Dickinson and Suczek, 1979). Sandstone compositions show a minor increase in the abundance of lithic grains between the Shanganchaigou and Xiaganchaigou formations, followed by a return to slightly higher quartz content in the overlying Shanyoushashan Formation (Fig. 2.10). Ubiquitous and diverse rock fragments attest to the proximity and/or complex geology of the catchment, but do not allow for identification of a specific source.

Detrital Zircon Geochronology

Detrital zircon U-Pb geochronologic analyses were employed to constrain Cenozoic sediment provenance for the Qaidam Basin. Shifts in detrital U-Pb ages allow discrimination among potential source areas and may be linked to changes in deformation patterns, shifting upstream drainage configurations, or unroofing of progressively deeper rock units.

METHODS

Detrital zircon U-Pb ages were obtained for 19 sandstone samples: 11 from Dahonggou and 8 from Huaitoutala. For each sample, ~5 kg of medium-grained sandstone was collected and processed according to standard mineral separation techniques. 120 zircon grains were randomly selected from the non-magnetic heavy mineral fraction of each sample and analyzed by LA-MC-ICP-MS at the Arizona Laserchron Center at the University of Arizona. Analyses were conducted using a laser spot size of 30 μm, avoiding impurities, and using a Sri Lankan zircon standard for calibration according to Arizona Laserchron Center protocols (Gehrels et al., 2008; 2011). Errors in determining $^{206}Pb/^{238}U$, $^{206}Pb/^{204}Pb$, $^{206}Pb/^{207}Pb$ and $^{206}Pb/^{204}Pb$ result in a measurement error of ~1-2% (at 2σ level), but can be substantially larger for grains younger than 1.0 Ga due to low intensity of the ^{207}Pb signal. $^{206}Pb/^{238}U$ ages are reported for grains with $^{206}Pb/^{238}U$ ages less than 900 Ma, whereas $^{206}Pb/^{207}Pb$ ages are reported for older grains. Only ages with <20% discordance or <5% reverse discordance were considered robust enough for interpretation. Analytical results (Table DR1) consist of 1999 analyses for 19 samples and are presented as age histograms and kernel density estimates (Fig. 2.11A) using the DensityPlotter routine outlined by Vermeesch (2012).

RESULTS

U-Pb results help constrain Cenozoic sediment provenance. Major populations in the Qaidam Basin samples include: (1) Permian-Triassic (299–200 Ma), (2) Late Cambrian to Early Devonian (500–400 Ma) and (3) Paleoproterozoic (2.5–1.6 Ga).

At the base of the section, two lower Lulehe samples (1DH0 and 2DH0) display a bimodal distribution, with peaks at 250 Ma and 436 Ma, and rare Proterozoic grains. Upsection, two upper Lulehe Formation samples (2DH224 and 220611-01) yield a unimodal early Paleozoic peak of ~440 Ma, a departure from samples below (2DH0) and above (2DH1184). Though rare, there is a significant increase in Proterozoic zircons in upper Lulehe samples (2DH224 and 220611-01). Three Xiaganchaigou Formation samples (2DH1184, 2DH1770, 2DH3040) show diverse zircon age spectra with peaks corresponding to the three aforementioned age populations, including the initial appearance of Late Triassic crystallization ages. Contrasting detrital zircon age spectra are revealed for two Shangganchaigou Formation samples (2DH3774, 2DH4580). Minor Precambrian peaks are present in both samples, though their frequency increases significantly at 2DH4580, continuing to the top of the section. The remaining 10 samples from the Dahonggou and Huaitoutala sections, from the Xiayoushashan, Shangyoushashan and Shizigou Formations (from Dahonggou: 2DH5484, 2DH6126; from Huaitoutala: 1QUA1, 2QUA144, 2QUA416, 160611-01, 160611-03, 160611-02, 160611-01, 190611-01), contain all three major age populations.

The D-value of the Kolmogorov-Smirnov test (K-S test) was used to compare detrital zircon U-Pb age cumulative distribution functions, and to determine the probability that samples are derived from the same parent population. The K-S test D-value is calculated as the maximum absolute difference between two samples' empirical cumulative distribution function and is a measure of the dissimilarity between two samples. Multi-dimensional scaling (MDS) was then used to create a spatial visualization or "map" (Fig. 2.11B) of the dissimilarity measure (Vermeesch, 2013). Three groups of similarly

sourced samples are identified using this metric: (1) 1DH0 and 2DH0, both displaying a zircon assemblage consisting of both **early Paleozoic and Permian-Triassic** ages, (2) 2DH224, 220611-01, and 2DH3774, which are dominated by a single **early Paleozoic** population, and (3) the remaining samples, which contain a **cosmopolitan** assemblage of all major detrital zircon populations (Fig. 2.11B).

Heavy Mineral Analysis

Further discrimination of sources was obtained through heavy mineral (density > 2.89 g/cm^3) analyses for sandstones from the Dahonggou section. Heavy minerals generally constitute a minor volume, but are a useful tracer of source evolution in orogenic belts and stratigraphic shifts in provenance (Mange and Maurer, 1992). Distinct petrologic characteristics of the Qilian Shan-Nan Shan and Kunlun Shan make heavy mineral analysis an important tool for understanding Qaidam Basin provenance.

METHODS

Ten heavy mineral fractions were separated from the same Dahonggou samples used for detrital zircon geochronology and analyzed using automated scanning electron microscopy (QEMSCAN) at the Colorado School of Mines. Four energy dispersive X-ray (EDX) spectrometers acquired spectra from each particle with a beam stepping interval of 15μm, an accelerating voltage of 25 keV, and a beam current of 5 nA and analyzed using the control program (iDiscover, FEI). BSE values and EDX spectra were compared with previously determined values and spectra for a representative catalog of diverse mineral phases, facilitating a compositional assignment for each acquisition point and generation of a compositional map for each mount. This approach reflects the instrument design,

which is optimized for rapid mineral identification rather than detailed intragranular compositional analysis (for which other techniques are more appropriate).

RESULTS

Results of QEMSCAN heavy mineral analyses reveal three groups with distinct assemblages (Fig. 2.12). In order to compare heavy mineral assemblages, index ratios ZTR (zircon-rutile-tourmaline) (Hubert, 1962), ATi (apatite-tourmaline index), RZi (rutile-zircon index) and MZi (monazite-zircon index) (Morton and Hallsworth, 1994) were used, comparing minerals of similar weathering and diagenetic stability, and hydraulic behavior. In addition, volume percent of each heavy mineral species was calculated for each sample.

Lulehe samples (1DH0, 2DH0 and 2DH224) contain a high volume percent of epidote (average 23.29) with increasing hornblende (average 18.95, increasing from 14.68 to 26.70) and tourmaline (average 0.12, increasing from 0.06 to 0.12). The highest GZi index (98.07) and lowest ATi index (80.93) are in this group. Whereas alumino-silicate metamorphic accessory minerals andalusite, kyanite and sillimanite are absent from this sample, these minerals are susceptible to dissolution and/or replacement due to both metamorphic and sedimentary processes. The association of epidote and hornblende, low volume percent of sphene (average 3.29), orthopyroxene (average 0.02) and monazite (average 0.02), and high GZi/ATi ratio (82.5), suggests a source terrane dominated by greenschist-facies metamorphic rocks.

Xiaganchaigou samples (2DH1184, 2DH1770 and 2DH3040) show a significant departure from Lulehe heavy mineral assemblages. There is a switch to low epidote (average 7.78) and hornblende (average 4.93), decreasing tourmaline (average 0.15,

decreasing from 0.20 to 0.12) as well as high volumes of apatite (average 9.37), TiO_2 polymorphs (average 30.95), siderite (average 25.67), zircon (average 6.75), monazite (average 0.07) and sphene (average 6.54). This interval has the highest mean ZTR index (37.36), and lowest mean GZi (55.46), RZi (82.39) and MZi (1.20) indices. Zircon, apatite, and sphene are all associated with igneous rocks, and the decrease in epidote and hornblende suggests either dilution or increasing removal of the low-grade metamorphic source. High ZTR indices characteristic of these samples is associated with enhanced recycling (Hubert, 1962).

Upper Xiaganchaigou and lower Shangganchaigou samples (2DH3040 and 2DH3774) has the highest volumes of hornblende (average 25.40), epidote (average 26.38), clinopyroxene (average 0.65), orthopyroxene (average 0.21) sphene (average 6.71) and andalusite/kyanite/sillimanite (average 0.02), yet lowest volumes of apatite (average 0.03), TiO2 polymorphs (average 14.90) and tourmaline (average 0.03). The lowest ZTR index (16.69) and highest ATi, RZi and MZi are in this zone. High abundance of metamorphic minerals (hornblende, epidote, pyroxene, andalusite/kyanite/sillimanite), low abundance of typically magmatic minerals (apatite, tourmaline), and high indices correspond to a shift from igneous (2DH1184, 2DH1770 and 2DH3040) to low–high grade metamorphic sources (2DH3774, 2DH4580, 2DH5484 and 2DH6126).

Provenance Interpretations

We identify four shifts in sediment provenance based on major changes in paleocurrent orientation, heavy mineral compositions, and detrital zircon age spectra. Consistent with previous research, changes in sandstone framework grain composition at

Dahonggou are minor and provide secondary constrains on provenance reconstructions (Rieser et al., 2005). The first shift involves a change from an early Paleozoic and Permian-Triassic zircon U-Pb assemblage to a largely unimodal early Paleozoic assemblage (Fig. 2.11A and B) above 220 m in the Lulehe Formation. The second shift occurs between 770 m and 1100 m in the Lulehe Formation and is characterized by a change in all three major proxies. At 770 m, paleoflow changes from eastward to southwest directed flow (Fig. 2.6). At ~1100 m there is a shift in U-Pb age spectra from an early Paleozoic assemblage to a cosmopolitan assemblage (Fig. 2.11A and B), and the heavy mineral assemblage shifts towards higher ZTR and lower GZi indices (Fig. 2.12). This shift is also accompanied by a minor increase in abundance of lithic grains in sandstone (Fig. 2.10). Between 3040 m and 3774 m there is a return to a single early Paleozoic-dominated zircon U-Pb age spectra coupled with a decrease in ZTR and GZi indices in the upper Xiaganchaigou–lower Shangganchaigou formations. There is also a return to less compositionally mature sandstones. Finally, the cosmopolitan zircon U-Pb age assemblage reemerges between 4580 m and 5484 m (uppermost Shangganchaigou Formation–lower Xiayoushashan Formation) in the Dahonggou section and synchronously dominates all samples in the Huaitoutala section (Fig. 2.11A).

E-directed paleocurrent orientations in the lower Lulehe Formation indicate sediment sources to the south or west of the Dahonggou location. Potential sources include (1) the Hoh Xil Basin, (2) Altyn Shan, (3), Western Kunlun Shan, and (4) Eastern Kunlun Shan.

(1) Detrital zircon age spectra (1DH0 and 2DH0) lack the large Neoproterozoic, Paleoproterozoic, and Cretaceous populations of contemporaneous Lhasa-Qiangtang-derived deposits in the Hoh Xil Basin to the south (Fig. 2.5; Dai et al., 2012; Staisch et

al., 2014), suggesting Paleogene appearance of a Kunlun Shan topographic barrier between the Qaidam and Hoh Xil basins.

(2) Initial displacement on the Altyn Tagh Fault and uplift of the Altyn Shan is usually ascribed to Oligocene-early Miocene time, with possible Mesozoic–early Cenozoic precursor faulting (Jolivet et al., 2001; Sobel et al., 2001; Yin et al., 2002, 2007a; Cowgill et al., 2004; Darby et al., 2005; Wang et al., 2005; Ritts et al., 2008). Because the Altyn Shan contains a major 1800–2000 Ma source (Yue et al., 2005; Gehrels et al., 2003a, 2003b) that is not observed in lower Lulehe results, it is eliminated as a possible source.

(3) On the basis of basin architecture and apatite fission track data, Wang et al. (2006) interpret a ~2000 km "paleo-Kunlun River" sourced in the Western Kunlun Shan to northeastern Pamir, following the incipient Altyn Tagh and Karakash faults. The expected provenance signature, however, would include early Paleozoic and Cretaceous zircons but would be dominated by Permian–Late Triassic ages (Fig. 2.5E, Cowgill et al., 2003; Zhang et al., 2007; Robinson et al., 2012; Carrapa et al., 2014). This association of ages is inconsistent with basal Lulehe results, which are dominated by early Paleozoic-aged zircons and include no Cretaceous ages (Fig. 2.11). However, exclusion of the Cretaceous-aged population would make the Western Kunlun Shan a viable secondary sediment source.

(4) Permian–Triassic and early Paleozoic age signatures from the lower Lulehe Formation (1DH0 and 2DH0) are compatible with the Kunlun arc terrane of the Eastern Kunlun Shan (west of Golmud) and southern Altyn Shan (Cowgill et al., 2003) and Triassic sedimentary units of the Kunlun Shan (Ding et al., 2013), and incompatible with

Late Triassic plutons of the easternmost Eastern Kunlun Shan (Mo et al., 2007). The high abundance of epidote, hornblende, tourmaline, and garnet is consistent with a metamorphic basement source. Whereas low temperature thermochronologic results from the easternmost Eastern Kunlun Shan support Oligocene-Miocene cooling (Mock et al., 1999; Jolivet et al., 2003; Yuan et al., 2006), this exhumation may be related to S-directed backthrusting following earlier Paleocene–Eocene N-directed thrusting in the Eastern Kunlun Shan (e.g., Yin et al., 2007a). Therefore, the westernmost Eastern Kunlun Shan is favored as the principal sediment source.

The switch to an early Paleozoic detrital zircon signature above 220 m occurs in the absence of a change in paleocurrent orientation, suggesting consistent derivation from the southern Qaidam Basin margin. The unimodal early Paleozoic zircon U-Pb age spectra is consistent with a westward shift in active exhumation to the northwestern Qimen Tagh region of the Eastern Kunlun Shan, adjacent to the Altyn Shan (Li et al., 2013) feeding the E-directed axial fluvial system.

There is a clear switch from variable axial paleocurrents of the lower–middle Lulehe Formation to SW-directed, transverse paleocurrents at 770 m in the uppermost Lulehe and Xiaganchaigou formations (Fig. 2.6). At the Dahonggou section this interval is characterized by a cosmopolitan detrital zircon signature with Permian-Triassic, early Paleozoic, and Proterozoic age peaks. Samples from the Xiaganchaigou Formation (2DH1184, 2DH1770, 2DH3040) include Paleozoic and Paleoproterozoic grains matching the Qilian Shan-Nan Shan basement (Fig. 2.5; Cowgill et al., 2003; Gehrels et al., 2003a, 2003b; Menold, 2006; Yan et al., 2010). The origin of Permian–Triassic grains is more complex, as such plutons are less common in the Qilian Shan-Nan Shan than the

Eastern Kunlun Shan. Given SW-directed paleocurrents and high ZTR heavy mineral index, the Permian–Triassic peak is attributed to grains recycled from Jurassic deposits, situated to the north in the Qilian Shan–Nan Shan, but originally shed from the Permian-Triassic Kunlun arc (Fig. 2.5). The heavy mineral assemblage represents dominantly igneous and recycled sedimentary sources, consistent with populations in the Qilian Shan-Nan Shan, where a well-established catchment eroded diverse source rocks. Absence of a significant metamorphic component, common in the North Qaidam terrane, suggests that high topography was confined to the northern Qilian Shan during Xiaganchaigou deposition.

A pronounced 400–500 Ma detrital zircon age peak and corresponding reduction or disappearance of other age peaks in the two Shangganchaigou Formation samples (2DH3774, 2DH4580) could be explained by several mechanisms. First, units containing recycled Permian-Triassic and Paleoproterozoic grains may have been preferentially eroded away, leaving only lower Paleozoic rocks. Second, new drainage networks may have contained local Paleozoic sources, before drainage expansion and elaboration provided more diverse populations. Neither option, however, is likely to have completely removed two source populations while maintaining early Paleozoic sources. A third explanation involves in-sequence deformation and growth of a topographic barrier along the Nan Shan-North Qaidam thrust belt (NQF in Fig. 2.1). At the same level, the increase in epidote and hornblende abundance and switch to high GZi and RZi heavy mineral indices requires deeper unroofing and/or exposures of metamorphic rocks. Paleoflow was to the southwest, consistent with a north/northeast source in the Qilian Shan. Possible sources include ophiolitic and ultra-high pressure metamorphic assemblages in the Nan

Shan-North Qaidam thrust belt along the Luliang and Xitieshan thrusts (Yin et al., 2008a), or possibly farther north in the Qilian Shan-Nan Shan.

Detrital zircon ages for the uppermost Xiayoushashan–Shizigou formations at both sections contain three major populations, including the early Paleozoic and reintroduction of Permian-Triassic and Proterozoic populations (Fig. 2.11). Metamorphic minerals continue to dominate heavy mineral assemblages. Lithofacies, sedimentation rates, and provenance shifts indicate continued in-sequence advance of the Luliang-Xitieshan thrust system along the southern front of the Qilian Shan-Nan Shan. Age populations can be traced to the southern Qilian Shan-Nan Shan: erosional unroofing of Paleoproterozoic basement, lower Paleozoic magmatic rocks, isolated Permian-Triassic plutons related to the Kunlun arc, as well as Mesozoic sedimentary units, collectively resulting in well-mixed detrital zircon age spectra.

DISCUSSION

BASIN RECONSTRUCTION

Sedimentologic, provenance, and geochronologic data support a reconstruction of Qaidam Basin evolution (Fig. 2.13) involving multiple source regions and variations in drainage patterns dictated by shifts in the tectonic development of flanking mountain ranges. Results presented here document the Cenozoic depositional record in the northeastern Qaidam Basin, and its relation to the broader northern Tibetan plateau. For this reconstruction, the chronology of the Dahonggou section is roughly correlated to nearby magnetostratigraphic sections (e.g., Lu and Xiong, 2009; Ke et al., 2013).

Lulehe Formation (Paleocene)

The composition and sediment dispersal pathways of Paleocene Lulehe Formation sediments are consistent with derivation from the westernmost Eastern Kunlun Shan (Fig. 2.2). This observation suggests that the Eastern Kunlun Shan had developed into a topographic edifice, largely or totally blocking drainage from the south (Fig. 2.13A). The drainage divide would have shed Permian–Triassic and early Paleozoic detritus to both the Qaidam and Hoh Xil basins, and blocked the majority of Neoproterozoic detritus from the Qiangtang and other southern terranes (Fig. 2.5). Detrital zircon U-Pb data and carbonate rock fragments in the Lulehe Formation in western Qaidam confirm early exhumation of the Eastern Kunlun Shan (Cheng et al., 2015). Finally, E- and NE-directed paleocurrent orientations at the Dahonggou location on the northern margin of the Qaidam Basin also strongly suggest that the Qilian Shan was not a significant topographic barrier in the Paleocene.

Lulehe Formation (Paleocene–Eocene transition)

The increased fluvial competence indicated by the upward coarsening trend may be attributed to increased precipitation and run-off or to enlargement of the catchment (Fig. 2.13B). However, the shift to a unimodal early Paleozoic detrital zircon peak in samples 2DH224 and 220611-01 (Fig. 2.11) is inconsistent with enlargement of the fluvial catchment. Oxygen isotopic values from sedimentary cements and paleosol carbonates from around the Qaidam Basin decrease from the lower to upper Lulehe Formation (Kent-Corson et al., 2009), consistent with enhanced precipitation in the late Paleocene–early Eocene. Low ZTR indices through this interval (Fig. 2.12), despite enhanced weathering in the warm Paleocene–Eocene climate, suggest rapid denudation and sediment transport to the Dahonggou site consistent with the increased grain size and

bedload proportions. Continued E-oriented paleoflow during this interval suggests quiescence in the Qilian Shan, continued sourcing of sediment from the SW–W basin margin, and a Qaidam Basin that remained open during this time interval.

Uppermost Lulehe–Xiaganhaigou formations (early–late Eocene)

Evidence for Eocene shortening in the Qilian Shan-Nan Shan (Fig. 2.13C and 2.13D) is revealed in the Dahonggou section by shifts in lithofacies and sediment dispersal. Results indicate Eocene establishment of the northern basin margin along the southern Qilian Shan-Nan Shan north of Daqaidam (Fig. 2.1), with the transition to the cosmopolitan zircon assemblage at sample DH1184. Provenance data presented here are complementary to the stratigraphic synthesis of Zhuang et al. (2011), in which they recognize Eocene accumulation of coarse sediment along the southern front of the Qilian Shan and Nan Shan-North Qaidam fold-thrust belt.

Shangganchaigou Formation (Oligocene)

The transition to a dominant early Paleozoic peak during the Oligocene-early Miocene with continued SW-directed paleoflow of a meandering fluvial system requires the southward advance of the Nan Shan-North Qaidam thrust belt within the Qilian Shan (Fig. 2.13E). This predicts isolation from earlier sources and a huge early Paleozoic signal from plutons along the Qilian Shan-Nan Shan thrust front. Consistent with this interpretation is the drastic shift in heavy minerals, from a recycled sedimentary to metamorphic source. The Nan Shan-North Qaidam thrust belt contains a early Paleozoic suture zone (Mattinson et al., 2007; Xiao et al., 2009) that underwent high and ultra-high pressure metamorphism, exposed along the Luliang and Xitie Shan faults (Fig. 2.4; Yang et al., 2001; Yin et al., 2008a; Menold et al., 2009).

The Qaidam Basin was fully closed at this stage, with organic-rich lacustrine deposits accumulating in the basin center (Hanson et al., 2001). At the Dahonggou site, marginal lacustrine deposits are interbedded with paleosols and meandering fluvial systems throughout this interval, as the depocenter shifted to the southeast due to flexural loading by the Nan Shan-North Qaidam thrust belt (Yin et al., 2008a, 2008b).

Xiayoushashan, Shangyoushan, and Shizigou formations (Miocene–Pliocene)

During Miocene deposition of the Xiayoushashan and Shangyoushashan formations, the Qaidam depocenter shifted eastward (Wang et al., 2006), the deposits begin coarsening upward at the 4800 m level in the Dahonggou section, and sedimentation initiated at the Huaitoutala section (Fang et al., 2007) in a piggyback hanging-wall setting on the S-directed Luliang and Xitieshan thrust system (Fig. 2.13F).

Growth strata, regional unconformities, and shifts in depositional systems and accumulation rates support a deformation phase commencing at 12-8 Ma and accelerating after ~3.6 Ma (Clark et al., 2010; Zheng et al., 2010; Lease et al., 2011; Yuan et al., 2014). This reorganization includes diminished slip along the Altyn Tagh fault and deformation migration in the southern Qilian Shan-Nan Shan to the south and east with the development of the Eastern Luliang, Xitie Shan, and Lenghu thrusts (Yue et al., 2005; Yin et al., 2008a). In the northwestern Qaidam Basin, a shift from magmatic to metamorphic sources (Jian et al., 2013) is attributed to unroofing of the Nan Shan-North Qaidam and South Qilian Shan belts. At the Dahonggou section, diverse detrital zircon and heavy mineral assemblages imply drainage integration and source unroofing, producing diverse grains from Paleoproterozoic basement, lower Paleozoic magmatic

rocks, and Permian-Triassic grains from recycled sedimentary, igneous and metamorphic sources.

Miocene and younger deposits preserve >2000 m of coarse-grained fill, with an upward coarsening and thickening pattern reflecting progradation of large distributive fluvial lobes from range front outlets. This succession is suggestive of the large area (>1000 km^2), low slope, and water-lain facies of fluvial megafans (Gupta, 1997; Horton and DeCelles, 2001; Hartley et al., 2010). During middle Miocene reorganization of deformation, a basin-wide grain-size increase and initiation of deposition in the Delingha depression (sub-basin containing the Huaitoutala section) represent significant topographic growth in surrounding ranges.

Modern drainage configuration and source areas were established during late Miocene–Pliocene deposition of the Shangyoushashan and Shizigou formations (Pullen et al., 2011). Coarse-grained sediment accumulation and growth strata formation continue to characterize the modern margins and interior of the Qaidam Basin (Wang and Coward, 1990).

Regional Implications

Basin isolation

The pattern of basin isolation for the Qaidam region (Fig. 2.13) is consistent with models for plateau expansion involving structural incorporation and partitioning of once-giant peripheral basins (Métivier et al., 1998; Meyer et al., 1998; Tapponnier et al., 2001; Horton et al., 2004; Carroll et al., 2010; Craddock et al., 2011b; Horton, 2012). In this model, growth of new basin-bounding ranges form critical topographic barriers to surface flow and atmospheric circulation, promoting sediment ponding and arid rain-shadow

conditions within the basin (Sobel et al., 2003; Strecker et al., 2007). Following surface uplift, basin-margin topographic barriers and associated arid conditions inhibit erosional evacuation. Progressive partitioning of large intraplate basins is supported by studies suggesting a shared Mesozoic history for the northwestern Qaidam Basin and the southeastern Tarim Basin (Ritts and Biffi, 2000, 2001; Meng and Feng, 2008; Craddock et al., 2011a; Johnson and Ritts, 2012). Tectonic subsidence waned in the Early Cretaceous and was followed by regional burial (Jolivet et al., 2001) and potential formation of a giant peripheral basin on the northern margin of the Tibetan Plateau. The sedimentary record presented here indicates that the early Cenozoic Kunlun Shan largely isolated the Hoh Xil and Qaidam basins by the Paleocene and would have constituted the southern margin of a formerly unified Qaidam-Tarim Basin (Ritts and Biffi, 2000, Fig. 2.13A and 2.13B).

Partitioning of this giant basin and progressive isolation of the Qaidam Basin from the Tarim Basin (to the WNW) and the Hexi Corridor (to the NE) began in the Paleogene. Paleocene to early Eocene isolation from the Hexi Corridor is documented by the provenance shift and SW-directed paleoflow documented in the uppermost Lulehe Formation, and displacement along thrusts bounding the NE margin of the Qaidam Basin (Fig. 2.13C, Yin et al., 2008a). Late Eocene–early Oligocene isolation from the Tarim Basin via movement on the Altyn Tagh fault is documented by thermochronology, and basin paleogeography for the NW Qaidam region (e.g., Yue et al., 2003, 2005; Wang et al., 2005; Meng and Feng, 2008; Ritts et al., 2008). By the middle Oligocene, the Qaidam Basin was tectonically isolated from basins to the north and west. SW-directed paleoflow at Dahonggou and endorheic lacustrine deposition in western Qaidam Basin

(Hanson et al., 2001) indicate that by the Oligocene, the Qaidam Basin was also hydrologically closed. Southward encroachment of Qilian Shan fold-thrust deformation into the Qaidam Basin focused sedimentation in transverse fluvial systems along basin margins (Fig. 2.13C–E). Connections to basins of the northeastern Tibetan Plateau are less clear. Increased exhumation is not documented in the Dulan-Chaka highland E of Qaidam Basin until the early Miocene (Duvall et al., 2013), raising the possibility that the Qaidam Basin remained tectonically integrated with regions to the east until at least the early Miocene.

The early Eocene onset of basin isolation is consistent with previous research suggesting that strain from Indo-Asian collision was transmitted rapidly to the northern edge of the modern Tibetan Plateau (e.g., Horton et al., 2004; Dupont-Nivet et al., 2004; Yin et al., 2008a; Clark et al., 2010). This may have been facilitated by high topography in the southern Tibetan Plateau (Ding et al., 2014), strong lithospheric blocks underlying the Qaidam-Tarim Basin (Braitenberg et al., 2003), and pre-existing zones of weakened lithosphere in basin-bounding mountain ranges due to pre-Cenozoic deformation (Ritts and Biffi, 2001; Wang et al., 2005; Johnson and Ritts, 2012). Oxygen isotopic data from basins in the vicinity of Qaidam Basin indicate topographic growth from Eocene to Oligocene, coincident with the timing of basin isolation (Graham et al., 2005; Kent-Corson et al., 2009). Surface uplift of Qaidam Basin and its bounding ranges may have stopped or slowed due to a potential early–middle Miocene shift from largely N-S shortening to a deformation regime dominated by eastward translation of crustal blocks along continental-scale strike-slip faults (Zhang et al., 2004; Gan et al., 2007; Duvall and Clark, 2010; Zheng et al., 2010; Lease et al., 2011; Yuan et al., 2013).

Factors favoring development of giant basins

The Qaidam Basin contrasts with basins in the southern Tibetan Plateau, as well as the mosaic of basins to its east in the northeastern Tibetan Plateau. Middle Miocene–Quaternary basins in the southern and central Tibetan Plateau are commonly related to extension or strike-slip faulting (e.g., Garzione et al., 2003; Spurlin et al., 2005; Kapp et al., 2008; Saylor et al., 2010; Sanchez et al., 2010; Horton, 2012; Taylor et al., 2012; Woodruff et al., 2013). Older basins in central Tibet such as Lunpola, Nima, Linzhou, and Hoh Xil (Fig. 2.1) formed in response to, or coeval with, shortening, and often contain only an early Cenozoic record of sedimentation after which they were exhumed during ongoing deformation (Xu, 1984; Leeder et al., 1988; Harrison et al., 1992; Liu and Wang, 2001; Liu et al., 2001; Horton et al., 2002; DeCelles et al., 2007; He et al., 2007; Kapp et al., 2007). However, the southern and central Tibetan basins are considerably smaller, thinner, and have shorter lifespans than the Qaidam Basin. Similarly, a mosaic of subbasins in the northeastern Tibetan Plateau have thinner stratigraphic sequences and discontinuous sedimentation reflecting late Eocene to late Miocene segregation events (Horton et al., 2004; Dupont-Nivet et al., 2008; Lease et al., 2011), and ultimately drainage integration and evacuation in the Pleistocene (Li et al., 1997; Fang et al., 2005; Craddock et al., 2010; Nie et al., 2015).

The Qaidam region shares elements with other large basins on the periphery of the Tibetan Plateau including the Tarim, Sichuan, and Hexi Corridor regions (Fig. 2.1) but also differs from them in several fundamental ways. The Qaidam and Tarim basins preserve the thickest and most complete Cenozoic sedimentary sequence of any of these

basins with up to 15 km of Cenozoic sediment accumulation. In the Hexi Corridor, 2.5–5 km of sediment accumulated in a restricted broken foreland basin above the basal Cretaceous-Oligocene unconformity (Bovet et al., 2009, and references therein). The Sichuan Basin contains thick sequences of Mesozoic strata, but only a thin (< 1 km) veneer of Cenozoic deposits (e.g., Guo et al., 1996; Meng et al., 2005).

High-elevation basins of the southern and central Tibetan Plateau and those on the periphery are also distinguished by the strength of their crustal basement relative to that of the surrounding mountain ranges, and development of syndepositional structural dams suggesting that these factors may control their evolution and accumulation histories. Low effective elastic thicknesses (typically <20 km) of basement underlying basins in the southern and central Tibetan Plateau (Masek et al., 1994; Braitenberg et al., 2003; Jordan and Watts, 2005), and a weak layer in the middle crust–upper mantle (Jin et al., 1994; Owens and Zandt, 1997; Klemperer, 2006) allow limited evolution of overlying basins before basins are disrupted and recycled (e.g., Kapp et al., 2008). The northeastern Tibetan region is characterized by lithosphere with moderately higher but laterally heterogeneous effective elastic thickness (Braitenberg et al., 2003; Jordan and Watts, 2005; Li et al., 2013) resulting in strain focusing in zones of weakness, disruption of once-contiguous basins during ongoing deformation, and development of the mosaic of basins. The Hexi Corridor is characterized by ~20–30 km effective elastic thicknesses, but is separated from the Qaidam Basin to the south by a low (<10 km) effective elastic thickness zone in the Qilian Shan-Nan Shan.

The Qaidam, Tarim and Sichuan basins are characterized by large regions with high effective elastic thicknesses, and high basement seismic velocities extending through the

lithosphere (Braitenberg et al., 2003; Jordan and Watts, 2005; Liang and Song, 2006; Li et al., 2008A, 2008b; Li et al., 2012; Yang et al., 2012). Whereas the Tarim and Qaidam basins developed thick Cenozoic sedimentary sequences by ponding due to Cenozoic deformation focused on the basin margins, no similar syndepositional structural dam developed in the Sichuan Basin resulting in widespread erosion of basin strata (Richardson et al. 2008). The onset of isolation and uplift of the Qaidam Basin relative to the Tarim Basin may be due either to injection of Tibetan lower crust beneath the Qaidam Basin (Yin et al., 2007a; Karplus et al., 2011) or structural transformation of Qaidam Basin into a crustal-scale piggyback basin (Yin et al., 2007a; Horton, 2012).

Effect of climate on basin filling and evacuation

Finally, late Eocene–early Oligocene isolation of the Qaidam Basin predates a regional increase in aridity starting in the early–middle Miocene (Kent-Corson et al., 2009; Miao et al., 2011). Endorheic conditions in Qaidam Basin also predate the increase in aridity and persist through the modern. This sequence of events points to early defeat of range-traversing rivers by tectonic uplift and development of rain-shadow related aridity within an isolated Qaidam Basin prior to Miocene regional aridification. On the other hand, Cenozoic strata in the multiple subbasins of northeastern Tibet point to periods of both sediment accumulation and large-scale evacuation of basin fill following regional aridification (e.g., Fang et al., 2003; Craddock et al., 2010, 2011b; Hough et al, 2011, 2014). As in the Qaidam Basin, local rain-shadow aridity is superimposed on the regional signal of aridification (Hough et al., 2014). However, excavation of the subbasins following regional aridification indicates that despite increased regional aridity

in the late Cenozoic, rivers maintained sufficient stream power to overcome structurally produced topographic barriers and effectively evacuate sediments that ponded upstream of those topographic barriers. The decoupling of regional climate changes and sediment accumulation or evacuation implies that regional climate change was not the primary factor in either the development or destruction of giant plateau-margin basins.

CONCLUSIONS

Constraints on the evolution of the Qaidam Basin provide insights into the Cenozoic deformation history of the northern Tibetan Plateau, which broadly includes Paleocene-Eocene exhumation of the Kunlun Shan followed by activation then outward growth of the Qilian Shan-Nan Shan. Supporting evidence consists of distinctive patterns and temporal shifts in depositional systems, detrital provenance, and sediment dispersal in the northeastern Qaidam Basin.

(1) Initial Cenozoic sedimentation in the northeastern Qaidam Basin involved eastward transport of sediment likely derived from the westernmost Eastern Kunlun Shan. Paleocene deposits (lower Lulehe Formation) contain major Permian-Triassic and early Paleozoic detrital zircon populations, with a heavy mineral assemblage of principally metamorphic origin, consistent with the Paleozoic basement, Permian-Triassic magmatic arc, and older metamorphic signatures along the Kunlun suture. These U-Pb detrital zircon ages support the existence of a drainage divide between the Qaidam Basin and the Hoh Xil Basin, preventing large volumes of Neoproterozoic grains of the Qiangtang terrane from reaching the Qaidam Basin. In the upper Lulehe Formation a shift from sandstone- to conglomerate-dominated facies and transition to early Paleozoic U-Pb detrital zircon ages indicates continued exhumation of the Eastern Kunlun Shan.

(2) The late Paleocene–Eocene shift is followed by an early Eocene switch to SW-directed paleoflow, igneous and recycled sedimentary heavy mineral assemblage, and diverse Permian-Triassic, early Paleozoic, and Proterozoic detrital zircon populations. This provenance analysis is consistent with the onset of extensive exhumation in the Qilian Shan-Nan Shan.

(3) In-sequence advance of the Qilian Shan-Nan Shan fold-thrust belt occurred during the Oligocene-early Miocene, with exhumation of metamorphic and ophiolitic complexes along the frontal Eastern Luliang, Xitie Shan, and Lenghu thrust faults and initial sedimentation at the Huaitoutala section located in the hanging wall of this frontal thrust belt. The Oligocene Shangganchaigou Formation preserves a significant provenance shift at the Dahonggou section, to a metamorphic heavy mineral assemblage and a unimodal early Paleozoic detrital zircon U-Pb peak.

(4) Since the middle Miocene, exhumation of the Qilian Shan-Nan Shan is recognizable in the detrital record preserved within the Qaidam Basin. Provenance data from both the Dahonggou and Huaitoutala sections show unroofing of Permian-Triassic, lower Paleozoic and Paleoproterozoic sources, with metamorphic heavy mineral assemblages, in the Qilian Shan-Nan Shan through the Xiayoushashan and Shangyoushashan Formations, continuing through the Pliocene Shizigou Formation.

(5) During the Paleogene the Qaidam Basin was sequentially isolated from the south, the west, and finally the north, becoming hydrologically closed by the Oligocene. The basin was eventually uplifted as a part of the Tibetan plateau and further isolated from the basins of the northeastern Tibetan plateau. This pattern of basin isolation and subsequent

uplift demonstrates the critical role of basin formation and filling as a component in the growth of the Tibetan plateau.

(6) This research joins a growing number of studies demonstrating the utility of an integrated approach to sediment provenance and quantitative comparison of detrital geochronology data. This is particularly true in regions where multiple sources have similar lithologies, compositions, or thermal histories or where recycling extensively masks provenance signals.

ACKNOWLEDGMENTS

This research was supported by the University of Texas at Austin Jackson School of the Geosciences Ronald K. DeFord Field Scholarship, American Association of Petroleum Geologists L. Austin Weeks Memorial Grant, Geological Society of America Graduate Student Grant, and International Association of Sedimentologists Post-Graduate Grant Scheme awarded to Bush, and a subaward to Saylor and Horton from NSF EAR-0958704 (awarded to Xiaoming Wang). Fieldwork was facilitated by awards to Nie from the National Basic Research Program of China (Grant 2013CB956400) and National Natural Science Foundation of China (Grant 41422204) and logistical assistance from Yunfa Miao, Kuang He, Wenbin Peng, and Shunchuan Ji of Lanzhou University. We thank the staff at the Arizona Laserchron Center (NSF-EAR 1032156) and Katharina Pfaff at the Colorado School of Mines QEMSCAN facility for laboratory assistance. The manuscript was improved by careful reviews by William Craddock, an anonymous reviewer, and editor Arlo Weil.

REFERENCES

Bally, A.W., Chou, I.-M., Clayton, R., Eugster, H.P., Kidwell, S., Meckel, L.D., Ryder, R.T., Watts, A.B., and Wilson, A.A., 1986, Notes on sedimentary basins in China--report of the American Sedimentary Basins Delegation to the People's Republic of China: Open–File Report 86, 327 p.

Bershaw, J., Garzione, C. N., Schoenbohm, L., Gehrels, G., and Tao, L., 2012, Cenozoic evolution of the Pamir plateau based on stratigraphy, zircon provenance, and stable isotopes of foreland basin sediments at Oytag (Wuyitake) in the Tarim Basin (west China): Journal of Asian Earth Sciences, v. 44, p. 136-148.

Besly, B.M., and Fielding, C.R., 1989, Palaeosols in Westphalian coal-bearing and red-bed sequences, central and northern England: Palaeogeography, Palaeoclimatology, Palaeoecology, v. 70, no. 4, p. 303–330, doi:10.1016/0031-0182(89)90110-7.

Bovet, P.M., Ritts, B.D., Gehrels, G.E., Abbink, A.O., Darby, B., and Hourigan, J.K., 2009, Evidence of Miocene crustal shortening in the North Qilian Shan from Cenozoic stratigraphy of the western Hexi Corridor, Gansu Province, China: American Journal of Science, v. 309, p. 290–329, doi:10.2475/00.4009.02.

Braitenberg, C., Wang, Y., Fang, J., Hsu, H.T., 2003, Spatial variations of flexure parameters over the Tibet-Quinghai plateau: Earth and Planetary Science Letters, v. 205, p. 211-224.

Cant, D.J., and Walker, R.G., 1978, Fluvial processes and facies sequences in the sandy braided South Saskatchewan River, Canada: Sedimentology, v. 25, p. 625–648.

Carrapa, B., Shazanee Mustapha, F., Cosca, M., Gehrels, G.E., Schoenbohm, L.M., Sobel, E.R., DeCelles, P.G., Russell, J., and Goodman, P., 2014, Multisystem dating of modern river detritus from Tajikistan and China: Implications for crustal evolution and exhumation of the Pamir: Lithosphere, L360.1, doi:10.1130/L360.1.

Carroll, A.R., Graham, S.A., and Smith, M., 2010, Walled sedimentary basins of China: Basin Research, v. 22, p. 17–32.

Chen, X.-H., Gehrels, G.E., Yin, A., Li, L., and Jiang, R.-B., 2012, Paleozoic and Mesozoic basement magmatisms of eastern Qaidam Basin, Northern Qinghai-Tibet Plateau: LA-ICP-MS Zircon U-Pb geochronology and its geological significance: Acta Geologica Sinica, v. 86, p. 350–369.

Cheng, F., Fu, S., Jolivet, M., Zhang, C., & Guo, Z., 2015, Source to sink relation between the Eastern Kunlun Range and the Qaidam Basin, northern Tibetan Plateau, during the Cenozoic: Geological Society of America Bulletin, B31260.1, http://doi.org/10.1130/B31260.1.

Clark, M.K., Farley, K. A., Zheng, D., Wang, Z., and Duvall, A.R., 2010, Early Cenozoic faulting of the northern Tibetan Plateau margin from apatite (U–Th)/He ages: Earth and Planetary Science Letters, v. 296, p. 78–88, doi:10.1016/j.epsl.2010.04.051.

Clark, M.K., and Royden, L.H., 2000, Topographic ooze : Building the eastern margin of Tibet by lower crustal flow: Geology, v. 28, p. 703–706, doi:10.1130/0091-7613(2000)28<703.

Cowgill, E., Yin, A., Harrison, T.M., and Wang, X.-F., 2003, Reconstruction of the Altyn Tagh fault based on U-Pb geochronology: Role of back thrusts, mantle sutures,

and heterogeneous crustal strength in forming the Tibetan Plateau: Journal of Geophysical Research, v. 108, B7, p. 2346, doi:10.1029/2002JB002080.

Craddock, W.H., Kirby, E., Harkins, N.W., Zhang, H., Shi, X., and Liu, J., 2010, Rapid fluvial incision along the Yellow River during headward basin integration: Nature Geoscience, v. 3, no. 3, p. 209–213.

Craddock, W.H., Kirby, E., Zhang, D., and Liu, J., 2011a, Tectonic setting of Cretaceous basins on the NE Tibetan Plateau: insights from the Jungong basin: Basin Research, p. 51-69, doi:10.1111/j.1365-2117.2011.00515.x.

Craddock, W.H., Kirby, E., and Zhang, H., 2011b, Late Miocene-Pliocene range growth in the interior of the northeastern Tibetan Plateau: Lithosphere, v. 3, p. 420–438, doi:10.1130/L159.1.

Dai, J., Zhao, X., Wang, C., Zhu, L., Li, Y., and Finn, D., 2012, The vast proto-Tibetan Plateau: New constraints from Paleogene Hoh Xil Basin: Gondwana Research, v. 22, p. 434–446, doi:10.1016/j.gr.2011.08.019.

Darby, B.J., Ritts, B.D., Yue, Y., and Meng, Q., 2005, Did the Altyn Tagh fault extend beyond the Tibetan Plateau?: Earth and Planetary Science Letters, v. 240, p. 425–435, doi:10.1016/j.epsl.2005.09.011.

Dayem, K. E., Molnar, P., Clark, M. K., and Houseman, G. A., 2009, Far-field lithospheric deformation in Tibet during continental collision: Tectonics, v. 28, p. 1–9, doi:10.1029/2008TC002344.

DeCelles, P., Kapp, P., Ding, L., and Gehrels, G., 2007, Late Cretaceous to middle Tertiary basin evolution in the central Tibetan Plateau: Changing environments in response to tectonic partitioning, aridification, and regional elevation gain: Geological Society of America Bulletin, v. 119, p. 654-680.

Dewey, J.F., Shackleton, R.M., Chengfa, C., and Yiyin, S., 1988, The Tectonic Evolution of the Tibetan Plateau: Philosophical Transactions of the Royal Society A: Mathematical, Physical and Engineering Sciences, v. 327, p. 379–413, doi:10.1098/rsta.1988.0135.

Dickinson, W.R., 1970, Interpreting detrital modes of greywacke and arkose: Journal of Sedimentary Petrology, v. 40, p. 695–707.

Dickinson, W.R., and Suczek, C.A., 1979, Plate Tectonics and Sandstone Compositions: AAPG Bulletin, v. 12, p. 2164–2182.

Dickinson, W.R., 1985, Interpreting provenance relations from detrital modes of sandstones, *in* Zuffa, G.G., ed., Provenance of arenites: Reidel Publishing Company, Dordrecht, Netherlands, p. 333–361.

Ding, L., Yang, D., Cai, F.L., Pullen, A., Kapp, P., Gehrels, G.E., Zhang, L.Y., Zhang, Q.H., Lai, Q.Z., Yue, Y.H., and Shi, R.D., 2013, Provenance analysis of the Mesozoic Hoh-Xil-Songpan-Ganzi turbidites in northern Tibet: Implications for the tectonic evolution of the eastern Paleo-Tethys Ocean: Tectonics, v. 32, p. 34–48, doi:10.1002/tect.20013.

Ding, L., Xu, Q., Yue, Y., Wang, H., Cai, F., Li, S., 2014, The Andean-type Gangdese Mountains: Paleoelevation record from the Paleocene–Eocene Linzhou Basin: Earth and Planetary Science Letters, v. 392, p. 250-264.

Dupont-Nivet, G., Butler, R.F., Yin, A., and Chen, X.-H., 2002, Paleomagnetism indicates no Neogene rotation of the Qaidam Basin in northern Tibet during Indo-

Asian collision: Geology, v. 30, p. 263–266, doi:10.1130/0091-7613(2002)030<0263.
Dupont-Nivet, G., Dai, S., Fang, X., Krijgsman, W., Erens, V., Reitsma, M., and Langereis, C.G., 2008, Timing and distribution of tectonic rotations in the northeastern Tibetan plateau: Geological Society of America Special Papers, v. 444, p. 73–87, doi:10.1130/2008.2444(05).
Dupont-Nivet, G., Horton, B.K., Butler, R.F., Wang, J., Zhou, J., and Waanders, G.L., 2004, Paleogene clockwise tectonic rotation of the Xining-Lanzhou region, northeastern Tibetan Plateau: Journal of Geophysical Research, v. 109, B04401, doi:10.1029/2003JB002620.
Duvall, A.R., and Clark, M.K., 2010, Dissipation of fast strike-slip faulting within and beyond northeastern Tibet: Geology, v. 38, p. 223–226, doi:10.1130/G30711.1.
Duvall, A.R., Clark, M.K., van der Pluijm, B. A., and Li, C., 2011, Direct dating of Eocene reverse faulting in northeastern Tibet using Ar-dating of fault clays and low-temperature thermochronometry: Earth and Planetary Science Letters, v. 304, p. 520–526, doi:10.1016/j.epsl.2011.02.028.
Duvall, A.R., Clark, M.K., Kirby, E., Farley, K. A., Craddock, W.H., Li, C., and Yuan, D.-Y., 2013, Low-temperature thermochronometry along the Kunlun and Haiyuan Faults, NE Tibetan Plateau: Evidence for kinematic change during late-stage orogenesis: Tectonics, v. 32, p. 1190–1211, doi:10.1002/tect.20072.
Enkelmann, E., Weislogel, A.L., Ratschbacher, L., Eide, E., Renno, A., and Wooden, J., 2007, How was the Triassic Songpan-Ganzi basin filled? A provenance study: Tectonics, v. 26, doi:10.1029/2006TC002078.
Ethridge, F.G., Skelly, R.L., and Bristow, C.S., 1999, Avulsion and crevassing in the sandy, braided Niobrara River: Complex response to base-level rise and aggradation, *in* Smith, N.D. and Rogers, J. eds., Fluvial Sedimentology VI, International Association of Sedimentologists, p. 179–191.
Fang, X., Garzione, C., Van der Voo, R., Li, J., Fan, M., 2003. Flexural subsidence by 29 Ma on the NE edge of Tibet from the magnetostratigraphy of Linxia Basin, China: Earth and Planetary Science Letters, v. 210, p. 545-560.
Fang, X.M., Yan, M.D., van der Voo, R., Rea, D.K., Song, C.H., Pares, J.M., Gao, J.P., Nie, J.S., and Dai, S., 2005, Late Cenozoic deformation and uplift of the NE Tibetan plateau: Evidence from high-resolution magneto stratigraphy of the Guide Basin, Qinghai Province, China: Geological Society of America Bulletin, v. 117, p. 1208–1225, doi:10.1130/B25727.1.
Fang, X., Zhang, W., Meng, Q., Gao, J., Wang, X., King, J.G., Song, C., Dai, S., and Miao, Y., 2007, High-resolution magnetostratigraphy of the Neogene Huaitoutala section in the eastern Qaidam Basin on the NE Tibetan Plateau, Qinghai Province, China and its implication on tectonic uplift of the NE Tibetan Plateau: Earth and Planetary Science Letters, v. 258, p. 293–306, doi:10.1016/j.epsl.2007.03.042.
Folk, R.L., 1980, Petrology of Sedimentary Rocks: Austin, Texas, Hemphill Publishing Company, 190 p.
Friend, P.F., Slater, M.J., and Williams, R.C., 1979, Vertical and lateral building of river sandstone bodies, Ebro Basin, Spain: Journal of the Geological Society of London, v. 136, p. 39–46.

Fu, B., and Awata, Y., 2007, Displacement and timing of left-lateral faulting in the Kunlun Fault Zone, northern Tibet, inferred from geologic and geomorphic features: Journal of Asian Earth Sciences, v. 29, p. 253–265, doi:10.1016/j.jseaes.2006.03.004.

Gan, W., Zhang, P., Shen, Z.K., Niu, Z., Wang, M., Wan, Y., Zhou, D., and Cheng, J., 2007, Present-day crustal motion within the Tibetan Plateau inferred from GPS measurements: Journal of Geophysical Research, v. 112, doi:10.1029/2005JB004120.

Garzione, C., DeCelles, P., Hodkinson, D., Ojha, T., and Upreti, B., 2003, East-west extension and Miocene environmental change in the southern Tibetan plateau: Thakkhola graben, central Nepal: Geological Society of America Bulletin, v. 115, p. 3-20.

Gazzi, P., 1966, Le minerali pesanti nei flysch arenacei fra Monte Ramaceto e Monte Molinatico (Appennino settent Ríonale): Mineralogica et Petrographica Acta, v. 11, p. 197–212.

Gehrels, G.E., Kapp, P., DeCelles, P.G., Pullen, A., Blakey, R., Weislogel, A.L., Ding, L., Guynn, J., Martin, A., McQuarrie, N., and Yin, A., 2011, Detrital zircon geochronology of pre-Tertiary strata in the Tibetan-Himalayan orogen: Tectonics, v. 30, doi:10.1029/2011TC002868.

Gehrels, G.E., Valencia, V.A., and Ruiz, J., 2008, Enhanced precision, accuracy, efficiency, and spatial resolution of U-Pb ages by laser ablation-multicollector-inductively coupled plasma-mass spectrometry: Geochemistry, Geophysics, Geosystems, v. 9, p. 1–13, doi:10.1029/2007GC001805.

Gehrels, G.E., Yin, A., and Wang, X.-F., 2003a, Detrital-zircon geochronology of the northeastern Tibetan plateau: Geological Society of America Bulletin, v. 115, p. 881–896, doi:10.1130/0016-7606(2003)115<0881:DGOTNT>2.0.CO;2.

Gehrels, G.E., Yin, A., and Wang, X.-F., 2003b, Magmatic history of the northeastern Tibetan Plateau: Journal of Geophysical Research, v. 108, no. B9, p. 1–14, doi:10.1029/2002JB001876.

George, A.D., Marshallsea, S.J., Wyrwoll, K.-H., Jie, C., and Yanchou, L., 2001, Miocene cooling in the northern Qilian Shan , northeastern margin of the Tibetan Plateau, revealed by apatite fission-track and vitrinite-reflectance analysis: Geology, v. 29, p. 939–942.

Graham, S.A., Chamberlain, C.P., Yue, Y., Ritts, B.D., Hanson, A.D., Horton, T.W., Waldbauer, J.R., Poage, M.A., and Feng, X., 2005, Stable isotope records of Cenozoic climate and topography, Tibetan plateau and Tarim basin: American Journal of Science, v. 305, p. 101–118, doi:10.2475/ajs.305.2.101.

Graham, S. A., Hendrix, M. S., Wang, L. B., and Carroll, A. R., 1993, Collisional successor basins of western China - Impact of tectonic inheritance on sand composition: Geological Society of America Bulletin, v. 105, no. 3, p. 323-344.

Guo, Z., Deng, K., and Han, Y., 1996, Formation and Evolution of the Sichuan Basin, Beijing, Geologic Publishing House, 200 p.

Gupta, S., 1997, Himalayan drainage patterns and the origin of fluvial megafans in the Ganges foreland basin: Geology, v. 25, p. 11–14, doi:10.1130/0091-7613(1997)025<0011.

Hanson, A. D., 1999, Organic geochemistry and petroleum geology, tectonics and basin analysis of southern Tarim and northern Qaidam basins, northwest China [Ph.D.: Stanford University, 388 p.

Hanson, A.D., Ritts, B.D., Zinniker, D., Moldowan, J.M., and Biffi, U., 2001, Upper Oligocene lacustrine source rocks and petroleum systems of the northern Qaidam basin, northwest China: AAPG Bulletin, v. 85, p. 601–619.

Harris, N.B.W., Ronghua, X., Lewis, C.L., and Chengwei, J., 1988, Plutonic rocks of the 1985 Tibet Geotraverse, Lhasa to Golmud: Philosophical Transactions of the Royal Society A: Mathematical, Physical and Engineering Sciences, v. 327, p. 145–168, doi:10.1098/rsta.1988.0124.

Harrison, T., Copeland, P., Kidd, W., and Yin, A., 1992, Raising Tibet: Science, v. 255, no. 5052, p. 1663-1670.

Hartley, A.J., Weissmann, G.S., Nichols, G.J., and Warwick, G.L., 2010, Large distributive fluvial systems: Characteristics, distribution, and controls on development: Journal of Sedimentary Research, v. 80, p. 167–183, doi:10.2110/jsr.2010.016.

He, S. D., Kapp, P., DeCelles, P. G., Gehrels, G. E., and Heizler, M., 2007, Cretaceous-Tertiary geology of the Gangdese Arc in the Linzhou area, southern Tibet: Tectonophysics, v. 433, p. 15-37.

Horton, B.K., and DeCelles, P.G., 2001, Modern and ancient fluvial megafans in the foreland basin system of the central Andes, southern Bolivia: implications for drainage network evolution in fold-thrust belts: Basin Research, v. 13, p. 43–63, doi:10.1046/j.1365-2117.2001.00137.x.

Horton, B.K., Dupont-Nivet, G., Zhou, J., Waanders, G.L. Butler, R.F., and Wang, J., 2004, Mesozoic-Cenozoic evolution of the Xining-Minhe and Dangchang basins, northeastern Tibetan plateau: Magnetostratigraphic and biostratigraphic results: Journal of Geophysical Research, v. 109, B04402, doi:10.1029/2003JB002913.

Horton, B. K., Yin, A., Spurlin, M. S., Zhou, J. Y., and Wang, J. H., 2002, Paleocene-Eocene syncontractional sedimentation in narrow, lacustrine-dominated basins of east-central Tibet: Geological Society of America Bulletin, v. 114, p. 771-786.

Horton, B.K., 2012, Cenozoic evolution of hinterland basins in the Andes and Tibet, *in* Busby, C., and Azor, A., editors, Tectonics of Sedimentary Basins: Recent Advances: Wiley-Blackwell, Oxford, UK, p. 427-444.

Hough, B.G., Garzione, C.N., Wang, Z., Lease, R.O., Burbank, D.W., and Yuan, D., 2011, Stable isotope evidence for topographic growth and basin segmentation: Implications for the evolution of the NE Tibetan Plateau: Bulletin of the Geological Society of America, v. 123, p. 168–185, doi:10.1130/B30090.1.

Hough, B.G., Garzione, C.N., Wang, Z., and Lease, R.O., 2014, Timing and spatial patterns of basin segmentation and climate change in northeastern Tibet: Geological Society of America Special Papers, v. 507, p. 129–153, doi:10.1130/2014.2507(07).

Hsü, K.J., Guitang, P., and Sengör, A., 1995, Tectonic evolution of the Tibetan Plateau: A working hypothesis based on the archipelago model of orogenesis: International Geology Review, v. 37, p. 473-508.

Hubert, J.F., 1962, A zircon-tourmaline-rutile maturity index and the interdependence of the composition of heavy mineral assemblages with the gross composition and texture of sandstones: Journal of Sedimentary Petrology, v. 32, p. 440–450.

Jian, X., Guan, P., Zhang, D.-W., Zhang, W., Feng, F., Liu, R.-J., and Lin, S.-D., 2013, Provenance of Tertiary sandstone in the northern Qaidam basin, northeastern Tibetan Plateau: Integration of framework petrography, heavy mineral analysis and mineral chemistry: Sedimentary Geology, v. 290, p. 109-125, doi:10.1016/j.sedgeo.2013.03.010.

Jin, Y., McNutt, M. K., and Zhu, Y., 1994, Evidence from gravity and topography data for folding of Tibet: Nature, v. 371, no. 6499, p. 669-674.

Johnson, C.L., and Ritts, B.D., 2012, Plate interior poly-phase basins, *in* Busby, C. and Azor, P.A. eds., Tectonics of Sedimentary Basins: Recent Advances, Hoboken, Wiley-Blackwell, p. 567–582.

Jolivet, M., Brunel, M., Seward, D., Xu, Z., Yang, J., Malavieille, J., Roger, F., Leyreloup, A., Arnaud, N., and Wu, C., 2003, Neogene extension and volcanism in the Kunlun Fault Zone, northern Tibet: New constraints on the age of the Kunlun Fault: Tectonics, v. 22, doi:10.1029/2002TC001428.

Jolivet, M., Brunel, M., Seward, D., Xu, Z., Yang, J., Roger, F., Tapponnier, P., Malavieille, J., Arnaud, N., and Wu, C., 2001, Mesozoic and Cenozoic tectonics of the northern edge of the Tibetan plateau: fission-track constraints: Tectonophysics, v. 343, p. 111–134, doi:10.1016/S0040-1951(01)00196-2.

Jordan, T., and Watts, A., 2005, Gravity anomalies, flexure and the elastic thickness structure of the India–Eurasia collisional system: Earth and Planetary Science Letters, v. 236, p. 732-750.

Kapp, P., DeCelles, P. G., Gehrels, G. E., Heizier, M., and Ding, L., 2007, Geological records of the Lhasa-Qiangtang and Indo-Asian collisions in the Nima area of central Tibet: Geological Society of America Bulletin, v. 119, p. 917-932.

Kapp, P., Taylor, M., Stockli, D., and Ding, L., 2008, Development of active low-angle normal fault systems during orogenic collapse: Insight from Tibet: Geology, v. 36, no. 1, p. 7-10.

Ke, X., Ji, J., Zhang, K., Kou, X., Song, B., and Wang, C., 2013, Magnetostratigraphy and anisotropy of magnetic susceptibility of the Lulehe formation in the northeastern Qaidam basin: Acta Geologica Sinica - English Edition, v. 87, p. 576–587.

Kent-Corson, M.L., Ritts, B.D., Zhuang, G., Bovet, P.M., Graham, S. A., and Chamberlain, P., 2009, Stable isotopic constraints on the tectonic, topographic, and climatic evolution of the northern margin of the Tibetan Plateau: Earth and Planetary Science Letters, v. 282, p. 158–166, doi:10.1016/j.epsl.2009.03.011.

Kirby, E., Harkins, N.W., Wang, E., Shi, X., Fan, C., and Burbank, D.W., 2007, Slip rate gradients along the eastern Kunlun fault: Tectonics, v. 26, p. 1–16, doi:10.1029/2006TC002033.

Klemperer, S. L., 2006, Crustal flow in Tibet: geophysical evidence for the physical state of Tibetan lithosphere, and inferred patterns of active flow, in Law, R. D., Searle, M. P., and Godin, L., eds., Channel Flow, Ductile Extrusion and Exhumation in Continental Collision Zones: London, Geological Society of London, Special Publications v. 268, p. 39-70.

Kraus, M., 1996, Avulsion deposits in lower Eocene alluvial rocks, Bighorn Basin, Wyoming: Journal of Sedimentary Research, v. 66, p. 354–363.

Lease, R.O., Burbank, D.W., Clark, M.K., Farley, K. A., Zheng, D., and Zhang, H., 2011, Middle Miocene reorganization of deformation along the northeastern Tibetan Plateau: Geology, v. 39, p. 359–362, doi:10.1130/G31356.1.

Leeder, M.R., Smith, A.B., and Yin, J., 1988, Sedimentology, palaeoecology and palaeoenvironmental evolution of the 1985 Lhasa to Golmud Geotraverse. Philosophical Transactions of the Royal Society of London, A327, 107–143.

Li, J.-J., Fang, X.-M., Van der Voo, R., Zhu, J.-J., Niocaill, C. M., Ono, Y., Pan, B.-T., Zhong, W., Wang, J.-L., Sasaki, T., Zhang, Y.-T., Cao, J.-X., Kang, S.-C., and Wang, J.-M., 1997, Magnetostratigraphic dating of river terraces: Rapid and intermittent incision by the Yellow River of the northeastern margin of the Tibetan Plateau during the Quaternary: Journal of Geophysical Research: Solid Earth, v. 102, p. 10121-10132.

Li, L., Guo, Z., Guan, S., Zhou, S., Wang, M., Fang, Y., and Zhang, C., 2015, Heavy mineral assemblage characteristics and the Cenozoic paleogeographic evolution in southwestern Qaidam Basin: Science China Earth Sciences, v. 58, p. 859–875, doi:10.1007/s11430-014-5050-x.

Li, L., Li, A., Shen, Y., Sandvol, E. A., Shi, D., Li, H., and Li, X., 2013, Shear wave structure in the northeastern Tibetan Plateau from Rayleigh wave tomography: Journal of Geophysical Research: Solid Earth, v. 118, p. 4170-4183.

Li, H., Li, S., Song, X., Gong, M., Li, X., and Jia, J., 2012, Crustal and uppermost mantle velocity structure beneath northwestern China from seismic ambient noise tomography: Geophysical Journal International, v. 188, p. 131-143.

Li, W., Neubauer, F., Liu, Y., Genser, J., Ren, S., Han, G., and Liang, C., 2013, Paleozoic evolution of the Qimantagh magmatic arcs, Eastern Kunlun Mountains: Constraints from zircon dating of granitoids and modern river sands: Journal of Asian Earth Sciences, v. 77, p. 183–202, doi:10.1016/j.jseaes.2013.08.030.

Li, C., van der Hilst, R. D., Engdahl, E. R., and Burdick, S., 2008a, A new global model for P wave speed variations in Earth's mantle: Geochemistry, Geophysics, Geosystems, v. 9, doi:10.1029/2007GC001806.

Li, C., Van der Hilst, R. D., Meltzer, A. S., and Engdahl, E. R., 2008b, Subduction of the Indian lithosphere beneath the Tibetan Plateau and Burma: Earth and Planetary Science Letters, v. 274, p. 157-168.

Liang, C., and Song, X., 2006, A low velocity belt beneath northern and eastern Tibetan Plateau from Pn tomography: Geophysical Research Letters, v. 33, L22306.

Lin, A., Fu, B., Guo, J., Zeng, Q., Dang, G., He, W., and Zhao, Y., 2002, Co-seismic strike-slip and rupture length produced by the 2001 Ms 8.1 Central Kunlun earthquake: Science, v. 296, no. 5575, p. 2015–7, doi:10.1126/science.1070879.

Liu, C., Mo, X., Luo, Z., Yu, X., Chen, H., Li, S., and Zhao, X., 2004, Mixing events between the crust- and mantle-derived magmas in Eastern Kunlun: Evidence from zircon SHRIMP II chronology: Chinese Science Bulletin, v. 49, p. 828–834, doi:10.1007/BF02889756.

Liu, Z. F., and Wang, C. S., 2001, Facies analysis and depositional systems of Cenozoic sediments in the Hoh Xil basin, northern Tibet: Sedimentary Geology, v. 140, p. 251-270.

Liu, Z., Wang, C., and Yi, H., 2001, Evolution and Mass Accumulation of the Cenozoic Hoh Xil Basin, Northern Tibet: Journal of Sedimentary Research, v. 71, p. 971-984.

Lu, H., Wang, E., Shi, X., and Meng, K., 2012, Cenozoic tectonic evolution of the Elashan range and its surroundings, northern Tibetan Plateau as constrained by paleomagnetism and apatite fission track analyses: Tectonophysics, v. 580, p. 150–161, doi:10.1016/j.tecto.2012.09.013.

Lu, H., and Xiong, S., 2009, Magnetostratigraphy of the Dahonggou section, northern Qaidam Basin and its bearing on Cenozoic tectonic evolution of the Qilian Shan and Altyn Tagh Fault: Earth and Planetary Science Letters, v. 288, p. 539–550, doi:10.1016/j.epsl.2009.10.016.

Makaske, B., 2001, Anastomosing rivers: a review of their classification, origin and sedimentary products: Earth-Science Reviews, v. 53, p. 149–196, doi:10.1016/S0012-8252(00)00038-6.

Mange, M., and Maurer, H.F.W., 1992, Heavy minerals in colour: Chapman & Hall, Hong Kong.

Mao, L., Xiao, A., Wu, L., Li, B., Wang, L., Lou, Q., Dong, Y., and Qin, S., 2014, Cenozoic tectonic and sedimentary evolution of southern Qaidam Basin, NE Tibetan Plateau and its implication for the rejuvenation of Eastern Kunlun Mountains: Science China Earth Sciences, v. 57, doi:10.1007/s11430-014-4951-z.

Masek, J. G., Isacks, B. L., Fielding, E. J., and Browaeys, J., 1994, Rift flank uplift in Tibet: Evidence for a viscous lower crust: Tectonics, v. 13, p. 659-667.

Mattinson, C.G., Menold, C.A., Zhang, J.X., and Bird, D.K., 2007, High- and Ultrahigh-Pressure Metamorphism in the North Qaidam and South Altyn Terranes, Western China: International Geology Review, v. 49, p. 969–995, doi:10.2747/0020-6814.49.11.969.

McRivette, M.W., 2011, The tectonic evolution of the Eastern Kunlun Range and central Tibetan plateau, China: Ph.D. dissertation, University of California, Los Angeles, 333 p.

Meng, Q.R., and Fang, X., 2008, Cenozoic tectonic development of the Qaidam Basin in the northeastern Tibetan Plateau: Geological Society of America Special Papers, v. 444, p. 1–24, doi:10.1130/2008.2444(01).

Meng, Q.-R., Wang, E., and Hu, J.-M., 2005, Mesozoic sedimentary evolution of the northwest Sichuan basin: Implication for continued clockwise rotation of the South China block: Geological Society of America Bulletin, v. 117, p. 396-410.

Menold, C.A., 2006, Tectonic and metamorphic evolution of the North Qaidam Ultrahigh-pressure metamorphic terrane, western China: Ph.D. dissertation, University of California, Los Angeles, 279 p.

Menold, C.A., Manning, C.E., Yin, A., Tropper, P., Chen, X.-H., and Wang, X.-F., 2009, Metamorphic evolution, mineral chemistry and thermobarometry of orthogneiss hosting ultrahigh-pressure eclogites in the North Qaidam metamorphic belt, Western China: Journal of Asian Earth Sciences, v. 35, p. 273–284, doi:10.1016/j.jseaes.2008.12.008.

Métivier, F., Gaudemer, Y., Tapponnier, P., and Meyer, B., 1998, Northeastward growth of the Tibet plateau deduced from balanced reconstruction of two depositional areas: Tectonics, v. 17, p. 823–842.

Meyer, B., Tapponnier, P., Bourjot, L., Metivier, F., Gaudemer, Y., Peltzer, G., Shunmin, G., and Zhitai, C., 1998, Crustal thickening in Gansu-Qinghai, lithospheric mantle subduction, and oblique, strike-slip controlled growth of the Tibetan Plateau: Geophysical Journal International, v. 135, p. 1–47.

Miall, A.D., 1977, A review of the braided-river depositional environment: Earth-Science Reviews, v. 13, p. 1–62, doi:10.1016/0012-8252(77)90055-1.

Miao, Y., Fang, X., Herrmann, M., Wu, F., Zhang, Y., and Liu, D., 2011, Miocene pollen record of KC-1 core in the Qaidam Basin, NE Tibetan Plateau and implications for evolution of the East Asian monsoon: Palaeogeography, Palaeoclimatology, Palaeoecology, v. 299, p. 30–38, doi:10.1016/j.palaeo.2010.10.026.

Miao, Y., Fang, X., Song, Z., Wu, F., Han, W., Dai, S., and Song, C., 2008, Late Eocene pollen records and palaeoenvironmental changes in northern Tibetan Plateau: Science in China Series D: Earth Sciences, v. 51, p. 1089–1098, doi:10.1007/s11430-008-0091-7.

Mo, X., Luo, Z., Deng, J., Yu, X., Liu, C., Chen, H., Yuan, W., and Liu, Y., 2007, Granitoids and crustal growth in the East-Kunlun orogenic belt: Geological Journal of China Universities, v. 13, p. 403–414.

Mock, C., Arnaud, N.O., and Cantagrel, J.-M., 1999, An early unroofing in northeastern Tibet ? Constraints from 40Ar / 39Ar thermochronology on granitoids from the eastern Kunlun range: Earth and Planetary Science Letters, v. 171, p. 107–122.

Morton, A.C., and Hallsworth, C.R., 1994, Identifying provenance-specific features of detrital heavy mineral assemblages in sandstones: Sedimentary Geology, v. 90, p. 241–256.

Nanson, G., 1980, Point bar and floodplain formation of the meandering Beatton River, northeastern British Columbia, Canada: Sedimentology, v. 27, p. 3–29.

Nemec, W., and Steel, R.J., 1984, Alluvial and coastal conglomerates: their significance and some comments on gravelly mass-flow deposits, *in* Koster, E.H. and Steel, R.J. eds., Sedimentology of Gravels and Conglomerates, Canadian Society of Petroleum Geologists Memoir 10, p. 1–31.

Nie, J., Stevens, T., Rittner, M., Stockli, D., Garzanti, E., Limonta, M., Bird, A., Ando, S., Vermeesch, P., Saylor, J., Lu, H., Breecker, D., Hu, X., Liu, S., Resentini, A., Vezzoli, G., Peng, W., Carter, A., Ji, S., and Pan, B., 2015, Loess Plateau storage of Northeastern Tibeta Plateau-derived Yellow River sediment: Nature Communications, v. 6, p. 8511 doi: 10.1038/ncomms9511.

Owens, T. J., and Zandt, G., 1997, Implications of crustal property variations for models of Tibetan plateau evolution: Nature, v. 387, no. 6628, p. 37-43.

Porter, R.J., and Gallois, R.W., 2008, Identifying fluvio–lacustrine intervals in thick playa-lake successions: An integrated sedimentology and ichnology of arenaceous members in the mid–late Triassic Mercia Mudstone Group of south-west England, UK: Palaeogeography, Palaeoclimatology, Palaeoecology, v. 270, p. 381–398, doi:10.1016/j.palaeo.2008.07.020.

Pullen, A., Kapp, P., Gehrels, G.E., Vervoort, J.D., and Ding, L., 2008, Triassic continental subduction in central Tibet and Mediterranean-style closure of the Paleo-Tethys Ocean: Geology, v. 36, p. 351, doi:10.1130/G24435A.1.

Pullen, A., Kapp, P., McCallister, A.T., Chang, H., Gehrels, G.E., Garzione, C.N., Heermance, R. V., and Ding, L., 2011, Qaidam Basin and northern Tibetan

Plateau as dust sources for the Chinese Loess Plateau and paleoclimatic implications: Geology, doi:10.1130/G32296.1.

Qinghai Bureau of Geology and Mineral Resources, 1991, Regional geology of Qinghai province.

Richardson, N. J., Densmore, A. L., Seward, D., Fowler, A., Wipf, M., Ellis, M. A., Yong, L., and Zhang, Y., 2008, Extraordinary denudation in the Sichuan Basin: Insights from low-temperature thermochronology adjacent to the eastern margin of the Tibetan Plateau: Journal of Geophysical Research: Solid Earth, v. 113, doi:10.1029/2006JB004739.

Rieser, A.B., Liu, Y., Genser, J., Neubauer, F., Handler, R., Friedl, G., and Ge, X., 2006a, 40Ar/39Ar ages of detrital white mica constrain the Cenozoic development of the intracontinental Qaidam Basin, China: Geological Society of America Bulletin, v. 118, p. 1522–1534, doi:10.1130/B25962.1.

Rieser, A. B., Liu, Y. J., Genser, J., Neubauer, F., Handler, R., and Ge, X. H., 2006b, Uniform Permian Ar-40/Ar-39 detrital mica ages in the eastern Qaidam Basin (NW China): where is the source?: Terra Nova, v. 18, no. 1, p. 79-87.

Rieser, A.B., Neubauer, F., Liu, Y., and Ge, X., 2005, Sandstone provenance of north-western sectors of the intracontinental Cenozoic Qaidam basin, western China: Tectonic vs. climatic control: Sedimentary Geology, v. 177, p. 1–18, doi:10.1016/j.sedgeo.2005.01.012.

Ritts, B.D., 1998, Mesozoic tectonics and sedimentation, and petroleum systems of the Qaidam and Tarim basins, NW China: Ph.D. dissertation, Stanford University, Stanford, California, 691 p.

Ritts, B.D. and Biffi, U., 2000, Magnitude of post-Middle Jurassic (Bajocian) displacement on the central Altyn Tagh fault system, northwest China: Geological Society of America Bulletin, v. 112, p. 61-74.

Ritts, B.D., and Biffi, U., 2001, Mesozoic northeast Qaidam basin: Response to contractional reactivation of the Qilian Shan, and implications for the extent of Mesozoic intracontinental deformation in Central Asia: Geological Society of America Memoirs, v. 194, p. 293–316, doi:10.1130/0-8137-1194-0.293.

Ritts, B.D., Yue, Y., Graham, S.A., Sobel, E.R., Abbink, A.O., and Stockli, D.F., 2008, From sea level to high elevation in 15 million years: Uplift history of the northern Tibetan Plateau margin in the Altun Shan: American Journal of Science, v. 308, p. 657–678, doi:10.2475/05.2008.01.

Robinson, A.C., Ducea, M., and Lapen, T.J., 2012, Detrital zircon and isotopic constraints on the crustal architecture and tectonic evolution of the northeastern Pamir: Tectonics, v. 31, doi:10.1029/2011TC003013.

Roger, F., Arnaud, N., Gilder, S., Tapponnier, P., Jolivet, M., Brunel, M., Malavieille, J., Xu, Z., and Yang, J., 2003, Geochronological and geochemical constraints on Mesozoic suturing in east central Tibet: Tectonics, v. 22, doi:10.1029/2002TC001466.

Rust, B.R., 1972, Structure and process in a braided river: Sedimentology, v. 18, p. 221–245.

Sanchez, V. I., Murphy, M. A., Dupré, W. R., Ding, L., and Zhang, R., 2010, Structural evolution of the Neogene Gar Basin, western Tibet: Implications for releasing

bend development and drainage patterns: Geological Society of America Bulletin, v. 122, p. 926-945.

Saylor, J. E., DeCelles, P. C., Gehrels, G., Murphy, M., Zhang, R., and Kapp, P., 2010, Basin formation in the High Himalaya by arc-parallel extension and tectonic damming: Zhada basin, southwestern Tibet: Tectonics, v. 29, TC1004.

Smith, S.A., 1990, The sedimentology and accretionary styles of an ancient gravel-bed stream: the Budleigh Salterton Pebble Beds (Lower Triassic), southwest England: Sedimentary Geology, v. 67, p. 199–219, doi:10.1016/0037-0738(90)90035-R.

Sobel, E.R., and Arnaud, N., 1999, A possible middle Paleozoic suture in the Altyn Tagh, NW China: Tectonics, v. 18, p. 64–74.

Sobel, E.R., Arnaud, N., Jolivet, M., and Ritts, B.D., 2001, Jurassic to Cenozoic exhumation history of the Altyn Tagh range, northwest China, constrained by 40Ar/39Ar and apatite fission track thermochronology: Geological Society Of America Memoirs, v. 194, p. 247–267, doi:10.1130/0-8137-1194-0.247.

Sobel, E. R., Hilley, G. E., and Strecker, M. R., 2003, Formation of internally drained contractional basins by aridity-limited bedrock incision: Journal of Geophysical Research-Solid Earth, v. 108, no. B7.

Song, B., Zhang, K., Chen, R., Wang, C., Luo, M., Zhang, J., and Jiang, S., 2013a, The sedimentary record in northern Qaidam basin and its response to the uplift of the southern Qilian Mountain at around 30 Ma: Acta Geologica Sinica - English Edition, v. 87, p. 528–539.

Song, B., Zhang, K., Lu, J., Wang, C., and Xu, Y., 2013b, The middle Eocene to early Miocene integrated sedimentary record in the Qaidam Basin and its implications for paleoclimate and early Tibetan Plateau uplift: Canadian Journal of Earth Sciences, v. 50, p. 183–196.

Spurlin, M. S., Yin, A., Horton, B. K., Zhou, J., and Wang, J., 2005, Structural evolution of the Yushu-Nangqian region and its relationship to syncollisional igneous activity east-central Tibet: Geological Society of America Bulletin, v. 117, p. 1293-1317.

Staisch, L.M., Niemi, N. A., Hong, C., Clark, M.K., Rowley, D.B., and Currie, B., 2014, A Cretaceous-Eocene depositional age for the Fenghuoshan Group, Hoh Xil Basin: Implications for the tectonic evolution of the northern Tibet Plateau: Tectonics, v. 33, p. 281-301, doi:10.1002/2013TC003367.

Strecker, M. R., Alonso, R. N., Bookhagen, B., Carrapa, B., Hilley, G. E., Sobel, E. R., and Trauth, M. H., 2007, Tectonics and climate of the southern central Andes: Annual Review of Earth and Planetary Sciences, v. 35, p. 747-787.

Sun, Z., Yang, Z., Pei, J., Ge, X., Wang, X., Yang, T., Li, W., and Yuan, S., 2005, Magnetostratigraphy of Paleogene sediments from northern Qaidam Basin, China: Implications for tectonic uplift and block rotation in northern Tibetan plateau: Earth and Planetary Science Letters, v. 237, p. 635–646, doi:10.1016/j.epsl.2005.07.007.

Tapponnier, P., Zhiqin, X., Meyer, B., and Arnaud, N., 2001, Oblique Stepwise Rise and Growth of the Tibet Plateau: Science, v. 294, no. 1671, p. 1671–1677, doi:10.1126/science.105978.

Taylor, M. H., Kapp, P. A., and Horton, B. K., 2012, Basin response to active extension and strike-slip deformation in the hinterland of the Tibetan Plateau, in Busby, C.,

and Azor, A., eds., Tectonics of Sedimentary Basins: Recent Advances, Blackwell Publishing Ltd., p. 445-460.

Tornqvist, T., 1993, Holocene alternation of meandering and anastomosing fluvial systems in the Rhine-Meuse delta (central Netherlands) controlled by sea-level rise and subsoil erodibility: Journal of Sedimentary Petrology, v. 63, p. 683–693.

Van Der Woerd, J., Ryerson, F.J., Tapponnier, P., Gaudemer, Y., Finkel, R., Meriaux, A. S., and Caffee, M., 1998, Holocene left-slip rate determined by cosmogenic surface dating on the Xidatan segment of the Kunlun fault (Qinghai, China): Geology, v. 26, p. 695–698, doi:10.1130/0091-7613(1998)026<0695:HLSRDB>2.3.CO;2.

Vermeesch, P., 2012, On the visualisation of detrital age distributions: Chemical Geology, v. 312-313, p. 190–194, doi:10.1016/j.chemgeo.2012.04.021.

Vermeesch, P., 2013, Multi-sample comparison of detrital age distributions: Chemical Geology, v. 341, p. 140–146, doi:10.1016/j.chemgeo.2013.01.010.

Wang, Q., and Coward, M.P., 1990, The Chaidam Basin (NW China): Formation and Hydrocarbon Potential: Journal of Petroleum Geology, v. 13, p. 93–112, doi:10.1306/BF9AB6C2-0EB6-11D7-8643000102C1865D.

Wang, F., Lo, C.-H., Li, Q., Yeh, M.-W., Wan, J., Zheng, D., and Wang, E., 2004, Onset timing of significant unroofing around Qaidam basin, northern Tibet, China: constraints from 40Ar/39Ar and FT thermochronology on granitoids: Journal of Asian Earth Sciences, v. 24, p. 59–69, doi:10.1016/j.jseaes.2003.07.004.

Wang, X., Qiu, Z., Li, Q., Wang, B., Qiu, Z., Downs, W.R., Xie, G., Xie, J., Deng, T., Takeuchi, G.T., Tseng, Z.J., Chang, M., Liu, J., Wang, Y., et al., 2007, Vertebrate paleontology, biostratigraphy, geochronology, and paleoenvironment of Qaidam Basin in northern Tibetan Plateau: Palaeogeography, Palaeoclimatology, Palaeoecology, v. 254, p. 363–385, doi:10.1016/j.palaeo.2007.06.007.

Wang, E., Xu, F.-Y., Zhou, J.-X., Wan, J., and Burchfiel, B.C., 2006, Eastward migration of the Qaidam basin and its implications for Cenozoic evolution of the Altyn Tagh fault and associated river systems: Geological Society of America Bulletin, v. 118, p. 349–365, doi:10.1130/B25778.1.

Wang, Y., Zhang, X.M., Wang, E., Zhang, A.F., Li, Q., Sun, G.H., 2005, Ar-40/Ar-39 thermochronological evidence for formation and Mesozoic evolution of the northern-central segment of the Altyn Tagh fault system in the northern Tibetan Plateau: Geological Society of America Bulletin, v. 117, p. 1336-1346.

Weislogel, A.L., 2008, Tectonostratigraphic and geochronologic constraints on evolution of the northeast Paleotethys from the Songpan-Ganzi complex, central China: Tectonophysics, v. 451, p. 331–345, doi:10.1016/j.tecto.2007.11.053.

Weislogel, A.L., Graham, S.A., Chang, E.Z., Wooden, J.L., and Gehrels, G.E., 2010, Detrital zircon provenance from three turbidite depocenters of the Middle-Upper Triassic Songpan-Ganzi complex, central China: Record of collisional tectonics, erosional exhumation, and sediment production: Geological Society of America Bulletin, v. 122, p. 2041–2062, doi:10.1130/B26606.1.

Weislogel, A.L., Graham, S.A., Chang, E.Z., Wooden, J.L., Gehrels, G.E., and Yang, H., 2006, Detrital zircon provenance of the Late Triassic Songpan-Ganzi complex: Sedimentary record of collision of the North and South China blocks: Geology, v. 34, p. 97, doi:10.1130/G21929.

Woodruff, W. H., Horton, B. K., Kapp, P. A., and Stockli, D. F., 2013, Late Cenozoic evolution of the Lunggar extensional basin, Tibet: Implications for basin growth and exhumation in hinterland plateaus: Geological Society of America Bulletin, v. 125, p. 343-358.

Wu, C., Yang, J., Wooden, J.L., Shi, R., Chen, S., Meibom, A., and Mattinson, C., 2004, Zircon U-Pb SHRIMP dating of the Yematan batholith in Dulan, North Qaidam, NW China: Chinese Science Bulletin, v. 49, p. 1736–1740, doi:10.1007/BF03184308.

Xia, W., Zhang, N., Yuan, X., Fan, L., and Zhang, B., 2001, Cenozoic Qaidam basin, China: A stronger tectonic inversed, extensional rifted basin: AAPG Bulletin, v. 85, p. 715–736.

Xiao, W.J., Windley, B.F., Chen, H.L., Zhang, G.C., and Li, J.L., 2002, Carboniferous-Triassic subduction and accretion in the western Kunlun, China: Implications for the collisional and accretionary tectonics of the northern Tibetan Plateau: Geology, v. 30, p. 295, doi:10.1130/0091-7613(2002)030<0295:CTSAAI>2.0.CO;2.

Xiao, W., Windley, B.F., Yong, Y., Yan, Z., Yuan, C., Liu, C., and Li, J., 2009, Early Paleozoic to Devonian multiple-accretionary model for the Qilian Shan, NW China: Journal of Asian Earth Sciences, v. 35, p. 323–333, doi:10.1016/j.jseaes.2008.10.001.

Xu, Z., 1984, Tertiary system and its petroleum potential in the Lunpola Basin, Xizang (Tibet). U.S. Geological Survey Open-File Report 84–420, 5 p.

Yan, Z., Xiao, W.J., Windley, B.F., Wang, Z.Q., and Li, J.L., 2010, Silurian clastic sediments in the North Qilian Shan, NW China: Chemical and isotopic constraints on their forearc provenance with implications for the Paleozoic evolution of the Tibetan Plateau: Sedimentary Geology, v. 231, p. 98–114, doi:10.1016/j.sedgeo.2010.09.001.

Yang, J., Xu, Z., Zhang, J., Chu, C.-Y., Zhang, R., and Liou, J.-G., 2001, Tectonic significance of early Paleozoic high-pressure rocks in Altun-Qaidam-Qilian Mountains, northwest China: Geological Society of America Memoirs, v. 194, p. 151–170, doi:10.1130/0-8137-1194-0.151.

Yang, Y., Ritzwoller, M. H., Zheng, Y., Shen, W., Levshin, A. L., and Xie, Z., 2012, A synoptic view of the distribution and connectivity of the mid-crustal low velocity zone beneath Tibet: Journal of Geophysical Research: Solid Earth (1978–2012), v. 117, B04303.

Yin, A., Butler, R., Harrison, T.M., Foster, D. a., Ingersoll, R. V., Zhou, X., Wang, X.-F., and Hanson, A.D., 2002, Tectonic history of the Altyn Tagh fault system in northern Tibet inferred from Cenozoic sedimentation: Geological Society of America Bulletin, v. 114, p. 1257–1295.

Yin, A., Dang, Y.-Q., Wang, L.-C., Jiang, W.-M., Zhou, S.-P., Chen, X.-H., Gehrels, G.E., and McRivette, M.W., 2008a, Cenozoic tectonic evolution of Qaidam basin and its surrounding regions (Part 1): The southern Qilian Shan-Nan Shan thrust belt and northern Qaidam basin: Geological Society of America Bulletin, v. 120, p. 813–846, doi:10.1130/B26180.1.

Yin, A., Dang, Y.-Q., Zhang, M., Chen, X.-H., and McRivette, M.W., 2008b, Cenozoic tectonic evolution of the Qaidam basin and its surrounding regions (Part 3):

Structural geology, sedimentation, and regional tectonic reconstruction: Geological Society of America Bulletin, v. 120, p. 847–876, doi:10.1130/B26232.1.

Yin, A., Dang, Y.-Q., Zhang, M., McRivette, M.W., Burgess, W.P., and Chen, X.-H., 2007a, Cenozoic tectonic evolution of Qaidam basin and its surrounding regions (part 2): Wedge tectonics in southern Qaidam basin and the Eastern Kunlun Range: Geological Society of America Special Papers, v. 433, p. 369, doi:10.1130/2007.2433(18).

Yin, A., and Harrison, T.M., 2000, Geologic evolution of the Himalayan-Tibetan orogen: Annual Review of Earth and Planetary Sciences, v. 28, no. 1, p. 211–280, doi:10.1146/annurev.earth.28.1.211.

Yin, A., Manning, C.E., Lovera, O., Menold, C.A., Chen, X., and Gehrels, G.E., 2007b, Early Paleozoic tectonic and thermomechanical evolution of ultrahigh-pressure (UHP) metamorphic rocks in the northern Tibetan Plateau, Northwest China: International Geology Review, v. 49, p. 681–716, doi:10.2747/0020-6814.49.8.681.

Yuan, W., Dong, J., Shicheng, W., and Carter, A., 2006, Apatite fission track evidence for Neogene uplift in the eastern Kunlun Mountains, northern Qinghai–Tibet Plateau, China: Journal of Asian Earth Sciences, v. 27, p. 847–856, doi:10.1016/j.jseaes.2005.09.002.

Yuan, C., Sun, M., Xiao, W., Wilde, S., Li, X., Liu, X., Long, X., Xia, X., Ye, K., and Li, J., 2009, Garnet-bearing tonalitic porphyry from East Kunlun, Northeast Tibetan Plateau: implications for adakite and magmas from the MASH Zone: International Journal of Earth Sciences, v. 98, p. 1489–1510, doi:10.1007/s00531-008-0335-y.

Yuan, D.-Y., Ge, W.-P., Chen, Z.-W., Li, C.-Y., Wang, Z.-C., Zhang, H.-P., Zhang, P.-Z., Zheng, D.-W., Zheng, W.-J., Craddock, W.H., Dayem, K.E., Duvall, A.R., Hough, B.G., Lease, R.O., et al., 2013, The growth of northeastern Tibet and its relevance to large-scale continental geodynamics: A review of recent studies: Tectonics, v. 32, p. 1358–1370, doi:10.1002/tect.20081.

Yue, Y., Graham, S. A., Ritts, B. D., and Wooden, J. L., 2005, Detrital zircon provenance evidence for large-scale extrusion along the Altyn Tagh fault: Tectonophysics, v. 406, p. 165–178. http://doi.org/10.1016/j.tecto.2005.05.023.

Yue, Y., Ritts, B.D., Graham, S.A., Wooden, J.L., Gehrels, G.E., and Zhang, Z., 2003, Slowing extrusion tectonics: lowered estimate of post-Early Miocene slip rate for the Altyn Tagh fault: Earth and Planetary Science Letters, v. 217, p. 111–122, doi:10.1016/S0012-821X(03)00544-2.

Zahid, K. M., and Barbeau, D. L., 2011, Constructing sandstone provenance and classification ternary diagrams using and electronic spreadsheet: Journal of Sedimentary Research, v. 81, p. 702-707.

Zhang, C.L., Lu, S.N., Yu, H.F., and Ye, H.M., 2007, Tectonic evolution of the Western Kunlun orogenic belt in northern Qinghai-Tibet Plateau: Evidence from zircon SHRIMP and LA-ICP-MS U-Pb geochronology: Science in China, Series D: Earth Sciences, v. 50, p. 825–835, doi:10.1007/s11430-007-2051-z.

Zhang, H.-P., Craddock, W.H., Lease, R.O., Wang, W., Yuan, D.-Y., Zhang, P.-Z., Molnar, P., Zheng, D.-W., and Zheng, W.-J., 2012, Magnetostratigraphy of the Neogene Chaka basin and its implications for mountain building processes in the

north-eastern Tibetan Plateau: Basin Research, v. 24, p. 31–50, doi:10.1111/j.1365-2117.2011.00512.x.

Zhang, J.Y., Ma, C.Q., Xiong, F.H., Liu, B., 2012, Petrogenesis and tectonic significance of the Late Permian-Middle Triassic calc-alkaline granites in the Balong region, eastern Kunlun Orogen, China: Geological Magazine, v. 149, p. 892-908.

Zhang, P.Z., Shen, Z., Wang, M., Gan, W., Bürgmann, R., Molnar, P., Wang, Q., Niu, Z., Sun, J., Wu, J., Hanrong, S., and Xinzhao, Y., 2004, Continuous deformation of the Tibetan Plateau from global positioning system data: Geology, v. 32, p. 809–812, doi:10.1130/G20554.1.

Zhang, Y., and Zheng, J., 1994, Geologic overview in Kokshili, Qinghai and adjacent areas: Seismological Publishing House, Beijing.

Zheng, D., Clark, M.K., Zhang, P., Zheng, W., and Farley, K. A., 2010, Erosion, fault initiation and topographic growth of the North Qilian Shan (northern Tibetan Plateau): Geosphere, v. 6, p. 937–941, doi:10.1130/GES00523.1.

Zhuang, G., Hourigan, J.K., Ritts, B.D., and Kent-Corson, M.L., 2011, Cenozoic multiple-phase tectonic evolution of the northern Tibetan Plateau: Constraints from sedimentary records from Qaidam basin, Hexi Corridor, and Subei basin, northwest China: American Journal of Science, v. 311, p. 116–152, doi:10.2475/02.2011.02.

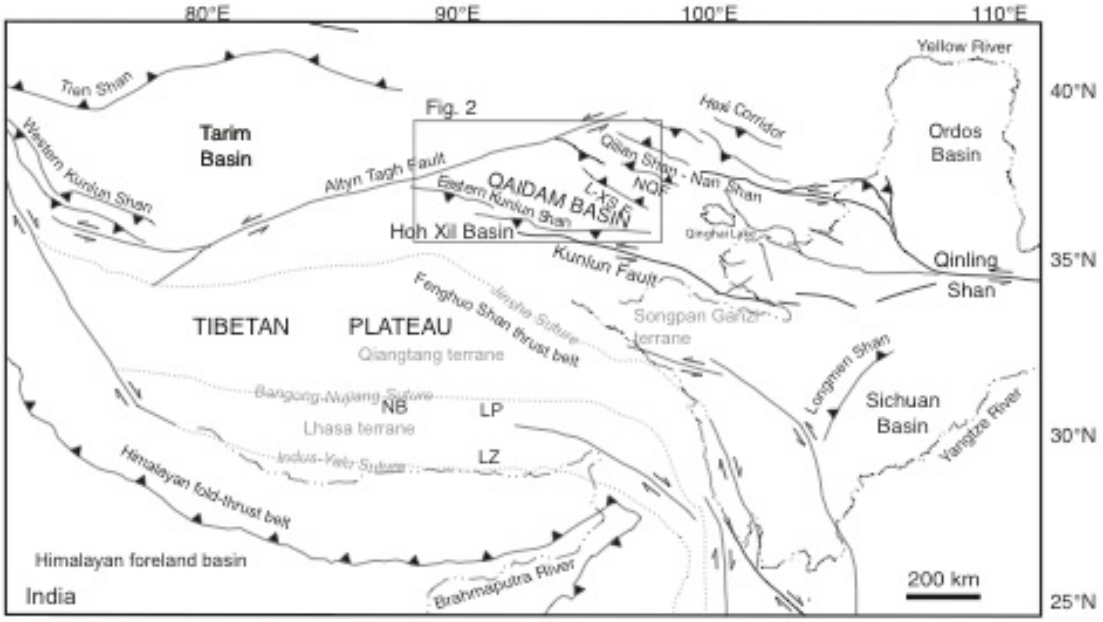

Figure 2.1: Tectonic map of the Tibetan Plateau showing major faults, Cenozoic basins, terranes, sutures, and rivers (Adapted from Horton et al., 2004). ATF: Altyn Tagh Fault; L-XS F: Lulian Shan-Xitie Shan Fault; LP: Lunpola Basin; LZ: Linzhou Basin; NM: Nima Basin; NQF: North Qaidam Fault.

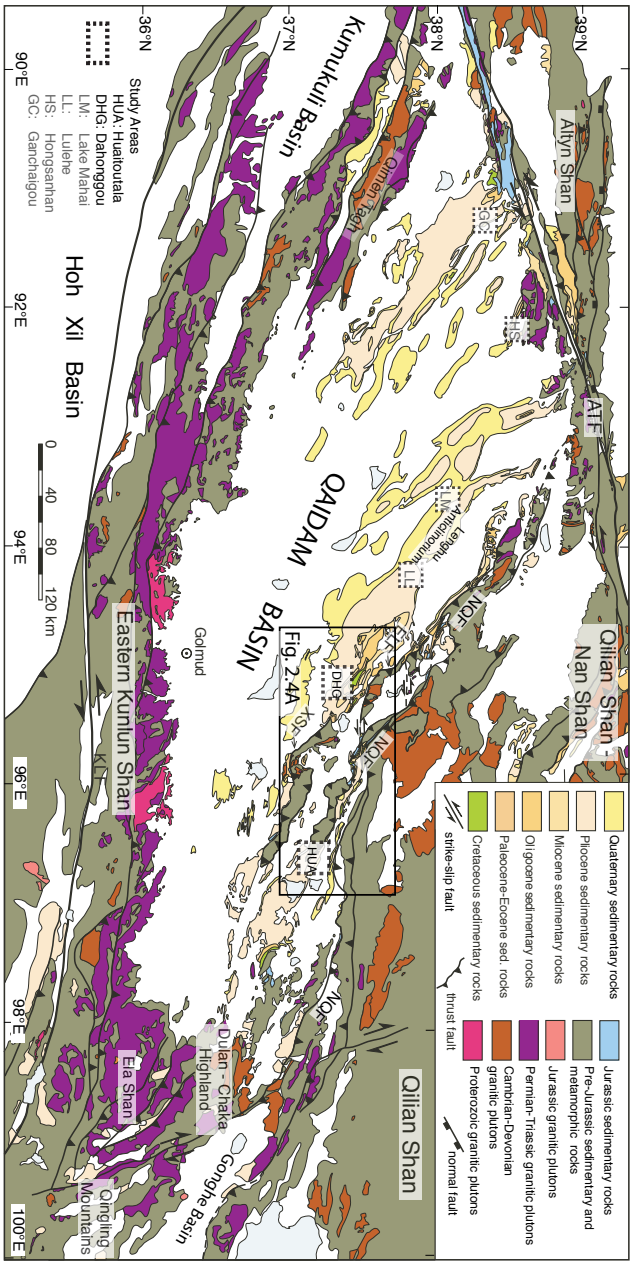

Figure 2.2: Geologic map of the Qaidam Basin (modified from Chen et al., 2012) and surroundings showing major structures, rock units, and study localities (dashed boxes) DHG and HUA (this study) and LM, LL, GC, and HS (Zhuang et al., 2011). ATF: Altyn Tagh Fault; ELF: East Luliang Fault; KLF: Kunlun Fault; NQF: North Qaidam Fault; XSF: Xitie Shan Thrust.

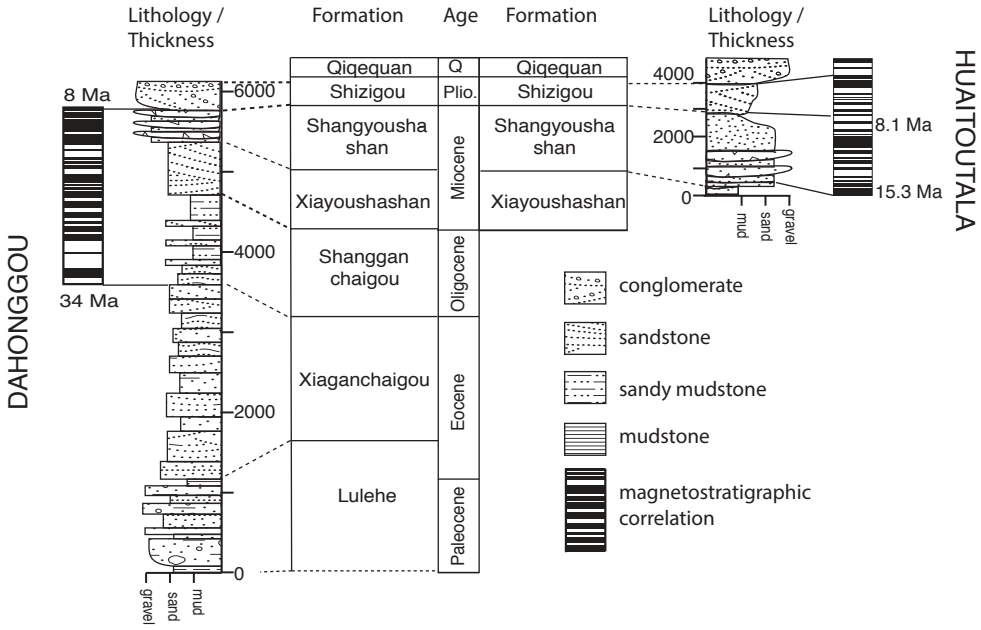

Figure 2.3: Stratigraphic framework for the Qaidam Basin, including formation names and ages, lithologies, meter levels, and magnetostratigraphic correlations for the Dahonggou (Lu and Xiong, 2009) and Huaitoutala (Fang et al., 2007) sections.

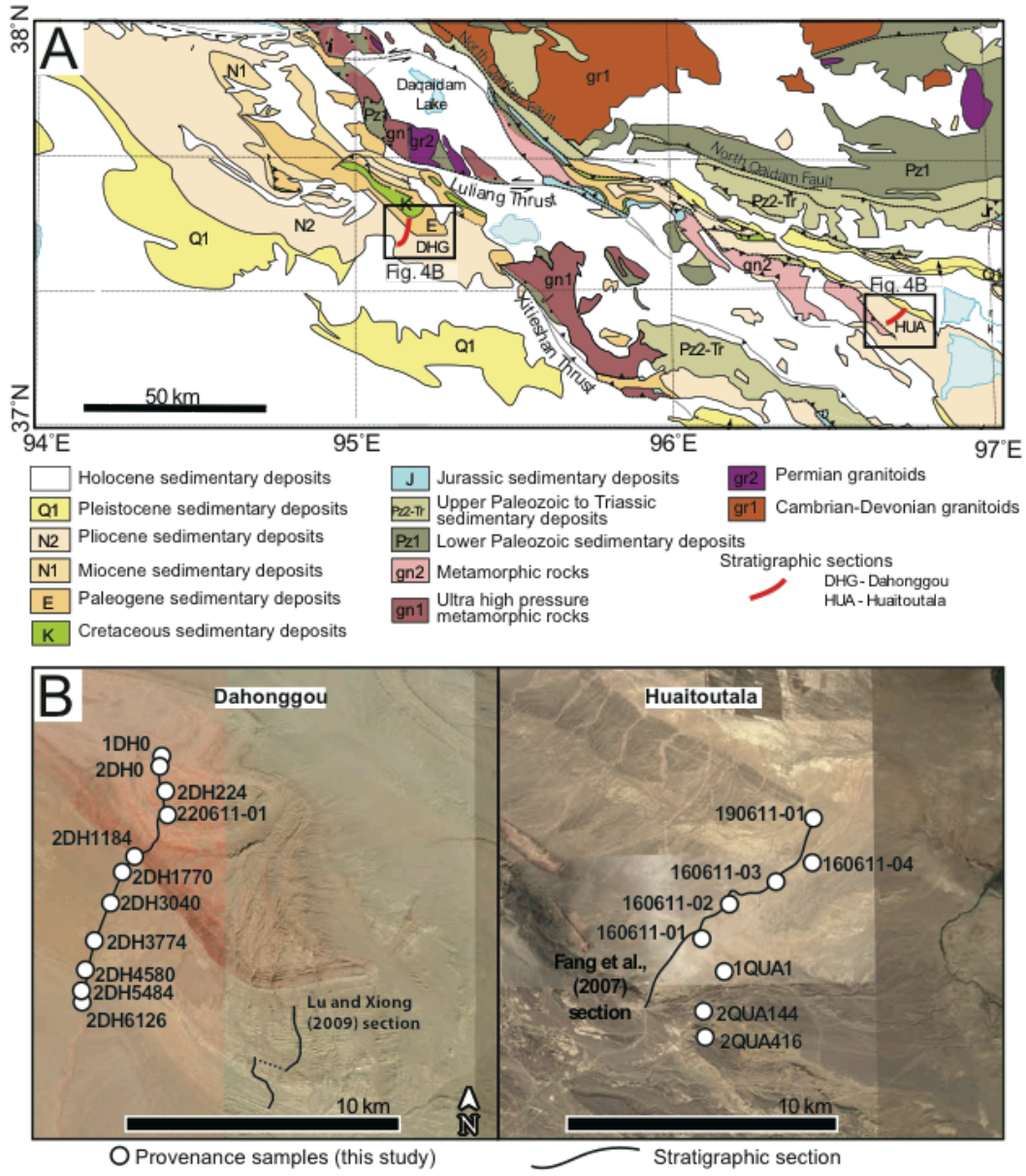

Figure 2.4: (A) Geologic map of the northern margin of the Qaidam Basin (modified from Yin et al., 2008a) showing localities for this study. (B) Satellite images of Dahonggou and Huaitoutala localities, with measured section traces (this study; Fang et al., 2007) and provenance samples locations.

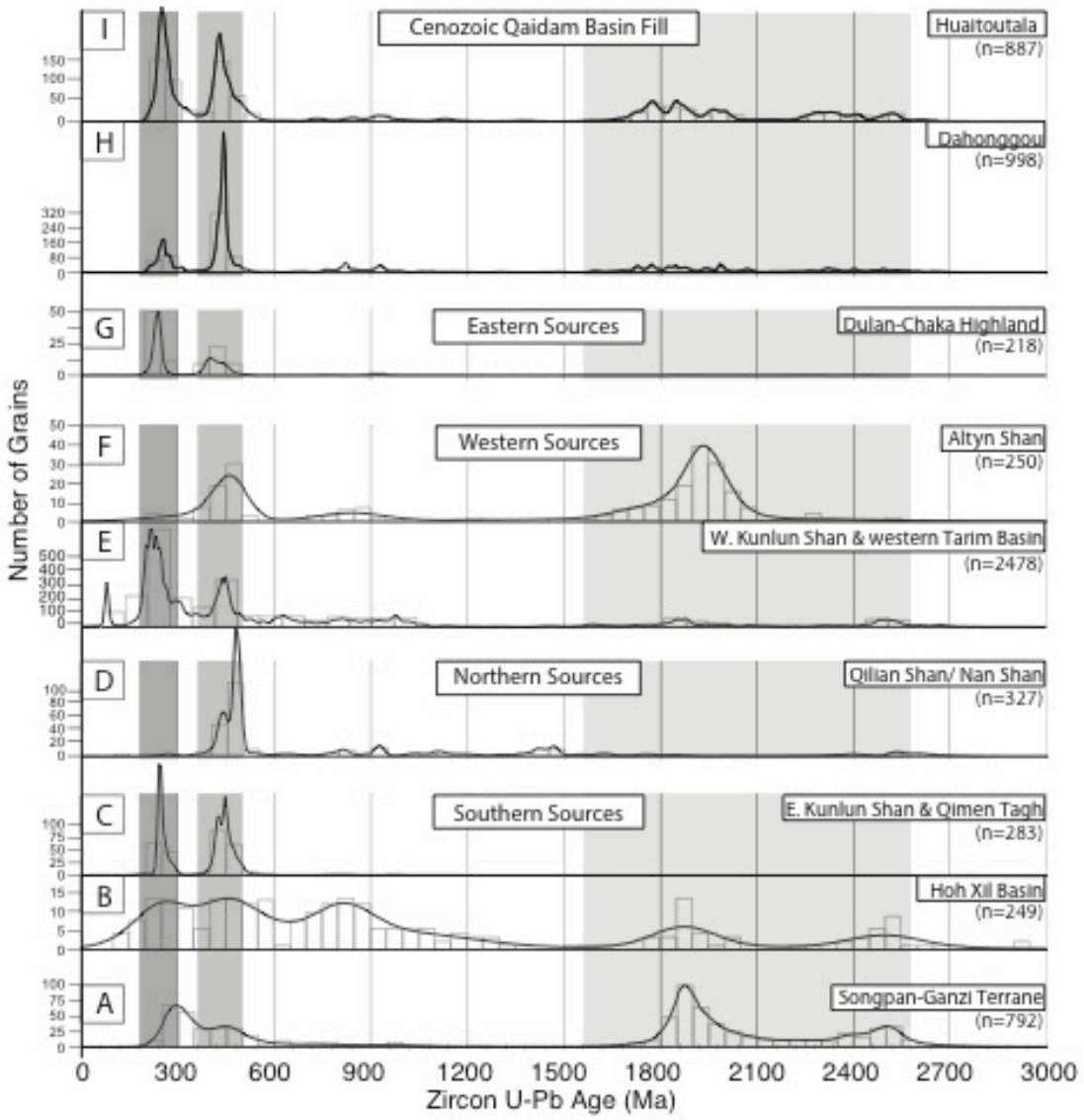

Figure 2.5: Histograms and kernel density estimates for source area detrital and magmatic zircon data. Grey vertical bars indicate the major populations identified in Cenozoic Qaidam Basin fill in this study. (A) Songpan-Ganzi Basin (Weislogel et al., 2010). (B) Hoh Xil Basin (Dai et al., 2012) (C) Eastern Kunlun Shan and Qimen Tagh (Cowgill et al., 2003; Pullen et al., 2011; Li et al., 2013). (D) Western Kunlun Shan and western Tarim Basin (Bershaw et al., 2012; Robinson et al., 2012; Carrapa et al., 2014). (E) Qilian Shan–Nan Shan, and North Qaidam (Cowgill et al., 2003; Gehrels et al., 2003; Menold, 2006; Yan et al., 2010). (F) Altyn Shan (Cowgill et al., 2003; Gehrels et al., 2003) (G) Dulan-Chaka highland (Liu et al., 2004; Wu et al., 2004; Chen et al., 2012) (H) All Dahonggou samples from this study. (I) All Huaitoutala samples from this study.

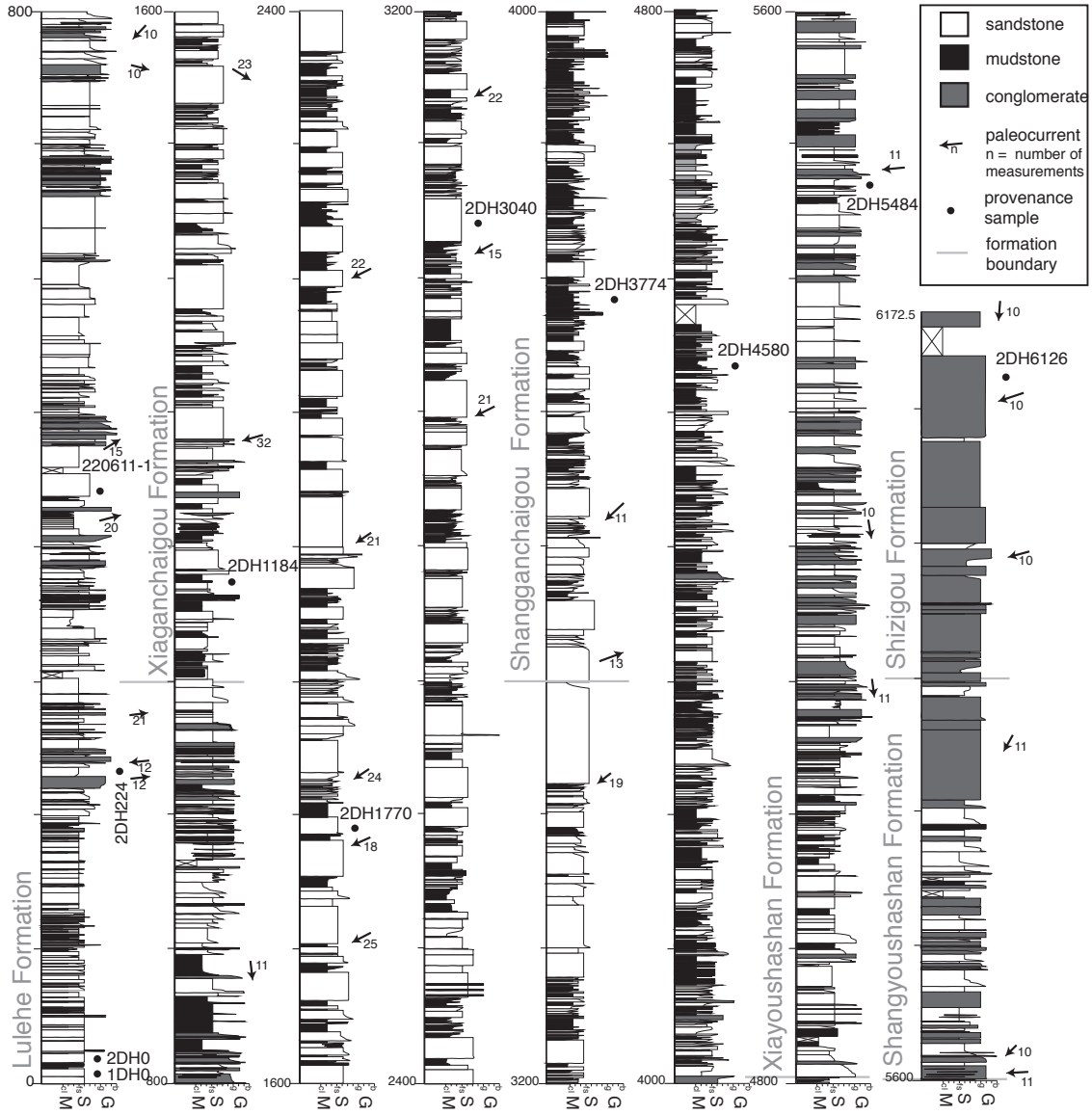

Figure 2.6: Measured stratigraphic section at the Dahonggou anticline, with paleocurrent orientations and provenance sample locations.

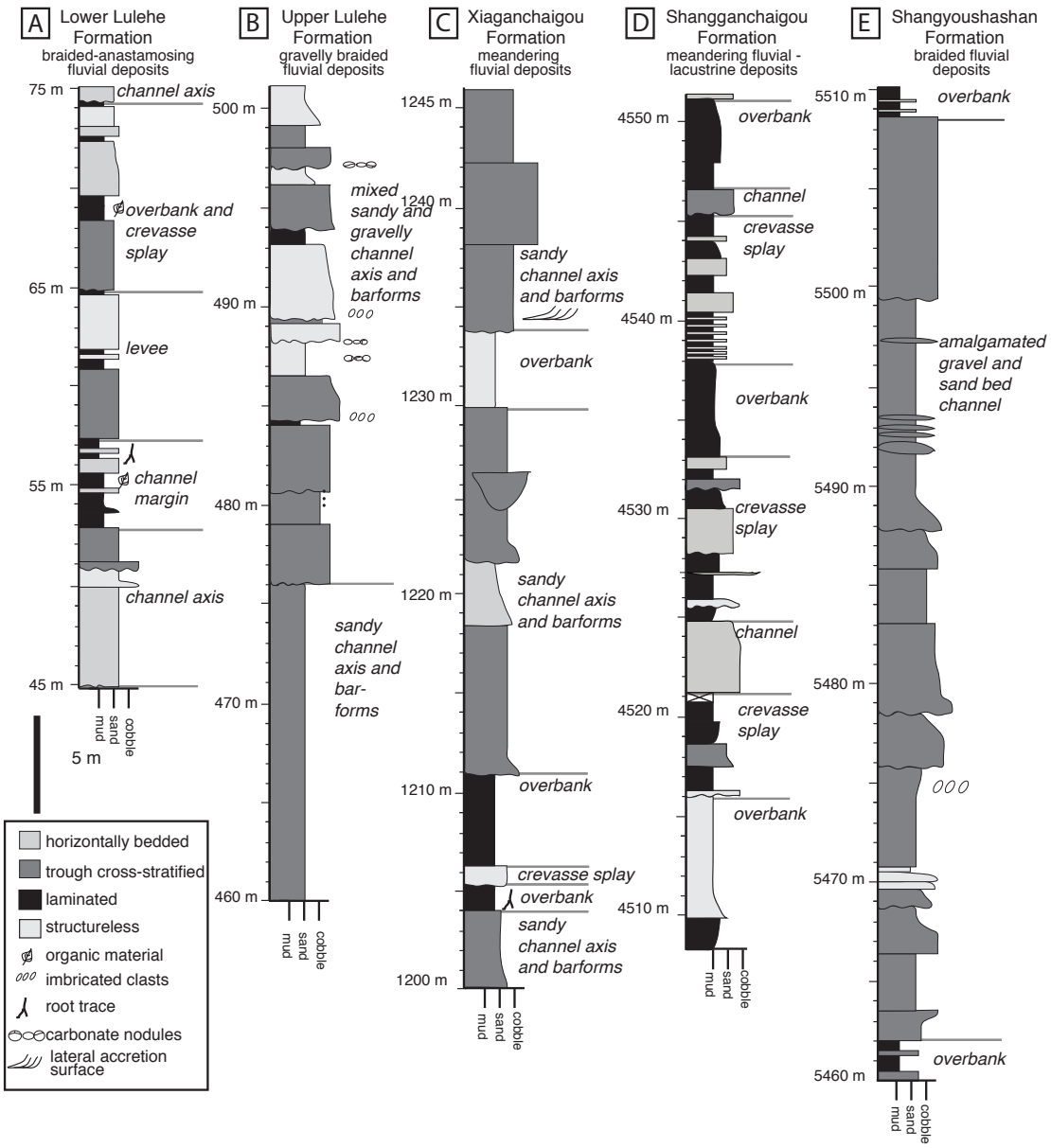

Figure 2.7: Representative stratigraphic columns for major depositional environments of the Dahonggou section. (A) Braided-anastomosing fluvial deposits of the Lower Lulehe Formation. (B) Gravelly braided fluvial deposits of the Upper Lulehe Formation. (C) Meandering fluvial deposits of the Xiaganchaigou Formation. (D) Meandering fluvial-lacustrine deposits of the Shangganchaigou Formation. (E) Braided fluvial deposits of the Shangyoushashan Formation.

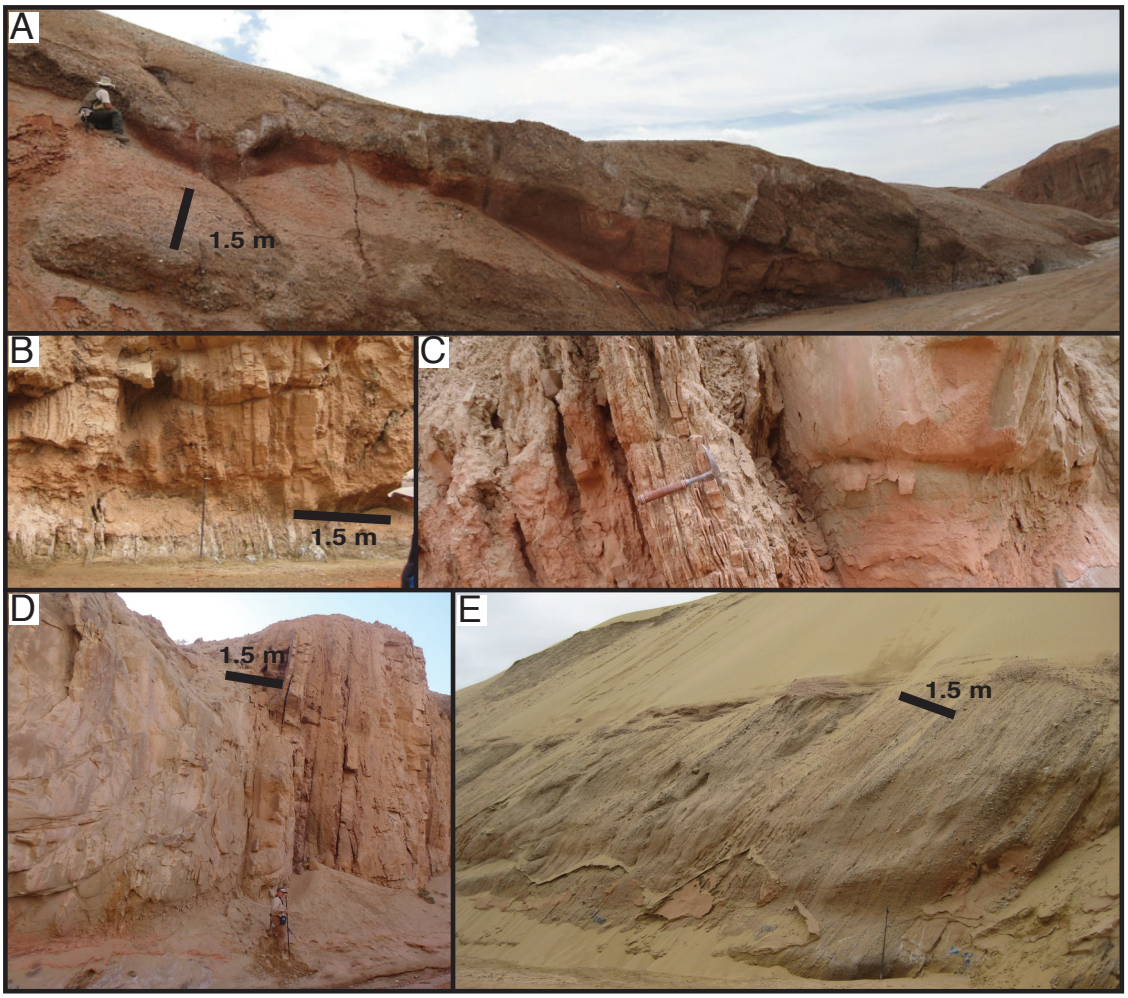

Figure 2.8: Field photographs of lithofacies and stratigraphic units at the Dahonggou section. Stratigraphic levels refer to Figure 2.6. (A) Erosive, laterally continuous conglomerate beds interbedded with structureless mudstone and sandstone. Lulehe Formation, 480 m. (B) Interbedded sandstone and mudstone. Sandstone packages thickness and frequency increases upwards. Xiaganchaigou Formation, 1940 m. (C) Structureless, red and green mottled mudstone. 1-10 cm beds of ripple cross-stratified and horizontally laminated fine-grained sandstone, increasing in thickness up to a sharp contact with trough cross-stratified medium-grained sandstone bed. Xiaganchaigou Formation, 2970 m. (D) Thick package of trough cross-stratified sandstone capped by interbedded mudstone and sandstone. Xiaganchaigou Formation, 3200 m. (E) Trough cross-stratified pebble conglomerate and medium- to coarse-grained sandstone. Shangyoushashan Formation, 5965 m.

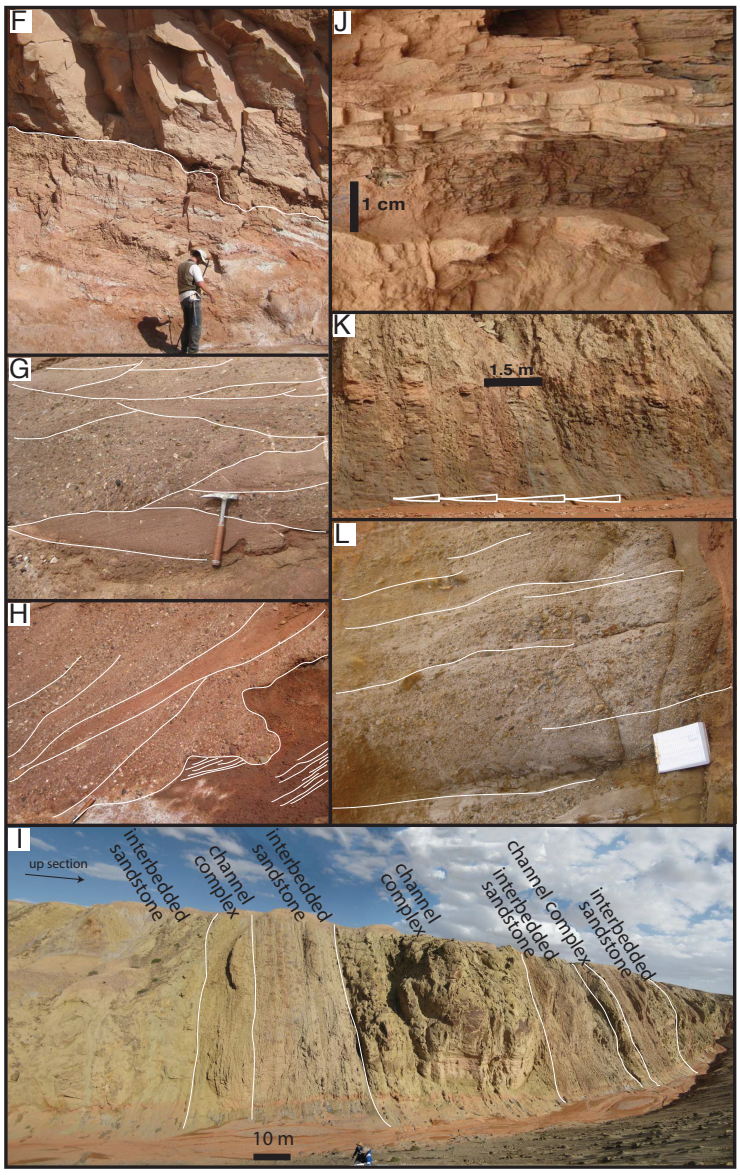

Figure 2.8, continued. (F) Amalgamated trough cross-stratified sandstone overlying laminated red mudstone. Lulehe Formation, ~50 m. (G) Interbedded coarse-grained cross-bedded sandstone and clast-supported pebble conglomerate, Lulehe Formation, 489 m. (H) Structureless to laminated red mudstone incised by trough cross-stratified clast-supported pebble conglomerate. Lulehe Formation, 815 m. (I) Two amalgamated channel complexes separated by interbedded sandstone and mudstone. Xiaganchaigou Formation, 2800 m. Upsection to the right. (J) Bidirectional current ripple cross stratification. Shangganchaigou Formation, 4523 m. (K) Upward coarsening packages of sandy siltstone to fine sandstone. Shangganchaigou Formation, 3659.7 m. (L) Horizontally bedded clast-supported pebble-cobble conglomerate interbedded with coarse- to very coarse-grained sandstone. Shangyoushashan Formation, 5603 m.

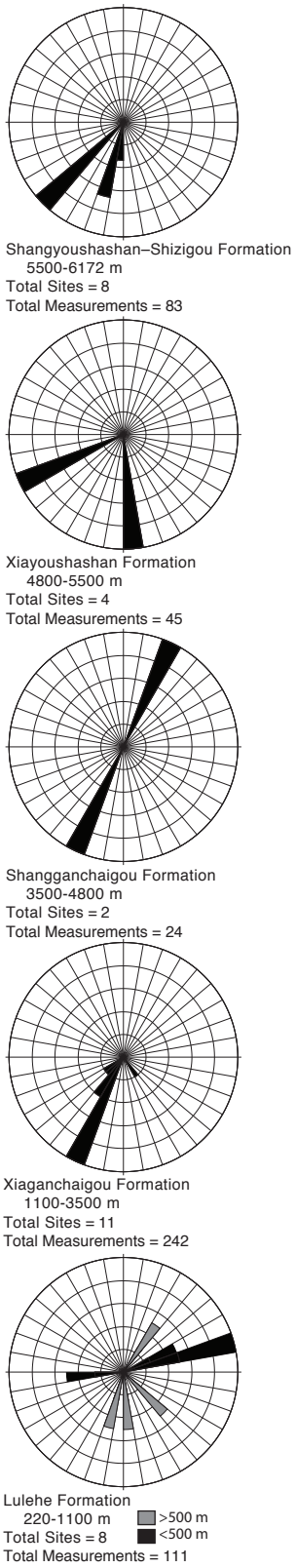

Figure 2.9: Rose diagrams for paleocurrents from Dahonggou section shown in Fig. 2.6.

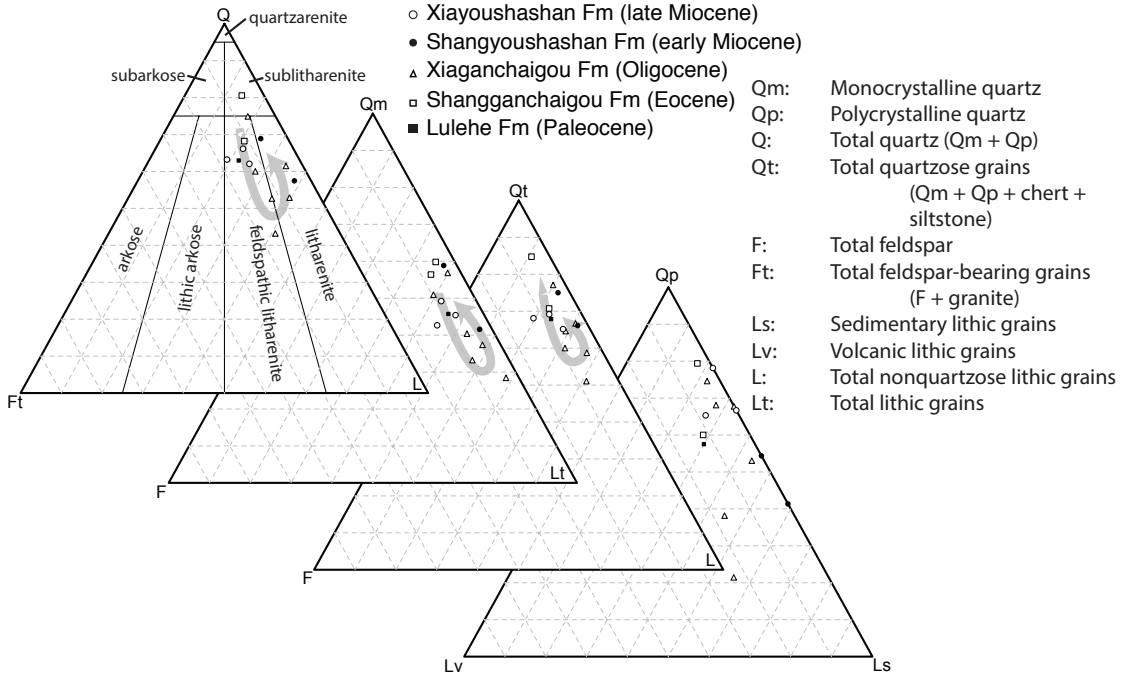

Figure 2.10: Ternary diagrams of sandstone petrographic data. Light grey arrow highlights an an upsection decrease in maturity between the Shangganchaigou and Xiaganchaigou formations followed by a return to more mature sandstone compositions between the Xiaganchaigou and Shangyoushashan formations. Fields for the leftmost ternary diagram are from Folk (1980). Ternary diagrams were created using Ternplot (Zahid and Barbeau, 2011).

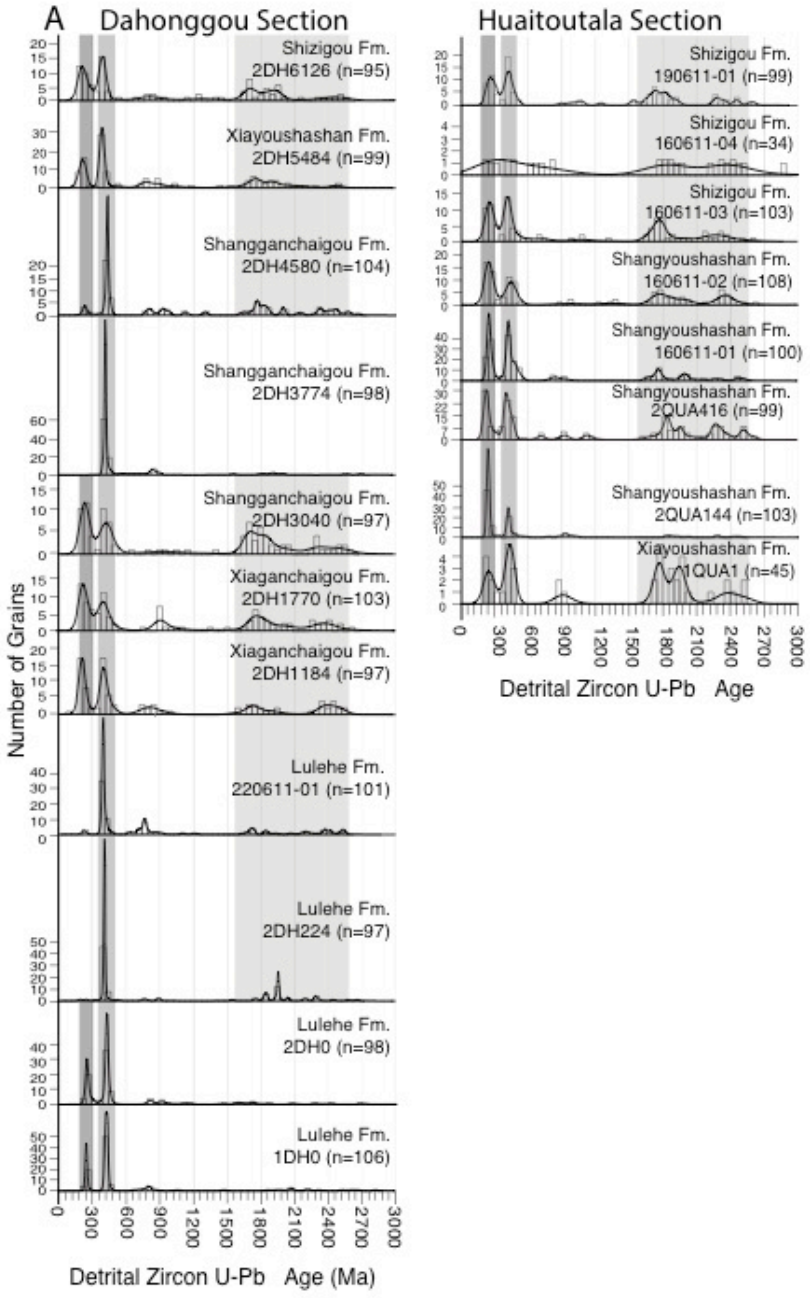

Figure 2.11: (A) Kernel density estimates and histograms for detrital zircon U-Pb age data showing geochronologic results for 11 samples from the Dahonggou section and 8 samples from the Huaitoutala section (locations shown in Figs. 2.2 and 2.5). Samples are presented in stratigraphic order and grouped by locality. Shaded bars indicate the presence or absence of major source populations: Permian-Triassic; early Paleozoic; Paleoproterozoic.

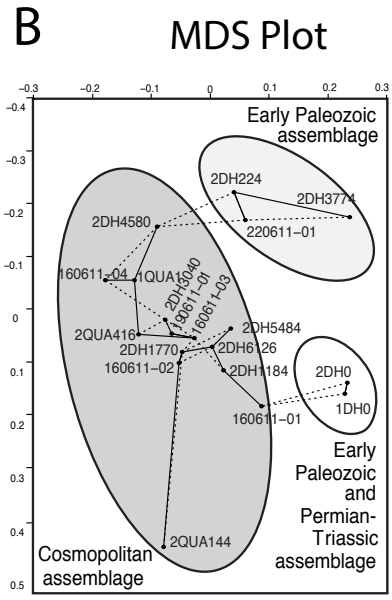

Figure 2.11, continued: (B) Multi-dimensional scaling plot (dimensionless space) for all Dahonggou and Huaitoutala detrital zircon samples, generated following methods outlined by Vermeesch (2013). Solid line indicates nearest neighbor, dashed line indicates second nearest neighbor.

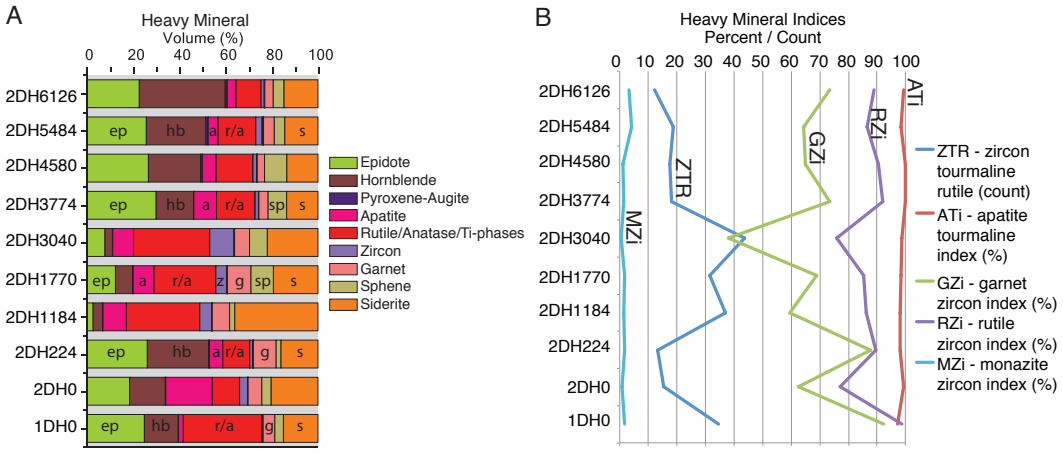

Figure 2.12: Heavy mineral assemblages from Dahonggou section, plotted in stratigraphic order. (A) Heavy mineral relative abundances for heavy minerals comprising >2% of the sample. (B) Heavy mineral indices. ZTR = zircon-tourmaline-rutile index (zircon + tourmaline + rutile counts), ATi = apatite-tourmaline index [100 x apatite count / (total apatite + tourmaline)], GZi = garnet-zircon index [100 x garnet count / (total garnet + tourmaline)], RZi = TiO_2 group - zircon index [100 x TiO_2 count / (total TiO_2 group + zircon)], MZi = monazite-zircon index [100 x monazite count / (total monazite + zircon)].

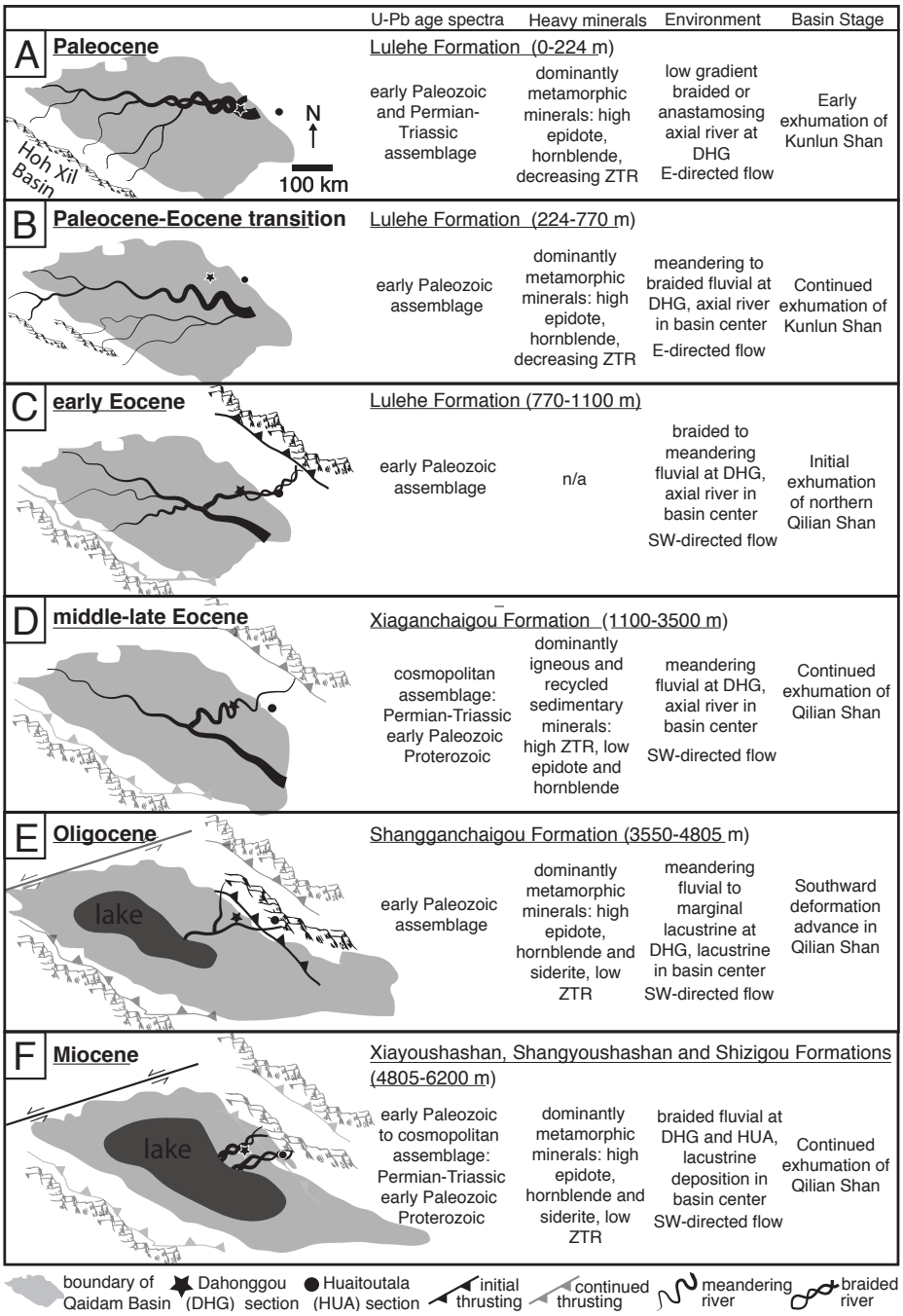

Figure 2.13: Schematic diagrams of the Cenozoic Qaidam Basin evolution. Shaded basin areas from Yin et al., 2008b isopach maps. (A) Paleocene (B) Paleocene-Eocene transition. (C) Early Eocene. (D) Middle-late Eocene. (E) Oligocene. (F) Miocene. Locations of sections shown with black star (Dahonggou) and black circle (Huaitoutala). Black fault and mountain symbols show initial deformation; grey fault and mountain symbols show continued deformation and unroofing.

Chapter 3: Detrital record of initial basement exhumation along the Laramide deformation front, southern Rocky Mountains[1]

ABSTRACT

New geochronological constraints on upper crustal exhumation in the southern Rocky Mountains help delineate the latest Cretaceous–Paleogene history of drainage reorganization and landscape evolution during Laramide flat-slab subduction beneath western North America. Detrital zircon U-Pb results for the Raton basin of southern Colorado and northern New Mexico define the inception of coarse-grained siliciclastic sedimentation and a distinctive shift in provenance, from distal to proximal sources, that recorded shortening-related uplift and unroofing along the Laramide deformation front of the northern Sangre de Cristo mountains. This Maastrichtian–early Paleocene (~70-65 Ma) change—from distal foreland accumulation of sediment derived from the thin-skinned Cordilleran (Sevier) fold-thrust belt to coarse-grained sedimentation proximal to a Laramide basement block uplift—reflects cratonward (eastward) deformation advance and reorganization of drainage systems that supplied a large volume of Paleocene–lower Eocene sediments to the Gulf of Mexico. The timing of unroofing along the eastern deformation front is synchronous with basement-involved shortening across the interior of the Laramide province, suggesting abrupt wholesale uplift rather than a systematic

[1]This chapter was published in September 2016. Author contributions to the authorship are as follows: M. Bush: 80%, B. Horton: 10%; M. Murphy: 5%; D. Stockli: 5%.

Bush, M.A., Horton, B.K., Murphy, M.A., and Stockli, D.F., 2016a, Detrital record of initial basement exhumation along the Laramide deformation front, southern Rocky Mountains: Tectonics, doi: 10.1002/2016TC004194.

inboard advance of deformation. The growth and infilling of broken foreland basins within the interior and margins of the Laramide province had a significant impact on continental-scale drainage systems, as several ponded/axial Laramide basins trapped large volumes of sediment and induced reorganization of major source-to-sink sediment pathways.

INTRODUCTION

Laramide basement uplift during Late Cretaceous–Paleogene shallow subduction of the oceanic Farallon slab triggered extensive landscape reorganization of western North America (Dickinson et al., 1988; Carroll et al., 2006; Lawton, 2008; Humphreys, 2009). In addition to large-scale partitioning of the Cordilleran (Sevier) foreland basin into a series of compartmentalized basins, vast segments of western North America underwent substantial changes in drainage configurations. The reorganization of major sediment pathways affected not only the plate-interior Laramide province but also the Cordilleran (Sevier) fold-thrust belt and Cordilleran (Sierra Nevada) magmatic arc, including the western (California-Nevada; Wernicke, 2011), northern (Idaho; Chetel, 2011), and southern (Colorado-New Mexico; Potochnik, 1989; Cather, 2004) zones of the Late Cretaceous–Paleogene convergent margin. Within this framework, the most pronounced shifts in continental-scale drainage patterns, including triggering of widespread closed drainage systems, were induced by uplift along the eastern deformation front of the Laramide orogenic system. However, the precise record of this shortening, which generated a >1000 km long topographic barrier—the Sangre de Cristo and Front Range systems of New Mexico and Colorado—remains incomplete (Tweto,

1975, 1980; Erslev, 1993; Lindsey, 1998; Chapin et al., 2014). Initial basement-involved shortening may have affected the entire Laramide province simultaneously, but the termination of deformation spanned from the Maastrichtian in Montana to the Oligocene in New Mexico and Colorado (Dickinson et al., 1988; Constenius, 1996; Copeland et al., 2011). Particularly in the southern Rocky Mountain Laramide province, it is unclear how (in terms of abrupt versus protracted uplift) and when (during the latest Cretaceous through Oligocene) the frontal topographic barrier was established.

In addition to important shifts in river drainage patterns, uplift of a plate-interior topographic barrier along the Laramide deformation front played an essential role in (1) governing the growth and isolation of a series of broken foreland basins (Dickinson et al., 1988; Carroll et al., 2006; Lawton, 2008), (2) generating a climatic response involving enhanced orographic precipitation versus aridification on opposing flanks of the barrier (Raynolds et al., 2007), and (3) triggering the initial influx of voluminous siliciclastic sediment into the Gulf of Mexico basin, including deposition of all major deepwater reservoir units (Winker, 1982; Galloway, 2011; Mackey et al., 2012). Furthermore, coupling of the Farallon and North American plates during flat slab subduction is suggested as the cause for Laramide deformation (Saleeby, 2003; Heller and Liu, 2016; Yonkee and Weil, 2015). Therefore, a more precise record of exhumation along the cratonal (eastern) limit of Laramide deformation provides critical ground truths for models describing the time-space evolution of Farallon-North America interactions, with specific constraints on the onset and duration of shortening along the deformation front defined by the Sangre de Cristo and Front Range systems.

GEOLOGIC FRAMEWORK

Thin-skinned structures of the Cordilleran (Sevier) retroarc fold-thrust belt propagated eastward from latest Jurassic through Cretaceous time, generating an eastward migrating foreland basin system characterized by a combination of marine and nonmarine sedimentation (Robinson Roberts and Kirschbaum, 1995; DeCelles, 2004). During the latest Cretaceous, an important shift took place in which shortening commenced across the Cordilleran foreland and was manifest as thick-skinned, basement-cored uplifts of the Laramide province of the North American interior. The eastern deformation front consisted of the linked Sangre de Cristo and Front Range systems of New Mexico and Colorado, key elements of the modern Rocky Mountains. Siliciclastic synorogenic strata in the Raton basin of northern New Mexico and southern Colorado provide a comprehensive detrital record of topographic growth and eastward advance of the Jurassic–Cretaceous Cordilleran (Sevier) fold-thrust belt to the Laramide basement province.

The Cretaceous–Paleogene Raton basin (Fig. 3.1) contains a depositional record of both Cordilleran thrusting and Laramide basement uplift. Basin-fill units (Fig. 3.2) represent a progradational sequence of marine, marginal marine, coastal and alluvial depositional environments influenced by major tectonic and climatic shifts (Cather, 2004).

Albian–Campanian Purgatoire Formation, Dakota Formation, Benton Group, and Niobrara Formation are regionally extensive siliciclastic units deposited principally in shallow marine settings of the Western Interior Seaway (MacKenzie and Poole, 1962; Baltz, 1965; McGookey, 1972; Robinson Roberts and Kirschbaum, 1995). The lower

units constitute an unconformity-bounded transgressive sequence of shales, sandstones, and conglomerates representing the maximum inundation of the seaway as it gradually covered northern New Mexico. The Niobrara Formation is comprised of both carbonate and clay-rich marine deposits.

Campanian to lower Maastrichtian deposits of the Pierre Shale and overlying Trinidad Sandstone (Fig. 3.2) mark the final regression and shift to nonmarine accumulation of the progressively more proximal deltaic, fluvial, and alluvial fan systems recorded by the Maastrichtian Vermejo Formation. Transgressive tongues of the Trinidad Sandstone within the Vermejo Formation are present along the southern margin of the Raton basin (Lee, 1917; Wanek, 1963).

Upper Campanian–Maastrichtian shallow marine deposits of the Trinidad and Vermejo Formations are unconformably overlain by the increasingly proximal, fluvial deposits of the upper Maastrichtian–Paleocene Raton Formation, Paleocene–Eocene Poison Canyon Formation, and Eocene–Oligocene Cuchara, Huerfano, and Farisita Formations (Fig. 3.2) (Johnson et al., 1966; Flores and Pillmore, 1987; Pillmore and Flores, 1987, 1990). In turn, these uppermost Maastrichtian–Oligocene sedimentary units are overprinted by late Oligocene to middle Miocene mafic to intermediate igneous rocks, including the Spanish Peaks stocks and radial dikes (Lipman et al., 1972; Penn and Lindsey, 1996).

The proximal western flank of the Raton basin is bounded by the Sangre de Cristo mountains (locally, Culebra range) (Fig. 3.1), a product of Laramide basement-involved shortening and uplift. The deep, east-vergent, range-bounding fault is thought to merge in the Phanerozoic sedimentary cover with a west-vergent thrust fault, defining a triangle

zone in the proximal foreland (Baltz, 1965; Lindsey, 1998). This Laramide fault system has controlled not only the uplift of the main Culebra range, but also the development of the north-trending La Veta syncline, which extends 120 km along the western basin margin with a steep western limb and gentle eastern limb, defining the axis of the Raton basin.

Potential Sediment Sources

Cretaceous through Eocene strata of the Raton basin may be derived from an array of potential sources. Depending on the drainage configurations, potential sediment sources include:

(1) Along the distal western margin, the Jurassic–Cretaceous Cordilleran (Sierra Nevada) magmatic arc produced calc-alkaline granitoid batholiths and related volcanic rocks on the western margin of North America from ~200 to 80 Ma (Busby-Spera et al., 1990; Barth and Wooden, 2006; Dickinson, 2006; Lamaskin, 2012), until the onset of Laramide flat-slab subduction. Two high-flux magmatic events are recorded in the Sierra Nevada batholith during the Jurassic (170–150 Ma) and Cretaceous (100–70 Ma), separated by a ~50 Myr magmatic gap (DeCelles et al., 2009).

(2) The Cordilleran (Sevier) fold-thrust belt formed by crustal shortening associated with ongoing convergence between the North American and Farallon plates, inducing large scale exhumation of principally Neoproterozoic–Mesozoic sedimentary units in thin-skinned thrust sheets (DeCelles, 2004; Horton et al., 2004; Painter et al., 2014; Szwarc et al., 2014).

(3) Jurassic–Cretaceous fill of the Cordilleran (Sevier) foreland basin was exhumed during eastward migration of the deformation front, representing another potential sediment source to the Raton basin (Lawton, 2008; Lawton and Bradford, 2011; Laskowski et al., 2013; Painter et al., 2014; Szwarc et al., 2014). The regionally extensive marine deposits of the Western Interior Seaway were largely recycled as Laramide basement block uplifts partitioned the expansive foreland basin into smaller, late-stage flexural basins.

(4) Basement exposures in the northern Sangre de Cristo mountains are primarily composed of Proterozoic gneiss and Pennsylvanian–Permian sedimentary rocks (Brill, 1952; Tweto, 1975; Lindsey, 1998). The Paleoproterozoic crystalline basement rocks range in age from ~1700-1800 Ma (Jones and Connelly, 2006), correlating them to the Yavapai province (Karlstrom and Humphreys, 1998; Whitmeyer and Karlstrom, 2007).

DETRITAL ZIRCON U-PB GEOCHRONOLOGY

Methods

Detrital zircon provenance analysis produces an age representation of the source components for a given rock sample. By generating a minimum of 117 U-Pb ages for each sandstone sample, this approach identifies all major source components (95% confidence for components comprising >5% of total; Vermeesch, 2004), which are represented in the resultant age-frequency plots (Fig. 3.3). We collected and analyzed 18 sandstone samples from the Raton basin and northern Sangre de Cristo mountains, spanning the Pennsylvanian–Permian Sangre de Cristo Formation to the Eocene–

Oligocene Farisita Formation (Fig. 3.2). Detrital zircon grains were separated using standard heavy mineral separation techniques, and analyzed by laser ablation inductively coupled plasma mass spectrometry (LA-ICP-MS) at the University of Texas at Austin, following methods outlined by Horton et al. (2016). Zircons were mounted on double-sided tape and the outer ~15 μm of each grain were depth profiled to obtain age-resolved profiles; this technique also has the greatest potential to preserve young, outer rims (Marsh and Stockli, 2015). $^{238}U/^{206}Pb$, $^{235}U/^{207}Pb$, and $^{207}Pb/^{206}Pb$ ages were obtained for at least 117 zircons from each sample, using a spot size of 30 μm. Zircon GJ-1 was used as a primary reference material (Jackson et al., 2004) and an in-house secondary age standard was used to evaluate accuracy. Data were processed and ages were calculated using the software package Iolite (Petrus and Kamber, 2012) Further details on sample locations, analytical methodology, and U-Pb data are provided in the supporting information (Appendix B).

Detrital zircon U-Pb ages from the Raton basin are plotted as histograms and probability density plots (Fig. 3.3). Zircon age populations and their ultimate origins include the following, from oldest to youngest: (1) 1600–1800 Ma basement ages representative of the Yavapai and Mazatzal provinces of southwestern North America; (2) ~1400 Ma ages associated with the Mid-Continent granite-rhyolite complex; (3) 1000–1200 Ma Grenvillian ages representative of basement blocks of eastern to southeastern North America, and (4) 400–600 Ma ages associated with Paleozoic rocks of the Appalachian-Ouachita system. Proterozoic grains are consistent with the ages of basement provinces accreted to Laurentia during the Yavapai and Mazatzal orogenies (Whitmeyer and Karlstrom, 2007). The latter two populations likely reflect recycling of

Paleozoic-Mesozoic strata of the Cordilleran hinterland and (Sevier) fold-thrust belt (Dickinson and Gehrels, 2003; 2008a; 2008b). The <250 Ma ages are particularly useful tracers of paleodrainage connectivity, and are diagnostic of arc magmatism in the westernmost Cordilleran system. The U-Pb signatures expressed in the Maastrichtian through Eocene siliciclastic succession of the Raton basin record major provenance changes, wholesale drainage reorganization reflective of basement-involved Laramide uplift, and large-scale unroofing of the northern Sangre de Cristo mountains.

Results

The U-Pb geochronological data help constrain differences in parent populations among the 18 sandstone samples (Fig. 3.2), as revealed in age histograms and probability density plots (Fig. 3.3). Individual U-Pb age concordia plots are presented in the Supporting Information, and U-Pb results are described below. A multi-dimensional scaling analysis (Vermeesch, 2013) based on the Kolmogorov-Smirnov test D value (see Appendix B) allows for the delineation of diagnostic provenance assemblages within the entire dataset (Fig. 3.4). Each assemblage represents derivation from statistically dissimilar parent populations. The two Paleozoic samples (RB105 and RB301) were not included in the multi-dimensional scaling analysis, as they are considered sedimentary basement and sourced from an earlier orogenic phase.

Ancestral Rocky Mountains provenance group

U-Pb ages for the Pennsylvanian-Permian Sangre de Cristo Formation (samples RB105 and RB301) reveal a dominantly unimodal signature of ~1700 Ma (ranging from 1500–1800 Ma), derived from Yavapai–Mazatzal basement rocks. A minor 1400 Ma

peak present in both samples can be associated with isolated plutons found throughout the Rocky Mountain province.

Sevier / Cordilleran provenance group

A very thin Triassic section is overlain by fluvial-eolian facies of the Jurassic Entrada Formation (sample RB302) and marine sandstones of the Cenomanian Dakota Formation (samples RB104 and RB303) deposited in the Western Interior Seaway, the Cordilleran foreland basin in front of the Cordilleran (Sevier) fold-thrust belt. For the Jurassic and Cenomanian samples, prominent peaks found at 171 Ma and 98 Ma (Fig. 3.3), correspond to magmatic high flux events in the Cordilleran magmatic arc (Ducea, 2001; DeCelles et al., 2009). Additional peaks at 421 Ma, 595 Ma, and 1000–1200 Ma are also present in the Paleozoic–Mesozoic strata of southwestern North America, particularly in deposits of the Colorado Plateau ultimately sourced from the Appalachian orogen (Dickinson and Gehrels, 2009). There is a diminished presence of Proterozoic grains in these samples, with very minor peaks at 1400 Ma and 1800 Ma.

A unimodal U-Pb age population centered at ~73 Ma characterizes the lower Maastrichtian Trinidad Formation (sample RB111) (Fig. 3.3). This age is consistent with the latest phases of volcanism in the Cordilleran arc. Approximately 30 Proterozoic-age grains dated from this sample indicate a minor input of basement and/or recycled sources.

Initial Laramide provenance group

The Maastrichtian Vermejo Formation (sample RB107) and lower Raton Formation (samples RB112, RB208, and RB207) have two age peaks in the Cordilleran arc range, at ~70 Ma and ~170 Ma (Fig. 3.3). Additionally, the first major input of Proterozoic ages in the Mesozoic units appears in these samples. The grains with 1400

Ma and 1700 Ma ages in these samples are likely derived directly from local basement exposures and/or from recycled grains derived from the erosion of the Pennsylvanian-Permian Sangre de Cristo Formation.

Laramide provenance group

In detrital zircon signatures from Paleocene Raton Formation (samples RB109 and RB206), the Paleocene-Eocene Poison Canyon Formation (samples RB113 and RB201) there is a significant absence of all arc-derived (<200 Ma) grains. Rather, these samples are dominated by Yavapai and Mazatzal ages (1600–1800 Ma).

Late Laramide provenance group

The uppermost sample from the Poison Canyon Formation (sample RB108), along with the Eocene Cuchara Formation (sample RB103), Huerfano Formation (sample RB402), and Farisita Formation (sample RB401) are comparable to the underlying Poison Canyon Formation samples with the addition of a second major Proterozoic peak, at ~1400 Ma.

SEDIMENT ACCUMULATION HISTORY

Depositional Age Constraints

The U-Pb ages help constrain the maximum depositional ages of several Upper Cretaceous–Paleocene units that have proven difficult to date by other means, largely due to lack of critical index fossils with a narrow age range (e.g., Pillmore and Flores, 1987; and references therein). For samples with a clear population of youngest U-Pb ages, we report a weighted mean age that represents the maximum depositional age of the sampled horizon (see Appendix B; Walker et al., 2012). In several cases, the ages are slightly

younger than the previously inferred depositional age, leading us to suggest that some results approximate the true depositional (stratigraphic) age. For these cases, the ultimate source of magmatic zircon is considered to be syndepositional volcanogenic processes in the western magmatic arc and long-distance transport, both by air and water, of zircon grains of volcanic origin.

Mid-Cretaceous deposition of the Dakota Formation is confirmed by young age peaks considered to approximate the depositional age. The lower and upper samples yield young grains clustered at 102–92 Ma, with weighted mean ages of 100.4 ± 6.3 Ma (n=3 youngest grains; RB303) and 93.7 ± 1.9 Ma (n=4 youngest grains; RB104), respectively, consistent with a late Albian–Cenomanian age of deposition (Tidwell et al., 2007; Currie et al., 2008).

The Trinidad Formation lacks diagnostic fossils but has been assigned a Maastrichtian age on the basis of its conformable relationship above the upper Pierre Shale, which is dated as Maastrichtian by ammonite fossils (Pillmore and Flores, 1987). The grains from Trinidad Formation sample RB111 are predominantly Cenozoic, and have not been corrected for common Pb. This results in discordant ages, but still provides general age constraints for the formation. The youngest 3 grains from the Trinidad Formation yield a weighted mean age of 66.9 ± 2.1 Ma (n=3 youngest grains; RB111). This result raises the possibility that facies that are lithostratigraphically defined as the upper Trinidad Formation may range into the early Paleocene.

The overlying Maastrichtian–lower Paleocene Vermejo and Raton Formations, which include the well-resolved K-Pg boundary from palynomorphs (Ash and Tidwell, 1976; Pillmore et al., 1984; Tschudy et al., 1984) and an iridium anomaly (Orth et al.,

1987), yield the following weighted mean ages: 64.1 ± 1.9 Ma (n=2 youngest grains; RB112); 64 ± 1.5 Ma (n=1 young grain; RB109); 62.6 ± 1.9 Ma (n=4 youngest grains; RB107). These results confirm an early Paleocene age and underscore a probable partial lateral equivalence of the Vermejo and Raton Formations. Two additional samples from higher levels of the Raton Formation yield Maastrichtian weighted mean ages that range from 72.2 ± 3.3 Ma (n=3 youngest grains; RB208) to 70.9 ± 0.81 Ma (n=4 youngest grains; RB207). Given the early Paleocene age confirmed for lower levels of the Raton Formation, the older (Maastrichtian) age populations in these two samples are attributed to grains derived from older, pre-depositional volcanic material, and therefore are unlikely to represent the true depositional ages.

Analyzed samples from the overlying Poison Canyon Formation contain a very limited proportion of possibly syndepositional zircon grains, and cannot be confidently regarded as estimates of actual depositional age. However, these single grain ages (61.3 ± 1.1 Ma for youngest grain in RB113 and 59.5 ± 0.7 Ma for youngest grain in RB108) are consistent with a mid- to late Paleocene age, in accordance with past age assignments (e.g., Johnson and Wood, 1956; Baltz, 1965).

Sediment Accumulation History

The tightly clustered Maastrichtian to early Paleocene U-Pb ages for the principal sandstone units—the Trinidad, Vermejo, Raton, and Poison Canyon Formations—highlight the rapid accumulation of siliciclastic material over a short period of time, from broadly 70 to 60 Ma. The composite thickness of these units commonly exceeds 2000 m, requiring a rapid accumulation rate of the Mesozoic–Cenozoic succession in the Raton basin.

In accordance with this result, a several-fold increase in accumulation rates is well documented by reconstructed burial histories based on drilled stratigraphic thicknesses, vitrinite reflectance values, and estimated peak temperatures (Higley, 2007). The long-term accumulation history for the Homer Smith no. 1 well (Fig. 3.5, location in Fig. 3.1) reveals an abrupt increase in sediment accumulation rates during Maastrichtian to early Paleocene basin filling. The ~70 Ma timing of this initial shift to rapid accumulation (Fig. 3.5) closely matches both the increase in grain size (Fig. 3.2) and shift in U-Pb age signatures (Fig. 3.3).

PROVENANCE AND EXHUMATION HISTORY

Six provenance assemblages are distinguished on the basis of chronostratigraphic order and statistical analysis of U-Pb results for the 18 sandstone samples (Fig. 3.4). Below we describe the six distinct provenance assemblages (Figs. 3.3 and 3.4) in the context of the regional tectonic history and the exhumation history of the Sangre de Cristo mountains along the Laramide deformation front (Fig. 3.6).

ANCESTRAL ROCKY MOUNTAINS

The detrital composition, depositional framework, and U-Pb age spectra of two samples from the Pennsylvanian–Permian Sangre de Cristo Formation (samples RB301 and RB105; Figs. 3.2, 3.3, and 3.5) are consistent with derivation from locally sourced basement exposures in the Ancestral Rocky Mountains (ARM) of Colorado and northern New Mexico (Brill, 1952; Mack and Rasmussen, 1984; Hoy and Ridgway, 2002). The Sangre de Cristo Formation is a nonmarine siliciclastic unit, consisting of red and green shale interbedded with medium- to coarse-grained sandstones and pebble-cobble conglomerate and associated with fluvial to alluvial fan deposition in a region proximal

to local basement uplifts. Based on regional isopach and subcrop mapping, several surrounding basement blocks (including the Sierra Grande uplift, Cimarron arch, and Wet Mountain uplift) would have been the principal sources of the first-cycle detritus composing the Sangre de Cristo Formation (Baltz, 1965; Hoy and Ridgway, 2002).

SEVIER (CORDILLERAN) FOLD-THRUST BELT

In the Albian–Campanian, the Western Interior Seaway spanned the Cordilleran foreland basin, from the Cordilleran (Sevier) fold-thrust belt eastward across the present-day Great Plains (Fig. 3.1). In the Raton basin, detrital zircon U-Pb results from the Dakota Formation (samples RB303 and RB104; Fig. 3.2) contains age populations originating in the Cordilleran magmatic arc and Phanerozoic sedimentary cover strata exposed in the growing Sevier (Cordilleran) fold-thrust belt (Figs. 3.3 and 3.5). This pattern suggests a direct paleodrainage connection between the study area and Jurassic–Cretaceous fluvial systems of the Colorado Plateau (Fig. 3.6A).

Studies of Cretaceous strata to the west of the Raton basin have attempted to differentiate between sources in the Sevier (Cordilleran) fold-thrust belt and the Mogollon highlands. Sources of Turonian strata to the west in the Black Mesa and San Juan basin regions are thought to be located to the south in the Mogollon highlands region, feeding into a major north- to northeast-directed longitudinal sediment delivery system (Dickinson and Gehrels, 2008a). By the Campanian, these sediment dispersal systems would have been sourced in the Sevier fold-thrust belt as well as the Mogollon highland (Dickinson and Gehrels, 2008a). Detrital zircon provenance signatures from these two regions do not allow for the differentiation of these two source areas, but for

this study either requires a continent-scale paleodrainage connection with western sources.

The terminal sedimentary basin during the Dakota Formation deposition was to the north in the Western Canadian Sedimentary Basin, as carbonate successions continued to accumulate in the Gulf of Mexico (Galloway et al., 2011; Blum and Pecha, 2014). Detrital zircon studies of the Albian Grand Rapids Formation and Clearwater Formation from Cold Lake in the Western Canadian Sedimentary Basin show similar provenance signatures to the Entrada and Dakota Formation from the Raton basin, and are interpreted as part of a continental-scale sediment dispersal systems integrated with the Cordilleran magmatic arc (Blum and Pecha, 2014). East of the Raton basin in the mid-continent and north-central regions of the Cordilleran foreland basin, the Dakota Formation preserves the record of west-flowing rivers with sources in the Appalachian region, lacking material associated with Cordilleran arc magmatism These sediment dispersal systems would have been sourced in the Sevier fold-thrust belt and possibly the Mogollon highlands.

The Colorado-New Mexico segment of this system appears to have been insensitive to the Appalachian-derived systems that occupied the mid-continent to north-central segments of North America (Blum and Pecha, 2014; Finzel, 2014).

Significant age populations derived from the Cordilleran arc, as preserved in the Maastrichtian Vermejo Formation (sample RB107; Figs. 3.3 and 3.5), have two possible explanations: (1) A direct routing connection with the Cordilleran magmatic arc or (2) early erosional recycling of arc-derived material contained in Jurassic–Cretaceous strata exhumed above nascent Laramide uplifts (DeCelles, 2004; Horton et al., 2004). The first

model, with east-flowing rivers sourced in the Cordilleran magmatic arc, is consistent with the absence of Grenvillian ages (recycled from the Cordilleran (Sevier) fold-thrust belt) but presence of both Cordilleran arc and local basement ages in this sample (Fig. 3.6B).

Following the abrupt increase in Cordilleran arc ages, a prominent Yavapai and Mazatzal (1800-1600 Ma) age population was introduced to the basin during later Maastrichtian deposition of the Raton Formation (samples RB112, RB208, and RB207; Figs. 3.3 and 3.5). Two explanations are considered for the introduction of these Proterozoic grains: (1) direct input from Yavapai–Mazatzal basement exposed in Laramide block uplifts of the southern Rocky Mountains, or (2) recycling from Permian–Triassic basin fill (such as the Sangre de Cristo Formation) of the Ancestral Rockies.

CORDILLERAN MAGMATISM

The lower Maastrichtian Trinidad Formation sample (RB111; Fig. 3.2) has a unique U-Pb age distribution (Figs. 3.3 and 3.5) composed almost exclusively of grains derived from the youngest phases of Cordilleran arc magmatism, with minor (<1/3) input of Proterozoic grains representative of local basement ages. This unimodal provenance signature requires both major input of ~70 Ma grains, likely associated with youthful volcanic sources, as well as a concurrent drainage reorganization capable of explaining the sharp reduction in detritus from the retroarc fold-thrust belt. Sandstones and mudstones of the Trinidad Formation represent deposition in a fluvially influenced delta-front environment (Flores and Tur, 1982; Flores and Pillmore, 1987). The relatively limited influence of the fold-thrust belt could potentially reflect input of airfall material from the magmatic arc, effectively flooding the drainage systems with a tremendous

volume of volcanogenic sediment. During the Campanian–Maastrichtian possible sources for major input of airfall volcanic material include magmatic systems to either the south in Arizona or to the north in Montana and Idaho (Christiansen et al., 1994).

INITIAL LARAMIDE SHORTENING

The Late Cretaceous transition from a regionally expansive marine foreland basin to an isolated, structurally controlled nonmarine Raton basin is evident from the detrital zircon U-Pb dataset presented here.

The Maastrichtian Vermejo Formation (sample RB107; Figs. 3.3 and 3.5) and lower Raton Formation (samples RB112, RB208, and RB207) contain all major zircon age populations (Figs. 3.3 and 3.5), indicating diverse sources in the Cordilleran magmatic arc, the Cordilleran (Sevier) fold-thrust belt, and local sources during initial exhumation of Laramide basement-involved uplifts. Based on continuity of the provenance distribution with the underlying deposits, we interpret continued input from western zones of the Cordilleran orogenic system as well as initial input of recycled sedimentary sources from the unroofing of Laramide block uplifts. The basement signals in the Vermejo Formation (1800-1600 Ma and minor ~ 1400 Ma populations) represent the first unambiguous provenance signatures for local derivation from nearby block uplifts, and therefore advance of the Laramide deformation front into the Front Range and Sangre de Cristo regions of Colorado and northern New Mexico.

MAIN LARAMIDE SHORTENING

A significant provenance shift is recorded within a sample of the Maastrichtian Raton Formation (sample RB109; Fig. 3.2), above which there is a nearly complete

absence of ages characteristic of the Cordilleran magmatic arc (Figs. 3.3 and 3.5). This change requires that by roughly 65 Ma the Raton basin was completely cut off from drainage system occupying the Cordilleran foreland basin due to Laramide surface uplift of the Sangre de Cristo mountains (also Culebra range or "San Luis highland") (Fig. 3.6C). U-Pb age distributions for the Maastrichtian–Paleocene Raton and Poison Canyon Formation (samples RB109, RB206, RB113 and RB201) contain nearly unimodal Yavapai and Mazatzal (1800-1600 Ma) age peaks corresponding to the unroofing of the upper Paleozoic sedimentary rocks and subjacent Proterozoic basement forming the core of the Sangre de Cristo mountains. In addition to the detrital zircon data presented here, a Maastrichtian inception of unroofing is confirmed by the appearance of Precambrian clasts in conglomerates of the lowermost Raton Formation (Johnson and Wood, 1956; Baltz, 1965).

LATE LARAMIDE SHORTENING

The uppermost Poison Canyon, Cuchara, Huerfano, and Farisita Formations (Figs 3.2 and 3.3) constitute the final provenance group and the youngest siliciclastic units exposed in the Raton basin. The U-Pb age signatures are comparable to the underlying Paleocene stratigraphic units, with the addition of a 1.4 Ga peak (Fig. 3.4). This additional age group indicates further unroofing and drainage integration in the Sangre de Cristo mountains. Modern exposures of 1.4 Ga rocks are found throughout the southern Rocky Mountains, both to the south of the Raton basin in the Santa Fe and Sandia ranges and to the north in the Wet Mountains (Karlstrom et al., 1997; Shaw et al., 2005).

DISCUSSION

Several paleodrainage scenarios have been suggested for reconstructions of Late Cretaceous–Paleogene landscape evolution in the Raton basin during Laramide mountain building. First, a major east-trending paleocanyon may have formed as an antecedent late Campanian–early Maastrichtian fluvial system that persisted and cut through the rising Sangre de Cristo basement-involved uplift, providing continuous input to the Raton basin from distal western sources (Cather, 2004). Alternatively, northward fault propagation and uplift of the northern Sangre de Cristo mountains during Maastrichtian to Eocene reverse faulting may have generated a growing topographic barrier, providing a local structural control for coarse-grained clastic sedimentation in the Raton basin (Lindsey, 1998). In this model, sediment input was accomplished exclusively by erosion of nearby sources above a growing basement block uplift, with no drainage connections to distal western sources. The data presented here supports the latter scenario, in which proximal sources from a major topographic barrier exclusively provided sediment to the Raton basin during Laramide basement deformation, effectively shutting off western sources.

The detrital zircon U-Pb signatures of the Vermejo Formation indicate a Maastrichtian age of initial exhumation of the basement-involved Sangre de Cristo uplift, as recorded by recycling of Yavapai and Mazatzal basement ages from the thick Pennsylvanian–Permian Sangre de Cristo Formation (Fig. 3.3). This initial Laramide exhumation was not accompanied by large-scale rerouting of fluvial systems. Rather, provenance records show that by early to mid-Paleocene deposition of the Raton and Poison Canyon Formations, uplift in the easternmost Laramide province had outpaced erosional processes, effectively cutting off the Raton basin from the large drainage systems farther

west. This challenges the Paleocene scenarios proposed by Cather (2004) and Blum and Pecha (2014), which propose fluvial systems linking the Cordilleran magmatic arc with the Gulf Coast through the southern Rocky Mountains.

Basin compartmentalization and basement block uplift in the North American plate interior had both climatic and tectonic implications. The growth of the topographic barrier defining the Laramide deformation front acted to enhance orographic precipitation (Sewall and Sloan, 2006; Raynolds et al., 2007; Snell et al., 2013) and resulted in a significant increase in clastic sediment supply to the Gulf of Mexico during the Paleocene (Winker, 1982; Cather and Chapin, 1990; Carroll et al., 2006; Hutto et al., 2009; Galloway et al., 2011; Mackey et al., 2012; Craddock and Kylander-Clark, 2013; Blum and Pecha, 2014).

During the Paleocene, large fluvial systems sourced in the Cordilleran hinterland and (Sevier) fold-thrust belt crossed the North American continental interior and discharged into the western Gulf of Mexico. Whereas the ancestral Mississippi and Rio Grande rivers have persisted, other rivers draining the central and southern Rocky Mountains have been modified, erased, or captured (Galloway et al., 2011; Blum and Pecha, 2014). The detrital zircon U-Pb geochronologic data presented here suggest that fluvial systems active from early Maastrichtian through Eocene time drained a major topographic barrier that developed along the Laramide deformation front (Sangre de Cristo and Front Range systems), issuing sediment to the east and southeast, across the Raton basin, in order to provide a critical source of voluminous sediment to the western Gulf of Mexico (Winker, 1982; Mackey et al., 2012). The establishment of major Laramide barriers in the southern Rocky Mountains of Colorado and New Mexico caused

a drastic reorganization of continental-scale drainage patterns as interior Laramide basins were cut off from eastern outlets. By the Paleocene, topographic isolation of these interior (ponded and axial) basins from the external (perimeter) basins of the Laramide province likely exerted a strong influence on the routing and volume of sediment supplied to downstream regions such as the Gulf of Mexico.

CONCLUSIONS

The reconstruction of drainage patterns for the North American interior largely hinges upon the patterns of basement uplift in the Laramide province of the U.S. Rocky Mountains. Late Cretaceous-Cenozoic variations in sediment flux to North American continental margins were a complex product of changes in uplift, exhumation, magmatism, climate, and sediment storage in intermontane to foreland regions during flattening and subsequent rollback of the subducted Farallon slab.

The distributions of detrital zircon U-Pb age populations within Cretaceous–Paleogene fill of the Raton basin provide a high-fidelity record of the initiation and growth of the Laramide deformation front in the southern Rocky Mountains. The Maastrichtian input of Proterozoic basement detritus, recycled from Ancestral Rocky Mountain basin fill, and the synchronous shift from marine to nonmarine depositional conditions, represent clear signals of Laramide basement-cored uplift in the northern Sangre de Cristo mountains of southern Colorado and northern New Mexico. By the Paleocene, the cutoff of western sources of Cordilleran magmatic arc materials to Raton basin strata highlights the significant degree of drainage reorganization during Laramide shortening, as major fluvial systems were rerouted around the high-relief Sangre de Cristo range. This pattern of basement exhumation followed by uplift and drainage cutoff

in the southern Rocky Mountains helps define the patterns and mechanisms for Late Cretaceous-Cenozoic basin reorganization in western North America, with general implications for drainage evolution in comparable zones of far-field deformation within continental plate interiors.

ACKNOWLEDGMENTS

This work was supported by a Geological Society of America Graduate Research Grant, American Association of Petroleum Geologists Wanek Memorial Grant, Gulf Coast Association of Geological Societies Graduate Research Grant, Colorado Scientific Society Research Grand, and a Statoil Graduate Research Fellowship to M.A. Bush. We thank Spencer Seman and Lisa Stockli for laboratory support, and George Gehrels, Bill Craddock, Marc Jolivet, and John Geissman for constructive reviews. Full analytical data are provided in the supporting information. Supporting data are included in the supporting information file associated with this manuscript.

REFERENCES

Ash, S.R., and Tidwell, W.D., 1976, Upper Cretaceous and Paleocene floras of the Raton Basin, Colorado and New Mexico, *in* Ewing, R.C. and Kues, B.S., eds., New Mexico Geological Society 27th Annual Fall Field Conference Guidebook, p. 197-203.

Baltz, E.H., 1965, Stratigraphy and history of the Raton basin and notes on the San Luis basin, Colorado-New Mexico: AAPG Bulletin, v. 49, no. 11, p. 2041–2075.

Barth, A.P., and Wooden, J.L., 2006, Timing of magmatism following initial convergence at a passive margin, Southwestern U.S. Cordillera, and ages of lower crustal magma sources: The Journal of Geology, v. 114, no. 2, p. 231–245, doi: 10.1086/499573.

Blum, M., and Pecha, M., 2014, Mid-Cretaceous to Paleocene North American drainage reorganization from detrital zircons: Geology, v. 42, no. 7, p. 607–610, doi: 10.1130/G35513.1.

Brill, K.G., 1952, Stratigraphy in the Permo-Pennsylvanian zeugogeosyncline of Colorado and Northern New Mexico: Geological Society of America Bulletin, v. 63, no. August, p. 809–880.

Busby-Spera, C.J., Mattinson, J.M., Riggs, N.R., and Schermer, E.R., 1990, The Triassic-Jurassic magmatic arc in the Mojave-Sonoran deserts and the Sierran-Klamath region; similarities and differences in paleogeographic evolution: Geological Society of America Special Papers, v. 255, p. 325–337, doi: 10.1130/SPE255-p325.

Cather, S.M., 2004, Laramide orogeny in central and northern New Mexico and southern Colorado: The Geology of New Mexico, A Geologic History, New Mexico Geological Society, p. 203–248.

Cather, S.M., and Chapin, C.E., 1990, Paleogeographic and paleotectonic setting of Laramide sedimentary basins in the central Rocky Mountain region: Alternative interpretation: Bulletin of the Geological Society of America, v. 102, p. 256-260.

Carroll, A.R., Chetel, L.M., and Smith, M.E., 2006, Feast to famine: Sediment supply control on Laramide basin fill: Geology, v. 34, no. 3, p. 197, doi: 10.1130/G22148.1.

Chapin, C.E., Kelley, S.A., and Cather, S.M., 2014, The Rocky Mountain Front, southwestern USA: Geosphere, v. 10; p. 1043–1060, doi:10.1130/GES01003.1.

Chetel, L.M., Janecke, S.U., Carroll, A.R., Beard, B.L., Johnson, C.M., and Singer, B.S., 2011, Paleogeographic reconstruction of the Eocene Idaho River, North American Cordillera: Geological Society of America Bulletin, v. 123, no. 1-2, p. 71–88, doi: 10.1130/B30213.1.

Christiansen, E.H., Kowallis, B.J., and Barton, M.D., 1994, Temporal and spatial distribution of volcanic ash in Mesozoic sedimentary rocks of the Western Interior: an alternative record of Mesozoic magmatism, in Mesozoic systems of the Rocky Mountain region, USA, Rocky Mountain Section SEPM, p. 73–94.

Coney, P.J., and Reynolds, S.J., 1977, Cordilleran Benioff zones: Nature, v. 270, p. 403-406.

Constenius, K.N., 1996, Late Paleogene extensional collapse of the Cordilleran foreland fold and thrust belt: Geological Society of America Bulletin, v. 108, p. 20–39.

Copeland, P., Murphy, M.A., Dupré, W.R., and Lapen, T.J., 2011, Oligocene Laramide deformation in southern New Mexico and its implications for Farallon plate geodynamics: Geosphere, v. 7, p. 1209-1219, doi:10.1130/GES00672.1.

Craddock, W.H., and Kylander-Clark, A.R.C., 2013, U-Pb ages of detrital zircons from the Tertiary Mississippi River Delta in central Louisiana: Insights into sediment provenance: Geosphere, v. 9, p. 1832–1851, doi: 10.1130/GES00917.1.

Currie, B. S., McPherson, M.L., Dark, J.P., and Pierson, J.S., 2008, Reservoir characterization of the Cretaceous Cedar Mountain and Dakota Formations, southern Uinta Basin, Utah: Year-two report: Utah Geological Survey Open-File Report 516, 71 p.

DeCelles, P.G., 2004, Late Jurassic to Eocene evolution of the Cordilleran thrust belt and foreland basin system, western USA: American Journal of Science, v. 304, no. February, p. 105–168.

DeCelles, P.G., Ducea, M.N., Kapp, P., and Zandt, G., 2009, Cyclicity in Cordilleran orogenic systems: Nature Geoscience, v. 2, p. 251–257, doi: 10.1038/ngeo469.

Dickinson, W.R., 2006, Geotectonic evolution of the Great Basin: Geosphere, v. 2, no. 7, p. 353, doi: 10.1130/GES00054.1.

Dickinson, W.R., and Gehrels, G.E., 2009, U-Pb ages of detrital zircons in Jurassic eolian and associated sandstones of the Colorado Plateau: Evidence for transcontinental dispersal and intraregional recycling of sediment: Geological Society of America Bulletin, v. 121, p. 408–433, doi: 10.1130/B26406.1.

Dickinson, W.R., and Gehrels, G.E., 2008a, Sediment delivery to the Cordilleran foreland basin: insights from U-Pb ages of detrital zircon in Upper Jurassic and Cretaceous strata of the Colorado Plateau: American Journal of Science, v. 308, no. December, p. 1041–1082, doi: 10.2475/10.2008.01.

Dickinson, W.R., and Gehrels, G.E., 2008b, U-Pb ages of detrital zircons in relation to paleogeography: Triassic paleodrainage networks and sediment dispersal across Southwest Laurentia: Journal of Sedimentary Research, v. 78, no. 1996, p. 745–764, doi: 10.2110/jsr.2008.088.

Dickinson, W.R., and Gehrels, G.E., 2003, U–Pb ages of detrital zircons from Permian and Jurassic eolian sandstones of the Colorado Plateau, USA: paleogeographic implications: Sedimentary Geology, v. 163, no. 1-2, p. 29–66, doi: 10.1016/S0037-0738(03)00158-1.

Dickinson, W.R., Klute, M.A., Hayes, M.J., Janecke, S.U., Lundin, E.R., McKittrick, M., and Olivares, M.D., 1988, Paleogeographic and paleotectonic setting of Laramide sedimentary basins in the central Rocky Mountain region: Bulletin of the Geological Society of America, v. 100, no. 7, p. 1023.

Dickinson, W.R., and Snyder, W.S., 1978, Plate tectonics of the Laramide orogeny, *in* Matthews, V., III, ed., Laramide folding associated with basement block faulting in the western United States: Geological Society of America Memoir 151, p. 355-366.

Ducea, M., 2001, The California arc: Thick granitic batholiths, eclogitic residues, lithospheric-scale thrusting, and magmatic flare-ups: GSA Today, v. 11, p. 4–10, doi: 10.1130/1052-5173(2001)011<0004:TCATGB>2.0.CO;2.

Erslev, E.A., 1993, Thrusts, back-thrusts, and detachment of Rocky Mountain foreland arches, *in* Schmidt, C.J., Chase, R.B., and Erslev, E.A., eds., Laramide basement

deformation in the Rocky Mountain foreland of the western United States: GSA Special Paper 280, p. 339-358.
Finzel, E.S., 2014, Detrital zircons from Cretaceous midcontinent strata reveal an Appalachian Mountains–Cordilleran foreland basin connection: Lithosphere, v. 6; p. 378–382.
Flores, R.M., and Pillmore, C.L., 1987, Tectonic control on alluvial paleoarchitecture of the Cretaceous and Tertiary Raton Basin, Colorado and New Mexico: Recent Developments in Fluvial Sedimentology, SEPM, v. 39.
Flores, R.M., and Tur, S., 1982, Characteristics of deltaic deposits in the Cretaceous Pierre Shale, Trinidad Sandstone, and Vermejo Formation, Raton basin, Colorado: The Mountain Geologist, v. 19, p. 25–40.
Galloway, W.E., Whiteaker, T.L., and Ganey-Curry, P., 2011, History of Cenozoic North American drainage basin evolution, sediment yield, and accumulation in the Gulf of Mexico basin: Geosphere, v. 7, no. 4, p. 938–973, doi: 10.1130/GES00647.1.
Higley, D.K., 2007, Petroleum systems and assessment of undiscovered oil and gas in the Raton Basin-Sierra Grande Uplift Province, Colorado and New Mexico- USGS Province 41: USGS.
Hoffman, G.K., and Jones, G.E., 2005, Availability of coal resources in the Vermejo and Raton formations, Raton coalfield, Raton Basin, northeast New Mexico: New Mexico Bureau of Geology and Mineral Resources Open-file Report, no. 490, 57 p.
Horton, B.K., Constenius, K.N., and DeCelles, P.G., 2004, Tectonic control on coarse-grained foreland-basin sequences: An example from the Cordilleran foreland basin, Utah: Geology, v. 32, p. 637-640.
Horton, B.K., Fuentes, F., Boll, A., Starck, D., Ramirez, S.G., and Stockli, D.F., 2016, Andean stratigraphic record of the transition from backarc extension to orogenic shortening: A case study from the northern Neuquén basin, Argentina: Journal of South American Earth Sciences, v. 71, p. 17–40, doi:10.1016/j.jsames.2016.06.003.
Hoy, R.G., and Ridgway, K.D., 2002, Syndepositional thrust-related deformation and sedimentation in an Ancestral Rocky Mountains basin, Central Colorado trough, Colorado, USA: Geological Society of America Bulletin, v. 114, p. 804-828.
Humphreys, E., 2009, Relation of flat subduction to magmatism and deformation in the western United States, *in* Kay, S.M., Ramos, V.A., and Dickinson, W.R., eds., Backbone of the Americas: Shallow Subduction, Plateau Uplift, and Ridge and Terrane Collision: GSA Memoir 204, p. 85-98, doi:10.1130/2009.1204(04).
Hutto, A.P., Yancey, T.E., and Miller, B. V, 2009, Provenance of Paleocene-Eocene Wilcox group sediments in Texas: the evidence from detrital zircons, in Gulf Coast Association of Geological Societies Transactions, v. 59, p. 357–362.
Jackson, S.E., Pearson, N.J., Griffin, W.L., and Belousova, E.A., 2004, The application of laser ablation-inductively coupled plasma-mass spectrometry to in situ U-Pb zircon geochronology: Chemical Geology, v. 211, p. 47–69, doi: 10.1016/j.chemgeo.2004.06.017.
Johnson, R., Dixon, G., and Wanek, A., 1966, Late Cretaceous and Tertiary stratigraphy of the Raton basin of New Mexico and Colorado: Guidebook, New Mexico Geological Society, v. 7th Field .

Johnson, R.B., and Wood, G.H., 1956, Stratigraphy of upper Cretaceous and Tertiary rocks of the Raton basin, Colorado and New Mexico: AAPG Bulletin, v. 40, no. 4, p. 707–721.

Jones, J., and Connelly, J., 2006, Proterozoic tectonic evolution of the Sangre de Cristo Mountains, southern Colorado, U.S.A.: Rocky Mountain Geology, v. 41, p. 79–116.

Karlstrom, K.E., Dallmeyer, R.D., and Grambling, J.A., 1997, 40Ar/39Ar evidence for 1.4 Ga regional metamorphism in New Mexico: Implications for thermal evolution of lithosphere in the Southwestern USA: The Journal of Geology, v. 105, p. 205–224, doi: 10.1086/515912.

Karlstrom, K.E., and Humphreys, E.D., 1998, Persistent influence of Proterozoic accretionary boundaries in the tectonic evolution of southwestern North America: Interaction of cratonic grain and mantle modification events: Rocky Mountain Geology, v. 33, p. 161–179.

LaMaskin, T.A., 2012, Detrital zircon facies of Cordilleran terranes in western North America: GSA Today, v. 22, p. 4–11, doi:10.1130/GSATG142A.1.

Laskowski, A.K., DeCelles, P.G., and Gehrels, G.E., 2013, Detrital zircon geochronology of Cordilleran retroarc foreland basin strata, western North America: Tectonics, v. 32, p. 1027–1048, doi: 10.1002/tect.20065.

Lawton, T.F., 2008, Laramide sedimentary basins, *in* Miall, A.D., Sedimentary Basins of the World: The Sedimentary Basins of the United States and Canada, v. 5, p. 429-450.

Lawton, T.F., and Bradford, B.A., 2011, Correlation and Provenance of Upper Cretaceous (Campanian) Fluvial Strata, Utah, U.S.A., from Zircon U-Pb Geochronology and Petrography: Journal of Sedimentary Research, v. 81, no. 7, p. 495–512, doi: 10.2110/jsr.2011.45.

Lee, W.T., and Knowlton, F.H., 1917, Geology and paleontology of the Raton Mesa and other regions in Colorado and New Mexico: USGS Professional Paper, v. 101.

Lindsey, D.A., 1998, Laramide structure of the central Sangre de Cristo mountains and adjacent Raton Basin, southern Colorado: The Mountain Geologist, v. 35, no. 2, p. 55-70.

Lipman, P.W., Prostka, H.J., and Christiansen, R.L., 1972, Cenozoic volcanism and plate-tectonic evolution of the western United States. I. Early and Middle Cenozoic: Philosophical Transactions of the Royal Society A: Mathematical, Physical and Engineering Sciences, v. 271, p. 217–248, doi: 10.1098/rsta.1972.0008.

Liu, L., Spasojevic, S., and Gurnis, M., 2008, Reconstructing Farallon plate subduction beneath North America back to the Late Cretaceous.: Science (New York, N.Y.), v. 322, November, p. 934–938, doi: 10.1126/science.1162921.

MacKenzie, D.B., and Poole, D.M., 1962, Provenance of Dakota Group sandstones of the Western Interior, *in* Enyert, R. L., and Curry, W. H., III., eds., Symposium on Early Cretaceous rocks of Wyoming and adjacent areas: Wyoming Geological Association, p. 62-71.

Mack, G. H., and Rasmussen, K. A., 1984, Alluvial-fan sedimentation of the Cutler Formation (Permo-Pennsylvanian) near Gateway, Colorado: Geological Society of America Bulletin, v. 95, p. 109-116.

Mackey, G.N., Horton, B.K., and Milliken, K.L., 2012, Provenance of the Paleocene-Eocene Wilcox Group, western Gulf of Mexico basin: Evidence for integrated

drainage of the southern Laramide Rocky Mountains and Cordilleran arc: Geological Society of America Bulletin, v. 124, no. 5-6, p. 1007–1024, doi: 10.1130/B30458.1.

Marsh, J.H., and Stockli, D.F., 2015, Zircon U-Pb and trace element zoning characteristics in an anatectic granulite domain: Insights from LASS-ICP-MS depth profiling: Lithos, v. 239, p. 170–185, doi: 10.1016/j.lithos.2015.10.017.

McGookey, D.P., 1972, Cretaceous System, *in* Mallory, W.W., ed., Geologic atlas of the Rocky Mountain region: Denver, Colorado, Rocky Mountain Association of Geologists, p. 190-228.

Merewether, E.A., Cobban, W.A., and Obradovich, J.D., 2011, Biostratigraphic data from Upper Cretaceous formations — eastern Wyoming, central Colorado, and northeastern New Mexico, U.S. Geological Survey Scientific Investigations Map 3175: 2 sheets, pamphlets, 10 p.

Orth, C., Gilmore, J., and Knight, J., 1987, Iridium anomaly at the Cretaceous-Tertiary boundary in the Raton Basin: New Mexico Geological Society Guidebook, v. 38, p. 265–269.

Painter, Clayton S., Barbara Carrapa, Peter G. DeCelles, George E. Gehrels, and S. N. Thomson, 2014, Exhumation of the North American Cordillera revealed by multi-dating of Upper Jurassic-Upper Cretaceous foreland basin deposits: Geological Society of America Bulletin, v. 126, no. 11-12, p. 1439–64, doi:10.1130/B30999.1

Penn, B.S., and Lindsey, D.A., 1996, Tertiary igneous rocks and Laramide structure and stratigraphy of the Spanish Peaks region, south-central Colorado: road log and descriptions from Walsenburg to La Veta (first day) and La Veta to Aguilar (second day), *in* Colorado Geological Survey OFR 96-4, p. [21].

Petrus, J.A., and Kamber, B.S., 2012, VizualAge: A novel approach to laser ablation ICP-MS U-Pb geochronology data reduction: Geostandards and Geoanalytical Research, v. 36, p. 247–270, doi: 10.1111/j.1751-908X.2012.00158.x.

Pillmore, C.L., and Flores, R.M., 1987, Stratigraphy and depositional environments of the Cretaceous-Tertiary boundary clay and associated rocks, Raton basin, New Mexico and Colorado: Geological Society of America Special Publication 209, p. 111–130.

Pillmore, C.L., and Flores, R.M., 1990, Cretaceous and Paleocene rocks of the Raton basin, New Mexico and Colorado-stratigraphic environmental framework: New Mexico Geological Society Guidebook, no. 41st Field Conference, p. 333–336.

Pillmore, C.L., Tschudy, R.H., Orth, C.J., Gilmore, J.S., and Knight, J.D., 1984, Geologic framework of nonmarine Cretaceous-Tertiary boundary sites, Raton basin, New Mexico and Colorado: Science, v. 223, no. 4641, p. 1180-1182.

Potochnik, A., 1989, Depositional style and tectonic implications of the Mogollon Rim Formation (Eocene), east-central Arizona: New Mexico Geological Society Guidebook, 40th Field Conference, p. 107–118.

Raynolds, R.G., Johnson, K.R., Ellis, B., Dechesne, M., and Miller, I.M., 2007, Earth history along Colorado's Front Range: Salvaging geologic data in the suburbs and sharing it with the citizens: GSA Today, v. 17, no. 12, p. 4–10, doi: 10.1130/GSAT01712A.1.

Robinson Roberts, L.N., and Kirschbaum, M.A., 1995, Paleogeography of the Late Cretaceous of the Western Interior of middle North America–Coal distribution and sediment accumulation: U.S. Geological Survey Professional Paper 1561, 115 p.

Saleeby, J., 2003, Segmentation of the Laramide Slab - Evidence from the southern Sierra Nevada region: Bulletin of the Geological Society of America, v. 115, no. 6, p. 655–668, doi: 10.1130/0016-7606(2003)115<0655:SOTLSF>2.0.CO;2.

Sewall, J.O., and Sloan, L.C., 2006, Come a little bit closer: A high-resolution climate study of the early Paleogene Laramide foreland: Geology, v. 34, p. 81–84, doi: 10.1130/G22177.1.

Shaw, C.A., Heizler, M.T., and Karlstrom, K.E., 2005, 40Ar/39 Ar thermochronologic record of 1.45-1.35 Ga intracontinental tectonism in the southern Rocky Mountains: Interplay of conductive and advective heating with intracontinental deformation, in The Rocky Mountain Region: An Evolving Lithosphere, American Geophysical Union, p. 163–184.

Snell, K.E., Thrasher, B.L., Eiler, J.M., Koch, P.L., Sloan, L.C., and Tabor, N.J., 2013, Hot summers in the Bighorn Basin during the early Paleogene: Geology, v. 41, p. 55–58, doi: 10.1130/G33567.1.

Szwarc, T.S., Johnson, C.L., Stright, L.E., and McFarlane, C.M., 2014, Interactions between axial and transverse drainage systems in the Late Cretaceous Cordilleran foreland basin: Evidence from detrital zircons in the Straight Cliffs Formation, southern Utah, USA: Geological Society of America Bulletin, , no. X, p. 1–21, doi: 10.1130/B31039.1.

Tschudy, R.H., Pillmore, C.L., Orth, C.J., Gilmore, J.S., and Knight, J.D., 1984, Disruptions of the terrestrial plant ecosystem at the Cretaceous- Tertiary boundary, Western Interior: Science, v. 225, no. 4666, p. 1030-1034.

Tidwell, W.D., Britt, B.B., and Tidwell, L.S., 2007, A review of the Cretaceous floras of east-central Utah and western Colorado: Central Utah–Diverse Geology of a Dynamic Landscape, Utah Geological Association, p. 467-482.

Tweto, O., 1975, Laramide (Late Cretaceous-early Tertiary) orogeny in the southern Rocky Mountains, *in* Curtis, B.F., ed., Cenozoic history of the southern Rocky Mountains: Geological Society of America Memoir 144, p. 1-44.

Tweto, O., 1980, Summary of Laramide orogeny in Colorado, *in* Kent, H.C., and Porter, K.W., eds., Colorado geology: Denver, Rocky Mountain Association of Geologists, p. 129-134.

Vermeesch, P., 2004, How many grains are needed for a provenance study? Earth and Planetary Science Letters, v. 224, p. 441–451, doi: 10.1016/j.epsl.2004.05.037.

Vermeesch, P., 2013, Multi-sample comparison of detrital age distributions: Chemical Geology, v. 341, p. 140–146, doi: 10.1016/j.chemgeo.2013.01.010.

Walker, J.D., Geissman, J.W., Bowring, S.A., and Babcock, L.E., 2012, GSA Geologic Time Scale (v. 4.0): Geological Society of America, http://www.geosociety.org/science/timescale/

Wanek, A. A., 1963, Geology and fuel resources of the southwestern part of the Raton coal field, Colfax County, New Mexico: U.S. Geological Survey Coal Investigations Map C-45.

Wernicke, B., 2011, The California River and its role in carving Grand Canyon: Geological Society of America Bulletin, v. 123, no. 7-8, p. 1288–1316, doi: 10.1130/B30274.1.

Whitmeyer, S.J., and Karlstrom, K.E., 2007, Tectonic model for the Proterozoic growth of North America: Geosphere, v. 3, no. 4, p. 220–259, doi: 10.1130/GES00055.1.

Winker, C.D., 1982, Cenozoic shelf margins, northwestern Gulf of Mexico basin: Gulf Coast Association of Geological Societies Transactions, v. 32, p. 427–448.

Yonkee, W.A., and Weil, A.B., 2015, Tectonic evolution of the Sevier and Laramide belts within the North American Cordillera orogenic system: Earth Science Reviews, v. 150, p. 531-593.

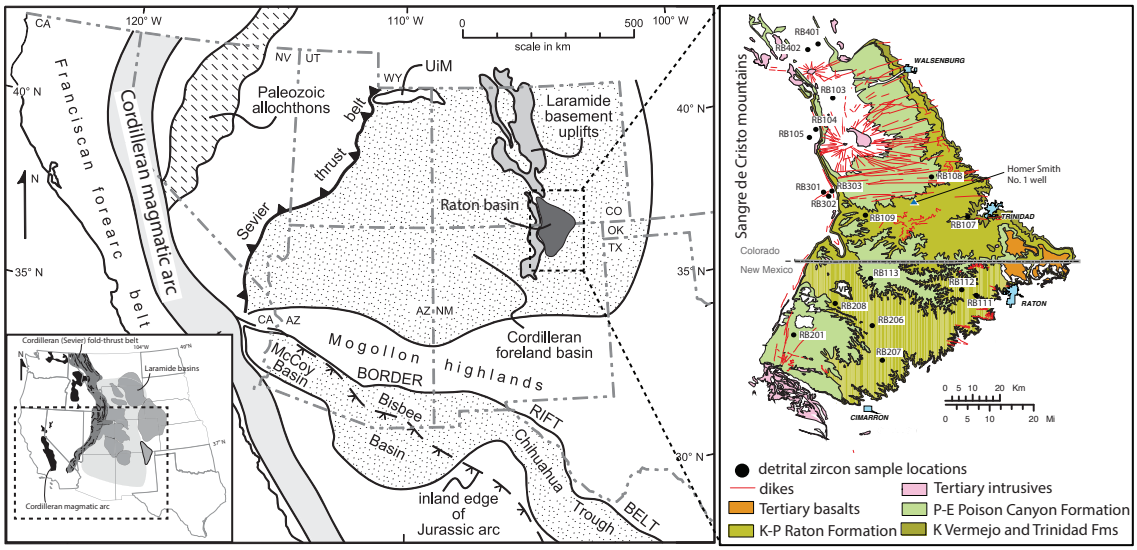

Figure 3.1. Regional tectonic map of western North America showing Laramide province (modified from Dickinson, 2008a). Geologic map of Raton basin (geology from Hoffman and Jones, 2005; Tweto, 1980). Inset map of the western United States (modified from Painter et al., 2014).

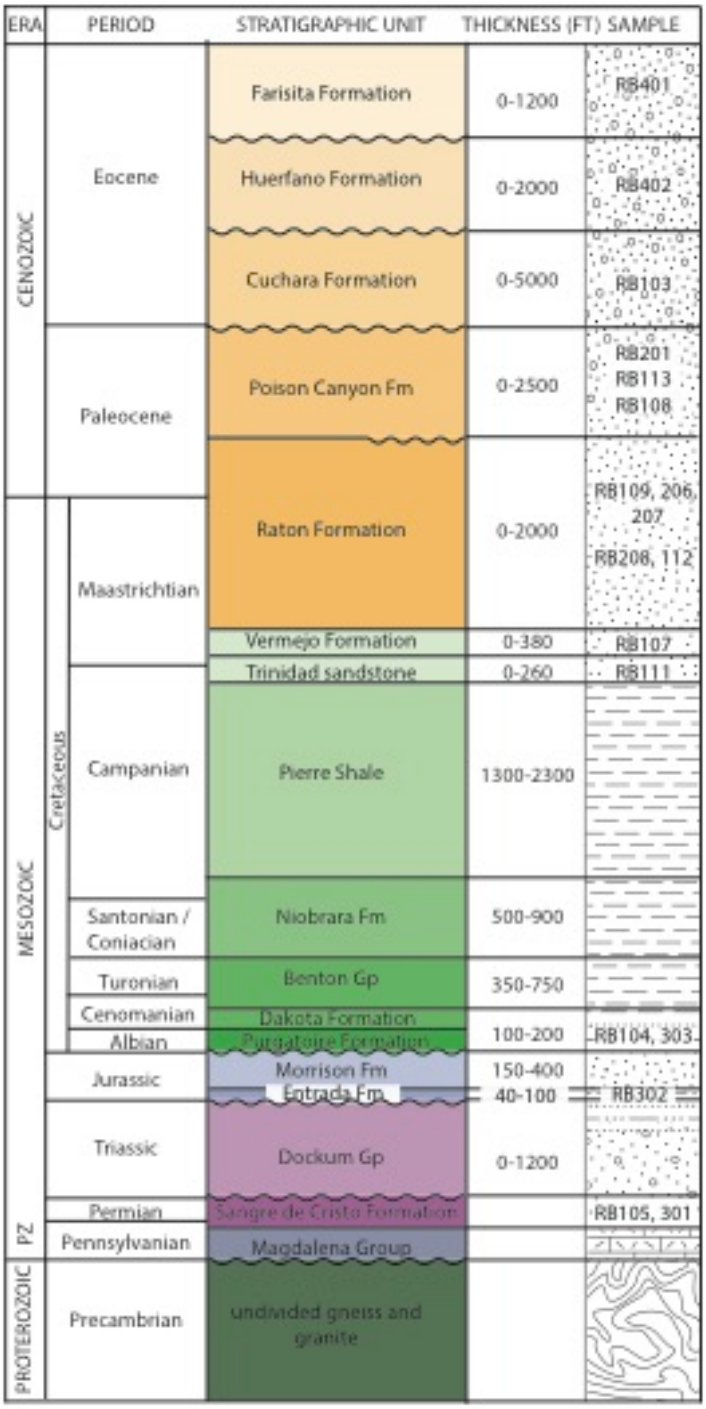

Figure 3.2. Stratigraphic column showing nomenclature, thickness, and lithology of major rock units of the Raton Basin. Ages from Merewether et al., 2011.

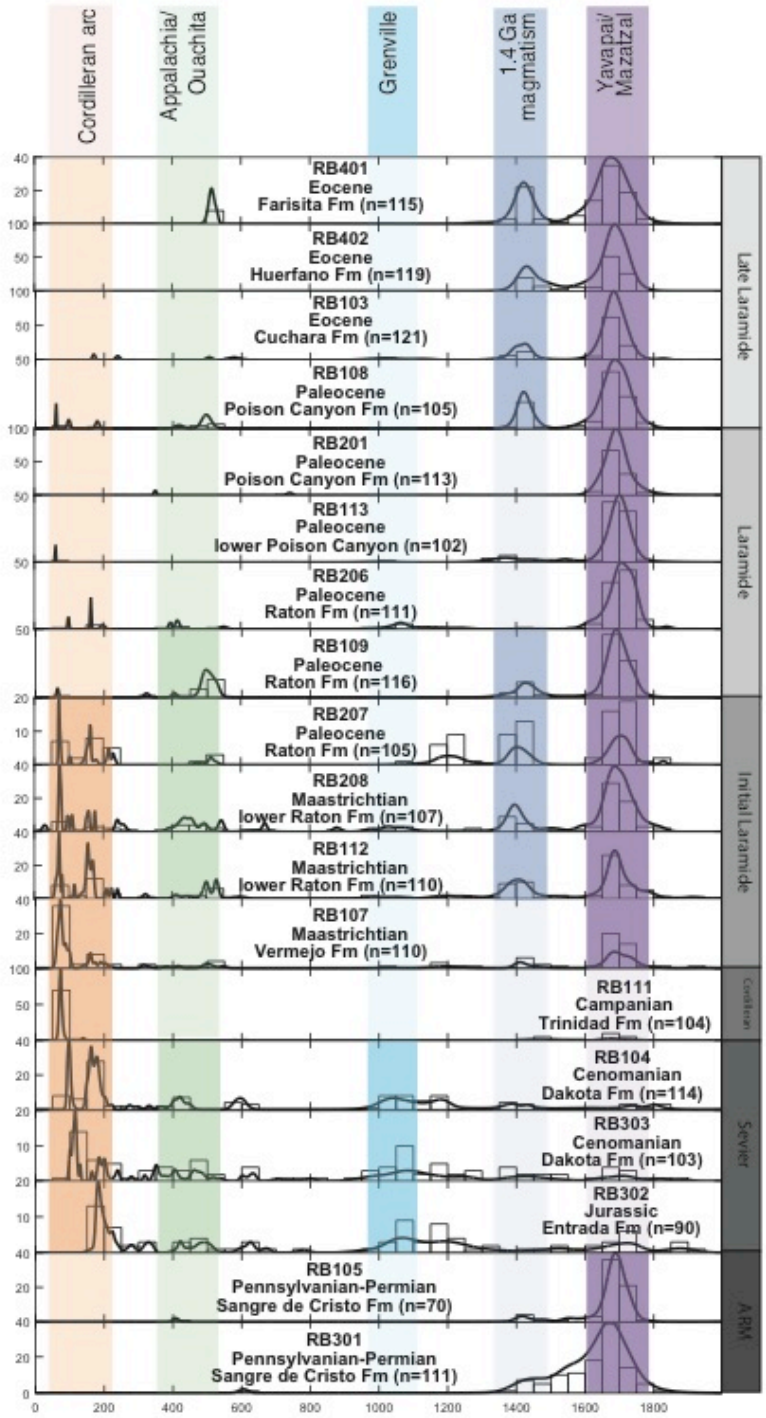

Figure 3.3. Plot of detrital zircon U-Pb age distributions for 17 sandstone samples from the Raton basin, arranged in stratigraphic order. U-Pb data are represented as age-probability density functions (black curves) and age histograms (open rectangles). Color shading denotes several major diagnostic age populations, highlighting stratigraphic variations.

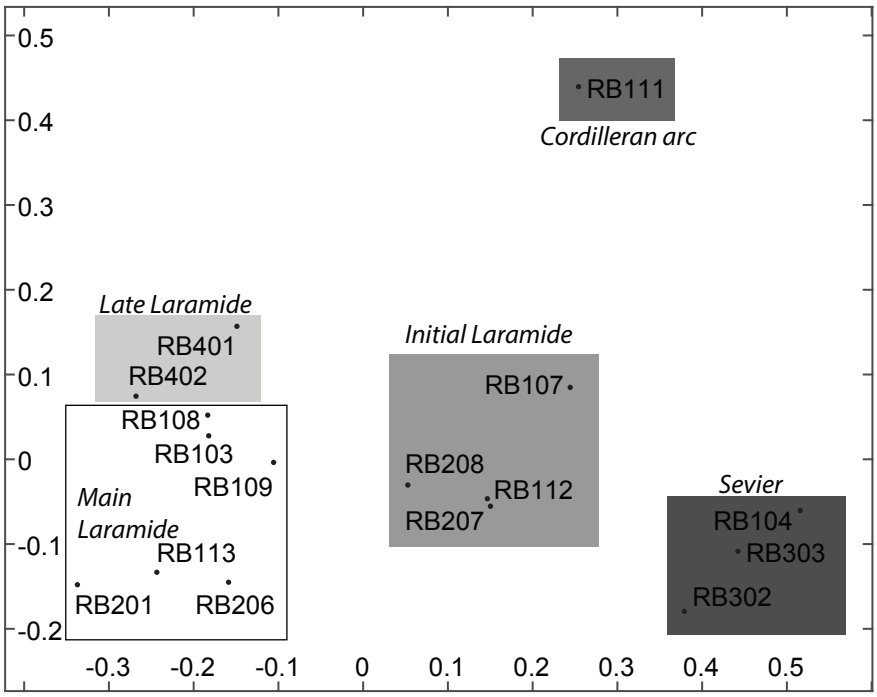

Figure 3.4. Multidimensional scaling (MDS) plot showing relative statistical similarity (based on the Kolmogorov-Smirnov test D value) among the 16 Mesozoic and Cenozoic samples. Paleozoic samples (RB105 and RB301) are not plotted here.

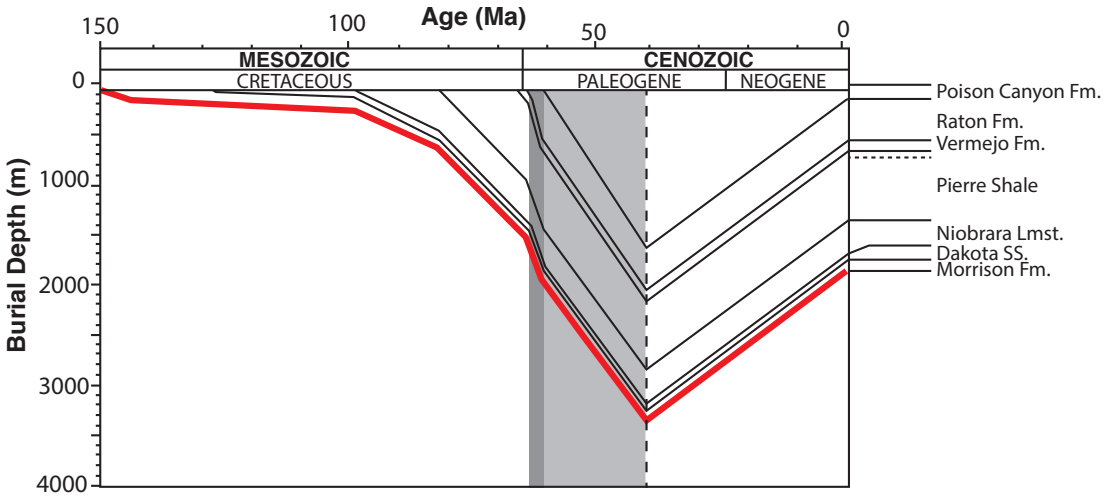

Figure 3.5. Sediment accumulation history for Homer Smith no. 1 well locality in central Raton basin (see Fig. 3.1). Modified from Higley, 2007 Fig. 11, based on vitrinite reflectance data from Close, 1988.

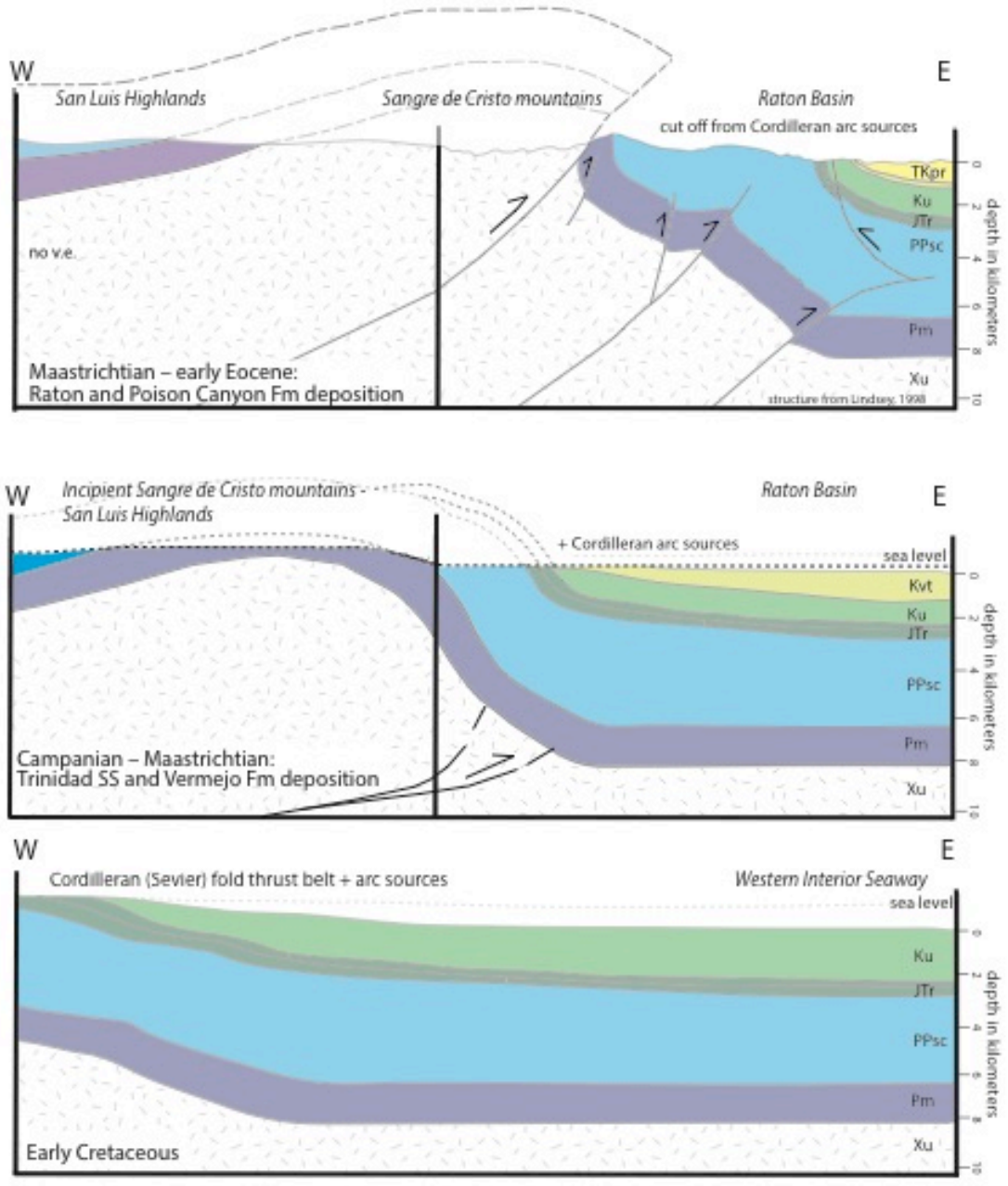

Figure 3.6. Schematic cross-section reconstruction showing progressive growth of the northern Sangre de Cristo mountains, emphasizing the structural geometry of the Culebra range and western Raton basin (all geology east of center line after Lindsey, 1998). A: Early Cretaceous cross-section, with an integrated basin connected to the Cordilleran arc and Sevier fold-thrust belt to the west. B: Campanian-Maastrichtian cross-section, with initial exhumation of local basement on growing uplifts but still connected basin. C: Maastrichtian-early Eocene, with formation of drainage divide to the west of the Raton basin.

Chapter 4: Laramide drainage evolution and sediment routing in the southern Rocky Mountains, USA: Implications for sediment delivery to the Gulf of Mexico[1]

ABSTRACT

The Campanian-Paleogene source-to-sink system connecting the Cordilleran hinterland and Laramide province to the Gulf of Mexico basin represents an important model for continent-scale drainage and sediment dispersal systems originating in contractional orogens. By focusing on the sedimentary record of several basins in the southern Rocky Mountains, this study informs our understanding of the production, storage, and transport of sediment in a continental plate interior. Detrital zircon geochronological results (1359 concordant U-Pb ages) and heavy mineral assemblages for samples from the San Juan, Galisteo-El Rito, and Raton basins of southern Colorado and northern New Mexico demonstrate Cordilleran arc (<250 Ma volcanic sources), Sevier fold-thrust belt (Paleozoic and Grenville-age recycled sedimentary sources), and Laramide basement sources (dominantly 1.4 and 1.7 Ga crystalline sources). These provenance data reveal an abrupt temporal transition from distal hinterland and thrust-belt sources for regionally integrated marine deposystems of the Sevier foreland basin, followed by input of crystalline basement detritus from initial Laramide shortening, and subsequent basin partitioning by uplift of the basement-cored Nacimiento and Sangre de Cristo ranges. Syndepositional U-Pb ages constrain the critical transition from distal to proximal sources to the early Paleocene. These phases of variable provenance and

[1] This chapter is currently under review in GSA Bulletin.

evolving basin architecture directly influenced continent-scale (>1000 km) drainage patterns and sediment budgets, as reflected in contrasting sediment volumes of siliciclastic material reaching the Gulf of Mexico during Campanian–Eocene orogenesis. Provenance analysis can track the introduction and exhumation of source areas, as new ranges are exhumed and as drainage networks alternatively become integrated or isolated. The structural framework and stratigraphic stacking patterns of these basins tracks the pattern of sediment storage versus bypass. The interplay of these factors during the Paleogene moderated the volume and timing of siliciclastic sediment reaching the Gulf of Mexico. Plate-interior deformation in continental regions such as the southern Rocky Mountains promotes large-scale reorganization of fluvial systems and basin drainage networks, inducing transient ponding of sediment behind topographic barriers and attendant alterations of regional base level.

INTRODUCTION

The temporal and spatial distribution of continental deformation in broad contractional orogen systems such as the Andes, Himalaya-Tibet, and North American Cordillera influence the accumulation and partitioning of sediment volumes among the orogenic source regions, intracontinental basins, and continental margin depocenters (Hovius, 1998; Metivier et al., 1999; Syvitski et al., 2003). Nonmarine strata from Upper Cretaceous–Paleogene broken foreland basins of the North American plate interior constrain the tectonic development of the Laramide province, providing insight into the

production, storage, and routing of sediment from the North American Cordillera to the Gulf of Mexico.

Isolated remnants of Laramide broken foreland basins are irregularly distributed along the Rocky Mountains and Colorado Plateau of western North America, preserving Upper Cretaceous to Eocene nonmarine sedimentary successions (Fig. 4.1A). These plate-interior basins record the temporal shift from thin- to thick-skinned shortening (Dickinson and Snyder, 1978; Dickinson et al., 1988; DeCelles, 2004; Cather et al., 2012;), structural partitioning of the Western Interior Seaway (Lawton, 2008; Fan and Carrapa, 2014), and resulting changes in depositional systems (Sewall and Sloan, 2006; Aschoff and Steel, 2011). Whereas conventional models of an advancing fold-thrust belt and adjacent foreland basin (Jordan, 1981; Heller et al., 1988; DeCelles and Giles, 1996) successfully predict the Late Cretaceous subsidence patterns observed in the Western Interior Seaway (Cordilleran foreland basin), the Campanian–Eocene phase of Laramide shortening in western North America resulted in less systematic and less predictable basin architectural trends (Peyton and Carrapa, 2013). Laramide basement deformation was largely influenced by inherited structural and stratigraphic frameworks overprinted by crustal-scale reverse faults; associated models of broken foreland basins (e.g., Beck et al., 1988; Fielding and Jordan, 1988; Jordan, 1995) have been developed to explain observations from the Laramide province of North America and the Sierras Pampeanas of Argentina (Jordan and Allmendinger, 1986; Ramos et al., 2002; Strecker et al., 2012).

Continental drainage networks are sensitive to changing patterns of crustal deformation, as fluvial systems respond to surface uplift and exhumation. By focusing on the sedimentary records in basins flanking intra-plate uplifts, the provenance signatures

simultaneously provide evidence for changing structural and depositional systems. While mountain belts analogous to the Cordilleran (Sevier) fold-thrust belt commonly display systematic histories (e.g., Davis et al., 1983; DeCelles, 2004; DeCelles and Graham, 2015), basement involved thrust-driven uplifts in the Laramide province appear more irregular with poorly understood evolutionary trends (Fig. 4.1A). Previous reconstructions of Laramide paleogeography have focused on basins in the northern Rocky Mountains (Beck et al., 1988; Liu et al., 2004; Carroll et al., 2006; Fan and Carrapa, 2014) and the connection to the western Canada and Gulf of Mexico basins (Galloway et al., 2011; Blum and Pecha, 2014). The same processes have been attributed to the southern Rocky Mountain Laramide uplifts, but neither the patterns of deformation and sedimentation nor the development of the connection to the Gulf of Mexico are clearly understood (Crabaugh, 2001; Galloway et al., 2011; Mackey et al., 2012).

This paper focuses on reconstructions of sediment routing and the regional paleogeography of the southern Rocky Mountains, integrating provenance data and sediment accumulation patterns from the San Juan, Galisteo-El Rito, and Raton basins of northern New Mexico and southern Colorado (Fig. 4.1B, 4.1C). These data allow us to evaluate the timing of deformation and drainage reorganization related to Laramide orogenesis, addressing sediment dispersal systems that span over 1500 km from sources in the southern Rocky Mountains to the sink in the Gulf of Mexico.

TECTONIC SETTING

The Cordilleran orogenic system formed during Jurassic–Eocene shortening in response to eastward subduction of the Farallon oceanic plate beneath the North

American continental plate (Atwater, 1970; Dewey and Bird, 1970; Coney, 1972; Jordan and Allmendinger, 1986). As the subduction angle of the Farallon slab decreased (Coney and Reynolds, 1977; Livaccari et al., 1981; Saleeby, 2003), the deformation front advanced rapidly eastward from the Cordilleran (Sevier) fold-thrust belt into the Laramide province of the craton interior (Fig. 4.1A). This cratonward migration in deformation was accompanied by changing magmatic and structural styles. The dominant structural style transitioned from the nearly continuous, thin-skinned Sevier fold-thrust belt to broken, basement-involved block uplifts of the Laramide province (Dickinson and Snyder, 1978; DeCelles and Mitra, 1995; DeCelles, 2004).

Structural Framework

During the Laramide orogeny, maximum shortening and structural development occurred in late Paleocene-early Eocene time (Kelley, 1955; Chapin and Cather, 1981), accompanied by cessation of volcanism, mineralization in the Colorado Mineral Belt (English et al., 2003; Chapin, 2012), and basement uplift from Montana to southern New Mexico (Mack and Clemons, 1988; Erslev, 1993. 2001; DeCelles, 2004). In northern New Mexico and southern Colorado, the major block uplifts include the N-trending Nacimiento and Sangre de Cristo mountains, as well as the NW-trending Lucero, Zuni, Defiance, and Brazos-Tusas uplifts (Fig. 4.1A).

The style of Campanian-Paleogene deformation is controversial, with debate surrounding both the type of faulting (reverse/thrust or transpressional faulting) and multi-directional versus unidirectional shortening (Chapin and Cather, 1981; Chapin, 1983; Gries, 1983; Karlstrom and Daniel, 1993; Yin and Ingersoll, 1997; Ruf and Erslev,

2005). Based on structural analysis throughout the region, the dominant shortening direction was ENE through the Paleocene with a possible clockwise shift at 45-40 Ma (Erslev, 2001; Bird, 2002; Wawrzyniec et al., 2002; Ruf and Erslev, 2005). Fracture studies from the southern Rocky Mountains have identified E-W shortening (Woodward et al., 1997; Lorenz and Cooper, 2003) as well as N-S right-lateral transpression (Cather, 1999).

Sedimentary Framework

Campanian through Eocene basement deformation resulted in a series of discontinuous uplifts and compartmentalized nonmarine basins, overprinting the marine deposystems of the formerly continuous Cordilleran (Sevier) foreland basin. These Laramide basins are variously categorized by geographic location, morphology, and tectonic style as (1) ponded and axial intermontane basins in the interior of the Laramide province and (2) perimeter basins south of the Colorado Plateau and flanking the eastern deformation front of the Laramide province (Chapin and Cather, 1981; Dickinson et al., 1988; Yin and Ingersoll, 1997; Lawton, 2008).

Nonmarine depositional systems characteristic of Laramide basins include alluvial fan, fluvial, and lacustrine systems. The location and orientation of block uplifts, rate of deformation, and source lithology all controlled the distribution of facies in the generally asymmetric Laramide basins, where subsidence was driven by thrust loading (Beck et al., 1988; Carroll et al., 2006; Lawton, 2008). Alluvial fan facies are concentrated in proximal zones adjacent to block uplifts and derived directly from local sources, preserving an inverted stratigraphy that records progressive exhumation of uplifted

hanging-wall blocks (DeCelles et al., 1991; Cather, 2004). Fluvial facies and associated floodplain deposits indicate both axial and transverse transport, with provenance signatures dependent upon source composition. Lacustrine facies include both siliciclastic and carbonate lithologies, as influenced by variable sediment supply and source lithologies (Carroll et al., 2006).

Perimeter basins such as the Powder River, Denver, and Raton basins contain alluvial fan facies near the Laramide thrust front with local lacustrine facies near basin depocenters and fluvial facies exiting distal basins to the east and ultimately reaching the Gulf of Mexico (Dickinson et al., 1988; Galloway et al., 2011). Ponded basins north of the Colorado Plateau, such as the Green River, Uinta, Piceance Creek, and Bighorn basins, situated between the Laramide and Cordilleran (Sevier) thrust fronts, drained large areas stretching west into the Cordilleran hinterland (Dickinson et al., 1988). These basins contain thick sections of lacustrine facies, deposited in periods of basin closure during which subsidence outpaced sediment delivery (Carroll et al., 2006; Smith et al., 2008; Davis et al., 2009). On the eastern margin of the Colorado Plateau, axial basins such as the Galisteo-El Rito, North Park, Middle Park, and South Park basins are distinguished by their small size and high structural relief, with alluvial fan and fluvial facies that connected these basins to larger fluvial networks and marginal basins (Yin and Ingersoll, 1997). In southern New Mexico and Arizona, the structural style of Laramide uplifts was modified by inherited extensional features, producing basins that are distinguished by their timing, orientation and style of faulting as well as contemporaneous magmatism (Seager, 1983; Seager and Mack, 1986; Mack and Clemons, 1988; Kelley and Chapin, 1997; Clinkscales and Lawton, 2015). These basins,

including the Baca and Carthage-La Joya basins, formed in the latest phase of Laramide shortening and are characterized by both reverse and strike-slip motion on W- and NW-trending faults (Cather and Johnson, 1986; Cather, 2004).

REGIONAL GEOLOGIC BACKGROUND

In the southern Rocky Mountains, exposures of post-marine, pre-volcanic Laramide deposits are limited to the San Juan, Galisteo-El Rito, and Raton basins (Fig. 4.1). Laramide shortening began at roughly 80–75 Ma across northern New Mexico, from the Sierra Nacimiento on the eastern flank of the San Juan basin to the Sangre de Cristo mountains between the Galisteo-El Rito and Raton basins.

The earliest phase of Laramide subsidence is identified based on regional stratigraphic patterns. Above the lower Campanian Menefee Formation, the uppermost Cretaceous units defined in the San Juan basin are absent in the Galisteo basin, indicating either non-deposition or later removal of upper Campanian and overlying units (Lisenbee, 2013). Stratigraphic thinning within Cretaceous units of the San Juan basin denote differential subsidence in the basin, marking initial Laramide shortening (Ayers and Kaiser, 1994; Cather, 2003). Apatite fission track ages from the Nacimiento, Sangre de Cristo, and Wet Mountain ranges indicate initial Laramide cooling commencing in Campanian time (Kelley, 1990; Kelley and Chapin, 1995).

Evidence for Laramide magmatism in the southern Rocky Mountains is limited to 75–60 Ma intermediate alkalic to mafic plutons in the western San Juan mountains of southwestern Colorado (Gonzales, 2015). Potential uplift linked to pluton emplacement in this southern zone of the Colorado Mineral Belt (Cunningham et al., 1994; Cather,

2012) may have redirected south-directed fluvial networks entering the northern San Juan basin.

The Nacimiento uplift forms the eastern boundary of the San Juan basin and has been subject to intense debate due to overlapping structural styles and its position along the eastern margin of the Colorado Plateau. Alternatively classified as a vertical dip-slip (Baltz, 1967; Woodward, 1987) or right-lateral strike-slip structure (Karlstrom and Daniel, 1993; Cather 1999), structural and geophysical data indicate primarily low-angle thrust faulting with minor dextral slip on the Nacimiento fault system during Laramide shortening (Erslev, 2001; Pollock et al., 2004; Ruf and Erslev, 2005). Paleocurrents and angular unconformities within the San Juan and Galisteo basins indicate syndeformational sediment accumulation in fluvial depositional systems draining the Nacimiento uplift (Gorham and Ingersoll, 1979; Cather 1992; Lucas et al., 1997; Erslev, 2001; Cather, 2004; Lisenbee, 2013).

West-dipping thrust and reverse faults bound tilted basement blocks in the Sangre de Cristo mountains (Applegate and Rose, 1985; Schavran, 1985; Lindsey, 1998). Evidence for initial exhumation of the Sangre de Cristo mountains comes from petrographic and clast compositional data from synorogenic strata in the Raton basin, with the first appearance of abundant feldspar and Precambrian clasts in the Maastrichtian Vermejo Formation (Johnson and Wood, 1956; Flores and Tur, 1982; Pillmore and Flores, 1990; Lindsey, 1998).

Raton basin

In the Raton basin, Cretaceous through Eocene strata preserve detrital records of uplift-induced exhumation in the Sangre de Cristo mountains (Fig. 4.1). Prior to 80 Ma,

the Raton basin region was the site of slow accumulation of marine shale in the Cretaceous Western Interior Seaway (Cather, 2004). Coastal plain deposits of the Vermejo Formation conformably overlie and interfinger with the deltaic Trinidad Formation, recording Maastrichtian regression and initial Laramide shortening. Above an unconformable contact are coarse-grained fluvial deposits of the upper Maastrichtian-Paleocene Raton Formation (Flores and Tur, 1982; Cather 2004). Conglomeratic facies of the Paleocene-Eocene Poison Canyon, Cuchara, Huerfano, and Farisita Formations thicken to the west and north, consistent with northward migration of the Raton basin depocenter due to thrust-sheet emplacement in the Culebra Range near the Colorado-New Mexico border (Johnson and Wood, 1956; Lindsey, 1998).

Galisteo-El Rito basin

The intermontane tectonic setting of the Galisteo-El Rito basin within the Laramide province (Fig. 4.1) helped promote axial depositional patterns controlled by local structural relief. Although undeformed Cretaceous units underlie the Diamond Tail and Galisteo Formations in the south, Mesozoic and Paleozoic units are deformed and eroded in the northern and western zones of the Galisteo-El Rito basin. The basin formed as a broad synclinal sag between the Sangre de Cristo and Nacimiento uplifts (Fig. 4.1C; Yin and Ingersoll, 1997), with deposition initiating later in the north. At the base of the Galisteo-El Rito succession, fluvial sandstones and mudstones of the Diamond Tail Formation thicken toward the Tijeras-Cañoncito fault (Lucas et al., 1997; Cather, 2004). Both SSW- and NE-directed paleocurrents have been reported for fluvial deposits of the Diamond Tail Formation, although exclusively S-directed paleocurrents are found in the unconformably overlying Galisteo Formation (Stearns, 1943; Gorham and Ingersoll,

1979; Cather, 1992; Abbott et al., 1995; Lucas et al., 1997). In the southern Galisteo-El Rito basin, the volcaniclastic Eocene-Oligocene Espinaso Formation caps the Galisteo Formation (Gorham and Ingersoll, 1979; Lucas, 1982). Deposition in the northern basin in the vicinity of Abiquiu and El Rito, New Mexico initiated in the Paleocene with the El Rito Formation. In this area, red clastic deposits up to 120 m thick (Smith, 1938; Bingler, 1968; Muehlberger, 1967) overlie an erosional surface that cuts across the Cretaceous Lewis Shale to Proterozoic basement in the San Luis (Brazos) uplift. Above an angular unconformity with the El Rito Formation, channel conglomerates and interbedded sandstones of the Ritito Formation (Maldonado, 2008) grade upsection into the Abiquiu Formation, early volcaniclastic deposits of the Rio Grande rift. Paleoflow indicators in the El Rito area are south directed in the El Rito Formation (Logsdon, 1981; Brister, 1992) and west directed in the Ritito Formation, consistent with south-dipping paleoslopes and north- and east-ward migration of the basin depocenter, related to increased tectonism along the Nacimiento and Brazos-Tusas uplifts (Smith, 1992).

San Juan basin

Maastricthian-early Paleocene paleoflow patterns for the upper Kirtland Shale and Ojo Alamo Formation are indicative of a shared northern source (Klute, 1986), although local unconformities and a missing Cretaceous-Paleogene boundary have been interpreted as an ~6 My period of bypass or erosion (Orth et al., 1982; Fassett and Steiner, 1997; Hunt and Lucas, 1992; Cather, 2003). The Paleocene Ojo Alamo and Nacimiento Formations fine upward from sandstone to mudstone, with ages constrained by magnetostratigraphy and biostratigraphy (Williamson and Lucas, 1992; Williamson, 1996). While there are local basin-margin unconformities, continuous basin-centered

subsidence is recorded from the Paleocene Nacimiento Formation to Eocene San Jose Formation (Baltz, 1965; Cather, 2003). Decreased accommodation relative to sediment supply during the deposition of the Cuba Mesa member of the San Jose Formation led to focused sedimentation in the basin center (Smith, 1992; Cather, 2004). The 550 m thick San Jose succession preserves south-flowing fluvial channels draining uplifted zones to the north and northeast (Smith and Lucas, 1991; Smith, 1992). An up to 1000 m thick interval of post-San Jose strata was deposited during middle Eocene-early Oligocene time, based on exposures in the Chuska Mountains (Fassett, 1985; Cather, 2003; Dickinson et al., 2010).

PROVENANCE ANALYSES

Multi-proxy provenance analyses of Upper Cretaceous–Eocene synorogenic clastic deposits from the southern Rocky Mountains help document the exhumation of Laramide ranges and associated reorganization of drainage networks. Fourteen samples of medium-grained sandstone from the San Juan and Galisteo-El Rito basins were collected and processed for detrital zircon U-Pb geochronological analyses. Samples from the Raton (Bush et al., 2016a) and Galisteo-El Rito basins were also processed for heavy mineral analyses, to further discriminate between potential source regions.

Detrital zircon U-Pb ages reflect five diagnostic populations linked to basement and recycled sources in western North America. (1) Ages of <250 Ma are derived principally from the Cordilleran magmatic arc to the west, with age peaks corresponding to the two main phases of arc magmatism (160–150 Ma and 98–86 Ma) recognized in the Sierra Nevada batholith (Barton, 1996; Coleman and Glazner, 1997; Ducea, 2001). (2)

Appalachian-Ouachita (400-600 Ma) and (3) Grenville (~1.0 Ga) U-Pb ages are largely recycled from sedimentary units eroded from the Cordilleran fold-thrust belt (Dickinson and Gehrels, 2003; Dickinson and Gehrels, 2009; Howard et al., 2014). The oldest detrital zircon age populations of (4) ~1.4 Ga and (5) ~1.7 Ga are consistent with contributions from the Mazatzal and Yavapai basement provinces in southwestern North America, the products of crustal formation and orogenesis at ~1.7 Ga and a subsequent ~1.4 Ga tectonothermal event (Jones and Connelly, 2006; Whitmeyer and Karlstrom, 2007; Daniel et al., 2013).

Heavy mineral assemblages allow further discrimination among potential source regions, specifically between recycled sedimentary sources and crystalline sources. The removal of sedimentary material precedes exposure and exhumation of crystalline basement, thus providing an important constraint on the depth of exhumation in Laramide uplifts.

Detrital Zircon U-Pb Geochronology

Detrital zircon U-Pb geochronological analyses help constrain the evolution of sediment source areas on the basis of variable geographic and stratigraphic occurrences of source crystallization ages. Tracking these provenance changes temporally within stratigraphic successions and spatially within and between basins allows for the reconstruction of paleodrainage configuration.

METHODS

Samples of medium-grained sandstones were collected from 14 localities in the San Juan and Galisteo-El Rito basins, in order to span the duration of pre-Laramide and

Laramide shortening. After zircon grains were separated from using standard density and magnetic separation techniques, ~120 zircon grains per sample were analyzed by laser ablation–inductively coupled plasma–mass spectrometry (LA-ICP-MS) at the University of Texas at Austin following methods outlined by Horton et al (2016). Zircons from each sample were mounted on double-sided tape and depth-profiled to ~15 μm to obtain age-resolved profiles. $^{238}U/^{206}Pb$, $^{235}U/^{207}Pb$, and $^{207}Pb/^{206}Pb$ ages were obtained using the standard zircon GJ-1. The software package Iolite was used to process data and calculate ages (Petrus and Kamber, 2012). Additional details on sample locations, analytical methodology, and U-Pb data are provided as supporting information (Appendix C).

RESULTS

San Juan basin. Six samples from Cretaceous–Eocene units of the San Juan basin yield U-Pb age distributions that reflect all five populations (Fig. 4.1D, 4.3, 4.4A; Table 1). The ages of the youngest zircon grains from the San Juan basin decrease upsection (Table 1, Fig. 4.4A), consistent with magmatic input from western arc sources.

Mancos Shale. The Mancos Shale is a widespread marine shale previously assigned a Late Cretaceous age based on ammonite biostratigraphy (Robinson Roberts and Kirschbaum, 1995). The maximum depositional age of the Mancos sample (SJ001) is early Campanian (82.4 ± 2.3 Ma), based on a single youngest grain which is not part of a continuous distribution of ages. For the 104 concordant U-Pb ages, there are two main age groups of 82–248 Ma (peaks at 93 Ma and 185 Ma) and ca. 1697 Ma, with the remaining <20% of grains in the 1.0–1.5 Ga range.

Mesaverde Group. The Mesaverde Group (SJ002) is assigned to the middle Campanian based on a youngest grain of 76.5 ± 1.2 Ma. Most (40%) of the 105

concordant ages in this sample are 77–218 Ma (age peaks at 97 and 174 Ma). Other major age groups include ca. 540 (10%), 1092 (19%), 1435 (11%), and 1732 (14%) Ma (Fig. 4.3, Table 1). This sample is distinguished by the most evenly distributed ages among the five provenance groups, with notably higher numbers of Paleozoic and Mesoproterozoic grains than other samples.

Pictured Cliffs Formation. The principal age groups from a sample of the Pictured Cliffs Formation (SJ005) are 77–250 Ma (40% of total grains, with peaks at 87 Ma and 194 Ma), 398–488, 1366–1522, and 1634–1817 Ma. A middle Campanian maximum depositional age is defined by a weighted average of the 6 youngest ages (77.49 ± 0.87 Ma, MSWD=0.44).

Ojo Alamo Formation. A single sample (SJ003) from the Ojo Alamo Formation produced a single youngest grain at 70.8 ± 1.4 Ma; this Maastrichtian grain is interpreted to be a pre-depositional age based on magnetostratigraphic and biostratigraphic assignments of a Paleocene age to the Ojo Alamo Formation (Lindsay et al., 1981; Fassett, 1985). Four age groups are identified from the 109 concordant U-Pb ages: 1703 Ma (40%); 1418 Ma (25%); 1187 Ma (18%); and a 71–224 Ma population (peaks at 81 and 178 Ma, 17% grains). The lack of Paleozoic ages in this sample persists throughout the overlying Nacimiento and San Jose Formations.

Nacimiento Formation. A sample from the Nacimiento Formation (SJ006) is dominated by a single peak at 74.6 Ma defined by 50% of the total ages. The remaining ages form smaller groups centered at ca. 81 and 1686 Ma. The weighted average of the 5 youngest grains is 71.35 ± 0.81 Ma (MSWD=0.49), which is interpreted to be a pre-depositional age, based on a Danian (66–61 Ma) biostratigraphic and

magnetostratigraphic age (Williamson and Lucas, 1992) as well as an Ar/Ar sanidine age of 65.59 +- 0.01 Ma (Peppe et al., 2013).

San Jose Formation. A sample from the Eocene San Jose Formation (SJ007) yields a youngest single grain of 67.7 ± 3.2 Ma, which is not part of a continuous distribution of ages. This Maastrichtian age is part of the youngest pre-depositional phases of volcanism in the San Juan mountains (Gonzales, 2015), but is inconsistent with the paleontologic and magnetostratigraphic age (Williamson and Lucas, 1992). Of the 105 concordant U-Pb ages, all of the major source populations are present. The largest group has a peak at 1686 Ma (44% of total grains), with smaller peaks at 91 Ma, 170 Ma, and 1.4 Ga.

A significant Cordilleran arc signature (<250 Ma) is present in all six samples. Three Cretaceous samples (SJ001, SJ002, and SJ005) are dominated by the Cordilleran arc signatures (~95 and ~173 Ma age peaks), with minor Appalachian, Grenville, and Proterozoic components (Fig. 4.3A). Upsection, the Cenozoic samples (SJ003, SJ006, and SJ007) generally contain greater proportions of Proterozoic (~1.4 and ~1.7 Ga) grains. However, the Paleocene Nacimiento Formation sample (SJ006) is anomalous in its nearly unimodal age distribution centered at 75 Ma (Fig. 4.3A, 4.5A).

Galisteo-El Rito basin. Detrital zircon U-Pb data obtained from eight Galisteo-El Rito basin samples are generally consistent with the age distributions for the San Juan basin (Fig. 4.3). Within the basin, two samples are from the northern (El Rito) depocenter (Fig. 4.3B) and six samples from the southern (Galisteo) depocenter (Fig. 4.3C).

Although the Cretaceous units below the Menefee Formation in the Galisteo basin are mapped as undivided, the detrital zircon data provide initial depositional age

constraints for two undivided Cretaceous samples (HB009 and HB007). The lower sample (HB009) has 100 concordant ages and a distribution of ages 152–219 Ma (53% total grains). The maximum depositional age is Kimmeridgian (Late Jurassic) based on the weighted average of the 3 youngest grains at 153.0 ±1.6 Ma (MSWD = 0.36). Two other age groups have minor peaks at ca. 1471 Ma (17%) and 1123 Ma (16%). The upper sample (HB007) yields 100 concordant ages, a single Campanian youngest grain at 74.8 ± 1.4 Ma, and three primary peaks at 91, 163, and 1720 Ma.

Menefee Formation. The 101 detrital zircon ages from a sample of the Menefee Formation (HB005) are consistent with prior studies of this unit (e.g., Dickinson et al., 2010). A Campanian age is confirmed by a 73.9 Ma single youngest grain. Abundant Cordilleran-arc derived grains (37%) are clustered in peaks of 91 and 163 Ma, indicating multiple Cordilleran sources. Grains derived from 1.7 Ga Yavapai basement (18%), 1.4 Ga plutons (18%), and 1.0–1.2 Ga Grenville-age sources (10%) are also present in the Menefee Formation.

Diamond Tail Formation. The maximum depositional age for a sample of the Diamond Tail Formation (HB002) is determined to be early Paleocene based on the single youngest grain of 64.7 ± 1.9 Ma. About half (46%) of the 108 analyses are Mesozoic, with peaks at 85 and 166 Ma. Additional age groups at 1714 and 1450 Ma each include ~20% of the grains, with another minor peak at 495 Ma.

Galisteo Formation. A late Paleocene (56.07 ± 0.99 Ma) maximum depositional age is obtained for a single grain from a sample of the Galisteo Formation (HB001). In this sample, 31% of the grains center on two Mesozoic peaks at 84 and 166 Ma, and 41% of the grains are Proterozoic with peaks at 1087, 1450, and 1707 Ma.

Espinaso Formation. A sample from the volcaniclastic Espinaso Formation (GB001) yields an early Eocene maximum depositional age from the single youngest grain (32.4 ± 1.2 Ma), consistent with previous chronostratigraphic results suggesting a 36–27 Ma age (Gorham and Ingersoll, 1979; Lisenbee, 2013). For this sample, syndepositional grains account for only 5% of the total grains, with major Proterozoic age peaks of 1706 Ma (42%) and 1433 Ma (31%).

El Rito Formation. In the northern Galisteo (El Rito) depocenter, a conglomeratic sample (RW003) from the pre-volcanic El Rito Formation (RW003) is dominated by clasts of the Proterozoic Ortega Quartzite (Logsdon, 1981), consistent with the U-Pb age population. Of the 95 concordant ages, 42% of grains center on a peak at 1743 Ma, with a secondary peak at 1132 Ma (19%). A single late Eocene youngest grain is the only Cenozoic age in this sample.

Ritito Formation. Overlying the El Rito Formation in the northern Galisteo (El Rito) depocenter is the Oligocene Ritito Formation. Although only 33 concordant ages were measured for the sample (RW007), the Oligocene maximum depositional age based on the youngest grain age of 29.8 ± 2.1 Ma is consistent with previous age determinations (Lipman et al., 1970; Maldonado, 2008). The majority (73%) of grains are of Paleoproterozoic age, with a range of 1669–1912 Ma.

In the northern (El Rito) depocenter (Fig. 4.3B), two samples from the Paleocene-Eocene El Rito Formation (RW003) and Oligocene Ritito Formation (RW007) contain primarily Yavapai-Mazatzal basement (~1.7 Ga) grains. Minor Cordilleran arc grains are found in both samples, with a decrease in Appalachian and Grenville ages from the El Rito Formation to the Ritito Formation (Fig. 4.4B).

In the southern (Galisteo) depocenter, Cordilleran arc ages persist throughout the section, with an overall increase in Proterozoic ages (~1.4 and ~1.7 Ga) upsection (Fig. 4.3C). The lowest Cretaceous sample (HB009) contains a single Cordilleran peak centered at 155 Ma, which persists through all samples from the southern depocenter. A second Cordilleran age peak characterizes the upper five samples, decreasing upsection from 91 Ma in the undivided Cretaceous (HB007) to 48 Ma in the Oligocene Espinaso Formation (GB001). Rare Appalachian and Grenville grains are present throughout the section. Collectively, the results for the southern (Galisteo) depocenter show continuous input of syndepositional grains with an upsection increase in locally derived Yavapai-Mazatzal basement material.

Raton basin. Detrital zircon U-Pb data from the Raton basin are included for regional comparison of Laramide basins across southern Colorado and northern New Mexico. Four provenance groups are identified for Cretaceous–Eocene samples from the Raton basin (Fig. 4.3D; Bush et al., 2016a), based on stratigraphic appearance and disappearance of age populations. The Jurassic Entrada Formation, Cretaceous Dakota Formation, and Cretaceous Trinidad Formation (RB302, RB303, RB104, and RB111; Bush et al., 2016a) is characterized by a major Cordilleran arc peak and minor Appalachian and Grenville ages. The Maastrichtian Vermejo Formation and lower Raton Formation (RB107, RB112, RB208, and RB207; Bush et al., 2016a) exhibits a Cordilleran arc peak accompanied by the two Proterozoic basement peaks at ~1.4 and ~1.7 Ga. The Paleocene upper Raton Formation and lower Poison Canyon Formation (RB109, RB206, RB113, and RB201; Bush et al., 2016a) are dominated by a single ~1.7 Ga Yavapai-Mazatzal peak. The Paleocene Poison Canyon Formation and Eocene

Cuchara, Huerfano, and Farisita Formations (RB108, RB103, RB402, and RB401) and contain both Proterozoic peaks at ~1.4 and ~1.7 Ga.

Heavy Mineral Assemblages

The composition and distribution of diagnostic heavy minerals were analyzed to discriminate between recycled and crystalline sources based on variations in the proportions of specific mineral species (Morton and Hallsworth, 1999). The appearance of heavy mineral assemblages consistent with crystalline sources is considered a key indicator that most sedimentary cover has been removed and crystalline basement exposed in developing Laramide block uplifts.

Methods

Heavy mineral fractions (density > 2.89 g/cm^3) from 10 samples from the Raton and Galisteo-El Rito basins were separated and then analyzed using automated scanning electron microscopy (QEMSCAN) at the Colorado School of Mines Automated Mineralogy Laboratory. Back-scattered electron (BSE) and X-ray dispersive (EDX) spectra were collected and analyzed using the control program (iDiscover, FEI) to generate a compositional map for the heavy mineral fractions for each sample. Spectra were acquired from each particle using a beam-stepping interval of 15 microns, an accelerating voltage of 25 keV, and a beam current of 5 nA. Results are reported by the percent abundance of each mineral.

RESULTS

The delineation of heavy mineral assemblages from 10 detrital samples helps constrain the compositional character of sediment source areas. In particular, the proportion of ultra-stable heavy minerals zircon, tourmaline, and rutile (ZTR) provide an important proxy for recycled sedimentary sources, owing to the fact that these species withstand multiple rounds of erosion, transport, burial, and exhumation. Other major heavy mineral species such as apatite, hornblende, epidote, garnet, alumino-silicate accessory minerals are more indicative of a crystalline (igneous or metamorphic) source area.

For the ten analyzed samples, there is an upsection decrease in the abundance of recycled heavy minerals in the Raton basin (Fig. 4.2), decreasing from 97% ZTR in the Cretaceous Dakota Formation to 8% ZTR in the Eocene Poison Canyon Formation. Accompanying this trend is a huge decrease in relative volumes of apatite, from 51% in the Cretaceous Trinidad and Raton Formation to ~2% in the Eocene upper Poison Canyon Formation. The relative abundances of garnet (from <10% in Cretaceous samples to >20% in Cenozoic samples) and epidote increase in the Raton basin (8-65%).

Heavy mineral signatures for two samples from the northern Galisteo-El Rito basin delineate a significant departure from the Raton basin. Both samples exhibit very low percentages (<20%) of recycled ZTR grain assemblages. However, high (>20%) volumes of garnet in Galisteo-El Rito samples are comparable to Eocene units from the Raton basin and characteristic of metamorphic sources. The maximum volume of aluminosilicate accessory minerals (38% andalusite, kyanite, sillimanite) is observed in the Paleocene-Eocene El Rito Formation, indicating a source area dominated by

metapelitic rocks. From the El Rito Formation to the Oligocene Ritito Formation there is an increase in the abundance of apatite, hornblende, epidote, and sphene.

QEMSCAN analyses reveal several general trends in detrital heavy mineral assemblages for the Raton and Galisteo-El Rito basins: (1) a recycled (ZTR) source dominates the Cretaceous Dakota Formation (RB303); (2) a mixed assemblage emblematic of recycled and crystalline sources defines the Cretaceous Trinidad Formation through lower Eocene Poison Canyon Formation (RB111, RB112, RB207, RB206, and RB113); and (3) a crystalline, probably metamorphic, assemblage is expressed in samples from the Galisteo-El Rito basin (RW003 and RW007) in the upper Poison Canyon Formation of the Raton basin (RB208 and RB201).

Provenance interpretations

Integration of detrital zircon U-Pb geochronology and heavy mineral analyses for the San Juan, Galisteo-El Rito, and Raton basins of the southern Rocky Mountains enables the differentiation of various phases of Laramide mountain building and basin reorganization that could not be dissociated by studies focused on a single basin or a particular analytical technique.

The Cordilleran provenance group is observed in all three basins. Jurassic through Campanian units contain an ultra-stable heavy mineral assemblage (high ZTR), indicative of recycled sources and/or long transport distances. The detrital zircon U-Pb ages from these units indicate a western source dominated by grains from the Cordilleran magmatic arc and minor populations of Paleozoic and Mesozoic ages recycled from the Cordilleran (Sevier) fold-thrust belt. These populations are observed through the Cretaceous Mancos

(SJ001), Mesaverde (SJ002), and Pictured Cliffs (SJ005) formations in the San Juan basin, the Jurassic-Cretaceous Entrada and Dakota formations in the Raton basin, and in the undivided Cretaceous (HB009 and HB007) through the Campanian Menefee Formation ((HB005) in the Galisteo basin.

For Maastrichtian through Eocene strata, provenance results indicate widespread exposure of crystalline basement. Heavy mineral results from the Raton basin show initial mixed crystalline and recycled assemblages, and then by the early Eocene, assemblages characteristic of a crystalline source. Detrital zircon U-Pb ages from all basins show progressive increases in Proterozoic basement ages. Western sources continued to supply Cordilleran arc grains to the San Juan basin and Galisteo-El Rito basin, but were cut off in the Paleocene from the Raton basin and northern (El Rito) depocenter of the Galisteo-El Rito basin

BASIN RECONSTRUCTION

San Juan Basin

The transition from regional Jurassic–Cretaceous marine deposition in the Cordilleran foreland basin to more restricted Maastrichtian–Eocene nonmarine deposition in the Laramide San Juan basin is preserved in detrital provenance signatures and accumulation patterns. Prior to the Maastrichtian, the primary sediment source area for San Juan basin was to the west in the Cordilleran arc and (Sevier) fold-thrust belt, and perhaps the Mogollon highland (Dickinson and Gehrels, 2008; Lawton and Bradford, 2011; Dickinson et al., 2012; Laskowski et al., 2013). In the Campanian, initial intra-foreland (Laramide) deformation is recognized based on thickness variations due to

changing subsidence patterns in the Pictured Cliffs Sandstone and time-equivalent Lewis Shale (Cather, 2003). While western sources in the Cordilleran arc and fold-thrust belt continued to source the San Juan basin throughout the Cretaceous (Fig. 4.3A, 4.5A), an influx of volcanic lithic detritus from the north is recorded in the Maastrichtian upper Kirtland Shale (Powell, 1973; Klute, 1986; Brister and Chapin, 1993), suggesting the introduction of a new, more proximal sediment source (Fig. 4.3A, 4.6A). This northern source can be related to initial deformation in the San Juan mountains, where uplift was amplified by pluton emplacement in the Colorado Mineral Belt (Cunningham et al., 1994; Cather, 2012; Gonzales, 2015).

Increased subsidence in the northeastern San Juan basin during the Paleocene resulted in fluvial sand deposition of the Ojo Alamo and Nacimiento Formations (Cather, 2003). Provenance signatures from the lower Paleocene Ojo Alamo Formation include Yavapai-Mazatzal basement and Cordilleran arc ages (Fig. 4.3A). Proterozoic grains were derived from southeast-flowing streams draining basement exposures in the San Juan uplift to the northwest, the uplifted San Juan sag to the northeast (underlying the modern San Luis Valley), and the Sierra Nacimiento to the east (Powell, 1973; Tweto, 1975; Gries, 1985; Lehman, 1985; Klute, 1986; Brister and Gries, 1994; Cather, 2003). Cordilleran grains were recycled from Jurassic–Cretaceous units eroded from local uplifts, western sources in the Cordilleran (Sevier) fold-thrust belt, and possible distal contributions from the Cordilleran arc itself. The unimodal U-Pb age distribution for the Paleocene Nacimiento Formation potentially reflects a large influx of volcanic detritus associated with a high-volume eruption from the San Juan mountains (Gonzales, 2015) and/or drainage reorganization depriving the system of the 1.7 and 1.4 Ga basement

sources. This signature is similar to the U-Pb age distribution from the Maastrichtian Trinidad Formation in the Raton basin (Bush et al., 2016a). To the northeast, Paleocene units from the San Juan sag confirm the unroofing of Cretaceous units and exposure of basement, consistent with exhumation of the Sangre de Cristo mountains (Brister and Chapin, 1994).

Deposition of the Eocene San Jose Formation occurred above an unconformity with the Nacimiento Formation, with provenance evidence from paleocurrents and detrital compositions suggesting the Nacimiento uplift as the primary source (Baltz, 1965). Significant input of both ~1.4 and ~1.7 Ga zircon populations is consistent with a local source, with western sources also continuing to supply Cordilleran age grains to the San Juan basin (Fig. 4.3A).

Galisteo-El Rito Basin

Prior to the Paleocene, the Galisteo-El Rito basin was part of a continuous basin system connected upstream to the San Juan basin and downstream to east-flowing fluvial networks draining to the Gulf of Mexico. Cretaceous units (mapped as undivided) are dominated by Cordilleran arc ages, which persisted in the Galisteo depocenter throughout Campanian–Eocene sedimentation (Fig. 4.3C). Minor Appalachian, Grenville, 1.4 Ga, and Yavapai-Mazatzal age grains are consistent with unroofing of Mesozoic units from the Cordilleran (Sevier) fold-thrust belt as well as local uplifts. Paleocene deposition of the Diamond Tail Formation (Lucas et al., 1997; Lisenbee, 2013) was focused in the Galisteo depocenter near the Tijeras-Canoncito fault, and the increasing input of 1.4 and 1.7 Ga zircon grains derived from nearby basement uplifts (Fig 4.4C). Expansion of Galisteo-El Rito depositional area across the Nacimiento (San Luis) uplift occurred

during the Paleocene with the initiation of deposition in the Galisteo and El Rito depocenters (Abbott et al., 1995; Cather, 2004). The Galisteo area received sediment from the Sangre de Cristo mountains to the NNE prior to any input from the Nacimiento uplift to the west.

In the El Rito depocenter, large paleochannels of the El Rito and Ritito formations cut from the upper Mesozoic units deeper into the Proterozoic Vadito Group. These quartzite conglomerate and quartzose sandstones contain a dominant 1.7 Ga U-Pb age population, and were deposited as part of a through-flowing drainage that connected alluvial fan deposits of the northern (El Rito) depocenter with the southern (Galisteo) depocenter (Fig. 4.3B). This northward expansion of the basin depositional area was concurrent with a change in source area between the Diamond Tail and Galisteo formations in the Galisteo depocenter (Gorham and Ingersoll, 1979). Distinct source areas to the northeast and northwest require separation from the San Juan basin by 50 Ma (Logsdon, 1981). Fluvial systems continued to supply basement and Cordilleran arc grains into the Oligocene Ritito Formation and Espinaso Formation of the Galisteo-El Rito basin, during increasingly volcaniclastic deposition of late Eocene-Oligocene and younger age (Fig. 4.3B, 4.4C).

Raton basin

The Cretaceous through Eocene record from the Raton basin illustrates the growth of Laramide block uplifts and contemporaneous regression of the Cretaceous Western Interior Seaway. Through the Campanian, marine deposits in the Raton basin are consistent with sedimentation patterns in other basins of western North America. Cather (2004) proposed that a late Campanian–early Maastrichtian fluvial system was

superimposed on San Luis Uplift (incipient Sangre de Cristo mountains), providing a point source for Trinidad Sandstone and cutting a paleocanyon during uplift of the San Luis Uplift / Sangre de Cristo mountains. While this model provides a direct supply of sediment to the deltaic deposits of the Trinidad Sandstone, there is a lack of evidence for deep incision in the Sangre de Cristo mountains or east-directed paleocurrents from the San Juan sag and San Juan basin to the west (Clark and Read, 1972; Bush et al., 2016a).

DISCUSSION

Based on provenance and stratigraphic evidence, we propose three stages of Campanian–Eocene basin evolution in the southern Rocky Mountain Laramide province. Using heavy mineral assemblages, U-Pb geochronology, accumulation rates, and stratigraphic gaps, we identify three phases of sedimentation and associated deformation (Fig. 4.6). These phases were largely controlled by the formation of topographic barriers and local infilling of basins, and ultimately expressed as changes in sediment routing and delivery of variable sediment volumes to the Gulf of Mexico.

Initial Laramide Phase

Maastrichtian through early Paleocene deposits in southern Rocky Mountain basins record partitioning of the Cordilleran foreland basin by incipient Laramide uplifts (Fig. 4.5A). These deposits are associated with the terminal retreat of the epicontinental sea from the interior of North America. Provenance signatures of the Ojo Alamo Formation of the San Juan basin, the Diamond Tail Formation of the Galisteo-El Rito basin, and the Raton Formation of the Raton basin are all typical of this phase of basin deposition. The transition from marine to nonmarine deposition was accompanied by

initial input of ~1.7 and ~1.4 Ga basement sources, as well as increasing sediment accumulation rates in local Laramide basins of the southern Rocky Mountains and in the Gulf of Mexico. A regional drop in base level and increased sediment supply dictated depositional patterns in these basins (Fig. 4.6). Base level change was driven by a combination of eustatic, climatic, and tectonic mechanisms that resulted in the retreat of the Western Interior Seaway from the Cordilleran foreland basin, and contributed to the eastward advance of deltaic, coastal plain, and fluvial depositional systems into the Cordilleran foreland. Initial deformation in the Laramide ranges resulted in localized depocenters throughout the southern Rocky Mountains as the Cordilleran foreland began to be compartmentalized into smaller basins. During this earliest phase, however, fluvial systems continued to be fully connected throughout the Laramide province, producing a provenance signal that can be traced to the Cordilleran magmatic arc, the Cordilleran (Sevier) fold-thrust belt, and growing Laramide uplifts. Longitudinal rivers crossed the interior of the continent, becoming integrated with the Gulf of Mexico in the Paleocene and providing the initial input of significant siliciclastic material to the Gulf of Mexico (Fig. 4.6).

Main Laramide Phase

The main phase of Laramide shortening and deposition occurred during the Paleocene (Fig. 4.5B). Provenance and depositional patterns of the upper Raton and Poison Canyon Formations in the Raton basin, the Nacimiento Formation in the San Juan basin, and the Galisteo and El Rito Formations in the Galisteo-El Rito basin indicate a major pulse of exhumation linked to shortening-induced uplift of various basement blocks. Provenance signatures from all three basins show a significant input of local

basement material, and sediment accumulation rates reach their maximum during this phase of Laramide deposition. At this time, the Sangre de Cristo range formed a topographic barrier between the Raton basin and western sources, cutting off fluvial systems that had previously connected these regions (Bush et al., 2016a). The increased local sediment supply can be attributed to unroofing of material from the Laramide ranges as they grew in relief and areal extent. Deposition behind the topographic barrier was focused in ponded and axial basins including the San Juan and Galisteo-El Rito basins. These basins maintained external drainage due to the low regional base level, supplying sediment derived from local uplifts and excavated from basin margins to feed major fluvial systems. These longitudinal rivers reached the Gulf of Mexico at the Rosita and southwest Texas river deltas, contributing to the massive increase in siliciclastic material reaching the Gulf of Mexico during the deposition of the Lower Wilcox Formation in the Paleocene (Fig. 4.6; Galloway et al., 2011). While sediment volumes in the Gulf of Meicxo derived from the southern Rocky Mountains was relatively minor compared to the northern Rocky Mountains and Sierra Madre, similar patterns of volume increase and decrease are observed at the local (western) and regional scale.

Post Laramide Phase

Upper Paleocene through Eocene deposits document the late stages of the Laramide orogeny (Fig. 4.5C). This phase is characterized by widespread infilling of basins due to internal drainage in the Rocky Mountains. In the Raton basin, the upper Poison Canyon through Farisita Formations include conglomerate and sandstone derived from local basement exposed in the Sangre de Cristo and Wet Mountain uplifts. In the Galisteo-El Rito basin, the channelized deposits of the El Rito and Ritito Formations in

the northern part of the basin coalesce into the Galisteo and Espinaso Formations in the southeastern part of the basin. By the middle Eocene the infilling of these basins progressed up the flanks of Laramide uplifts and persisted across the Front Range to the Great Plains, creating a low relief surface that has been mapped throughout the region (Epis and Chapin, 1975; McMillan et al., 2006).

The storage of significant quantities of sediment within axial and ponded basins behind topographic barriers prevented large-scale mass transfer from the orogen interior to the foreland (Dickinson et al., 1988). This reduced the erosional capacity of channels on the perimeter of the orogen as catchment size was reduced, effectively retarding incision of a through-going drainage across the barrier (Burbank et al., 1996; Whipple and Tucker, 1999; Sobel et al., 2003).

Continent-scale drainage patterns

The sediment accumulation history of the Gulf of Mexico shows two distinct phases associated with Laramide deformation: (1) an initial, voluminous influx of sediment marked by deposition of the Lower Wilcox Formation during the early, main phase of Laramide shortening, followed by (2) drastically diminished sediment volumes in late Paleocene through Eocene time (Fig. 4.6; Galloway et al., 2011). Previously these patterns have been attributed slowing of Laramide deformation as the region transitioned into relative tectonic stability in the Eocene (Galloway et al., 2011). However, the provenance and depositional record from the southern Rocky Mountains do not support the interpretation of a hiatus or slowing of Laramide shortening. Rather, provenance data from Paleocene–Eocene strata confirm the sustained exhumation of crystalline basement

in the Sangre de Cristo and Nacimiento ranges, and continuous sedimentation in both the San Juan and Raton basins. In fact, the late Paleocene–Eocene are thought to have been the time of the most intense tectonism and rapid sedimentation in New Mexico (Chapin and Cather, 1981; Lucas and Ingersoll, 1981). Though only limited exposures of upper Paleocene–Eocene rocks remain in these basins, outcrops in the Chuska Mountains and the Spanish Peaks stocks (quartz syenite, granodiorite porphyry, and granite porphyry) require at least one kilometer of sediment to have been removed since Eocene time (Fassett, 1985; Cather, 2003). Thus, while axial rivers persisted through the San Juan and southern Galisteo-El Rito basins, the Sangre de Cristo range effectively blocked sediment delivery to the Gulf of Mexico. This pattern of basin infilling is consistent with the record in the northern Rocky Mountains, where topographic growth during the late stages of the Laramide orogeny resulted in the integration of the Green River, Uinta, and Piceance Creek basin systems and hydrologic closure of the Laramide foredeep at ~52 Ma (Carroll et al., 2006; Davis et al., 2009).

The Laramide basins share many elements with basins in high continental plateaus of contractional orogens such as the Andes and Tibet (e.g., Horton, 2012; Bush et al., 2016b), but they also differ from these examples in several fundamental ways. Laramide deformation involved rapid shortening, exhumation, and uplift, as well as the exposure of resistant lithologies, but there is no contemporaneous evidence for a significant increase in aridity in the North American plate interior. In contrast, aridity is considered a necessary condition to maintain closed drainage in plateau interiors of the Andes and Tibet (Sobel et al., 2003; Garcia-Castellanos, 2006; Carroll, 2010; Strecker et al., 2012). Furthermore, the proposed high-elevation plateau in North America (the

"Nevadaplano" of DeCelles, 2004), a potential equivalent to the Altiplano or Tibetan plateau, was associated with the earlier phase of Cordilleran mountain building and located much farther west in the Cordilleran hinterland. Thus, the plate-interior basins of the Laramide province are characterized by thick accumulations of synorogenic sedimentary strata, but not necessarily the long-term internal drainage that is typical of other contractional orogenic settings.

CONCLUSIONS

Detrital zircon U-Pb provenance results reveal a switch from accumulation of distal sediments in a regional foreland basin with Cordilleran arc sources, to more proximal sedimentation in partitioned flexural basins fed principally by basement-cored Laramide uplifts. This pattern is consistent across the San Juan, Galisteo-El Rito, and Raton basins of the southern Colorado and northern New Mexico (Fig. 4.5). Syndepositional detrital zircon U-Pb ages as well as other chronostratigraphic evidence constrains the timing of this provenance switch to the early Paleocene. In the San Juan and Galisteo-El Rito basins, the youngest detrital zircon populations systematically decrease in age upsection, supporting the interpretation that a syndepositional volcanic source from the San Juan range, as well as possibly a more distal Cordilleran arc source, was connected to the basin system throughout the Sevier-Laramide orogeny. In addition to these syndepositional volcanic sources, 1.7 Ga Yavapai basement and 1.4 Ga local plutonic sources provide evidence of the initial exposure of Precambrian crystalline basement within the cores of uplifting Laramide ranges. Uplift of the San Juan, Nacimiento, and Sangre de Cristo ranges can be tracked in both the provenance signals

and in basin architecture. Whereas the Cretaceous marine units associated with the Sevier foreland basin persist regionally across the southern Rocky Mountains, the Maastrichtian–Eocene sedimentary units are much more localized in their extent and character, and contain more significant internal unconformities. This regional contrast in provenance and stratigraphic framework is indicative of the complex patterns of basin partitioning associated with uplift of topographic barriers such as the Sangre de Cristo range to the west of the Raton basin, and the Nacimiento range between the San Juan and Galisteo-El Rito basins.

Overall, we interpret three major phases in the Laramide drainage evolution of the southern Rocky Mountains. First, initial exhumation in Laramide uplifts provided the first pulse of basement material to a still interconnected regional foreland basin. Then, the Sangre de Cristo range was uplifted to the point of forming a topographic barrier between the San Juan–Galisteo-El Rito basins to the west and the Raton basin to the east. Finally, uplift in the Nacimiento range and both uplift and volcanism in the San Juan range partitioned the (upstream) San Juan basin and the (downstream) Galisteo-El Rito basin.

We propose that drainage reorganization was critical not only to the evolution of the proximal basins of the southern Rocky Mountains, but also influenced changes in the sedimentary budgets of the continental-scale source-to-sink system spanning from the Laramide uplifts of the southern Rocky Mountains to the Gulf of Mexico (Fig. 4.6). In this interpretation, we emphasize the contemporaneous input of significant Laramide material in proximal basins and increase in sediment volumes reaching the Gulf of Mexico during Maastrichtian to Paleocene time. Likewise, the drop in sediment volumes in the Gulf of Mexico during the late Paleocene to Eocene is compatible with uplift of

topographic barriers (Sangre de Cristo and Nacimiento ranges) and partial blockage of formerly through going drainage systems in the southern Rocky Mountains. Finally, the subsequent post-Eocene dissection of these topographic barriers and re-integration of the southern Rocky Mountain sedimentary basins is mirrored by the stabilization of siliciclastic sedimentary volumes in the Gulf of Mexico.

REFERENCES

Abbott, J.C., Cather, S.M., and Goodwin, L.B., 1995, Paleogene synorogenic sedimentation in the Galisteo basin related to the Tijeras-Canoncito Fault System: New Mexico Geological Society Guidebook, p. 271–278.

Applegate, J.K., and Rose, P.R., 1985, Structure of the Raton Basin from a regional seismic line, *in* Gries, R.R., and Dyer, R.C., eds, Seismic exploration of the Rocky Mountain region: Rocky Mountain Association of Geologists and Denver Geophysical Society, p. 259-265.

Aschoff, J.L. and Steel, R.J., 2011, Anomalous clastic wedge development during the Sevier-Laramide transition in the Cordilleran Foreland Basin, USA: Geological Society of America Bulletin, v. 123, p. 1822-1835.

Atwater, T., 1970, Implications of plate tectonics for the Cenozoic tectonic evolution of western North America: Geological Society of America Bulletin, v. 81, p. 3513.

Ayers, W.B. Jr., and Kaiser, W.R., 1994, Coalbed methane in the Upper Cretaceous Fruitland Formation, San Juan Basin, New Mexico and Colorado: New Mexico Bureau of Mines and Mineral Resources, Bulletin 146, 216 p.

Baltz, E.H., 1965, Stratigraphy and history of the Raton basin and notes on the San Luis basin, Colorado-New Mexico: AAPG Bulletin, v. 49, p. 2041–2075.

Baltz, E. H., 1967, Stratigraphy and regional tectonic implications of part of Upper Cretaceous and Tertiary rocks, eastcentral San Juan Basin, New Mexico: U.S. Geological Survey Professional Paper 552, 101 p.

Barton, M.D., 1996, Granitic magmatism and metallogeny of southwestern North America: Transactions of the Royal Society of Edinburgh: Earth Sciences, v. 87, p. 261–280.

Beck, R.A., Vondra, C.F., Filkins, J.E., and Olander, J.D., 1988, Syntectonic sedimentation and Laramide basement thrusting, Cordilleran foreland; Timing of deformation: Geological Society of America Memoir, v. 171, p. 465–487.

Bingler, E.C., 1968, Geology and mineral resources of Rio Arriba County, New Mexico: New Mexico Bureau of Geology and Mineral Resources Bulletin, v. 91, p. 175.

Blum, M., and Pecha, M., 2014, Mid-Cretaceous to Paleocene North American drainage reorganization from detrital zircons: Geology, v. 42, p. 607–610, doi: 10.1130/G35513.1.

Brister, B.S., 1992, The Blanco Basin formation (Eocene), San Juan Mountains Region, Colorado and New Mexico: New Mexico Geological Society Guidebook, v. 43rd Field, p. 321–331.

Brister, B.S., and Chapin, C.E., 1994, Sedimentation and Tectonics of the Laramide San Juan Sag, Southwestern Colorado: The Mountain Geologist, v. 31, p. 2–18.

Brister, B.S., and Gries, R.R., 1994, Tertiary stratigraphy and tectonic development of the Alamosa basin (northern San Luis Basin), Rio Grande rift, south-central Colorado, *in* Keller, G.R., and Cather, S.M., eds., Basins of the Rio Grande rift: Structure, stratigraphy, and tectonic setting: GSA Special Paper 291, p. 39-58.

Burbank, D.W., Meigs, A., and Brozovic, N., 1996, Interactions of growing folds and coeval depositional systems: Basin Research, v. 8, p. 199–223, doi: 10.1046/j.1365-2117.1996.00181.x.

Bush, M.A., Horton, B.K., Murphy, M.A., and Stockli, D.F., 2016a, Detrital record of initial basement exhumation along the Laramide deformation front, southern Rocky Mountains: Tectonics, doi: 10.1002/2016TC004194.

Bush, M.A., Saylor, J.E., Horton, B.K., and Nie, J., 2016b, Growth of the Qaidam Basin during Cenozoic exhumation in the northern Tibetan Plateau: Inferences from depositional patterns and multiproxy detrital provenance signatures: Lithosphere, v. 8, p. 58-82, doi:10.1130/L449.1.

Carroll, A.R., Chetel, L.M., and Smith, M.E., 2006, Feast to famine: Sediment supply control on Laramide basin fill: Geology, v. 34, p. 197, doi: 10.1130/G22148.1.

Carroll, A.R., Graham, S.A., and Smith, M.E., 2010, Walled sedimentary basins of China: Basin Research, v. 22, p. 17–32.

Carvajal, C., and Steel, R.J., 2012, Source-to-sink sediment volumes within a tectono-stratigraphic model for a Laramide shelf-to-deep-water basin : methods and results, *in* Busby, C. and Azor, A. eds., Tectonics of Sedimentary Basins: Recent Advances, Blackwell Scientific Publications, p. 131–151.

Cather, S.M., 1999, Implications of Jurassic, Cretaceous, and Proterozoic piercing lines for Laramide oblique-slip faulting in New Mexico and rotation of the Colorado Plateau: Geological Society of America Bulletin, v. 111, p. 849–868, doi: 10.1130/0016-7606(1999)111<0849:IOJCAP>2.3.CO;2.

Cather, S.M., 2003, Polyphase Laramide tectonism and sedimentation in the San Juan Basin, New Mexico: New Mexico Geological Society Guidebook, v. 54, p. 119–132.

Cather, S.M., 2004, Laramide orogeny in central and northern New Mexico and southern Colorado, *in* Mack, G.H. and Giles, K.A. eds., The Geology of New Mexico, a Geologic History, New Mexico Geological Society, p. 203–248.

Cather, S.M., 1992, Suggested revisions to the Tertiary tectonic history of north-central New Mexico: New Mexico Geological Society Guidebook, v. 43rd Field, p. 109–122.

Cather, S.M., Chapin, C.E., and Kelley, S.A., 2012, Diachronous episodes of Cenozoic erosion in southwestern North America and their relationship to surface uplift, paleoclimate, paleodrainage, and paleoaltimetry: Geosphere, v. 8, p. 1177–1206, doi: 10.1130/GES00801.1.

Cather, S.M., and Johnson, B.D., 1986, Eocene depositional systems and tectonic framework of west-central New Mexico and eastern Arizona, *in* Paleotectonics and sedimentation in the Rocky Mountains, AAPG, p. 623–652.

Chapin, C.E., 1983, An overview of Laramide wrench faulting in the southern Rocky Mountains with emphasis on petroleum exploration, *in* Lowell, J.D. and Gries, R.R. eds., Rocky Mountain Foreland Basins and Uplifts, Denver, CO, Rocky Mountain Association of Geologists, p. 169–179.

Chapin, C.E., 2012, Origin of the Colorado Mineral Belt: Geosphere, v. 8, p. 28–43, doi: 10.1130/GES00694.1.

Chapin, C.E., and Cather, S.M., 1981, Eocene tectonics and sedimentation in the Colorado Plateau - Rocky Mountain area, *in* Dickinson, W.R. and Payne, W.D. eds., Relations of Tectonics to ore deposits in the southern Cordillera: Arizona Geological Society Digest, v. 14, p. 173–198.

Clark, K.F., and Read, C.B., 1972, Geology and ore deposits of Eagle Nest area, New Mexico: New Mexico Bureau of Mines and Mineral Resources Bulletin 94, p. 152.

Clinkscales, C.A., and Lawton, T.F., 2015, Timing of Late Cretaceous shortening and basin development, Little Hatchet Mountains, southwestern New Mexico, USA - implications for regional Laramide tectonics: Basin Research, v. 27, p. 453–472, doi: 10.1111/bre.12083.

Coleman, D.S., and Glazner, A.F., 1997, The Sierra Crest magmatic event: Rapid formation of juvenile crust during the Late Cretaceous in California: International Geology Review, v. 39, p. 768–787, doi: 10.1080/00206819709465302.

Coney, P.J., 1972, Cordilleran tectonics and North American plate motion: American Journal of Science, v. 272, p. 603–628.

Coney, P.J., and Reynolds, S.J., 1977, Cordilleran Benioff zones: Nature, v. 270, p. 403–406.

Crabaugh, J.P., 2001, Nature and growth of nonmarine-to-marine clastic wedges: Examples from the Upper Cretaceous Iles Formation, Western Interior (Colorado) and the Lower Paleogene Wilcox Group of the Gulf of Mexico basin (Texas) [Ph.D. thesis]: University of Wyoming, 235 p.

Cunningham, C.G., Naeser, C.W., Marvin, R.F., Luedke, R.G., and Wallace, A.R., 1994, Ages of Selected Intrusive Rocks ana Associated Ore Deposits in the Colorado Mineral Belt: U.S. Geological Survey Bulletin, v. 2109.

Daniel, C.G., Pfeifer, L.S., Jones, J. V., and McFarlane, C.M., 2013, Detrital zircon evidence for non-Laurentian provenance, Mesoproterozoic (ca. 1490-1450 Ma) deposition and orogenesis in a reconstructed orogenic belt, northern New Mexico, USA: Defining the Picuris orogeny: Geological Society of America Bulletin, v. 125, p. 1423–1441, doi: 10.1130/B30804.1.

Davis, D., Suppe, J., and Dahlen, F.A., 1983, Mechanics of fold-and-thrust belts and accretionary wedges: Journal of Geophysical Research, p. 1153-1172.

Davis, S.J., Mix, H.T., Wiegand, B.A., Carroll, A.R., and Chamberlain, C.P., 2009, Synorogenic evolution of large-scale drainage patterns: Isotope paleohydrology of sequential Laramide basins: American Journal of Science, v. 309, p. 549–602, doi: 10.2475/07.2009.02.

DeCelles, P.G., 2004, Late Jurassic to Eocene evolution of the Cordilleran thrust belt and foreland basin system, western USA: American Journal of Science, v. 304, p. 105–168.

DeCelles, P.G., 1991, Kinematic history of a foreland uplift from Paleocene synorogenic conglomerate, Beartooth Range, Wyoming and Montana: Geological Society of America Bulletin, v. 103, p. 1458–1475.

DeCelles, P.G., and Giles, K.A., 1996, Foreland basin systems: Basin Research, v. 8, p. 105–123, doi: 10.1046/j.1365-2117.1996.01491.x.

DeCelles, P.G., and Graham, S.A., 2015, Cyclical processes in the North American Cordilleran orogenic system: Geology, v. 43, p. 499-502.

DeCelles, P.G., and Mitra, G., 1995, History of the Sevier orogenic wedge in terms of critical taper models, northeast Utah and southwest Wyoming: Geological Society of America Bulletin, v. 107, p. 454–462, doi: 10.1130/0016-7606(1995)107<0454:HOTSOW>2.3.CO;2.

Dewey, J.F., and Bird, J.M., 1970, Mountain belts and the new global tectonics: Journal of Geophysical Research, v. 75, p. 2625–2646, doi: 10.1029/JB075i014p02625.

Dickinson, W.R., and Gehrels, G.E., 2008, Sediment delivery to the Cordilleran foreland basin: insights from U-Pb ages of detrital zircon in Upper Jurassic and Cretaceous strata of the Colorado Plateau: American Journal of Science, v. 308, p. 1041–1082, doi: 10.2475/10.2008.01.

Dickinson, W.R., and Gehrels, G.E., 2003, U–Pb ages of detrital zircons from Permian and Jurassic eolian sandstones of the Colorado Plateau, USA: paleogeographic implications: Sedimentary Geology, v. 163, p. 29–66, doi: 10.1016/S0037-0738(03)00158-1.

Dickinson, W.R., and Gehrels, G.E., 2009, U-Pb ages of detrital zircons in Jurassic eolian and associated sandstones of the Colorado Plateau: Evidence for transcontinental dispersal and intraregional recycling of sediment: Geological Society of America Bulletin, v. 121, p. 408–433, doi: 10.1130/B26406.1.

Dickinson, W.R., Cather, S.M., and Gehrels, G.E., 2010, Detrital zircon evidence for derivation of arkosic sand in the eolian Narbona Pass Member of the Chuska Sandstone from Precambrian basement rocks in central Arizona, in Fassett. J.E., Zeigler, K.E., and Lueth, V.W., eds., Geology of the Four Corners Country: New Mexico Geological Society 61st Annual Field Conference, p. 125–134.

Dickinson, W.R., Klute, M.A., Hayes, M.J., Janecke, S.U., Lundin, E.R., McKittrick, M., and Olivares, M.D., 1988, Paleogeographic and paleotectonic setting of Laramide sedimentary basins in the central Rocky Mountain region: Bulletin of the Geological Society of America, v. 100, p. 1023.

Dickinson, W.R., and Snyder, W., 1978, Plate tectonics of the Laramide orogeny: Geological Society of America Memoir, v. 151, p. 355–366.

Ducea, M.N., 2001, The California arc: Thick granitic batholiths, eclogitic residues, lithospheric-scale thrusting, and magmatic flare-ups: GSA Today, v. 11, p. 4–10, doi: 10.1130/1052-5173(2001)011<0004:TCATGB>2.0.CO;2.

English, J.M., Johnston, S.T., and Wang, K., 2003, Thermal modelling of the Laramide orogeny: Testing the flat-slab subduction hypothesis: Earth and Planetary Science Letters, v. 214, p. 619–632, doi: 10.1016/S0012-821X(03)00399-6.

Epis, R., and Chapin, C.E., 1975, Geomorphic and tectonic implications of the post-Laramide, late Eocene erosion surface in the southern Rocky Mountains: Geological Society Of America Memoirs, v. 144, p. 45–74.

Erslev, E.A., 1993, Thrusts, back-thrusts, and detachment of Rocky Mountain foreland arches, *in* Schmidt, C.J., Chase, R.B., and Erslev, E.A., eds., Laramide basement deformation in the Rocky Mountain foreland of the western United States: Geological Society of America Special Paper 280, p. 339–358.

Erslev, E.A., 2001, Multistage, multidirectional Tertiary shortening and compression in north-central New Mexico: Geological Society of America Bulletin, v. 113, p. 63–74, doi: 10.1130/0016-7606(2001)113<0063:MMTSAC>2.0.CO;2.

Fan, M., and Carrapa, B., 2014, Late Cretaceous – early Eocene Laramide uplift, exhumation, and basin subsidence in Wyoming: Crustal responses to flat slab subduction: Tectonics, v. 33, p. 509–529, doi: 10.1002/2012TC003221.Received.

Fassett, J.E., and Steiner, M.B., 1997, Precise age of C33N-C32R magnetic-polarity reversal, San Juan basin, New Mexico and Colorado, *in* Anderson, O., Kues, B., and

Lucas, S.G. eds., Mesozoic Geology and Paleontology of the Four Corners Area: New Mexico Geological Survey Guidebook v. 48, p. 105–111.
Fassett, J.E., 1985, Early Tertiary paleogeography and paleotectonics of the San Juan Basin Area, New Mexico and Colorado, *in* Cenozoic Paleogeography of west-central United States, Rocky Mountain Section SEPM Symposium 3, p. 317–334.
Fielding, E.J., and Jordan, T.E., 1988, Active deformation at the boundary between the Precordillera and Sierras Pampeanas, Argentina, and comparison with ancient Rocky Mountain deformation: Geological Society of America Memoir, v. 171, p. 143–163.
Flores, R.M., and Tur, S., 1982, Characteristics of deltaic deposits in the Cretaceous Pierre Shale, Trinidad Sandstone, and Vermejo Formation, Raton basin, Colorado: The Mountain Geologist, v. 19, p. 25–40.
Galloway, W.E., Whiteaker, T.L., and Ganey-Curry, P., 2011, History of Cenozoic North American drainage basin evolution, sediment yield, and accumulation in the Gulf of Mexico basin: Geosphere, v. 7, p. 938–973, doi: 10.1130/GES00647.1.
Gonzales, D.A., 2015, New U-Pb Zircon and 40Ar/39Ar age constraints on the Late Mesozoic to Cenozoic plutonic record in the western San Juan Mountains: The Mountain Geologist, v. 52, p. 5–42.
Gorham, T.W., and Ingersoll, R. V., 1979, Evolution of the Eocene Galisteo basin, north-central New Mexico: New Mexico Geological Society Guidebook, v. 30th Field, p. 219–225.
Gries, R., 1983, North-south compression of Rocky Mountain foreland structures, *in* Rocky Mountain Foreland Basins and Uplifts, Rocky Mountain Association of Geologists, p. 9–32.
Gries, R.R., 1985, San Juan sag: Cretaceous Rocks in a volcanic-covered basin, south central Colorado: The Mountain Geologist,. The Mountain Geologist, v. 22, p. 167–179.
Heller, P.L., Angevine, C.L., Winslow, N.S., and Paola, C., 1988, Two-phase stratigraphic model of foreland-basin sequences: Geology, v. 16, p. 501.
Horton, B.K., 2012, Cenozoic evolution of hinterland basins in the Andes and Tibet, in Busby, C., and Azor, A., eds., Tectonics of Sedimentary Basins: Recent Advances: Wiley-Blackwell, Oxford, UK, p. 427–444.
Horton, B.K., Fuentes, F., Boll, A., Starck, D., Ramirez, S.G., and Stockli, D.F., 2016, Andean stratigraphic record of the transition from backarc extension to orogenic shortening: A case study from the northern Neuquén basin, Argentina: Journal of South American Earth Sciences, v. 71, p. 17–40, doi:10.1016/j.jsames.2016.06.003.
Hovius, N., 1998, Controls on sediment supply by large rivers, *in* Shanley, K.W. and McCabe, P.J. eds., Relative Role of Eustasy, Climate and Tectonism in Continental Rocks, SEPM Society for Sedimentary Geology, p. 3–16.
Howard, A.L., Farmer, G.L., Amato, J.M., and Fedo, C.M., 2015, Zircon U – Pb ages and Hf isotopic compositions indicate multiple sources for Grenvillian detrital zircon deposited in western Laurentia: Earth and Planetary Science Letters, v. 432, p. 300–310.
Hunt, A.P., and Lucas, S.G., 1992, Stratigraphy, paleontology and age of the Fruitland and Kirtland formations (upper Cretaceous), San Juan Basin, New Mexico, *in* Lucas, S.G., Kues, B., Williamson, T.E., and Hunt, A.P. eds., San Juan Basin IV, New

Mexico Geological Soceity 43rd Annual Fall Field Conference Guidebook, p. 217–239.
Johnson, R.B., and Wood, G.H., 1956, Stratigraphy of upper Cretaceous and Tertiary rocks of the Raton basin, Colorado and New Mexico: AAPG Bulletin, v. 40, p. 707–721.
Jones, J., and Connelly, J., 2006, Proterozoic tectonic evolution of the Sangre de Cristo Mountains, southern Colorado, U.S.A.: Rocky Mountain Geology, v. 41, p. 79–116.
Jordan, T.E., 1981, Thrust loads and foreland basin evolution, Cretaceous, western United States: AAPG Bulletin, v. 65, p. 2506-2520.
Jordan, T.E., 1995, Retroarc foreland and related basins, *in* Busby, C.J. and Ingersoll, R.V. eds., Tectonics of Sedimentary Basins, Oxford, Blackwell Science, p. 331–362.
Jordan, T.E., and Allmendinger, R.W., 1986, The Sierras Pampeanas of Argentina: A modern analogue of Rocky Mountain foreland deformation: American Journal of Science, v. 286, p. 737–764.
Karlstrom, K.E., and Daniel, C.G., 1993, Restoration of Laramide right-lateral strike slip in northern New Mexico by using Proterozoic piercing points: tectonic implications from the Proterozoic to the Cenozoic: Geology, v. 21, p. 1139–1142, doi: 10.1130/0091-7613(1993)021<1139:ROLRLS>2.3.CO;2.
Kelley, S.A., 1990, Late Mesozoic to Cenozoic cooling histories of the Sangre de Cristo Mountains, Colorado and New Mexico: New Mexico Geological Society Guidebook, v. 41st Annua, p. 123–132.
Kelley, S.A., and Chapin, C.E., 1995, Apatite fission-track thermochronology of the southern Rocky Mountain - Rio Grande rift - western High Plains province: New Mexico Geological Society Guidebook, v. 46th Annua, p. 87–96.
Kelley, S., and Chapin, C.E., 1997, Internal structure of the southern Front Range, Colorado, from an apatite fission-track thermochronology perspective, *in* Bolyard, D.W. and Sonnenberg, S.A. eds., Colorado Front Range Guidebook, Denver, Rocky Mountain Association of Geologists, p. 19–30.
Kelley, V.C., 1955, Monoclines of the Colorado Plateau: Geological Society of America Bulletin, v. 66, p. 789–804.
Klute, M.A., 1986, Sedimentology and sandstone petrography of the upper Kirtland Shale and Ojo Alamo Sandstone, Cretaceous-Tertiary boundary, western and southern San Juan basin, New Mexico: American Journal of Science, v. 286, p. 463–488.
Laskowski, A.K., DeCelles, P.G., and Gehrels, G.E., 2013, Detrital zircon geochronology of Cordilleran retroarc foreland basin strata, western North America: Tectonics, v. 32, p. 1027–1048, doi: 10.1002/tect.20065.
Lawton, T.F., 2008, Laramide Sedimentary Basins, *in* The Sedimentary Basins of the United States and Canada, Sedimentary Basins of the World v.5, Sedimentary Basins of the World, Elsevier, p. 429–450.
Lawton, T.F., and Bradford, B.A., 2011, Correlation and Provenance of Upper Cretaceous (Campanian) Fluvial Strata, Utah, U.S.A., from Zircon U-Pb Geochronology and Petrography: Journal of Sedimentary Research, v. 81, p. 495–512, doi: 10.2110/jsr.2011.45.
Lehman, T.M., 1985, Depositional environments of the Naashobito Member of the Kirtland Shale, Upper Cretaceous, San Juan Basin, New Mexico, *in* Wolberg, D.L.

ed., Contributions to Late Cretaceous paleontology and stratigraphy of New Mexico: New Mexico Bureau of Mines and Mineral Resources, Circular 195, p. 55–79.
Lindsay, E.H., Butler, R.F., and Johnson, N.M., 1981, Magnetic polarity zonation and biostratigraphy of late Cretaceous and Paleocene continental deposits, San Juan basin, New Mexico: American Journal of Science, v. 281, p. 390–435.
Lindsey, D.A., 1998, Laramide structure of the central Sangre de Cristo mountains and adjacent Raton Basin, southern Colorado: The Mountain Geologist, v. 35, p. 55-70.
Lipman, P.W., Steven, T.A., and Mehnert, H.H., 1970, Volcanic history of the San Juan Mountains, Colorado, as indicated by potassium-argon dating: Geological Society of America Bulletin, v. 81, p. 2329–2352.
Lisenbee, A.L., 2013, Multi-stage Laramide deformation in the area of the southern Santa Fe embayment (Rio Grande rift), north-central New Mexico: Geological Society of America Special Papers, v. 494, p. 239–260, doi: 10.1130/2013.2494(10).
Liu, S., Nummedal, D., and Liu, L., 2011, Migration of dynamic subsidence across the Late Cretaceous United States Western Interior Basin in response to Farallon plate subduction: Geology, v. 39, p. 555–558, doi: 10.1130/G31692.1.
Livaccari, R.F., Burke, K., and Şengör, A.M.C., 1981, Was the Laramide orogeny related to subduction of an oceanic plateau? Nature, v. 289, p. 276–278, doi: 10.1038/289276a0.
Logsdon, M.J., 1981, A preliminary basin analysis of the El Rito Formation (Eocene), north-central New Mexico: Geological Society of America Bulletin, v. 92, p. 968, doi: 10.1130/0016-7606(1981)92<968:APBAOT>2.0.CO;2.
Lorenz, J.C., and Cooper, S.P., 2003, Tectonic Setting and Characteristics of Natural Fractures in Mesaverde and Dakota Reservoirs of the San Juan, New Mexico and Colorado: New Mexico Geology, v. 25, p. 3-14.
Lucas, S.G., 1982, Vertebrate paleontology, stratigraphy and biostratigraphy of Eocene Galisteo Formation, north-central New Mexico, *in* New Mexico Bureau of Geology and Mineral Resources Circular 1, Socorro, NM, New Mexico Bureau of Mines and Mineral Resources.
Lucas, S.G., Cather, S.M., Abbott, J.C., and Williamson, T.E., 1997, Stratigraphy and tectonic implications of Paleogene strata in the Laramide Galisteo Basin, north-central New Mexico: New Mexico Geology, p. 89–95.
Lucas, S.G., and Ingersoll, R. V., 1981, Cenozoic continental deposits of New Mexico: An overview: Geological Society of America Bulletin, v. 92, p. 917–932.
Mack, G.H., and Clemons, R.E., 1988, Structural and stratigraphic evidence for the Laramide (early Tertiary) Burro uplift in southwestern New Mexico: New Mexico Bureau of Geology and Mineral Resources Field Conference Guidebook, v. 39th, p. 59–66.
Mackey, G.N., Horton, B.K., and Milliken, K.L., 2012, Provenance of the Paleocene-Eocene Wilcox Group, western Gulf of Mexico basin: Evidence for integrated drainage of the southern Laramide Rocky Mountains and Cordilleran arc: Geological Society of America Bulletin, v. 124, p. 1007–1024, doi: 10.1130/B30458.1.
Maldonado, F., 2008, Geologic map of the Abiquiu quadrangle, Rio Arriba County, New Mexico: U.S. Geological Survey Scientific Investigations Map 2998, scale 1:24 000.

Marine Geoscience Data System, 2016, GeoMapApp: http://www.geomapapp.org (accessed July 2016).

Marshak, S., Karlstrom, K.E., and Timmons, J.M., 2000, Inversion of Proterozoic extensional faults: An explanation for the pattern of Laramide and Ancestral Rockies intracratonic deformation, United States: Geology, v. 28, p. 735–738, doi: 10.1130/0091-7613(2000)28<735.

Métivier, F., Gaudemer, Y., Tapponnier, P., Klein, M., 1999, Mass accumulation rates in Asia during the Cenozoic: Geophysical Journal International, v. 137, p. 280-318.

Morton, A.C., and Hallsworth, C.R., 1999, Processes controlling the composition of heavy mineral assemblages in sandstones: Sedimentary Geology, v. 124, p. 3-29.

Muehlberger, W.R., 1967, Geology of Chama Quadrangle, New Mexico: New Mexico Bureau of Mines and Mineral Resources Bulletin 89. 114 p.

Orth, C., Gilmore, J.S., Knight, J.D., Pillmore, C.L., Tschudy, R.H., and Fassett, J.E., 1982, Iridium abundance measurements across the Cretaceous/Tertiary boundary in the San Juan and Raton basins of northern New Mexico: Geological Society of America Special Papers, v. 190, p. 423–434, doi: 10.1130/SPE190-p423.

Peppe, D.J., Heizler, M.T., Williamson, T.E., Masson, I.P., Brusatte, S., Weil, A., and Secord, R., 2013, New age constrains on the late Cretaceous through early Paleocene rocks in the San Juan basin, New Mexico, in Geological Society of America Annual Meeting 2013, Denver, CO.

Petrus, J.A., and Kamber, B.S., 2012, VizualAge: A novel approach to laser ablation ICP-MS U-Pb geochronology data reduction: Geostandards and Geoanalytical Research, v. 36, p. 247–270, doi: 10.1111/j.1751-908X.2012.00158.x.

Peyton, S.L., and Carrapa, B., 2013, An overview of tow-temperature thermochronology in the Rocky Mountains and its application to petroleum system analysis, *in* Knight, C. and Cuzella, J. eds., Applications of structural methods to Rocky Mountain hydrocarbon exploration and development: AAPG Studies in Geology 65, p. 37–70.

Powell, J.S., 1973, Paleontology and sedimentation models of the Kimbeto Member of the Ojo Alamo Sandstone, in Cretaceous and Tertiary rocks of the southern Colorado Plateau: Four Corners Geological Society Memoir, p. 111–122.

Pillmore, C.L., and Flores, R.M., 1990, Cretaceous and Paleocene rocks of the Raton basin, New Mexico and Colorado-stratigraphic environmental framework: New Mexico Geological Society Guidebook, p. 333–336.

Pollock, C.J., Stewart, K.G., Hibbard, J.P., Wallace, L., and Giral, R.A., 2004, Thrust wedge tectonics and strike-slip faulting in the Sierra Nacimiento, New Mexico: New Mexico Bureau of Geology and Mineral Resources Bulletin, p. 97–112.

Ramos, V.A., Cristallini, E., and Perez, D.J., 2002, The Pampean flat-slab of the Central Andes: Journal of South American Earth Sciences, v. 15, p. 59–78, doi: 10.1016/S0895-9811(02)00006-8.

Reed, J.C., Jr., Wheeler, J.O., and Tucholke, J.E., comps., 2005a, Geologic map of North America: Boulder, Colo., Geological Society of America, Decade of North American Geology Continental Scale Map 001, scale 1:5,000,000, http://rock.geosociety.org/bookstore/default.asp?oID= 0&catID=2&pID=CSM001F.

Reed, J.C., Jr., Wheeler, J.O., and Tucholke, B.E., 2005b, Geologic map of North America—Perspectives and explanation: Boulder, Colo., Geological Society of America, Decade of North American Geology, 28 p.

Robinson Roberts, L.N.R., and Kirschbaum, M.A., 1995, Paleogeography of the Late Cretaceous of the Western Interior of middle North America- Coal distribution and sediment accumulation: USGS Professional Paper, v. 1561.

Royden, L.H., 1996, Coupling and decoupling of crust and mantle in convergent orogens: Implications for strain partitioning in the crust: Journal of Geophysical Research, v. 101, p. 17679–17.

Ruf, J.C., and Erslev, E.A., 2005, Origin of Cretaceous to Holocene fractures in the northern San Juan Basin, Colorado and New Mexico: Rocky Mountain Geology, v. 40, p. 91–114, doi: 10.2113/40.1.91.

Saleeby, J., 2003, Segmentation of the Laramide Slab — evidence from the southern Sierra Nevada region: Geological Society of America Bulletin, v. 115, p. 655, doi: 10.1130/0016-7606(2003)115<0655.

Schavran, G., 1985, Structural features in the Huerfano Park area, east flank, Sangre de Cristo range, Colorado: The Mountain Geologist, v. 22, p. 33–39.

Seager, W.R., 1983, Laramide wrench faults, basement-cored upifts, and complimentary basins in southern New Mexico: New Mexico Geology, v. 5, p. 69–76.

Seager, W.R., and Mack, G.H., 1986, Laramide paleotectonics of southern New Mexico, *in* Paleotectonics and sedimentation in the Rocky Mountain region, United States, AAPG Memoir 41, p. 669–685.

Sewall, J.O., and Sloan, L.C., 2006, Come a little bit closer: A high-resolution climate study of the early Paleogene Laramide foreland: Geology, v. 34, p. 81–84, doi: 10.1130/G22177.1.

Smith, H.T.U., 1938, Tertiary geology of the Abiquiu quadrangle, New Mexico: The Journal of Geology, v. 46, p. 933–965.

Smith, L.N., 1992, Stratigraphy, sediment dispersal and paleogeography of the lower Eocene San Jose Formation, San Juan Basin, New Mexico, *in* San Juan Basin IV, New Mexico Geological Soceity 43rd Annual Fall Field Conference Guidebook, p. 265–296.

Smith, M.E., Carroll, A.R., and Singer, B.S., 2008, Synoptic reconstruction of a major ancient lake system: Eocene Green River Formation, western United States: Geological Society of America Bulletin, v. 120, p. 54–84, doi: 10.1130/B26073.1.

Sobel, E.R., Hilley, G.E., and Strecker, M.R., 2003, Formation of internally drained contractional basins by aridity-limited bedrock incision: Journal of Geophysical Research, v. 108, doi: 10.1029/2002JB001883.

Stearns, C.E.., 1943, The Galisteo Formation of north-central New Mexico: The Journal of Geology, v. 51, p. 301–319.

Stewart, J.H., 1972, Initial deposits in the Cordilleran geosyncline: Evidence of a Late Precambrian (<850 m.y.) continental separation: Geological Society of America Bulletin, v. 83, p. 1345–1360.

Strecker, M.R., Alonso, R.N., Bookhagen, B., Carrapa, B., Coutand, I., Hain, M.P., Hilley, G.E., Mortimer, E., Schoenbohm, L.M., and Sobel, E.R., 2009, Does the topographic distribution of the central Andean Puna Plateau result from climatic or geodynamic processes? Geology, v. 37, p. 643–646, doi: 10.1130/G25545A.1.

Strecker, M.R., Hilley, G.E., Bookhagen, B., and Sobel, E.R., 2012, Structural, geomorphic, and depositional characteristics of contiguous and broken foreland basins: examples from the eastern flanks of the central Andes in Bolivia and NW

Argentina, *in* Busby, C., and Azor, A., eds., Tectonics of Sedimentary Basins: Recent Advances: Wiley-Blackwell, Oxford, UK, p. 508-521.

Syvitski, J.P.M., Peckham, S.D., Hilberman, R., and Mulder, T., 2003, Predicting the terrestrial flux of sediment to the global ocean: a planetary perspective: Sedimentary Geology, v. 162, p. 5–24, doi: 10.1016/S0037-0738(03)00232-X.

Tweto, O., 1975, Laramide (Late Cretaceous-early Tertiary) orogeny in the southern Rocky Mountains, in Curtis, B.F., ed., Cenozoic history of the southern Rocky Mountains, GSA Memoir 144, p. 1-44.

Wawrzyniec, T.F., Geissman, J.W., Melker, M.D. and Hubbard, M., 2002. Dextral shear along the eastern margin of the Colorado Plateau: A kinematic link between Laramide contraction and Rio Grande rifting (ca. 75–13 Ma). The Journal of Geology, 110(3), pp.305-324.

Whitmeyer, S.J., and Karlstrom, K.E., 2007, Tectonic model for the Proterozoic growth of North America: Geosphere, v. 3, p. 220–259, doi: 10.1130/GES00055.1.

Whipple, K. X., and G. E. Tucker, Dynamics of the stream-power river incision model: Implications for height limits of mountain ranges, land- scape response timescales, and research needs, J. Geophys. Res., 104, 17,661–17,674, 1999

Willett, S.D., 1999, Orogeny and orography : The effects of erosion on the structure Processes: Journal of Geophysical Research, v. 104, p. 28957–28981.

Willett, S.D., and Beaumont, C., 1994, Subduction of Asian lithospheric mantle beneath Tibet inferred from models of continental collision: Nature, v. 369, p. 642–646.

Williamson, T.E., and Lucas, S.G., 1992, Stratigraphy and mammalian biostratigraphy of the Paleocene Nacimiento Formation, southern San Juan Basin, *in* Lucas, S.G., Kues, B., Williamson, T.E., and Hunt, A.P. eds., San Juan Basin IV, New Mexico Geological Soceity 43rd Annual Fall Field Conference Guidebook, p. 265–296.

Williamson, T.E., 1996, The beginning of the age of mammals in the San Juan Basin, New Mexico; biostratigraphy and evolution of Paleocene mammals of the Nacimiento Formation: New Mexico Museum of Natural History and Science Bulletin, v. 8, p. 1–141.

Woodward, L. A., 1987, Geology and mineral resources of Sierra Nacimiento and vicinity, New Mexico: New Mexico Bureau of Mines and Mineral Resources, Memoir 42, 84 p.

Woodward, L.A., Anderson, O.J., and Lucas, S.G., 1997, Mesozoic stratigraphic constraints on Laramide right slip on the east side of the Colorado Plateau: Geology, v. 25, p. 843–846, doi: 10.1130/0091-7613(1997)025<0843:MSCOLR>2.3.CO;2.

Yin, A., and Ingersoll, R. V., 1997, A model for evolution of Laramide axial basins in the southern Rocky Mountains: International geology review, v. 39, p. 1113–1123.

Yonkee, W.A., Dehler, C.D., Link, P.K., Balgord, E.A., Keeley, J.A., Hayes, D.S., Wells, M.L., Fanning, C.M., and Johnston, S.M., 2014, Tectono-stratigraphic framework of Neoproterozoic to Cambrian strata, west-central U.S.: Protracted rifting, glaciation, and evolution of the North American Cordilleran margin: Earth-Science Reviews, v. 136, p. 59–95, doi: 10.1016/j.earscirev.2014.05.004.

TABLE 4.1. DETRITAL ZIRCON U-PB SAMPLE DATA FOR SAN JUAN AND GALISTEO-EL RITO SAMPLES

Sample Number / Formation	Total grains (number)	Maximum depositional age (Ma)	Cordilleran; <250 Ma	Appalachian; 400-600 Ma	Grenville; 1.0-1.2 Ga	1.4 Ga magmatism	Yavapai; 1.6-1.8 Ga
San Juan Basin							
SJ001 / Mancos	104	82.4 ± 2.3	39% (93, 185 Ma)	0	7%	11% (1449 Ma)	37% (1697 Ma)
SJ002 / Mesa Verde	105	76.5 ± 1.2	40% (97, 174 Ma)	10% (540 Ma)	19% (1092 Ma)	11% (1435 Ma)	14% (1732 Ma)
SJ005 / Pictured Cliffs	103	77.5±0.9	40% (87, 194 Ma)	14% (495 Ma)	7%	12% (1475 Ma)	21% (1688 Ma)
SJ003 / Ojo Alamo	109	70.8 ± 1.4	17% (80.7, 178 Ma)	0	18% (1187 Ma)	25% (1418 Ma)	40% (1703 Ma)
SJ006 / Nacimiento	86	71.35±.81	50% (75 Ma)	0	0	8%	42% (1683 Ma)
SJ007 / San Jose	105	67.7 ± 3.2	28% (91, 170 Ma)	5%	3%	20% (1419 Ma)	44% (1686 Ma)
Galisteo-El Rito Basin							
RW007 / Ritito Fm	33	29.8±2.1	12%	0	0	6%	73% (1743 Ma)
RW003 / El Rito Fm	95	*36.5±1.4*	5%	9%	19% (1132 Ma)	7%	42% (1724 Ma)
GB001 / Espinaso Fm	98	32.4±1.2	18% (71, 175 Ma)	2%	3%	31% (1433 Ma)	40% (1706 Ma)
HB001 / Galisteo Fm.	110	56 ±.99	48% (83, 178 Ma)	3%	14% (1087 Ma)	15% (1450 Ma)	20% (1707 Ma)
HB002 / Diamond Tail	108	64.7±1.9	31% (84, 166 Ma)	11% (495 Ma)	8%	19% (1427 Ma)	22% (1714 Ma)
HB005 / Menefee	101	73.9± 3	46% (85, 166 Ma)	1%	10% (1054 Ma)	10% (1431 Ma)	26% (1681 Ma)
HB007	100	74.8±1.4	37% (91, 163 Ma)	8%	2%	18% (1407 Ma)	32% (1720 Ma)
HB009	100	153±1.6	53% (181 Ma)	4%	16% (1123 Ma)	17% (1471 Ma)	5%

Notes: For each of the five provenance groups, the relative percentage of ages is reported along with peak ages for major populations (>10% of the sample ages).

.

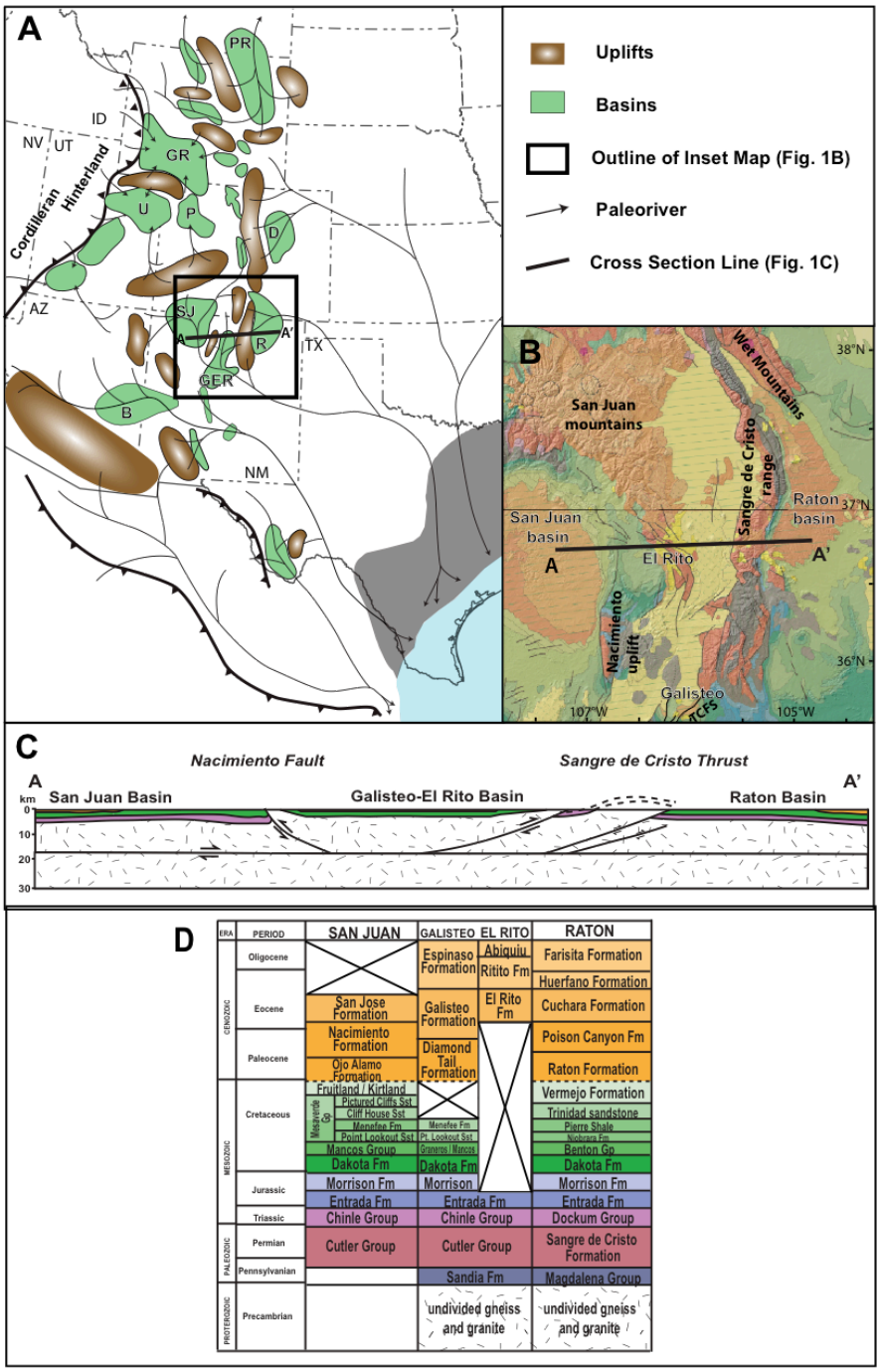

Figure 4.1. (A) Regional map of Laramide uplifts and basins. Paleorivers from Galloway, 2011. (Based on Dickinson et al., 1988, Lawton, 2008, and Galloway, 2011.) (B) Geologic map of study areas. Topography from Marine Geoscience Data Systems, 2016; geology from Reed et al., 2005a and 2005b. TCFS: Tijeras-Cañoncito fault system. (C) Cross-section of Laramide uplifts and basins of the southern Rocky Mountains (A-A' on Fig. 4.1A and 4.1B). Modified from Yin and Ingersoll, 1997. (D) Stratigraphic columns for San Juan basin, Galisteo-El Rito basin, and Raton basin.

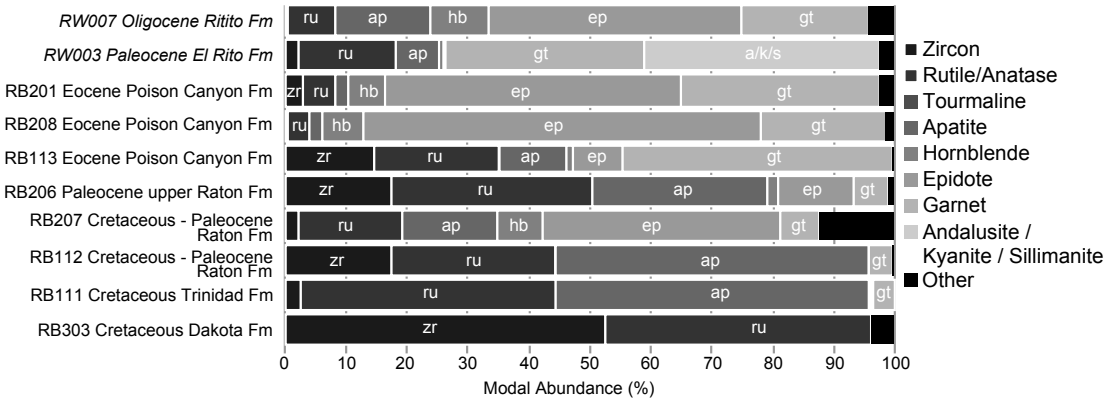

Figure 4.2. QEMSCAN detrital heavy mineral assemblage data for Raton basin and *El Rito depocenter of Galisteo-El Rito basin* (italics). 'Other' category includes: monazite, staurolite, olivine, and sphene.

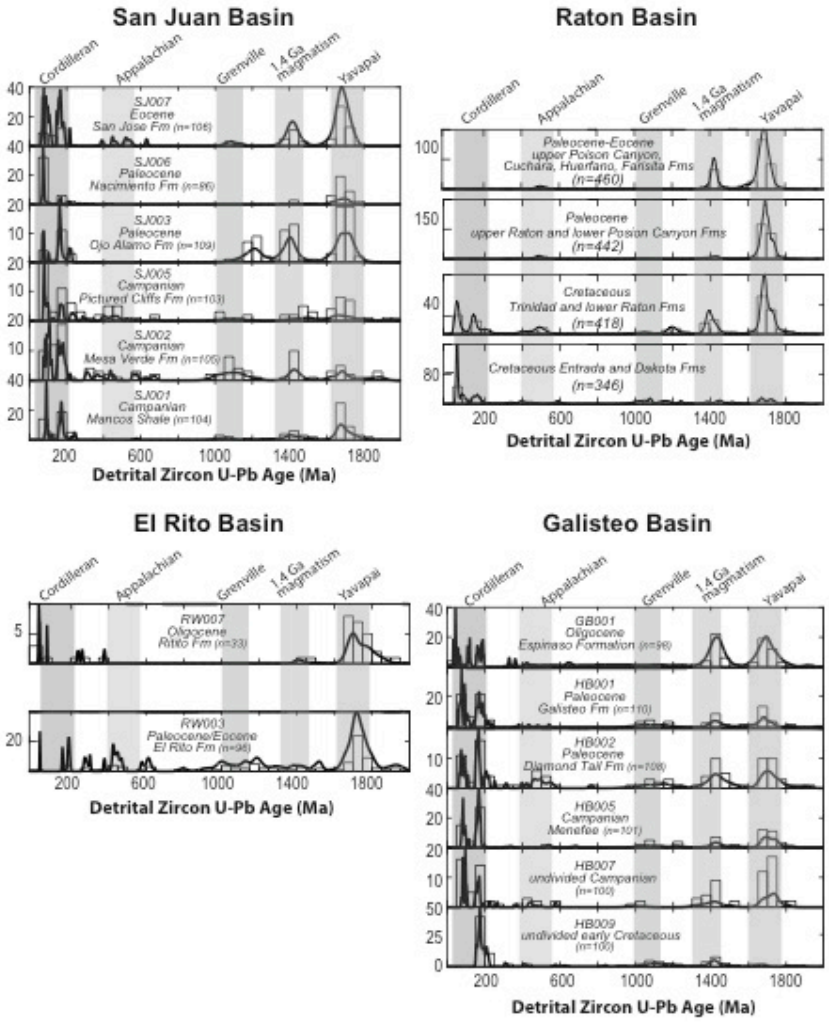

Figure 4.3. Detrital zircon U-Pb geochronology data, plotted as histograms and probability density plots, from 0-2000 Ma. (A) San Juan basin. (B) El Rito depocenter of Galisteo-El Rito basin. (C) Galisteo depocenter of Galisteo-El Rito basin. (D) Raton basin (data from Bush et al., 2016a).

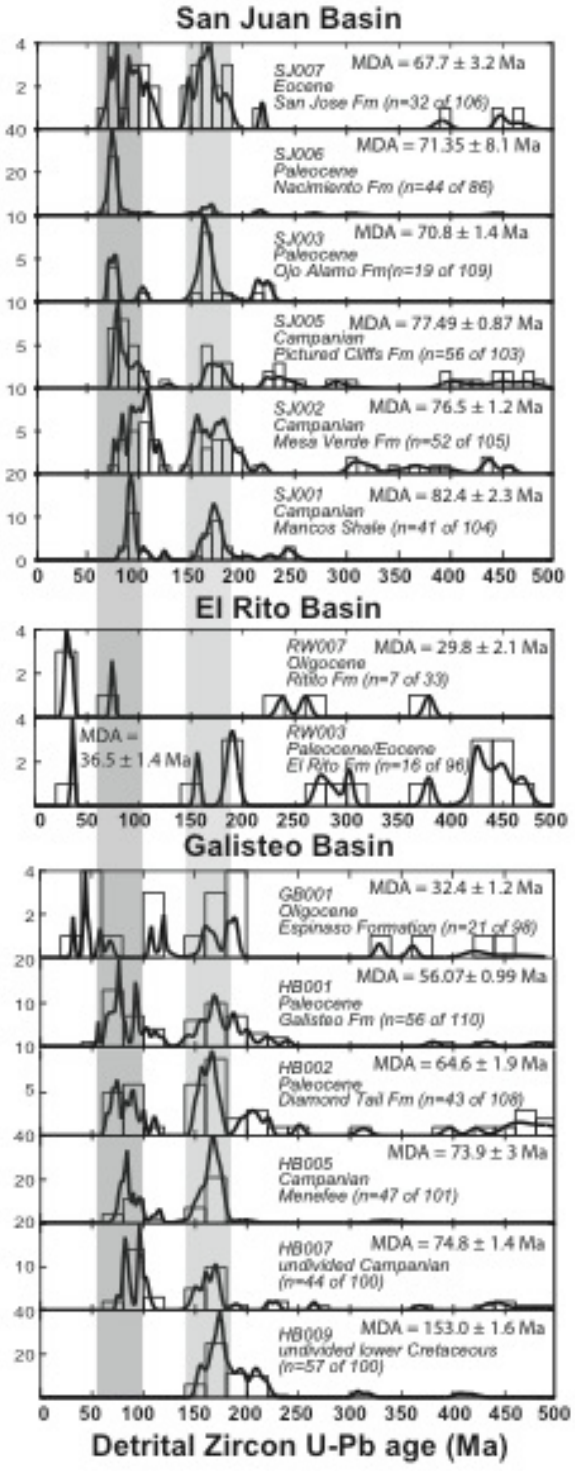

Figure 4.4. Detrital zircon U-Pb geochronology data, plotted as histograms and probability density plots, from 0-500 Ma. (A) San Juan basin. (B) El Rito depocenter of Galisteo-El Rito basin. (C) Galisteo depocenter of Galisteo-El Rito basin.

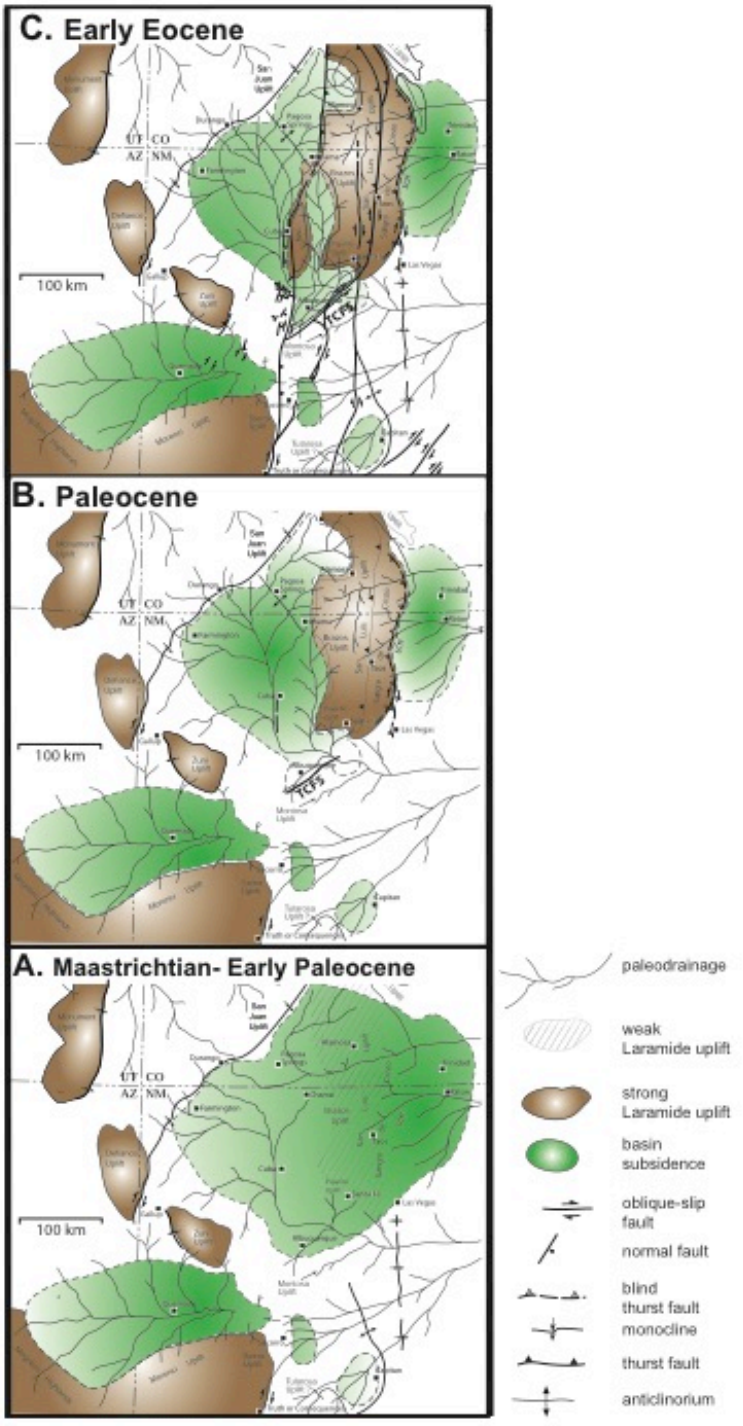

Figure 4.5. Paleogeographic reconstruction for Four Corners region, highlighting areas of subsidence and uplift as well as paleodrainage networks during the (A) Early Eocene; (B) Paleocene; (C) Maastrichtian – Early Paleocene. (Adapted from Cather, 2004).

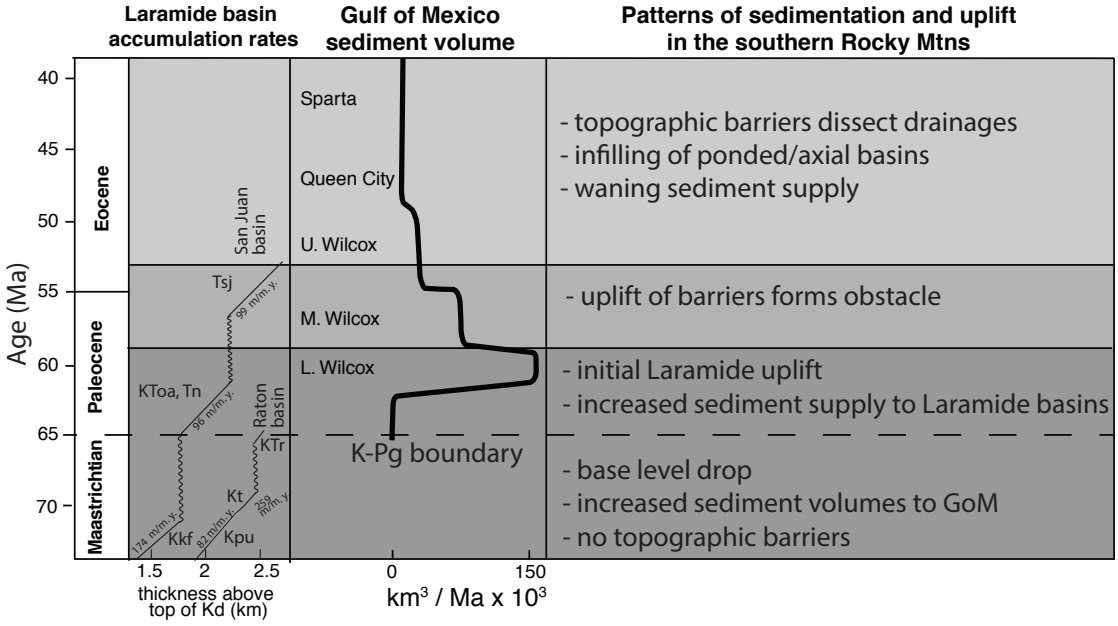

Figure 4.6. Chart of southern Rocky Mountain basin accumulation rates, Gulf of Mexico sediment volumes, and southern Rocky Mountain sedimentation and uplift patterns. Gulf of Mexico sediment volumes from Galloway et al., 2011. San Juan and Raton basin sediment accumulation rates and thicknesses from Cather, 2004. Kkf, Fruitland and Kirtland Formation; Kpu, Pierre shale; Kt, Trinidad sandstone; KTr, Raton Formation; KToa, Ojo Alamo Formation; Tn, Nacimiento Formation; Tsj, San Jose Formation.

Chapter 5: Synthesis and Conclusions

Each chapter of this dissertation contains detailed conclusions regarding the relevant projects. Here, general conclusions of the dissertation are summarized. Provenance data from plate interior basins preserve an important component of the multi-stage histories of convergent orogens. Data sets from the Qaidam basin of the Tibetan plateau and the San Juan, Galisteo-El Rito, and Raton basins of the southern Rocky Mountains allow for the evaluation of the stratigraphic signatures of mountain building. This integrated approach to basin analysis using stratigraphic as well as multi-proxy provenance analysis is sensitive to shifting patterns of deformation and sedimentation in the plate interior, allowing for the recognition of changes that would not be identifiable from one single technique alone. Large-scale trends identified in these basins include (1) initial deformation identified by a shift to more proximal depositional facies and new provenance signatures, (2) ongoing exhumation, and (3) basin isolation.

Patterns of Basin Filling

These basins preserve the record of changing source areas, sedimentation rates, and depositional systems. Though each basin system has a unique geologic context, similar signals of initial deformation, unroofing of major bounding ranges, and basin isolation can be identified.

Detailed analysis of the Cenozoic section from Qaidam basin on the northern margin of the Tibetan plateau (Chapter 2) reveals several significant episodes of mountain building: Paleocene deformation in the Eastern Kunlun Shan followed initial uplift in the Northern Qilian Shan and southward advance of the deformation front into the Qaidam basin (Figure 2.13). Evidence for major shifts in depositional patterns are

recognized based on multiple provenance signals, including shifts in the paleocurrent directions and the elimination or diversification of source signatures.

As in the Qaidam basin, detailed basin analysis reveals major shifts in source areas and depositional patterns for the San Juan, Galisteo-El Rito, and Raton basins of the southern Rocky Mountains (Chapters 3 and 4). In the San Juan and Galisteo-El Rito basins, the diversification of provenance signals (introduction of basement material) is interpreted to record the unroofing of proximal Laramide uplifts as well as the regional integration of drainage systems (Figure 4.6). At the same time, the removal of Phanerozoic sources from the Raton basin during the Paleocene is consistent with isolation from the other Laramide basins to the west due to the uplift of the Sangre de Cristo range as a topographic barrier (Figure 3.6).

In these far-field (>1000 km from the convergent plate boundary) intra-continental basins, several important patterns of basin filling are common:

1. Initial deformation nearly co-incident with zones of the orogen closer to the plate boundary (across the Tibetan plateau or Laramide province)
2. Later complexity due to ongoing deformation, leading to further basin partitioning and isolation

Continental-scale drainage patterns and sediment routing

The formation of these major plate interior basins has major implications for continental-scale fluvial networks. In both the Tibetan plateau and the mid-continental of North America, convergent deformation partitioned large, intracraton basins into smaller, walled basins. New uplifts in the plate interior have the effect of rerouting of fluvial systems, both introducing new source areas and lithologies into the system and in some

cases eliminating connection to former source terranes. Significant volumes of sediment can be stored in these basins over long time scales, disrupting the mass balance between the orogenic hinterland and the ultimate, marine systems that serve as the long-term sink for sediment.

Dramatic changes in sediment volumes reaching the Gulf of Mexico have been recorded during the Cenozoic (Figure 4.6), coincident with Laramide shortening in the plate interior. Initial Laramide-age and –style shortening in the Rocky Mountains can be correlated to the Paleocene increase in sediment accumulation in local basins. The Paleocene increase and later drop in Gulf of Mexico sediment volumes during continued exhumation of Laramide ranges may be linked to the increase in sediment storage basins such as the San Juan, Galisteo-El Rito, and Raton basins. By the Oligocene-Miocene, the near-complete burial of the Laramide ranges across the Rocky Mountain region by fine-grained fluvial and aeolian deposits such as the White River Group, the Arikaree Group, the Santa Fe Group, and, most significantly across the plate interior, the Ogallala Formation.

Summary

The research presented in this dissertations reveals important dynamics of plate interior basins in zones of convergent orogenesis. The sensitivity of sedimentary systems such as the Qaidam basin of the Tibetan plateau and the San Juan, Galisteo-El Rito, and Raton basins of the southern Rocky Mountains highlights the need for careful consideration of these plate interior systems as important sites of sediment storage, preserving both the record of exhumation in the hinterland, and providing important constraints on continental-scale mass balance.

Appendix A: Supplementary data and charts for Chapter 2

Sample locations, heavy mineral data, petrography data, paleocurrent data, and detrital zircon U-Pb data.

Sample Locations

Sample Name	Latitude/ Longitude
1DH0	N 37.54844 E 95.16530
2DH0	N 37.54844 E 95.16531
2DH224	N 37.54079 E 95.06621
2DH1184	N 37.52181 E 95.15259
2DH1770	N 37.51764 E 95.14830
2DH2230	N 37.51328 E 95.14707
2DH3040	N 37.50674 E 95.14290
2DH3774	N 37.50113 E 95.13887
2DH4580	N 37.49367 E 95.13673
2DH5484	N 37.48496 E 95.13280
2DH6126	N 37.47780 E 95.13190
2QUA144	N37.20403 E96.72632
2QUA416	N37.20028 E96.72707
1QUA1	N37.2217 E96.73396
160611-01	N37.23241 E9672549
160611-02	N37.2427 E96.7363
160611-03	N37.24995 E96.75486
160611-04	N37.25574 E96.76928
190611-01	N37.26778 E96.77027
220611-01	N37.53483 E95.16772

Heavy Mineral Data

Volume (%)		1	2	3	4	5	6	7	8	9	10
		1DH0:	2DH0:	2DH224:	2DH1184:	2DH1770:	2DH3040:	2DH3774:	2DH4580:	2DH5484:	2DH6126:
Minerals	Epidote	25.00	18.60	26.28	2.86	12.51	7.98	30.10	26.75	25.85	22.81
	Hornblende	14.68	15.48	26.70	4.07	7.50	3.22	16.28	22.55	25.69	37.11
	Pyroxene-Augite	0.00	0.01	0.00	0.00	0.00	0.01	0.02	0.75	0.97	0.86

	Tourmaline (Dravite)	0.06	0.18	0.12	0.20	0.14	0.12	0.01	0.00	0.07	0.03
	Apatite	2.07	20.08	5.82	10.09	9.03	8.99	9.78	5.99	4.29	3.82
	Rutile/Anatase/other Ti-phases	33.95	11.81	11.65	31.74	26.69	32.94	16.68	15.89	16.23	10.82
	Andalusite/Ky/Sill	0.00	0.00	0.00	0.00	0.04	0.00	0.00	0.01	0.07	0.00
	Zircon	0.42	3.54	1.36	5.11	4.62	10.53	1.43	1.69	2.56	1.33
	Pyroxene-En-Fs	0.01	0.02	0.04	0.04	0.16	0.05	0.13	0.05	0.50	0.14
	Monazite	0.01	0.03	0.02	0.08	0.08	0.05	0.02	0.02	0.11	0.04
	Staurolite	0.01	0.02	0.06	0.07	0.06	0.05	0.02	0.04	0.06	0.00
	Olivine	0.10	0.04	0.04	0.08	0.04	0.06	0.04	0.03	0.09	0.08
	Garnet	5.08	5.93	9.84	7.51	10.21	6.45	3.98	3.15	4.64	3.65
	Sphene	3.69	4.05	2.11	2.24	9.70	7.68	8.00	9.65	4.55	4.66
	Siderite	14.91	20.20	15.95	35.93	19.23	21.86	13.53	13.43	14.31	14.65
	Epidote	0.00	0.00	0.00	0.00	0.00	0.00	0.00	0.00	0.00	0.00

Petrography Data

Paleocurrent Data

Stratigraphic Level	Strike / Dip of Bedding	Trend of Paleoflow	Plunge of Paleoflow	Sense of Paleoflow	Type of Data	Formation	Number of Measurements
226	111 22SW	79	51	NE	Trough	Lulehe	12
245	111 22SW	260	44	SW	Imbrication	Lulehe	12
281	099 19SW	78	55	NE	Trough	Lulehe	21
428	124 10SW	60	67	NE	Imbrication	Lulehe	20
490	124 10SW	32	58	NE	Imbrication	Lulehe	15
753	151 22SW	135	65	SE	Imbrication	Lulehe	10
770	151 22SW	194	89	SW	Imbrication	Lulehe	10
879	155 38SW	177	48	S	Imbrication	Lulehe	11
1290	134 63SW	232	0	NE/SW	Trough	Xia Ganchaigou	32
1550	130 80SW	143	68	SE	Trough	Xia Ganchaigou	23
1704	119 85SW	210	3	SW	Trough	Xia Ganchaigou	25
1770	135 76SW	222	9	SW	Trough	Xia Ganchaigou	18
1832	114 85SW	204	1	SW	Trough	Xia Ganchaigou	24
2000	114 85SW	204	5	SW	Trough	Xia Ganchaigou	21
2200	117 85SW			NE	Trough	Xia Ganchaigou	22
2900	120 85SW	211	2	SW	Trough	Xia Ganchaigou	21
3030	116 82SW	208	3	SW	Trough	Xia Ganchaigou	15
3142	116 82SW	206	14	SW	Trough	Shang Ganchaigou	22
3430	117 82SW	209	2	SW	Trough	Shang Ganchaigou	19
3520	117 82SW	29	10	NE	Trough	Shang Ganchaigou	13
3623	112 75SW	200	18	SW	Trough	Shang Ganchaigou	11

5055	120 68SW	177	73	SE	Imbrication	Xia Youshashan	13
5099	125 70SW	176	54	S	Imbrication	Xia Youshashan	11
5201	125 70SW	243	75	SW	Imbrication	Shang Youshashan	10
5477	125 70SW	244	52	SW	Imbrication	Shang Youshashan	11
5602	120 65SW	197	66	SW	Imbrication	Shang Youshashan	11
5614	120 65SW	190	63	SW	Imbrication	Shang Youshashan	10
5860	125 65SW	229	62	SW	Imbrication	Shang Youshashan	11
5989	127 59SW	222	67	SW	Imbrication	Shang Youshashan	10
6114.8	125 25SW	182	57	S	Trough	Shang Youshashan	10
6761	130 10SW	220	62	SW	Imbrication	Shang Youshashan	10

Detrital Zircon U-Pb Geochronology

Attached separately.

Appendix B: Supplementary Data for Chapter 3

Detrital zircon U-Pb data attached separately.
Also available as supplementary data file with publication:

Bush, M.A., Horton, B.K., Murphy, M.A., and Stockli, D.F., 2016a, Detrital record of initial basement exhumation along the Laramide deformation front, southern Rocky Mountains: Tectonics, doi: 10.1002/2016TC004194.

Appendix C: Supplementary Data for Chapter 4

Detrital zircon U-Pb data attached separately.

References

Abbott, J.C., Cather, S.M., and Goodwin, L.B., 1995, Paleogene synorogenic sedimentation in the Galisteo basin related to the Tijeras-Canoncito Fault System: New Mexico Geological Society Guidebook, p. 271–278.

Applegate, J.K., and Rose, P.R., 1985, Structure of the Raton Basin from a regional seismic line, *in* Gries, R.R., and Dyer, R.C., eds, Seismic exploration of the Rocky Mountain region: Rocky Mountain Association of Geologists and Denver Geophysical Society, p. 259-265.

Aschoff, J.L. and Steel, R.J., 2011, Anomalous clastic wedge development during the Sevier-Laramide transition in the Cordilleran Foreland Basin, USA: Geological Society of America Bulletin, v. 123, p. 1822-1835.

Ash, S.R., and Tidwell, W.D., 1976, Upper Cretaceous and Paleocene floras of the Raton Basin, Colorado and New Mexico, *in* Ewing, R.C. and Kues, B.S., eds., New Mexico Geological Society 27th Annual Fall Field Conference Guidebook, p. 197-203.

Atwater, T., 1970, Implications of plate tectonics for the Cenozoic tectonic evolution of western North America: Geological Society of America Bulletin, v. 81, p. 3513.

Ayers, W.B. Jr., and Kaiser, W.R., 1994, Coalbed methane in the Upper Cretaceous Fruitland Formation, San Juan Basin, New Mexico and Colorado: New Mexico Bureau of Mines and Mineral Resources, Bulletin 146, 216 p.

Bally, A.W., Chou, I.-M., Clayton, R., Eugster, H.P., Kidwell, S., Meckel, L.D., Ryder, R.T., Watts, A.B., and Wilson, A.A., 1986, Notes on sedimentary basins in China--report of the American Sedimentary Basins Delegation to the People's Republic of China: Open–File Report 86, 327 p.

Baltz, E.H., 1965, Stratigraphy and history of the Raton basin and notes on the San Luis basin, Colorado-New Mexico: AAPG Bulletin, v. 49, p. 2041–2075.

Baltz, E. H., 1967, Stratigraphy and regional tectonic implications of part of Upper Cretaceous and Tertiary rocks, eastcentral San Juan Basin, New Mexico: U.S. Geological Survey Professional Paper 552, 101 p.

Barth, A.P., and Wooden, J.L., 2006, Timing of magmatism following initial convergence at a passive margin, Southwestern U.S. Cordillera, and ages of lower crustal magma sources: The Journal of Geology, v. 114, no. 2, p. 231–245, doi: 10.1086/499573.

Barton, M.D., 1996, Granitic magmatism and metallogeny of southwestern North America: Transactions of the Royal Society of Edinburgh: Earth Sciences, v. 87, p. 261–280.

Beck, R.A., Vondra, C.F., Filkins, J.E., and Olander, J.D., 1988, Syntectonic sedimentation and Laramide basement thrusting, Cordilleran foreland; Timing of deformation: Geological Society of America Memoir, v. 171, p. 465–487.

Bershaw, J., Garzione, C. N., Schoenbohm, L., Gehrels, G., and Tao, L., 2012, Cenozoic evolution of the Pamir plateau based on stratigraphy, zircon provenance, and stable isotopes of foreland basin sediments at Oytag (Wuyitake) in the Tarim Basin (west China): Journal of Asian Earth Sciences, v. 44, p. 136-148.

Besly, B.M., and Fielding, C.R., 1989, Palaeosols in Westphalian coal-bearing and red-bed sequences, central and northern England: Palaeogeography, Palaeoclimatology, Palaeoecology, v. 70, no. 4, p. 303–330, doi:10.1016/0031-0182(89)90110-7.

Bingler, E.C., 1968, Geology and mineral resources of Rio Arriba County, New Mexico: New Mexico Bureau of Geology and Mineral Resources Bulletin, v. 91, p. 175.

Blum, M., and Pecha, M., 2014, Mid-Cretaceous to Paleocene North American drainage reorganization from detrital zircons: Geology, v. 42, p. 607–610, doi: 10.1130/G35513.1.

Bovet, P.M., Ritts, B.D., Gehrels, G.E., Abbink, A.O., Darby, B., and Hourigan, J.K., 2009, Evidence of Miocene crustal shortening in the North Qilian Shan from Cenozoic stratigraphy of the western Hexi Corridor, Gansu Province, China: American Journal of Science, v. 309, p. 290–329, doi:10.2475/00.4009.02.

Braitenberg, C., Wang, Y., Fang, J., Hsu, H.T., 2003, Spatial variations of flexure parameters over the Tibet-Quinghai plateau: Earth and Planetary Science Letters, v. 205, p. 211-224.

Brill, K.G., 1952, Stratigraphy in the Permo-Pennsylvanian zeugogeosyncline of Colorado and Northern New Mexico: Geological Society of America Bulletin, v. 63, no. August, p. 809–880.

Brister, B.S., 1992, The Blanco Basin formation (Eocene), San Juan Mountains Region, Colorado and New Mexico: New Mexico Geological Society Guidebook, v. 43rd Field, p. 321–331.

Brister, B.S., and Chapin, C.E., 1994, Sedimentation and Tectonics of the Laramide San Juan Sag, Southwestern Colorado: The Mountain Geologist, v. 31, p. 2–18.

Brister, B.S., and Gries, R.R., 1994, Tertiary stratigraphy and tectonic development of the Alamosa basin (northern San Luis Basin), Rio Grande rift, south-central Colorado, in Keller, G.R., and Cather, S.M., eds., Basins of the Rio Grande rift: Structure, stratigraphy, and tectonic setting: GSA Special Paper 291, p. 39-58.

Burbank, D.W., Meigs, A., and Brozovic, N., 1996, Interactions of growing folds and coeval depositional systems: Basin Research, v. 8, p. 199–223, doi: 10.1046/j.1365-2117.1996.00181.x.

Busby-Spera, C.J., Mattinson, J.M., Riggs, N.R., and Schermer, E.R., 1990, The Triassic-Jurassic magmatic arc in the Mojave-Sonoran deserts and the Sierran-Klamath region; similarities and differences in paleogeographic evolution: Geological Society of America Special Papers, v. 255, p. 325–337, doi: 10.1130/SPE255-p325.

Bush, M.A., Horton, B.K., Murphy, M.A., and Stockli, D.F., 2016a, Detrital record of initial basement exhumation along the Laramide deformation front, southern Rocky Mountains: Tectonics, doi: 10.1002/2016TC004194.

Bush, M.A., Saylor, J.E., Horton, B.K., and Nie, J., 2016b, Growth of the Qaidam Basin during Cenozoic exhumation in the northern Tibetan Plateau: Inferences from depositional patterns and multiproxy detrital provenance signatures: Lithosphere, v. 8, p. 58-82, doi:10.1130/L449.1.

Cant, D.J., and Walker, R.G., 1978, Fluvial processes and facies sequences in the sandy braided South Saskatchewan River, Canada: Sedimentology, v. 25, p. 625–648.

Carrapa, B., Shazanee Mustapha, F., Cosca, M., Gehrels, G.E., Schoenbohm, L.M., Sobel, E.R., DeCelles, P.G., Russell, J., and Goodman, P., 2014, Multisystem dating

of modern river detritus from Tajikistan and China: Implications for crustal evolution and exhumation of the Pamir: Lithosphere, L360.1, doi:10.1130/L360.1.
Carroll, A.R., Chetel, L.M., and Smith, M.E., 2006, Feast to famine: Sediment supply control on Laramide basin fill: Geology, v. 34, p. 197, doi: 10.1130/G22148.1.
Carroll, A.R., Graham, S.A., and Smith, M.E., 2010, Walled sedimentary basins of China: Basin Research, v. 22, p. 17–32.
Carvajal, C., and Steel, R.J., 2012, Source-to-sink sediment volumes within a tectono-stratigraphic model for a Laramide shelf-to-deep-water basin : methods and results, *in* Busby, C. and Azor, A. eds., Tectonics of Sedimentary Basins: Recent Advances, Blackwell Scientific Publications, p. 131–151.
Cather, S.M., 1999, Implications of Jurassic, Cretaceous, and Proterozoic piercing lines for Laramide oblique-slip faulting in New Mexico and rotation of the Colorado Plateau: Geological Society of America Bulletin, v. 111, p. 849–868, doi: 10.1130/0016-7606(1999)111<0849:IOJCAP>2.3.CO;2.
Cather, S.M., 2003, Polyphase Laramide tectonism and sedimentation in the San Juan Basin, New Mexico: New Mexico Geological Society Guidebook, v. 54, p. 119–132.
Cather, S.M., 2004, Laramide orogeny in central and northern New Mexico and southern Colorado, *in* Mack, G.H. and Giles, K.A. eds., The Geology of New Mexico, a Geologic History, New Mexico Geological Society, p. 203–248.
Cather, S.M., 1992, Suggested revisions to the Tertiary tectonic history of north-central New Mexico: New Mexico Geological Society Guidebook, v. 43rd Field, p. 109–122.
Cather, S.M., and Chapin, C.E., 1990, Paleogeographic and paleotectonic setting of Laramide sedimentary basins in the central Rocky Mountain region: Alternative interpretation: Bulletin of the Geological Society of America, v. 102, p. 256-260.
Cather, S.M., Chapin, C.E., and Kelley, S.A., 2012, Diachronous episodes of Cenozoic erosion in southwestern North America and their relationship to surface uplift, paleoclimate, paleodrainage, and paleoaltimetry: Geosphere, v. 8, p. 1177–1206, doi: 10.1130/GES00801.1.
Cather, S.M., and Johnson, B.D., 1986, Eocene depositional systems and tectonic framework of west-central New Mexico and eastern Arizona, *in* Paleotectonics and sedimentation in the Rocky Mountains, AAPG, p. 623–652.
Carroll, A.R., Chetel, L.M., and Smith, M.E., 2006, Feast to famine: Sediment supply control on Laramide basin fill: Geology, v. 34, no. 3, p. 197, doi: 10.1130/G22148.1.
Chapin, C.E., 1983, An overview of Laramide wrench faulting in the southern Rocky Mountains with emphasis on petroleum exploration, *in* Lowell, J.D. and Gries, R.R. eds., Rocky Mountain Foreland Basins and Uplifts, Denver, CO, Rocky Mountain Association of Geologists, p. 169–179.
Chapin, C.E., 2012, Origin of the Colorado Mineral Belt: Geosphere, v. 8, p. 28–43, doi: 10.1130/GES00694.1.
Chapin, C.E., and Cather, S.M., 1981, Eocene tectonics and sedimentation in the Colorado Plateau - Rocky Mountain area, *in* Dickinson, W.R. and Payne, W.D. eds., Relations of Tectonics to ore deposits in the southern Cordillera: Arizona Geological Society Digest, v. 14, p. 173–198.

Chapin, C.E., Kelley, S.A., and Cather, S.M., 2014, The Rocky Mountain Front, southwestern USA: Geosphere, v. 10; p. 1043–1060, doi:10.1130/GES01003.1.

Chen, X.-H., Gehrels, G.E., Yin, A., Li, L., and Jiang, R.-B., 2012, Paleozoic and Mesozoic basement magmatisms of eastern Qaidam Basin, Northern Qinghai-Tibet Plateau: LA-ICP-MS Zircon U-Pb geochronology and its geological significance: Acta Geologica Sinica, v. 86, p. 350–369.

Cheng, F., Fu, S., Jolivet, M., Zhang, C., & Guo, Z., 2015, Source to sink relation between the Eastern Kunlun Range and the Qaidam Basin, northern Tibetan Plateau, during the Cenozoic: Geological Society of America Bulletin, B31260.1, http://doi.org/10.1130/B31260.1.

Chetel, L.M., Janecke, S.U., Carroll, A.R., Beard, B.L., Johnson, C.M., and Singer, B.S., 2011, Paleogeographic reconstruction of the Eocene Idaho River, North American Cordillera: Geological Society of America Bulletin, v. 123, no. 1-2, p. 71–88, doi: 10.1130/B30213.1.

Christiansen, E.H., Kowallis, B.J., and Barton, M.D., 1994, Temporal and spatial distribution of volcanic ash in Mesozoic sedimentary rocks of the Western Interior: an alternative record of Mesozoic magmatism, in Mesozoic systems of the Rocky Mountain region, USA, Rocky Mountain Section SEPM, p. 73–94.

Clark, K.F., and Read, C.B., 1972, Geology and ore deposits of Eagle Nest area, New Mexico: New Mexico Bureau of Mines and Mineral Resources Bulletin 94, p. 152.

Clark, M.K., Farley, K. A., Zheng, D., Wang, Z., and Duvall, A.R., 2010, Early Cenozoic faulting of the northern Tibetan Plateau margin from apatite (U–Th)/He ages: Earth and Planetary Science Letters, v. 296, p. 78–88, doi:10.1016/j.epsl.2010.04.051.

Clark, M.K., and Royden, L.H., 2000, Topographic ooze : Building the eastern margin of Tibet by lower crustal flow: Geology, v. 28, p. 703–706, doi:10.1130/0091-7613(2000)28<703.

Clinkscales, C.A., and Lawton, T.F., 2015, Timing of Late Cretaceous shortening and basin development, Little Hatchet Mountains, southwestern New Mexico, USA - implications for regional Laramide tectonics: Basin Research, v. 27, p. 453–472, doi: 10.1111/bre.12083.

Coleman, D.S., and Glazner, A.F., 1997, The Sierra Crest magmatic event: Rapid formation of juvenile crust during the Late Cretaceous in California: International Geology Review, v. 39, p. 768–787, doi: 10.1080/00206819709465302.

Coney, P.J., 1972, Cordilleran tectonics and North American plate motion: American Journal of Science, v. 272, p. 603–628.

Coney, P.J., and Reynolds, S.J., 1977, Cordilleran Benioff zones: Nature, v. 270, p. 403–406.

Constenius, K.N., 1996, Late Paleogene extensional collapse of the Cordilleran foreland fold and thrust belt: Geological Society of America Bulletin, v. 108, p. 20–39.

Copeland, P., Murphy, M.A., Dupré, W.R., and Lapen, T.J., 2011, Oligocene Laramide deformation in southern New Mexico and its implications for Farallon plate geodynamics: Geosphere, v. 7, p. 1209-1219, doi:10.1130/GES00672.1.

Cowgill, E., Yin, A., Harrison, T.M., and Wang, X.-F., 2003, Reconstruction of the Altyn Tagh fault based on U-Pb geochronology: Role of back thrusts, mantle sutures, and heterogeneous crustal strength in forming the Tibetan Plateau: Journal of Geophysical Research, v. 108, B7, p. 2346, doi:10.1029/2002JB002080.

Crabaugh, J.P., 2001, Nature and growth of nonmarine-to-marine clastic wedges: Examples from the Upper Cretaceous Iles Formation, Western Interior (Colorado) and the Lower Paleogene Wilcox Group of the Gulf of Mexico basin (Texas) [Ph.D. thesis]: University of Wyoming, 235 p.

Craddock, W.H., Kirby, E., Harkins, N.W., Zhang, H., Shi, X., and Liu, J., 2010, Rapid fluvial incision along the Yellow River during headward basin integration: Nature Geoscience, v. 3, no. 3, p. 209–213.

Craddock, W.H., Kirby, E., Zhang, D., and Liu, J., 2011a, Tectonic setting of Cretaceous basins on the NE Tibetan Plateau: insights from the Jungong basin: Basin Research, p. 51-69, doi:10.1111/j.1365-2117.2011.00515.x.

Craddock, W.H., Kirby, E., and Zhang, H., 2011b, Late Miocene-Pliocene range growth in the interior of the northeastern Tibetan Plateau: Lithosphere, v. 3, p. 420–438, doi:10.1130/L159.1.

Craddock, W.H., and Kylander-Clark, A.R.C., 2013, U-Pb ages of detrital zircons from the Tertiary Mississippi River Delta in central Louisiana: Insights into sediment provenance: Geosphere, v. 9, p. 1832–1851, doi: 10.1130/GES00917.1.

Cunningham, C.G., Naeser, C.W., Marvin, R.F., Luedke, R.G., and Wallace, A.R., 1994, Ages of Selected Intrusive Rocks ana Associated Ore Deposits in the Colorado Mineral Belt: U.S. Geological Survey Bulletin, v. 2109.

Currie, B. S., McPherson, M.L., Dark, J.P., and Pierson, J.S., 2008, Reservoir characterization of the Cretaceous Cedar Mountain and Dakota Formations, southern Uinta Basin, Utah: Year-two report: Utah Geological Survey Open-File Report 516, 71 p.

Dai, J., Zhao, X., Wang, C., Zhu, L., Li, Y., and Finn, D., 2012, The vast proto-Tibetan Plateau: New constraints from Paleogene Hoh Xil Basin: Gondwana Research, v. 22, p. 434–446, doi:10.1016/j.gr.2011.08.019.

Daniel, C.G., Pfeifer, L.S., Jones, J. V., and McFarlane, C.M., 2013, Detrital zircon evidence for non-Laurentian provenance, Mesoproterozoic (ca. 1490-1450 Ma) deposition and orogenesis in a reconstructed orogenic belt, northern New Mexico, USA: Defining the Picuris orogeny: Geological Society of America Bulletin, v. 125, p. 1423–1441, doi: 10.1130/B30804.1.

Darby, B.J., Ritts, B.D., Yue, Y., and Meng, Q., 2005, Did the Altyn Tagh fault extend beyond the Tibetan Plateau?: Earth and Planetary Science Letters, v. 240, p. 425–435, doi:10.1016/j.epsl.2005.09.011.

Davis, D., Suppe, J., and Dahlen, F.A., 1983, Mechanics of fold-and-thrust belts and accretionary wedges: Journal of Geophysical Research, p. 1153-1172.

Davis, S.J., Mix, H.T., Wiegand, B.A., Carroll, A.R., and Chamberlain, C.P., 2009, Synorogenic evolution of large-scale drainage patterns: Isotope paleohydrology of sequential Laramide basins: American Journal of Science, v. 309, p. 549–602, doi: 10.2475/07.2009.02.

Dayem, K. E., Molnar, P., Clark, M. K., and Houseman, G. A., 2009, Far-field lithospheric deformation in Tibet during continental collision: Tectonics, v. 28, p. 1–9, doi:10.1029/2008TC002344.

DeCelles, P.G., 2004, Late Jurassic to Eocene evolution of the Cordilleran thrust belt and foreland basin system, western USA: American Journal of Science, v. 304, p. 105–168.

DeCelles, P.G., 1991, Kinematic history of a foreland uplift from Paleocene synorogenic conglomerate, Beartooth Range, Wyoming and Montana: Geological Society of America Bulletin, v. 103, p. 1458–1475.

DeCelles, P.G., Ducea, M.N., Kapp, P., and Zandt, G., 2009, Cyclicity in Cordilleran orogenic systems: Nature Geoscience, v. 2, p. 251–257, doi: 10.1038/ngeo469.

DeCelles, P.G., and Giles, K.A., 1996, Foreland basin systems: Basin Research, v. 8, p. 105–123, doi: 10.1046/j.1365-2117.1996.01491.x.

DeCelles, P.G., and Graham, S.A., 2015, Cyclical processes in the North American Cordilleran orogenic system: Geology, v. 43, p. 499-502.

DeCelles, P., Kapp, P., Ding, L., and Gehrels, G., 2007, Late Cretaceous to middle Tertiary basin evolution in the central Tibetan Plateau: Changing environments in response to tectonic partitioning, aridification, and regional elevation gain: Geological Society of America Bulletin, v. 119, p. 654-680.

DeCelles, P.G., and Mitra, G., 1995, History of the Sevier orogenic wedge in terms of critical taper models, northeast Utah and southwest Wyoming: Geological Society of America Bulletin, v. 107, p. 454–462, doi: 10.1130/0016-7606(1995)107<0454:HOTSOW>2.3.CO;2.

Dewey, J.F., and Bird, J.M., 1970, Mountain belts and the new global tectonics: Journal of Geophysical Research, v. 75, p. 2625–2646, doi: 10.1029/JB075i014p02625.

Dewey, J.F., Shackleton, R.M., Chengfa, C., and Yiyin, S., 1988, The Tectonic Evolution of the Tibetan Plateau: Philosophical Transactions of the Royal Society A: Mathematical, Physical and Engineering Sciences, v. 327, p. 379–413, doi:10.1098/rsta.1988.0135.

Dickinson, W.R., 1970, Interpreting detrital modes of greywacke and arkose: Journal of Sedimentary Petrology, v. 40, p. 695–707.

Dickinson, W.R., 1985, Interpreting provenance relations from detrital modes of sandstones, *in* Zuffa, G.G., ed., Provenance of arenites: Reidel Publishing Company, Dordrecht, Netherlands, p. 333–361.

Dickinson, W.R., 2006, Geotectonic evolution of the Great Basin: Geosphere, v. 2, no. 7, p. 353, doi: 10.1130/GES00054.1.

Dickinson, W.R., and Gehrels, G.E., 2008, Sediment delivery to the Cordilleran foreland basin: insights from U-Pb ages of detrital zircon in Upper Jurassic and Cretaceous strata of the Colorado Plateau: American Journal of Science, v. 308, p. 1041–1082, doi: 10.2475/10.2008.01.

Dickinson, W.R., and Gehrels, G.E., 2008b, U-Pb ages of detrital zircons in relation to paleogeography: Triassic paleodrainage networks and sediment dispersal across Southwest Laurentia: Journal of Sedimentary Research, v. 78, no. 1996, p. 745–764, doi: 10.2110/jsr.2008.088.

Dickinson, W.R., and Gehrels, G.E., 2003, U–Pb ages of detrital zircons from Permian and Jurassic eolian sandstones of the Colorado Plateau, USA: paleogeographic implications: Sedimentary Geology, v. 163, p. 29–66, doi: 10.1016/S0037-0738(03)00158-1.

Dickinson, W.R., and Gehrels, G.E., 2009, U-Pb ages of detrital zircons in Jurassic eolian and associated sandstones of the Colorado Plateau: Evidence for transcontinental dispersal and intraregional recycling of sediment: Geological Society of America Bulletin, v. 121, p. 408–433, doi: 10.1130/B26406.1.

Dickinson, W.R., Cather, S.M., and Gehrels, G.E., 2010, Detrital zircon evidence for derivation of arkosic sand in the eolian Narbona Pass Member of the Chuska Sandstone from Precambrian basement rocks in central Arizona, in Fassett. J.E., Zeigler, K.E., and Lueth, V.W., eds., Geology of the Four Corners Country: New Mexico Geological Society 61st Annual Field Conference, p. 125–134.

Dickinson, W.R., Klute, M.A., Hayes, M.J., Janecke, S.U., Lundin, E.R., McKittrick, M., and Olivares, M.D., 1988, Paleogeographic and paleotectonic setting of Laramide sedimentary basins in the central Rocky Mountain region: Bulletin of the Geological Society of America, v. 100, p. 1023.

Dickinson, W.R., and Snyder, W., 1978, Plate tectonics of the Laramide orogeny: Geological Society of America Memoir, v. 151, p. 355–366.

Dickinson, W.R., and Suczek, C.A., 1979, Plate Tectonics and Sandstone Compositions: AAPG Bulletin, v. 12, p. 2164–2182.

Ding, L., Yang, D., Cai, F.L., Pullen, A., Kapp, P., Gehrels, G.E., Zhang, L.Y., Zhang, Q.H., Lai, Q.Z., Yue, Y.H., and Shi, R.D., 2013, Provenance analysis of the Mesozoic Hoh-Xil-Songpan-Ganzi turbidites in northern Tibet: Implications for the tectonic evolution of the eastern Paleo-Tethys Ocean: Tectonics, v. 32, p. 34–48, doi:10.1002/tect.20013.

Ding, L., Xu, Q., Yue, Y., Wang, H., Cai, F., Li, S., 2014, The Andean-type Gangdese Mountains: Paleoelevation record from the Paleocene–Eocene Linzhou Basin: Earth and Planetary Science Letters, v. 392, p. 250-264.

Ducea, M.N., 2001, The California arc: Thick granitic batholiths, eclogitic residues, lithospheric-scale thrusting, and magmatic flare-ups: GSA Today, v. 11, p. 4–10, doi: 10.1130/1052-5173(2001)011<0004:TCATGB>2.0.CO;2.

Dupont-Nivet, G., Butler, R.F., Yin, A., and Chen, X.-H., 2002, Paleomagnetism indicates no Neogene rotation of the Qaidam Basin in northern Tibet during Indo-Asian collision: Geology, v. 30, p. 263–266, doi:10.1130/0091-7613(2002)030<0263.

Dupont-Nivet, G., Dai, S., Fang, X., Krijgsman, W., Erens, V., Reitsma, M., and Langereis, C.G., 2008, Timing and distribution of tectonic rotations in the northeastern Tibetan plateau: Geological Society of America Special Papers, v. 444, p. 73–87, doi:10.1130/2008.2444(05).

Dupont-Nivet, G., Horton, B.K., Butler, R.F., Wang, J., Zhou, J., and Waanders, G.L., 2004, Paleogene clockwise tectonic rotation of the Xining-Lanzhou region, northeastern Tibetan Plateau: Journal of Geophysical Research, v. 109, B04401, doi:10.1029/2003JB002620.

Duvall, A.R., and Clark, M.K., 2010, Dissipation of fast strike-slip faulting within and beyond northeastern Tibet: Geology, v. 38, p. 223–226, doi:10.1130/G30711.1.

Duvall, A.R., Clark, M.K., van der Pluijm, B. A., and Li, C., 2011, Direct dating of Eocene reverse faulting in northeastern Tibet using Ar-dating of fault clays and low-temperature thermochronometry: Earth and Planetary Science Letters, v. 304, p. 520–526, doi:10.1016/j.epsl.2011.02.028.

Duvall, A.R., Clark, M.K., Kirby, E., Farley, K. A., Craddock, W.H., Li, C., and Yuan, D.-Y., 2013, Low-temperature thermochronometry along the Kunlun and Haiyuan Faults, NE Tibetan Plateau: Evidence for kinematic change during late-stage orogenesis: Tectonics, v. 32, p. 1190–1211, doi:10.1002/tect.20072.

Enkelmann, E., Weislogel, A.L., Ratschbacher, L., Eide, E., Renno, A., and Wooden, J., 2007, How was the Triassic Songpan-Ganzi basin filled? A provenance study: Tectonics, v. 26, doi:10.1029/2006TC002078.

English, J.M., Johnston, S.T., and Wang, K., 2003, Thermal modelling of the Laramide orogeny: Testing the flat-slab subduction hypothesis: Earth and Planetary Science Letters, v. 214, p. 619–632, doi: 10.1016/S0012-821X(03)00399-6.

Epis, R., and Chapin, C.E., 1975, Geomorphic and tectonic implications of the post-Laramide, late Eocene erosion surface in the southern Rocky Mountains: Geological Society Of America Memoirs, v. 144, p. 45–74.

Erslev, E.A., 1993, Thrusts, back-thrusts, and detachment of Rocky Mountain foreland arches, in Schmidt, C.J., Chase, R.B., and Erslev, E.A., eds., Laramide basement deformation in the Rocky Mountain foreland of the western United States: Geological Society of America Special Paper 280, p. 339–358.

Erslev, E.A., 2001, Multistage, multidirectional Tertiary shortening and compression in north-central New Mexico: Geological Society of America Bulletin, v. 113, p. 63–74, doi: 10.1130/0016-7606(2001)113<0063:MMTSAC>2.0.CO;2.

Ethridge, F.G., Skelly, R.L., and Bristow, C.S., 1999, Avulsion and crevassing in the sandy, braided Niobrara River: Complex response to base-level rise and aggradation, in Smith, N.D. and Rogers, J. eds., Fluvial Sedimentology VI, International Association of Sedimentologists, p. 179–191.

Fan, M., and Carrapa, B., 2014, Late Cretaceous – early Eocene Laramide uplift, exhumation, and basin subsidence in Wyoming: Crustal responses to flat slab subduction: Tectonics, v. 33, p. 509–529, doi: 10.1002/2012TC003221.Received.

Fang, X., Garzione, C., Van der Voo, R., Li, J., Fan, M., 2003. Flexural subsidence by 29 Ma on the NE edge of Tibet from the magnetostratigraphy of Linxia Basin, China: Earth and Planetary Science Letters, v. 210, p. 545-560.

Fang, X.M., Yan, M.D., van der Voo, R., Rea, D.K., Song, C.H., Pares, J.M., Gao, J.P., Nie, J.S., and Dai, S., 2005, Late Cenozoic deformation and uplift of the NE Tibetan plateau: Evidence from high-resolution magneto stratigraphy of the Guide Basin, Qinghai Province, China: Geological Society of America Bulletin, v. 117, p. 1208–1225, doi:10.1130/B25727.1.

Fang, X., Zhang, W., Meng, Q., Gao, J., Wang, X., King, J.G., Song, C., Dai, S., and Miao, Y., 2007, High-resolution magnetostratigraphy of the Neogene Huaitoutala section in the eastern Qaidam Basin on the NE Tibetan Plateau, Qinghai Province, China and its implication on tectonic uplift of the NE Tibetan Plateau: Earth and Planetary Science Letters, v. 258, p. 293–306, doi:10.1016/j.epsl.2007.03.042.

Fassett, J.E., and Steiner, M.B., 1997, Precise age of C33N-C32R magnetic-polarity reversal, San Juan basin, New Mexico and Colorado, in Anderson, O., Kues, B., and Lucas, S.G. eds., Mesozoic Geology and Paleontology of the Four Corners Area: New Mexico Geological Survey Guidebook v. 48, p. 105–111.

Fassett, J.E., 1985, Early Tertiary paleogeography and paleotectonics of the San Juan Basin Area, New Mexico and Colorado, *in* Cenozoic Paleogeography of west-central United States, Rocky Mountain Section SEPM Symposium 3, p. 317–334.

Fielding, E.J., and Jordan, T.E., 1988, Active deformation at the boundary between the Precordillera and Sierras Pampeanas, Argentina, and comparison with ancient Rocky Mountain deformation: Geological Society of America Memoir, v. 171, p. 143–163.

Flemings, P.B., and Jordan, T.E., 1989, A synthetic stratigraphic model of foreland basin development: Journal of Geophysical Research, v. 94, p. 3851–3866.

Finzel, E.S., 2014, Detrital zircons from Cretaceous midcontinent strata reveal an Appalachian Mountains–Cordilleran foreland basin connection: Lithosphere, v. 6; p. 378–382.

Flores, R.M., and Pillmore, C.L., 1987, Tectonic control on alluvial paleoarchitecture of the Cretaceous and Tertiary Raton Basin, Colorado and New Mexico: Recent Developments in Fluvial Sedimentology, SEPM, v. 39.

Flores, R.M., and Tur, S., 1982, Characteristics of deltaic deposits in the Cretaceous Pierre Shale, Trinidad Sandstone, and Vermejo Formation, Raton basin, Colorado: The Mountain Geologist, v. 19, p. 25–40.

Folk, R.L., 1980, Petrology of Sedimentary Rocks: Austin, Texas, Hemphill Publishing Company, 190 p.

Friend, P.F., Slater, M.J., and Williams, R.C., 1979, Vertical and lateral building of river sandstone bodies, Ebro Basin, Spain: Journal of the Geological Society of London, v. 136, p. 39–46.

Fu, B., and Awata, Y., 2007, Displacement and timing of left-lateral faulting in the Kunlun Fault Zone, northern Tibet, inferred from geologic and geomorphic features: Journal of Asian Earth Sciences, v. 29, p. 253–265, doi:10.1016/j.jseaes.2006.03.004.

Galloway, W.E., Whiteaker, T.L., and Ganey-Curry, P., 2011, History of Cenozoic North American drainage basin evolution, sediment yield, and accumulation in the Gulf of Mexico basin: Geosphere, v. 7, p. 938–973, doi: 10.1130/GES00647.1.

Gan, W., Zhang, P., Shen, Z.K., Niu, Z., Wang, M., Wan, Y., Zhou, D., and Cheng, J., 2007, Present-day crustal motion within the Tibetan Plateau inferred from GPS measurements: Journal of Geophysical Research, v. 112, doi:10.1029/2005JB004120.

Garzione, C., DeCelles, P., Hodkinson, D., Ojha, T., and Upreti, B., 2003, East-west extension and Miocene environmental change in the southern Tibetan plateau: Thakkhola graben, central Nepal: Geological Society of America Bulletin, v. 115, p. 3-20.

Gazzi, P., 1966, Le minerali pesanti nei flysch arenacei fra Monte Ramaceto e Monte Molinatico (Appennino settent Ríonale): Mineralogica et Petrographica Acta, v. 11, p. 197–212.

Gehrels, G.E., Kapp, P., DeCelles, P.G., Pullen, A., Blakey, R., Weislogel, A.L., Ding, L., Guynn, J., Martin, A., McQuarrie, N., and Yin, A., 2011, Detrital zircon geochronology of pre-Tertiary strata in the Tibetan-Himalayan orogen: Tectonics, v. 30, doi:10.1029/2011TC002868.

Gehrels, G.E., Valencia, V.A., and Ruiz, J., 2008, Enhanced precision, accuracy, efficiency, and spatial resolution of U-Pb ages by laser ablation-multicollector-inductively coupled plasma-mass spectrometry: Geochemistry, Geophysics, Geosystems, v. 9, p. 1–13, doi:10.1029/2007GC001805.

Gehrels, G.E., Yin, A., and Wang, X.-F., 2003a, Detrital-zircon geochronology of the northeastern Tibetan plateau: Geological Society of America Bulletin, v. 115, p. 881–896, doi:10.1130/0016-7606(2003)115<0881:DGOTNT>2.0.CO;2.

Gehrels, G.E., Yin, A., and Wang, X.-F., 2003b, Magmatic history of the northeastern Tibetan Plateau: Journal of Geophysical Research, v. 108, no. B9, p. 1–14, doi:10.1029/2002JB001876.

George, A.D., Marshallsea, S.J., Wyrwoll, K.-H., Jie, C., and Yanchou, L., 2001, Miocene cooling in the northern Qilian Shan , northeastern margin of the Tibetan Plateau, revealed by apatite fission-track and vitrinite-reflectance analysis: Geology, v. 29, p. 939–942.

Gonzales, D.A., 2015, New U-Pb Zircon and 40Ar/39Ar age constraints on the Late Mesozoic to Cenozoic plutonic record in the western San Juan Mountains: The Mountain Geologist, v. 52, p. 5–42.

Gorham, T.W., and Ingersoll, R. V., 1979, Evolution of the Eocene Galisteo basin, north-central New Mexico: New Mexico Geological Society Guidebook, v. 30th Field, p. 219–225.

Graham, S.A., Chamberlain, C.P., Yue, Y., Ritts, B.D., Hanson, A.D., Horton, T.W., Waldbauer, J.R., Poage, M.A., and Feng, X., 2005, Stable isotope records of Cenozoic climate and topography, Tibetan plateau and Tarim basin: American Journal of Science, v. 305, p. 101–118, doi:10.2475/ajs.305.2.101.

Graham, S. A., Hendrix, M. S., Wang, L. B., and Carroll, A. R., 1993, Collisional successor basins of western China - Impact of tectonic inheritance on sand composition: Geological Society of America Bulletin, v. 105, no. 3, p. 323-344.

Gries, R., 1983, North-south compression of Rocky Mountain foreland structures, in Rocky Mountain Foreland Basins and Uplifts, Rocky Mountain Association of Geologists, p. 9–32.

Gries, R.R., 1985, San Juan sag: Cretaceous Rocks in a volcanic-covered basin, south central Colorado: The Mountain Geologist,. The Mountain Geologist, v. 22, p. 167–179.

Guo, Z., Deng, K., and Han, Y., 1996, Formation and Evolution of the Sichuan Basin, Beijing, Geologic Publishing House, 200 p.

Gupta, S., 1997, Himalayan drainage patterns and the origin of fluvial megafans in the Ganges foreland basin: Geology, v. 25, p. 11–14, doi:10.1130/0091-7613(1997)025<0011.

Hanson, A. D., 1999, Organic geochemistry and petroleum geology, tectonics and basin analysis of southern Tarim and northern Qaidam basins, northwest China [Ph.D.: Stanford University, 388 p.

Hanson, A.D., Ritts, B.D., Zinniker, D., Moldowan, J.M., and Biffi, U., 2001, Upper Oligocene lacustrine source rocks and petroleum systems of the northern Qaidam basin, northwest China: AAPG Bulletin, v. 85, p. 601–619.

Harris, N.B.W., Ronghua, X., Lewis, C.L., and Chengwei, J., 1988, Plutonic rocks of the 1985 Tibet Geotraverse, Lhasa to Golmud: Philosophical Transactions of the Royal Society A: Mathematical, Physical and Engineering Sciences, v. 327, p. 145–168, doi:10.1098/rsta.1988.0124.

Harrison, T., Copeland, P., Kidd, W., and Yin, A., 1992, Raising Tibet: Science, v. 255, no. 5052, p. 1663-1670.

Hartley, A.J., Weissmann, G.S., Nichols, G.J., and Warwick, G.L., 2010, Large distributive fluvial systems: Characteristics, distribution, and controls on

development: Journal of Sedimentary Research, v. 80, p. 167–183, doi:10.2110/jsr.2010.016.
He, S. D., Kapp, P., DeCelles, P. G., Gehrels, G. E., and Heizler, M., 2007, Cretaceous-Tertiary geology of the Gangdese Arc in the Linzhou area, southern Tibet: Tectonophysics, v. 433, p. 15-37.
Heller, P.L., Angevine, C.L., Winslow, N.S., and Paola, C., 1988, Two-phase stratigraphic model of foreland-basin sequences: Geology, v. 16, p. 501.
Higley, D.K., 2007, Petroleum systems and assessment of undiscovered oil and gas in the Raton Basin-Sierra Grande Uplift Province, Colorado and New Mexico- USGS Province 41: USGS.
Hoffman, G.K., and Jones, G.E., 2005, Availability of coal resources in the Vermejo and Raton formations, Raton coalfield, Raton Basin, northeast New Mexico: New Mexico Bureau of Geology and Mineral Resources Open-file Report, no. 490, 57 p.
Horton, B.K., 2012, Cenozoic evolution of hinterland basins in the Andes and Tibet, in Busby, C., and Azor, A., eds., Tectonics of Sedimentary Basins: Recent Advances: Wiley-Blackwell, Oxford, UK, p. 427–444.
Horton, B.K., Constenius, K.N., and DeCelles, P.G., 2004, Tectonic control on coarse-grained foreland-basin sequences: An example from the Cordilleran foreland basin, Utah: Geology, v. 32, p. 637-640.
Horton, B.K., and DeCelles, P.G., 2001, Modern and ancient fluvial megafans in the foreland basin system of the central Andes, southern Bolivia: implications for drainage network evolution in fold-thrust belts: Basin Research, v. 13, p. 43–63, doi:10.1046/j.1365-2117.2001.00137.x.
Horton, B.K., Dupont-Nivet, G., Zhou, J., Waanders, G.L. Butler, R.F., and Wang, J., 2004, Mesozoic-Cenozoic evolution of the Xining-Minhe and Dangchang basins, northeastern Tibetan plateau: Magnetostratigraphic and biostratigraphic results: Journal of Geophysical Research, v. 109, B04402, doi:10.1029/2003JB002913.
Horton, B.K., Fuentes, F., Boll, A., Starck, D., Ramirez, S.G., and Stockli, D.F., 2016, Andean stratigraphic record of the transition from backarc extension to orogenic shortening: A case study from the northern Neuquén basin, Argentina: Journal of South American Earth Sciences, v. 71, p. 17–40, doi:10.1016/j.jsames.2016.06.003.
Horton, B. K., Yin, A., Spurlin, M. S., Zhou, J. Y., and Wang, J. H., 2002, Paleocene-Eocene syncontractional sedimentation in narrow, lacustrine-dominated basins of east-central Tibet: Geological Society of America Bulletin, v. 114, p. 771-786.
Hough, B.G., Garzione, C.N., Wang, Z., Lease, R.O., Burbank, D.W., and Yuan, D., 2011, Stable isotope evidence for topographic growth and basin segmentation: Implications for the evolution of the NE Tibetan Plateau: Bulletin of the Geological Society of America, v. 123, p. 168–185, doi:10.1130/B30090.1.
Hough, B.G., Garzione, C.N., Wang, Z., and Lease, R.O., 2014, Timing and spatial patterns of basin segmentation and climate change in northeastern Tibet: Geological Society of America Special Papers, v. 507, p. 129–153, doi:10.1130/2014.2507(07).
Hovius, N., 1998, Controls on sediment supply by large rivers, *in* Shanley, K.W. and McCabe, P.J. eds., Relative Role of Eustasy, Climate and Tectonism in Continental Rocks, SEPM Society for Sedimentary Geology, p. 3–16.
Howard, A.L., Farmer, G.L., Amato, J.M., and Fedo, C.M., 2015, Zircon U – Pb ages and Hf isotopic compositions indicate multiple sources for Grenvillian detrital zircon

deposited in western Laurentia: Earth and Planetary Science Letters, v. 432, p. 300–310.

Hoy, R.G., and Ridgway, K.D., 2002, Syndepositional thrust-related deformation and sedimentation in an Ancestral Rocky Mountains basin, Central Colorado trough, Colorado, USA: Geological Society of America Bulletin, v. 114, p. 804-828.

Hsü, K.J., Guitang, P., and Sengör, A., 1995, Tectonic evolution of the Tibetan Plateau: A working hypothesis based on the archipelago model of orogenesis: International Geology Review, v. 37, p. 473-508.

Hubert, J.F., 1962, A zircon-tourmaline-rutile maturity index and the interdependence of the composition of heavy mineral assemblages with the gross composition and texture of sandstones: Journal of Sedimentary Petrology, v. 32, p. 440–450.

Humphreys, E., 2009, Relation of flat subduction to magmatism and deformation in the western United States, *in* Kay, S.M., Ramos, V.A., and Dickinson, W.R., eds., Backbone of the Americas: Shallow Subduction, Plateau Uplift, and Ridge and Terrane Collision: GSA Memoir 204, p. 85-98, doi:10.1130/2009.1204(04).

Hunt, A.P., and Lucas, S.G., 1992, Stratigraphy, paleontology and age of the Fruitland and Kirtland formations (upper Cretaceous), San Juan Basin, New Mexico, *in* Lucas, S.G., Kues, B., Williamson, T.E., and Hunt, A.P. eds., San Juan Basin IV, New Mexico Geological Soceity 43rd Annual Fall Field Conference Guidebook, p. 217–239.

Hutto, A.P., Yancey, T.E., and Miller, B. V, 2009, Provenance of Paleocene-Eocene Wilcox group sediments in Texas: the evidence from detrital zircons, in Gulf Coast Association of Geological Societies Transactions, v. 59, p. 357–362.

Jackson, S.E., Pearson, N.J., Griffin, W.L., and Belousova, E.A., 2004, The application of laser ablation-inductively coupled plasma-mass spectrometry to in situ U-Pb zircon geochronology: Chemical Geology, v. 211, p. 47–69, doi: 10.1016/j.chemgeo.2004.06.017.

Jian, X., Guan, P., Zhang, D.-W., Zhang, W., Feng, F., Liu, R.-J., and Lin, S.-D., 2013, Provenance of Tertiary sandstone in the northern Qaidam basin, northeastern Tibetan Plateau: Integration of framework petrography, heavy mineral analysis and mineral chemistry: Sedimentary Geology, v. 290, p. 109-125, doi:10.1016/j.sedgeo.2013.03.010.

Jin, Y., McNutt, M. K., and Zhu, Y., 1994, Evidence from gravity and topography data for folding of Tibet: Nature, v. 371, no. 6499, p. 669-674.

Johnson, C.L., and Ritts, B.D., 2012, Plate interior poly-phase basins, *in* Busby, C. and Azor, P.A. eds., Tectonics of Sedimentary Basins: Recent Advances, Hoboken, Wiley-Blackwell, p. 567–582.

Johnson, R., Dixon, G., and Wanek, A., 1966, Late Cretaceous and Tertiary stratigraphy of the Raton basin of New Mexico and Colorado: Guidebook, New Mexico Geological Society, v. 7th Field .

Johnson, R.B., and Wood, G.H., 1956, Stratigraphy of upper Cretaceous and Tertiary rocks of the Raton basin, Colorado and New Mexico: AAPG Bulletin, v. 40, p. 707–721.

Jolivet, M., Brunel, M., Seward, D., Xu, Z., Yang, J., Malavieille, J., Roger, F., Leyreloup, A., Arnaud, N., and Wu, C., 2003, Neogene extension and volcanism in

the Kunlun Fault Zone, northern Tibet: New constraints on the age of the Kunlun Fault: Tectonics, v. 22, doi:10.1029/2002TC001428.

Jolivet, M., Brunel, M., Seward, D., Xu, Z., Yang, J., Roger, F., Tapponnier, P., Malavieille, J., Arnaud, N., and Wu, C., 2001, Mesozoic and Cenozoic tectonics of the northern edge of the Tibetan plateau: fission-track constraints: Tectonophysics, v. 343, p. 111–134, doi:10.1016/S0040-1951(01)00196-2.

Jones, J., and Connelly, J., 2006, Proterozoic tectonic evolution of the Sangre de Cristo Mountains, southern Colorado, U.S.A.: Rocky Mountain Geology, v. 41, p. 79–116.

Jordan, T.E., 1981, Thrust loads and foreland basin evolution, Cretaceous, western United States: AAPG Bulletin, v. 65, p. 2506-2520.

Jordan, T.E., 1995, Retroarc foreland and related basins, *in* Busby, C.J. and Ingersoll, R.V. eds., Tectonics of Sedimentary Basins, Oxford, Blackwell Science, p. 331–362.

Jordan, T.E., and Allmendinger, R.W., 1986, The Sierras Pampeanas of Argentina: A modern analogue of Rocky Mountain foreland deformation: American Journal of Science, v. 286, p. 737–764.

Jordan, T., and Watts, A., 2005, Gravity anomalies, flexure and the elastic thickness structure of the India–Eurasia collisional system: Earth and Planetary Science Letters, v. 236, p. 732-750.Karlstrom, K.E., Dallmeyer, R.D., and Grambling, J.A., 1997, 40Ar/39Ar evidence for 1.4 Ga regional metamorphism in New Mexico: Implications for thermal evolution of lithosphere in the Southwestern USA: The Journal of Geology, v. 105, p. 205–224, doi: 10.1086/515912.

Kapp, P., DeCelles, P. G., Gehrels, G. E., Heizier, M., and Ding, L., 2007, Geological records of the Lhasa-Qiangtang and Indo-Asian collisions in the Nima area of central Tibet: Geological Society of America Bulletin, v. 119, p. 917-932.

Kapp, P., Taylor, M., Stockli, D., and Ding, L., 2008, Development of active low-angle normal fault systems during orogenic collapse: Insight from Tibet: Geology, v. 36, no. 1, p. 7-10.

Karlstrom, K.E., and Daniel, C.G., 1993, Restoration of Laramide right-lateral strike slip in northern New Mexico by using Proterozoic piercing points: tectonic implications from the Proterozoic to the Cenozoic: Geology, v. 21, p. 1139–1142, doi: 10.1130/0091-7613(1993)021<1139:ROLRLS>2.3.CO;2.

Karlstrom, K.E., and Humphreys, E.D., 1998, Persistent influence of Proterozoic accretionary boundaries in the tectonic evolution of southwestern North America: Interaction of cratonic grain and mantle modification events: Rocky Mountain Geology, v. 33, p. 161–179.

Ke, X., Ji, J., Zhang, K., Kou, X., Song, B., and Wang, C., 2013, Magnetostratigraphy and anisotropy of magnetic susceptibility of the Lulehe formation in the northeastern Qaidam basin: Acta Geologica Sinica - English Edition, v. 87, p. 576–587.

Kelley, S.A., 1990, Late Mesozoic to Cenozoic cooling histories of the Sangre de Cristo Mountains, Colorado and New Mexico: New Mexico Geological Society Guidebook, v. 41st Annua, p. 123–132.

Kelley, S.A., and Chapin, C.E., 1995, Apatite fission-track thermochronology of the southern Rocky Mountain - Rio Grande rift - western High Plains province: New Mexico Geological Society Guidebook, v. 46th Annua, p. 87–96.

Kelley, S., and Chapin, C.E., 1997, Internal structure of the southern Front Range, Colorado, from an apatite fission-track thermochronology perspective, *in* Bolyard,

D.W. and Sonnenberg, S.A. eds., Colorado Front Range Guidebook, Denver, Rocky Mountain Association of Geologists, p. 19–30.
Kelley, V.C., 1955, Monoclines of the Colorado Plateau: Geological Society of America Bulletin, v. 66, p. 789–804.
Kent-Corson, M.L., Ritts, B.D., Zhuang, G., Bovet, P.M., Graham, S. A., and Chamberlain, P., 2009, Stable isotopic constraints on the tectonic, topographic, and climatic evolution of the northern margin of the Tibetan Plateau: Earth and Planetary Science Letters, v. 282, p. 158–166, doi:10.1016/j.epsl.2009.03.011.
Kirby, E., Harkins, N.W., Wang, E., Shi, X., Fan, C., and Burbank, D.W., 2007, Slip rate gradients along the eastern Kunlun fault: Tectonics, v. 26, p. 1–16, doi:10.1029/2006TC002033.
Klemperer, S. L., 2006, Crustal flow in Tibet: geophysical evidence for the physical state of Tibetan lithosphere, and inferred patterns of active flow, in Law, R. D., Searle, M. P., and Godin, L., eds., Channel Flow, Ductile Extrusion and Exhumation in Continental Collision Zones: London, Geological Society of London, Special Publications v. 268, p. 39-70.
Klute, M.A., 1986, Sedimentology and sandstone petrography of the upper Kirtland Shale and Ojo Alamo Sandstone, Cretaceous-Tertiary boundary, western and southern San Juan basin, New Mexico: American Journal of Science, v. 286, p. 463–488.
Kraus, M., 1996, Avulsion deposits in lower Eocene alluvial rocks, Bighorn Basin, Wyoming: Journal of Sedimentary Research, v. 66, p. 354–363.
LaMaskin, T.A., 2012, Detrital zircon facies of Cordilleran terranes in western North America: GSA Today, v. 22, p. 4–11, doi:10.1130/GSATG142A.1.
Laskowski, A.K., DeCelles, P.G., and Gehrels, G.E., 2013, Detrital zircon geochronology of Cordilleran retroarc foreland basin strata, western North America: Tectonics, v. 32, p. 1027–1048, doi: 10.1002/tect.20065.
Lawton, T.F., 2008, Laramide Sedimentary Basins, in The Sedimentary Basins of the United States and Canada, Sedimentary Basins of the World v.5, Sedimentary Basins of the World, Elsevier, p. 429–450.
Lawton, T.F., and Bradford, B.A., 2011, Correlation and Provenance of Upper Cretaceous (Campanian) Fluvial Strata, Utah, U.S.A., from Zircon U-Pb Geochronology and Petrography: Journal of Sedimentary Research, v. 81, p. 495–512, doi: 10.2110/jsr.2011.45.
Lease, R.O., Burbank, D.W., Clark, M.K., Farley, K. A., Zheng, D., and Zhang, H., 2011, Middle Miocene reorganization of deformation along the northeastern Tibetan Plateau: Geology, v. 39, p. 359–362, doi:10.1130/G31356.1.
Lee, W.T., and Knowlton, F.H., 1917, Geology and paleontology of the Raton Mesa and other regions in Colorado and New Mexico: USGS Professional Paper, v. 101.
Leeder, M.R., Smith, A.B., and Yin, J., 1988, Sedimentology, palaeoecology and palaeoenvironmental evolution of the 1985 Lhasa to Golmud Geotraverse. Philosophical Transactions of the Royal Society of London, A327, 107–143.
Lehman, T.M., 1985, Depositional environments of the Naashobito Member of the Kirtland Shale, Upper Cretaceous, San Juan Basin, New Mexico, in Wolberg, D.L. ed., Contributions to Late Cretaceous paleontology and stratigraphy of New Mexico: New Mexico Bureau of Mines and Mineral Resources, Circular 195, p. 55–79.

Li, J.-J., Fang, X.-M., Van der Voo, R., Zhu, J.-J., Niocaill, C. M., Ono, Y., Pan, B.-T., Zhong, W., Wang, J.-L., Sasaki, T., Zhang, Y.-T., Cao, J.-X., Kang, S.-C., and Wang, J.-M., 1997, Magnetostratigraphic dating of river terraces: Rapid and intermittent incision by the Yellow River of the northeastern margin of the Tibetan Plateau during the Quaternary: Journal of Geophysical Research: Solid Earth, v. 102, p. 10121-10132.

Li, L., Guo, Z., Guan, S., Zhou, S., Wang, M., Fang, Y., and Zhang, C., 2015, Heavy mineral assemblage characteristics and the Cenozoic paleogeographic evolution in southwestern Qaidam Basin: Science China Earth Sciences, v. 58, p. 859–875, doi:10.1007/s11430-014-5050-x.

Li, L., Li, A., Shen, Y., Sandvol, E. A., Shi, D., Li, H., and Li, X., 2013, Shear wave structure in the northeastern Tibetan Plateau from Rayleigh wave tomography: Journal of Geophysical Research: Solid Earth, v. 118, p. 4170-4183.

Li, H., Li, S., Song, X., Gong, M., Li, X., and Jia, J., 2012, Crustal and uppermost mantle velocity structure beneath northwestern China from seismic ambient noise tomography: Geophysical Journal International, v. 188, p. 131-143.

Li, W., Neubauer, F., Liu, Y., Genser, J., Ren, S., Han, G., and Liang, C., 2013, Paleozoic evolution of the Qimantagh magmatic arcs, Eastern Kunlun Mountains: Constraints from zircon dating of granitoids and modern river sands: Journal of Asian Earth Sciences, v. 77, p. 183–202, doi:10.1016/j.jseaes.2013.08.030.

Li, C., van der Hilst, R. D., Engdahl, E. R., and Burdick, S., 2008a, A new global model for P wave speed variations in Earth's mantle: Geochemistry, Geophysics, Geosystems, v. 9, doi:10.1029/2007GC001806.

Li, C., Van der Hilst, R. D., Meltzer, A. S., and Engdahl, E. R., 2008b, Subduction of the Indian lithosphere beneath the Tibetan Plateau and Burma: Earth and Planetary Science Letters, v. 274, p. 157-168.

Liang, C., and Song, X., 2006, A low velocity belt beneath northern and eastern Tibetan Plateau from Pn tomography: Geophysical Research Letters, v. 33, L22306.

Lin, A., Fu, B., Guo, J., Zeng, Q., Dang, G., He, W., and Zhao, Y., 2002, Co-seismic strike-slip and rupture length produced by the 2001 Ms 8.1 Central Kunlun earthquake: Science, v. 296, no. 5575, p. 2015–7, doi:10.1126/science.1070879.

Lindsay, E.H., Butler, R.F., and Johnson, N.M., 1981, Magnetic polarity zonation and biostratigraphy of late Cretaceous and Paleocene continental deposits, San Juan basin, New Mexico: American Journal of Science, v. 281, p. 390–435.

Lindsey, D.A., 1998, Laramide structure of the central Sangre de Cristo mountains and adjacent Raton Basin, southern Colorado: The Mountain Geologist, v. 35, p. 55-70.

Lipman, P.W., Prostka, H.J., and Christiansen, R.L., 1972, Cenozoic volcanism and plate-tectonic evolution of the western United States. I. Early and Middle Cenozoic: Philosophical Transactions of the Royal Society A: Mathematical, Physical and Engineering Sciences, v. 271, p. 217–248, doi: 10.1098/rsta.1972.0008.

Lipman, P.W., Steven, T.A., and Mehnert, H.H., 1970, Volcanic history of the San Juan Mountains, Colorado, as indicated by potassium-argon dating: Geological Society of America Bulletin, v. 81, p. 2329–2352.

Lisenbee, A.L., 2013, Multi-stage Laramide deformation in the area of the southern Santa Fe embayment (Rio Grande rift), north-central New Mexico: Geological Society of America Special Papers, v. 494, p. 239–260, doi: 10.1130/2013.2494(10).

Liu, C., Mo, X., Luo, Z., Yu, X., Chen, H., Li, S., and Zhao, X., 2004, Mixing events between the crust- and mantle-derived magmas in Eastern Kunlun: Evidence from zircon SHRIMP II chronology: Chinese Science Bulletin, v. 49, p. 828–834, doi:10.1007/BF02889756.

Liu, L., Spasojevic, S., and Gurnis, M., 2008, Reconstructing Farallon plate subduction beneath North America back to the Late Cretaceous.: Science (New York, N.Y.), v. 322, November, p. 934–938, doi: 10.1126/science.1162921.

Liu, S., Nummedal, D., and Liu, L., 2011, Migration of dynamic subsidence across the Late Cretaceous United States Western Interior Basin in response to Farallon plate subduction: Geology, v. 39, p. 555–558, doi: 10.1130/G31692.1.

Liu, Z. F., and Wang, C. S., 2001, Facies analysis and depositional systems of Cenozoic sediments in the Hoh Xil basin, northern Tibet: Sedimentary Geology, v. 140, p. 251-270.

Liu, Z., Wang, C., and Yi, H., 2001, Evolution and Mass Accumulation of the Cenozoic Hoh Xil Basin, Northern Tibet: Journal of Sedimentary Research, v. 71, p. 971-984.

Livaccari, R.F., Burke, K., and Şengör, A.M.C., 1981, Was the Laramide orogeny related to subduction of an oceanic plateau? Nature, v. 289, p. 276–278, doi: 10.1038/289276a0.

Logsdon, M.J., 1981, A preliminary basin analysis of the El Rito Formation (Eocene), north-central New Mexico: Geological Society of America Bulletin, v. 92, p. 968, doi: 10.1130/0016-7606(1981)92<968:APBAOT>2.0.CO;2.

Lorenz, J.C., and Cooper, S.P., 2003, Tectonic Setting and Characteristics of Natural Fractures in Mesaverde and Dakota Reservoirs of the San Juan, New Mexico and Colorado: New Mexico Geology, v. 25, p. 3-14.

Lu, H., Wang, E., Shi, X., and Meng, K., 2012, Cenozoic tectonic evolution of the Elashan range and its surroundings, northern Tibetan Plateau as constrained by paleomagnetism and apatite fission track analyses: Tectonophysics, v. 580, p. 150–161, doi:10.1016/j.tecto.2012.09.013.

Lu, H., and Xiong, S., 2009, Magnetostratigraphy of the Dahonggou section, northern Qaidam Basin and its bearing on Cenozoic tectonic evolution of the Qilian Shan and Altyn Tagh Fault: Earth and Planetary Science Letters, v. 288, p. 539–550, doi:10.1016/j.epsl.2009.10.016.

Lucas, S.G., 1982, Vertebrate paleontology, stratigraphy and biostratigraphy of Eocene Galisteo Formation, north-central New Mexico, *in* New Mexico Bureau of Geology and Mineral Resources Circular 1, Socorro, NM, New Mexico Bureau of Mines and Mineral Resources.

Lucas, S.G., Cather, S.M., Abbott, J.C., and Williamson, T.E., 1997, Stratigraphy and tectonic implications of Paleogene strata in the Laramide Galisteo Basin, north-central New Mexico: New Mexico Geology, p. 89–95.

Lucas, S.G., and Ingersoll, R. V., 1981, Cenozoic continental deposits of New Mexico: An overview: Geological Society of America Bulletin, v. 92, p. 917–932.

Mack, G.H., and Clemons, R.E., 1988, Structural and stratigraphic evidence for the Laramide (early Tertiary) Burro uplift in southwestern New Mexico: New Mexico

Bureau of Geology and Mineral Resources Field Conference Guidebook, v. 39th, p. 59–66.
Mack, G. H., and Rasmussen, K. A., 1984, Alluvial-fan sedimentation of the Cutler Formation (Permo-Pennsylvanian) near Gateway, Colorado: Geological Society of America Bulletin, v. 95, p. 109-116.
MacKenzie, D.B., and Poole, D.M., 1962, Provenance of Dakota Group sandstones of the Western Interior, *in* Enyert, R. L., and Curry, W. H., III., eds., Symposium on Early Cretaceous rocks of Wyoming and adjacent areas: Wyoming Geological Association, p. 62-71.
Mackey, G.N., Horton, B.K., and Milliken, K.L., 2012, Provenance of the Paleocene-Eocene Wilcox Group, western Gulf of Mexico basin: Evidence for integrated drainage of the southern Laramide Rocky Mountains and Cordilleran arc: Geological Society of America Bulletin, v. 124, p. 1007–1024, doi: 10.1130/B30458.1.
Makaske, B., 2001, Anastomosing rivers: a review of their classification, origin and sedimentary products: Earth-Science Reviews, v. 53, p. 149–196, doi:10.1016/S0012-8252(00)00038-6.
Maldonado, F., 2008, Geologic map of the Abiquiu quadrangle, Rio Arriba County, New Mexico: U.S. Geological Survey Scientific Investigations Map 2998, scale 1:24 000.
Mange, M., and Maurer, H.F.W., 1992, Heavy minerals in colour: Chapman & Hall, Hong Kong.
Mao, L., Xiao, A., Wu, L., Li, B., Wang, L., Lou, Q., Dong, Y., and Qin, S., 2014, Cenozoic tectonic and sedimentary evolution of southern Qaidam Basin, NE Tibetan Plateau and its implication for the rejuvenation of Eastern Kunlun Mountains: Science China Earth Sciences, v. 57, doi:10.1007/s11430-014-4951-z.
Marine Geoscience Data System, 2016, GeoMapApp: http://www.geomapapp.org (accessed July 2016).
Marsh, J.H., and Stockli, D.F., 2015, Zircon U-Pb and trace element zoning characteristics in an anatectic granulite domain: Insights from LASS-ICP-MS depth profiling: Lithos, v. 239, p. 170–185, doi: 10.1016/j.lithos.2015.10.017.
Marshak, S., Karlstrom, K.E., and Timmons, J.M., 2000, Inversion of Proterozoic extensional faults: An explanation for the pattern of Laramide and Ancestral Rockies intracratonic deformation, United States: Geology, v. 28, p. 735–738, doi: 10.1130/0091-7613(2000)28<735.
Masek, J. G., Isacks, B. L., Fielding, E. J., and Browaeys, J., 1994, Rift flank uplift in Tibet: Evidence for a viscous lower crust: Tectonics, v. 13, p. 659-667.
Mattinson, C.G., Menold, C.A., Zhang, J.X., and Bird, D.K., 2007, High- and Ultrahigh-Pressure Metamorphism in the North Qaidam and South Altyn Terranes, Western China: International Geology Review, v. 49, p. 969–995, doi:10.2747/0020-6814.49.11.969.
McGookey, D.P., 1972, Cretaceous System, *in* Mallory, W.W., ed., Geologic atlas of the Rocky Mountain region: Denver, Colorado, Rocky Mountain Association of Geologists, p. 190-228.
McRivette, M.W., 2011, The tectonic evolution of the Eastern Kunlun Range and central Tibetan plateau, China: Ph.D. dissertation, University of California, Los Angeles, 333 p.

Meng, Q.R., and Fang, X., 2008, Cenozoic tectonic development of the Qaidam Basin in the northeastern Tibetan Plateau: Geological Society of America Special Papers, v. 444, p. 1–24, doi:10.1130/2008.2444(01).

Meng, Q.-R., Wang, E., and Hu, J.-M., 2005, Mesozoic sedimentary evolution of the northwest Sichuan basin: Implication for continued clockwise rotation of the South China block: Geological Society of America Bulletin, v. 117, p. 396-410.

Menold, C.A., 2006, Tectonic and metamorphic evolution of the North Qaidam Ultrahigh-pressure metamorphic terrane, western China: Ph.D. dissertation, University of California, Los Angeles, 279 p.

Menold, C.A., Manning, C.E., Yin, A., Tropper, P., Chen, X.-H., and Wang, X.-F., 2009, Metamorphic evolution, mineral chemistry and thermobarometry of orthogneiss hosting ultrahigh-pressure eclogites in the North Qaidam metamorphic belt, Western China: Journal of Asian Earth Sciences, v. 35, p. 273–284, doi:10.1016/j.jseaes.2008.12.008.

Merewether, E.A., Cobban, W.A., and Obradovich, J.D., 2011, Biostratigraphic data from Upper Cretaceous formations — eastern Wyoming, central Colorado, and northeastern New Mexico, U.S. Geological Survey Scientific Investigations Map 3175: 2 sheets, pamphlets, 10 p.

Métivier, F., Gaudemer, Y., Tapponnier, P., Klein, M., 1999, Mass accumulation rates in Asia during the Cenozoic: Geophysical Journal International, v. 137, p. 280-318.

Meyer, B., Tapponnier, P., Bourjot, L., Metivier, F., Gaudemer, Y., Peltzer, G., Shunmin, G., and Zhitai, C., 1998, Crustal thickening in Gansu-Qinghai, lithospheric mantle subduction, and oblique, strike-slip controlled growth of the Tibetan Plateau: Geophysical Journal International, v. 135, p. 1–47.

Miall, A.D., 1977, A review of the braided-river depositional environment: Earth-Science Reviews, v. 13, p. 1–62, doi:10.1016/0012-8252(77)90055-1.

Miao, Y., Fang, X., Herrmann, M., Wu, F., Zhang, Y., and Liu, D., 2011, Miocene pollen record of KC-1 core in the Qaidam Basin, NE Tibetan Plateau and implications for evolution of the East Asian monsoon: Palaeogeography, Palaeoclimatology, Palaeoecology, v. 299, p. 30–38, doi:10.1016/j.palaeo.2010.10.026.

Miao, Y., Fang, X., Song, Z., Wu, F., Han, W., Dai, S., and Song, C., 2008, Late Eocene pollen records and palaeoenvironmental changes in northern Tibetan Plateau: Science in China Series D: Earth Sciences, v. 51, p. 1089–1098, doi:10.1007/s11430-008-0091-7.

Mo, X., Luo, Z., Deng, J., Yu, X., Liu, C., Chen, H., Yuan, W., and Liu, Y., 2007, Granitoids and crustal growth in the East-Kunlun orogenic belt: Geological Journal of China Universities, v. 13, p. 403–414.

Mock, C., Arnaud, N.O., and Cantagrel, J.-M., 1999, An early unroofing in northeastern Tibet ? Constraints from 40Ar / 39Ar thermochronology on granitoids from the eastern Kunlun range: Earth and Planetary Science Letters, v. 171, p. 107–122.

Morton, A.C., and Hallsworth, C.R., 1999, Processes controlling the composition of heavy mineral assemblages in sandstones: Sedimentary Geology, v. 124, p. 3-29.

Muehlberger, W.R., 1967, Geology of Chama Quadrangle, New Mexico: New Mexico Bureau of Mines and Mineral Resources Bulletin 89. 114 p.

Nanson, G., 1980, Point bar and floodplain formation of the meandering Beatton River, northeastern British Columbia, Canada: Sedimentology, v. 27, p. 3–29.

Nemec, W., and Steel, R.J., 1984, Alluvial and coastal conglomerates: their significance and some comments on gravelly mass-flow deposits, *in* Koster, E.H. and Steel, R.J. eds., Sedimentology of Gravels and Conglomerates, Canadian Society of Petroleum Geologists Memoir 10, p. 1–31.

Nie, J., Stevens, T., Rittner, M., Stockli, D., Garzanti, E., Limonta, M., Bird, A., Ando, S., Vermeesch, P., Saylor, J., Lu, H., Breecker, D., Hu, X., Liu, S., Resentini, A., Vezzoli, G., Peng, W., Carter, A., Ji, S., and Pan, B., 2015, Loess Plateau storage of Northeastern Tibeta Plateau-derived Yellow River sediment: Nature Communications, v. 6, p. 8511 doi: 10.1038/ncomms9511.

Owens, T. J., and Zandt, G., 1997, Implications of crustal property variations for models of Tibetan plateau evolution: Nature, v. 387, no. 6628, p. 37-43.

Orth, C., Gilmore, J.S., Knight, J.D., Pillmore, C.L., Tschudy, R.H., and Fassett, J.E., 1982, Iridium abundance measurements across the Cretaceous/Tertiary boundary in the San Juan and Raton basins of northern New Mexico: Geological Society of America Special Papers, v. 190, p. 423–434, doi: 10.1130/SPE190-p423.

Painter, Clayton S., Barbara Carrapa, Peter G. DeCelles, George E. Gehrels, and S. N. Thomson, 2014, Exhumation of the North American Cordillera revealed by multi-dating of Upper Jurassic-Upper Cretaceous foreland basin deposits: Geological Society of America Bulletin, v. 126, no. 11-12, p. 1439–64, doi:10.1130/B30999.1

Penn, B.S., and Lindsey, D.A., 1996, Tertiary igneous rocks and Laramide structure and stratigraphy of the Spanish Peaks region, south-central Colorado: road log and descriptions from Walsenburg to La Veta (first day) and La Veta to Aguilar (second day), in Colorado Geological Survey OFR 96-4, p. [21].

Peppe, D.J., Heizler, M.T., Williamson, T.E., Masson, I.P., Brusatte, S., Weil, A., and Secord, R., 2013, New age constrains on the late Cretaceous through early Paleocene rocks in the San Juan basin, New Mexico, in Geological Society of America Annual Meeting 2013, Denver, CO.

Petrus, J.A., and Kamber, B.S., 2012, VizualAge: A novel approach to laser ablation ICP-MS U-Pb geochronology data reduction: Geostandards and Geoanalytical Research, v. 36, p. 247–270, doi: 10.1111/j.1751-908X.2012.00158.x.

Peyton, S.L., and Carrapa, B., 2013, An overview of tow-temperature thermochronology in the Rocky Mountains and its application to petroleum system analysis, *in* Knight, C. and Cuzella, J. eds., Applications of structural methods to Rocky Mountain hydrocarbon exploration and development: AAPG Studies in Geology 65, p. 37–70.

Pillmore, C.L., and Flores, R.M., 1987, Stratigraphy and depositional environments of the Cretaceous-Tertiary boundary clay and associated rocks, Raton basin, New Mexico and Colorado: Geological Society of America Special Publication 209, p. 111–130.

Pillmore, C.L., and Flores, R.M., 1990, Cretaceous and Paleocene rocks of the Raton basin, New Mexico and Colorado-stratigraphic environmental framework: New Mexico Geological Society Guidebook, no. 41st Field Conference, p. 333–336.

Pillmore, C.L., Tschudy, R.H., Orth, C.J., Gilmore, J.S., and Knight, J.D., 1984, Geologic framework of nonmarine Cretaceous-Tertiary boundary sites, Raton basin, New Mexico and Colorado: Science, v. 223, no. 4641, p. 1180-1182.

Porter, R.J., and Gallois, R.W., 2008, Identifying fluvio–lacustrine intervals in thick playa-lake successions: An integrated sedimentology and ichnology of arenaceous members in the mid–late Triassic Mercia Mudstone Group of south-west England,

UK: Palaeogeography, Palaeoclimatology, Palaeoecology, v. 270, p. 381–398, doi:10.1016/j.palaeo.2008.07.020.

Powell, J.S., 1973, Paleontology and sedimentation models of the Kimbeto Member of the Ojo Alamo Sandstone, in Cretaceous and Tertiary rocks of the southern Colorado Plateau: Four Corners Geological Society Memoir, p. 111–122.

Pillmore, C.L., and Flores, R.M., 1990, Cretaceous and Paleocene rocks of the Raton basin, New Mexico and Colorado-stratigraphic environmental framework: New Mexico Geological Society Guidebook, p. 333–336.

Pollock, C.J., Stewart, K.G., Hibbard, J.P., Wallace, L., and Giral, R.A., 2004, Thrust wedge tectonics and strike-slip faulting in the Sierra Nacimiento, New Mexico: New Mexico Bureau of Geology and Mineral Resources Bulletin, p. 97–112.

Potochnik, A., 1989, Depositional style and tectonic implications of the Mogollon Rim Formation (Eocene), east-central Arizona: New Mexico Geological Society Guidebook, 40th Field Conference, p. 107–118.

Pullen, A., Kapp, P., Gehrels, G.E., Vervoort, J.D., and Ding, L., 2008, Triassic continental subduction in central Tibet and Mediterranean-style closure of the Paleo-Tethys Ocean: Geology, v. 36, p. 351, doi:10.1130/G24435A.1.

Pullen, A., Kapp, P., McCallister, A.T., Chang, H., Gehrels, G.E., Garzione, C.N., Heermance, R. V., and Ding, L., 2011, Qaidam Basin and northern Tibetan Plateau as dust sources for the Chinese Loess Plateau and paleoclimatic implications: Geology, doi:10.1130/G32296.1.

Qinghai Bureau of Geology and Mineral Resources, 1991, Regional geology of Qinghai province.

Ramos, V.A., Cristallini, E., and Perez, D.J., 2002, The Pampean flat-slab of the Central Andes: Journal of South American Earth Sciences, v. 15, p. 59–78, doi: 10.1016/S0895-9811(02)00006-8.

Raynolds, R.G., Johnson, K.R., Ellis, B., Dechesne, M., and Miller, I.M., 2007, Earth history along Colorado's Front Range: Salvaging geologic data in the suburbs and sharing it with the citizens: GSA Today, v. 17, no. 12, p. 4–10, doi: 10.1130/GSAT01712A.1.

Reed, J.C., Jr., Wheeler, J.O., and Tucholke, J.E., comps., 2005a, Geologic map of North America: Boulder, Colo., Geological Society of America, Decade of North American Geology Continental Scale Map 001, scale 1:5,000,000, http://rock.geosociety.org/bookstore/default.asp?oID= 0&catID=2&pID=CSM001F.

Reed, J.C., Jr., Wheeler, J.O., and Tucholke, B.E., 2005b, Geologic map of North America—Perspectives and explanation: Boulder, Colo., Geological Society of America, Decade of North American Geology, 28 p.

Richardson, N. J., Densmore, A. L., Seward, D., Fowler, A., Wipf, M., Ellis, M. A., Yong, L., and Zhang, Y., 2008, Extraordinary denudation in the Sichuan Basin: Insights from low-temperature thermochronology adjacent to the eastern margin of the Tibetan Plateau: Journal of Geophysical Research: Solid Earth, v. 113, doi:10.1029/2006JB004739.

Rieser, A.B., Liu, Y., Genser, J., Neubauer, F., Handler, R., Friedl, G., and Ge, X., 2006a, 40Ar/39Ar ages of detrital white mica constrain the Cenozoic development of the intracontinental Qaidam Basin, China: Geological Society of America Bulletin, v. 118, p. 1522–1534, doi:10.1130/B25962.1.

Rieser, A. B., Liu, Y. J., Genser, J., Neubauer, F., Handler, R., and Ge, X. H., 2006b, Uniform Permian Ar-40/Ar-39 detrital mica ages in the eastern Qaidam Basin (NW China): where is the source?: Terra Nova, v. 18, no. 1, p. 79-87.

Rieser, A.B., Neubauer, F., Liu, Y., and Ge, X., 2005, Sandstone provenance of north-western sectors of the intracontinental Cenozoic Qaidam basin, western China: Tectonic vs. climatic control: Sedimentary Geology, v. 177, p. 1–18, doi:10.1016/j.sedgeo.2005.01.012.

Ritts, B.D., 1998, Mesozoic tectonics and sedimentation, and petroleum systems of the Qaidam and Tarim basins, NW China: Ph.D. dissertation, Stanford University, Stanford, California, 691 p.

Ritts, B.D. and Biffi, U., 2000, Magnitude of post-Middle Jurassic (Bajocian) displacement on the central Altyn Tagh fault system, northwest China: Geological Society of America Bulletin, v. 112, p. 61-74.

Ritts, B.D., and Biffi, U., 2001, Mesozoic northeast Qaidam basin: Response to contractional reactivation of the Qilian Shan, and implications for the extent of Mesozoic intracontinental deformation in Central Asia: Geological Society of America Memoirs, v. 194, p. 293–316, doi:10.1130/0-8137-1194-0.293.

Ritts, B.D., Yue, Y., Graham, S.A., Sobel, E.R., Abbink, A.O., and Stockli, D.F., 2008, From sea level to high elevation in 15 million years: Uplift history of the northern Tibetan Plateau margin in the Altun Shan: American Journal of Science, v. 308, p. 657–678, doi:10.2475/05.2008.01.

Robinson, A.C., Ducea, M., and Lapen, T.J., 2012, Detrital zircon and isotopic constraints on the crustal architecture and tectonic evolution of the northeastern Pamir: Tectonics, v. 31, doi:10.1029/2011TC003013.

Robinson Roberts, L.N.R., and Kirschbaum, M.A., 1995, Paleogeography of the Late Cretaceous of the Western Interior of middle North America- Coal distribution and sediment accumulation: USGS Professional Paper, v. 1561.

Roger, F., Arnaud, N., Gilder, S., Tapponnier, P., Jolivet, M., Brunel, M., Malavieille, J., Xu, Z., and Yang, J., 2003, Geochronological and geochemical constraints on Mesozoic suturing in east central Tibet: Tectonics, v. 22, doi:10.1029/2002TC001466.

Royden, L.H., 1996, Coupling and decoupling of crust and mantle in convergent orogens: Implications for strain partitioning in the crust: Journal of Geophysical Research, v. 101, p. 17679–17.

Ruf, J.C., and Erslev, E.A., 2005, Origin of Cretaceous to Holocene fractures in the northern San Juan Basin, Colorado and New Mexico: Rocky Mountain Geology, v. 40, p. 91–114, doi: 10.2113/40.1.91.

Rust, B.R., 1972, Structure and process in a braided river: Sedimentology, v. 18, p. 221–245.

Ryan, W.B.F., S.M. Carbotte, J.O. Coplan, S. O'Hara, A. Melkonian, R. Arko, R.A. Weissel, V. Ferrini, A. Goodwillie, F. Nitsche, J. Bonczkowski, and R. Zemsky, 2009, Global Multi-Resolution Topography synthesis, Geochem. Geophys. Geosyst., 10, Q03014, doi:10.1029/2008GC002332.

Saleeby, J., 2003, Segmentation of the Laramide Slab — evidence from the southern Sierra Nevada region: Geological Society of America Bulletin, v. 115, p. 655, doi: 10.1130/0016-7606(2003)115<0655.

Sanchez, V. I., Murphy, M. A., Dupré, W. R., Ding, L., and Zhang, R., 2010, Structural evolution of the Neogene Gar Basin, western Tibet: Implications for releasing bend development and drainage patterns: Geological Society of America Bulletin, v. 122, p. 926-945.

Saylor, J. E., DeCelles, P. C., Gehrels, G., Murphy, M., Zhang, R., and Kapp, P., 2010, Basin formation in the High Himalaya by arc-parallel extension and tectonic damming: Zhada basin, southwestern Tibet: Tectonics, v. 29, TC1004.

Schavran, G., 1985, Structural features in the Huerfano Park area, east flank, Sangre de Cristo range, Colorado: The Mountain Geologist, v. 22, p. 33–39.

Seager, W.R., 1983, Laramide wrench faults, basement-cored upifts, and complimentary basins in southern New Mexico: New Mexico Geology, v. 5, p. 69–76.

Seager, W.R., and Mack, G.H., 1986, Laramide paleotectonics of southern New Mexico, *in* Paleotectonics and sedimentation in the Rocky Mountain region, United States, AAPG Memoir 41, p. 669–685.

Sewall, J.O., and Sloan, L.C., 2006, Come a little bit closer: A high-resolution climate study of the early Paleogene Laramide foreland: Geology, v. 34, p. 81–84, doi: 10.1130/G22177.1.

Shaw, C.A., Heizler, M.T., and Karlstrom, K.E., 2005, 40Ar/39 Ar thermochronologic record of 1.45-1.35 Ga intracontinental tectonism in the southern Rocky Mountains: Interplay of conductive and advective heating with intracontinental deformation, in The Rocky Mountain Region: An Evolving Lithosphere, American Geophysical Union, p. 163–184.

Smith, H.T.U., 1938, Tertiary geology of the Abiquiu quadrangle, New Mexico: The Journal of Geology, v. 46, p. 933–965.

Smith, L.N., 1992, Stratigraphy, sediment dispersal and paleogeography of the lower Eocene San Jose Formation, San Juan Basin, New Mexico, *in* San Juan Basin IV, New Mexico Geological Soceity 43rd Annual Fall Field Conference Guidebook, p. 265–296.

Smith, M.E., Carroll, A.R., and Singer, B.S., 2008, Synoptic reconstruction of a major ancient lake system: Eocene Green River Formation, western United States: Geological Society of America Bulletin, v. 120, p. 54–84, doi: 10.1130/B26073.1.

Smith, S.A., 1990, The sedimentology and accretionary styles of an ancient gravel-bed stream: the Budleigh Salterton Pebble Beds (Lower Triassic), southwest England: Sedimentary Geology, v. 67, p. 199–219, doi:10.1016/0037-0738(90)90035-R.

Snell, K.E., Thrasher, B.L., Eiler, J.M., Koch, P.L., Sloan, L.C., and Tabor, N.J., 2013, Hot summers in the Bighorn Basin during the early Paleogene: Geology, v. 41, p. 55–58, doi: 10.1130/G33567.1.

Sobel, E.R., and Arnaud, N., 1999, A possible middle Paleozoic suture in the Altyn Tagh, NW China: Tectonics, v. 18, p. 64–74.

Sobel, E.R., Arnaud, N., Jolivet, M., and Ritts, B.D., 2001, Jurassic to Cenozoic exhumation history of the Altyn Tagh range, northwest China, constrained by 40Ar/39Ar and apatite fission track thermochronology: Geological Society Of America Memoirs, v. 194, p. 247–267, doi:10.1130/0-8137-1194-0.247.

Sobel, E.R., Hilley, G.E., and Strecker, M.R., 2003, Formation of internally drained contractional basins by aridity-limited bedrock incision: Journal of Geophysical Research, v. 108, doi: 10.1029/2002JB001883.

Song, B., Zhang, K., Chen, R., Wang, C., Luo, M., Zhang, J., and Jiang, S., 2013a, The sedimentary record in northern Qaidam basin and its response to the uplift of the southern Qilian Mountain at around 30 Ma: Acta Geologica Sinica - English Edition, v. 87, p. 528–539.

Song, B., Zhang, K., Lu, J., Wang, C., and Xu, Y., 2013b, The middle Eocene to early Miocene integrated sedimentary record in the Qaidam Basin and its implications for paleoclimate and early Tibetan Plateau uplift: Canadian Journal of Earth Sciences, v. 50, p. 183–196.

Spurlin, M. S., Yin, A., Horton, B. K., Zhou, J., and Wang, J., 2005, Structural evolution of the Yushu-Nangqian region and its relationship to syncollisional igneous activity east-central Tibet: Geological Society of America Bulletin, v. 117, p. 1293-1317.

Staisch, L.M., Niemi, N. A., Hong, C., Clark, M.K., Rowley, D.B., and Currie, B., 2014, A Cretaceous-Eocene depositional age for the Fenghuoshan Group, Hoh Xil Basin: Implications for the tectonic evolution of the northern Tibet Plateau: Tectonics, v. 33, p. 281-301, doi:10.1002/2013TC003367.

Stearns, C.E.., 1943, The Galisteo Formation of north-central New Mexico: The Journal of Geology, v. 51, p. 301–319.

Stewart, J.H., 1972, Initial deposits in the Cordilleran geosyncline: Evidence of a Late Precambrian (<850 m.y.) continental separation: Geological Society of America Bulletin, v. 83, p. 1345–1360.

Strecker, M. R., Alonso, R. N., Bookhagen, B., Carrapa, B., Hilley, G. E., Sobel, E. R., and Trauth, M. H., 2007, Tectonics and climate of the southern central Andes: Annual Review of Earth and Planetary Sciences, v. 35, p. 747-787.

Strecker, M.R., Alonso, R.N., Bookhagen, B., Carrapa, B., Coutand, I., Hain, M.P., Hilley, G.E., Mortimer, E., Schoenbohm, L.M., and Sobel, E.R., 2009, Does the topographic distribution of the central Andean Puna Plateau result from climatic or geodynamic processes? Geology, v. 37, p. 643–646, doi: 10.1130/G25545A.1.

Strecker, M.R., Hilley, G.E., Bookhagen, B., and Sobel, E.R., 2012, Structural, geomorphic, and depositional characteristics of contiguous and broken foreland basins: examples from the eastern flanks of the central Andes in Bolivia and NW Argentina, *in* Busby, C., and Azor, A., eds., Tectonics of Sedimentary Basins: Recent Advances: Wiley-Blackwell, Oxford, UK, p. 508-521.

Sun, Z., Yang, Z., Pei, J., Ge, X., Wang, X., Yang, T., Li, W., and Yuan, S., 2005, Magnetostratigraphy of Paleogene sediments from northern Qaidam Basin, China: Implications for tectonic uplift and block rotation in northern Tibetan plateau: Earth and Planetary Science Letters, v. 237, p. 635–646, doi:10.1016/j.epsl.2005.07.007.

Syvitski, J.P.M., Peckham, S.D., Hilberman, R., and Mulder, T., 2003, Predicting the terrestrial flux of sediment to the global ocean: a planetary perspective: Sedimentary Geology, v. 162, p. 5–24, doi: 10.1016/S0037-0738(03)00232-X.

Szwarc, T.S., Johnson, C.L., Stright, L.E., and McFarlane, C.M., 2014, Interactions between axial and transverse drainage systems in the Late Cretaceous Cordilleran foreland basin: Evidence from detrital zircons in the Straight Cliffs Formation, southern Utah, USA: Geological Society of America Bulletin, , no. X, p. 1–21, doi: 10.1130/B31039.1.

Tapponnier, P., Zhiqin, X., Meyer, B., and Arnaud, N., 2001, Oblique Stepwise Rise and Growth of the Tibet Plateau: Science, v. 294, no. 1671, p. 1671–1677, doi:10.1126/science.105978.

Taylor, M. H., Kapp, P. A., and Horton, B. K., 2012, Basin response to active extension and strike-slip deformation in the hinterland of the Tibetan Plateau, in Busby, C., and Azor, A., eds., Tectonics of Sedimentary Basins: Recent Advances, Blackwell Publishing Ltd., p. 445-460.

Tidwell, W.D., Britt, B.B., and Tidwell, L.S., 2007, A review of the Cretaceous floras of east-central Utah and western Colorado: Central Utah–Diverse Geology of a Dynamic Landscape, Utah Geological Association, p. 467-482.

Tornqvist, T., 1993, Holocene alternation of meandering and anastomosing fluvial systems in the Rhine-Meuse delta (central Netherlands) controlled by sea-level rise and subsoil erodibility: Journal of Sedimentary Petrology, v. 63, p. 683–693.

Tschudy, R.H., Pillmore, C.L., Orth, C.J., Gilmore, J.S., and Knight, J.D., 1984, Disruptions of the terrestrial plant ecosystem at the Cretaceous- Tertiary boundary, Western Interior: Science, v. 225, no. 4666, p. 1030-1034.

Tweto, O., 1975, Laramide (Late Cretaceous-early Tertiary) orogeny in the southern Rocky Mountains, in Curtis, B.F., ed., Cenozoic history of the southern Rocky Mountains, GSA Memoir 144, p. 1-44.

Tweto, O., 1980, Summary of Laramide orogeny in Colorado, *in* Kent, H.C., and Porter, K.W., eds., Colorado geology: Denver, Rocky Mountain Association of Geologists, p. 129-134.

Van Der Woerd, J., Ryerson, F.J., Tapponnier, P., Gaudemer, Y., Finkel, R., Meriaux, A. S., and Caffee, M., 1998, Holocene left-slip rate determined by cosmogenic surface dating on the Xidatan segment of the Kunlun fault (Qinghai, China): Geology, v. 26, p. 695–698, doi:10.1130/0091-7613(1998)026<0695:HLSRDB>2.3.CO;2.

Vermeesch, P., 2004, How many grains are needed for a provenance study? Earth and Planetary Science Letters, v. 224, p. 441–451, doi: 10.1016/j.epsl.2004.05.037.

Vermeesch, P., 2012, On the visualisation of detrital age distributions: Chemical Geology, v. 312-313, p. 190–194, doi:10.1016/j.chemgeo.2012.04.021.

Vermeesch, P., 2013, Multi-sample comparison of detrital age distributions: Chemical Geology, v. 341, p. 140–146, doi: 10.1016/j.chemgeo.2013.01.010.

Walker, J.D., Geissman, J.W., Bowring, S.A., and Babcock, L.E., 2012, GSA Geologic Time Scale (v. 4.0): Geological Society of America, http://www.geosociety.org/science/timescale/

Wanek, A. A., 1963, Geology and fuel resources of the southwestern part of the Raton coal field, Colfax County, New Mexico: U.S. Geological Survey Coal Investigations Map C-45.

Wang, Q., and Coward, M.P., 1990, The Chaidam Basin (NW China): Formation and Hydrocarbon Potential: Journal of Petroleum Geology, v. 13, p. 93–112, doi:10.1306/BF9AB6C2-0EB6-11D7-8643000102C1865D.

Wang, F., Lo, C.-H., Li, Q., Yeh, M.-W., Wan, J., Zheng, D., and Wang, E., 2004, Onset timing of significant unroofing around Qaidam basin, northern Tibet, China: constraints from 40Ar/39Ar and FT thermochronology on granitoids: Journal of Asian Earth Sciences, v. 24, p. 59–69, doi:10.1016/j.jseaes.2003.07.004.

Wang, X., Qiu, Z., Li, Q., Wang, B., Qiu, Z., Downs, W.R., Xie, G., Xie, J., Deng, T., Takeuchi, G.T., Tseng, Z.J., Chang, M., Liu, J., Wang, Y., et al., 2007, Vertebrate paleontology, biostratigraphy, geochronology, and paleoenvironment of Qaidam Basin in northern Tibetan Plateau: Palaeogeography, Palaeoclimatology, Palaeoecology, v. 254, p. 363–385, doi:10.1016/j.palaeo.2007.06.007.

Wang, E., Xu, F.-Y., Zhou, J.-X., Wan, J., and Burchfiel, B.C., 2006, Eastward migration of the Qaidam basin and its implications for Cenozoic evolution of the Altyn Tagh fault and associated river systems: Geological Society of America Bulletin, v. 118, p. 349–365, doi:10.1130/B25778.1.

Wang, Y., Zhang, X.M., Wang, E., Zhang, A.F., Li, Q., Sun, G.H., 2005, Ar-40/Ar-39 thermochronological evidence for formation and Mesozoic evolution of the northern-central segment of the Altyn Tagh fault system in the northern Tibetan Plateau: Geological Society of America Bulletin, v. 117, p. 1336-1346.

Wawrzyniec, T.F., Geissman, J.W., Melker, M.D. and Hubbard, M., 2002. Dextral shear along the eastern margin of the Colorado Plateau: A kinematic link between Laramide contraction and Rio Grande rifting (ca. 75–13 Ma). The Journal of Geology, 110(3), pp.305-324.

Weislogel, A.L., 2008, Tectonostratigraphic and geochronologic constraints on evolution of the northeast Paleotethys from the Songpan-Ganzi complex, central China: Tectonophysics, v. 451, p. 331–345, doi:10.1016/j.tecto.2007.11.053.

Weislogel, A.L., Graham, S.A., Chang, E.Z., Wooden, J.L., and Gehrels, G.E., 2010, Detrital zircon provenance from three turbidite depocenters of the Middle-Upper Triassic Songpan-Ganzi complex, central China: Record of collisional tectonics, erosional exhumation, and sediment production: Geological Society of America Bulletin, v. 122, p. 2041–2062, doi:10.1130/B26606.1.

Weislogel, A.L., Graham, S.A., Chang, E.Z., Wooden, J.L., Gehrels, G.E., and Yang, H., 2006, Detrital zircon provenance of the Late Triassic Songpan-Ganzi complex: Sedimentary record of collision of the North and South China blocks: Geology, v. 34, p. 97, doi:10.1130/G21929.

Wernicke, B., 2011, The California River and its role in carving Grand Canyon: Geological Society of America Bulletin, v. 123, no. 7-8, p. 1288–1316, doi: 10.1130/B30274.1.

Whitmeyer, S.J., and Karlstrom, K.E., 2007, Tectonic model for the Proterozoic growth of North America: Geosphere, v. 3, p. 220–259, doi: 10.1130/GES00055.1.

Whipple, K. X., and G. E. Tucker, Dynamics of the stream-power river incision model: Implications for height limits of mountain ranges, land- scape response timescales, and research needs, J. Geophys. Res., 104, 17,661–17,674, 1999

Willett, S.D., 1999, Orogeny and orography : The effects of erosion on the structure Processes: Journal of Geophysical Research, v. 104, p. 28957–28981.

Willett, S.D., and Beaumont, C., 1994, Subduction of Asian lithospheric mantle beneath Tibet inferred from models of continental collision: Nature, v. 369, p. 642–646.

Williamson, T.E., and Lucas, S.G., 1992, Stratigraphy and mammalian biostratigraphy of the Paleocene Nacimiento Formation, southern San Juan Basin, *in* Lucas, S.G., Kues, B., Williamson, T.E., and Hunt, A.P. eds., San Juan Basin IV, New Mexico Geological Soceity 43rd Annual Fall Field Conference Guidebook, p. 265–296.

Williamson, T.E., 1996, The beginning of the age of mammals in the San Juan Basin, New Mexico; biostratigraphy and evolution of Paleocene mammals of the Nacimiento Formation: New Mexico Museum of Natural History and Science Bulletin, v. 8, p. 1–141.

Winker, C.D., 1982, Cenozoic shelf margins, northwestern Gulf of Mexico basin: Gulf Coast Association of Geological Societies Transactions, v. 32, p. 427–448.

Woodward, L. A., 1987, Geology and mineral resources of Sierra Nacimiento and vicinity, New Mexico: New Mexico Bureau of Mines and Mineral Resources, Memoir 42, 84 p.

Woodward, L.A., Anderson, O.J., and Lucas, S.G., 1997, Mesozoic stratigraphic constraints on Laramide right slip on the east side of the Colorado Plateau: Geology, v. 25, p. 843–846, doi: 10.1130/0091-7613(1997)025<0843:MSCOLR>2.3.CO;2.

Woodruff, W. H., Horton, B. K., Kapp, P. A., and Stockli, D. F., 2013, Late Cenozoic evolution of the Lunggar extensional basin, Tibet: Implications for basin growth and exhumation in hinterland plateaus: Geological Society of America Bulletin, v. 125, p. 343-358.

Wu, C., Yang, J., Wooden, J.L., Shi, R., Chen, S., Meibom, A., and Mattinson, C., 2004, Zircon U-Pb SHRIMP dating of the Yematan batholith in Dulan, North Qaidam, NW China: Chinese Science Bulletin, v. 49, p. 1736–1740, doi:10.1007/BF03184308.

Xia, W., Zhang, N., Yuan, X., Fan, L., and Zhang, B., 2001, Cenozoic Qaidam basin, China: A stronger tectonic inversed, extensional rifted basin: AAPG Bulletin, v. 85, p. 715–736.

Xiao, W.J., Windley, B.F., Chen, H.L., Zhang, G.C., and Li, J.L., 2002, Carboniferous-Triassic subduction and accretion in the western Kunlun, China: Implications for the collisional and accretionary tectonics of the northern Tibetan Plateau: Geology, v. 30, p. 295, doi:10.1130/0091-7613(2002)030<0295:CTSAAI>2.0.CO;2.

Xiao, W., Windley, B.F., Yong, Y., Yan, Z., Yuan, C., Liu, C., and Li, J., 2009, Early Paleozoic to Devonian multiple-accretionary model for the Qilian Shan, NW China: Journal of Asian Earth Sciences, v. 35, p. 323–333, doi:10.1016/j.jseaes.2008.10.001.

Xu, Z., 1984, Tertiary system and its petroleum potential in the Lunpola Basin, Xizang (Tibet). U.S. Geological Survey Open-File Report 84–420, 5 p.

Yan, Z., Xiao, W.J., Windley, B.F., Wang, Z.Q., and Li, J.L., 2010, Silurian clastic sediments in the North Qilian Shan, NW China: Chemical and isotopic constraints on their forearc provenance with implications for the Paleozoic evolution of the Tibetan Plateau: Sedimentary Geology, v. 231, p. 98–114, doi:10.1016/j.sedgeo.2010.09.001.

Yang, J., Xu, Z., Zhang, J., Chu, C.-Y., Zhang, R., and Liou, J.-G., 2001, Tectonic significance of early Paleozoic high-pressure rocks in Altun-Qaidam-Qilian Mountains, northwest China: Geological Society of America Memoirs, v. 194, p. 151–170, doi:10.1130/0-8137-1194-0.151.

Yang, Y., Ritzwoller, M. H., Zheng, Y., Shen, W., Levshin, A. L., and Xie, Z., 2012, A synoptic view of the distribution and connectivity of the mid-crustal low velocity zone beneath Tibet: Journal of Geophysical Research: Solid Earth (1978–2012), v. 117, B04303.

Yin, A., Butler, R., Harrison, T.M., Foster, D. a., Ingersoll, R. V., Zhou, X., Wang, X.-F., and Hanson, A.D., 2002, Tectonic history of the Altyn Tagh fault system in northern Tibet inferred from Cenozoic sedimentation: Geological Society of America Bulletin, v. 114, p. 1257–1295.

Yin, A., Dang, Y.-Q., Wang, L.-C., Jiang, W.-M., Zhou, S.-P., Chen, X.-H., Gehrels, G.E., and McRivette, M.W., 2008a, Cenozoic tectonic evolution of Qaidam basin and its surrounding regions (Part 1): The southern Qilian Shan-Nan Shan thrust belt and northern Qaidam basin: Geological Society of America Bulletin, v. 120, p. 813–846, doi:10.1130/B26180.1.

Yin, A., Dang, Y.-Q., Zhang, M., Chen, X.-H., and McRivette, M.W., 2008b, Cenozoic tectonic evolution of the Qaidam basin and its surrounding regions (Part 3): Structural geology, sedimentation, and regional tectonic reconstruction: Geological Society of America Bulletin, v. 120, p. 847–876, doi:10.1130/B26232.1.

Yin, A., Dang, Y.-Q., Zhang, M., McRivette, M.W., Burgess, W.P., and Chen, X.-H., 2007a, Cenozoic tectonic evolution of Qaidam basin and its surrounding regions (part 2): Wedge tectonics in southern Qaidam basin and the Eastern Kunlun Range: Geological Society of America Special Papers, v. 433, p. 369, doi:10.1130/2007.2433(18).

Yin, A., and Harrison, T.M., 2000, Geologic evolution of the Himalayan-Tibetan orogen: Annual Review of Earth and Planetary Sciences, v. 28, no. 1, p. 211–280, doi:10.1146/annurev.earth.28.1.211.

Yin, A., and Ingersoll, R. V., 1997, A model for evolution of Laramide axial basins in the southern Rocky Mountains: International geology review, v. 39, p. 1113–1123.

Yin, A., Manning, C.E., Lovera, O., Menold, C.A., Chen, X., and Gehrels, G.E., 2007b, Early Paleozoic tectonic and thermomechanical evolution of ultrahigh-pressure (UHP) metamorphic rocks in the northern Tibetan Plateau, Northwest China: International Geology Review, v. 49, p. 681–716, doi:10.2747/0020-6814.49.8.681.

Yonkee, W.A., Dehler, C.D., Link, P.K., Balgord, E.A., Keeley, J.A., Hayes, D.S., Wells, M.L., Fanning, C.M., and Johnston, S.M., 2014, Tectono-stratigraphic framework of Neoproterozoic to Cambrian strata, west-central U.S.: Protracted rifting, glaciation, and evolution of the North American Cordilleran margin: Earth-Science Reviews, v. 136, p. 59–95, doi: 10.1016/j.earscirev.2014.05.004.

Yonkee, W.A., and Weil, A.B., 2015, Tectonic evolution of the Sevier and Laramide belts within the North American Cordillera orogenic system: Earth Science Reviews, v. 150, p. 531-593.

Yuan, W., Dong, J., Shicheng, W., and Carter, A., 2006, Apatite fission track evidence for Neogene uplift in the eastern Kunlun Mountains, northern Qinghai–Tibet Plateau, China: Journal of Asian Earth Sciences, v. 27, p. 847–856, doi:10.1016/j.jseaes.2005.09.002.

Yuan, C., Sun, M., Xiao, W., Wilde, S., Li, X., Liu, X., Long, X., Xia, X., Ye, K., and Li, J., 2009, Garnet-bearing tonalitic porphyry from East Kunlun, Northeast Tibetan Plateau: implications for adakite and magmas from the MASH Zone: International Journal of Earth Sciences, v. 98, p. 1489–1510, doi:10.1007/s00531-008-0335-y.

Yuan, D.-Y., Ge, W.-P., Chen, Z.-W., Li, C.-Y., Wang, Z.-C., Zhang, H.-P., Zhang, P.-Z., Zheng, D.-W., Zheng, W.-J., Craddock, W.H., Dayem, K.E., Duvall, A.R., Hough, B.G., Lease, R.O., et al., 2013, The growth of northeastern Tibet and its relevance to large-scale continental geodynamics: A review of recent studies: Tectonics, v. 32, p. 1358–1370, doi:10.1002/tect.20081.

Yue, Y., Graham, S. A., Ritts, B. D., and Wooden, J. L., 2005, Detrital zircon provenance evidence for large-scale extrusion along the Altyn Tagh fault: Tectonophysics, v. 406, p. 165–178. http://doi.org/10.1016/j.tecto.2005.05.023.

Yue, Y., Ritts, B.D., Graham, S.A., Wooden, J.L., Gehrels, G.E., and Zhang, Z., 2003, Slowing extrusion tectonics: lowered estimate of post-Early Miocene slip rate for the Altyn Tagh fault: Earth and Planetary Science Letters, v. 217, p. 111–122, doi:10.1016/S0012-821X(03)00544-2.

Zahid, K. M., and Barbeau, D. L., 2011, Constructing sandstone provenance and classification ternary diagrams using and electronic spreadsheet: Journal of Sedimentary Research, v. 81, p. 702-707.

Zhang, C.L., Lu, S.N., Yu, H.F., and Ye, H.M., 2007, Tectonic evolution of the Western Kunlun orogenic belt in northern Qinghai-Tibet Plateau: Evidence from zircon SHRIMP and LA-ICP-MS U-Pb geochronology: Science in China, Series D: Earth Sciences, v. 50, p. 825–835, doi:10.1007/s11430-007-2051-z.

Zhang, H.-P., Craddock, W.H., Lease, R.O., Wang, W., Yuan, D.-Y., Zhang, P.-Z., Molnar, P., Zheng, D.-W., and Zheng, W.-J., 2012, Magnetostratigraphy of the Neogene Chaka basin and its implications for mountain building processes in the north-eastern Tibetan Plateau: Basin Research, v. 24, p. 31–50, doi:10.1111/j.1365-2117.2011.00512.x.

Zhang, J.Y., Ma, C.Q., Xiong, F.H., Liu, B., 2012, Petrogenesis and tectonic significance of the Late Permian-Middle Triassic calc-alkaline granites in the Balong region, eastern Kunlun Orogen, China: Geological Magazine, v. 149, p. 892-908.

Zhang, P.Z., Shen, Z., Wang, M., Gan, W., Bürgmann, R., Molnar, P., Wang, Q., Niu, Z., Sun, J., Wu, J., Hanrong, S., and Xinzhao, Y., 2004, Continuous deformation of the Tibetan Plateau from global positioning system data: Geology, v. 32, p. 809–812, doi:10.1130/G20554.1.

Zhang, Y., and Zheng, J., 1994, Geologic overview in Kokshili, Qinghai and adjacent areas: Seismological Publishing House, Beijing.

Zheng, D., Clark, M.K., Zhang, P., Zheng, W., and Farley, K. A., 2010, Erosion, fault initiation and topographic growth of the North Qilian Shan (northern Tibetan Plateau): Geosphere, v. 6, p. 937–941, doi:10.1130/GES00523.1.

Zhuang, G., Hourigan, J.K., Ritts, B.D., and Kent-Corson, M.L., 2011, Cenozoic multiple-phase tectonic evolution of the northern Tibetan Plateau: Constraints from sedimentary records from Qaidam basin, Hexi Corridor, and Subei basin, northwest China: American Journal of Science, v. 311, p. 116–152, doi:10.2475/02.2011.02.